THE UNIVERSITY OF MANITOBA

YIELDING CRITERIA AND LIMIT-STATE IN A WINNIPEG CLAY

by

KHEW VOON LEW

A THESIS

SUBMITTED TO THE FACULTY OF GRADUATE STUDIES

IN PARTIAL FULFILLMENT OF THE REQUIREMENTS FOR THE DEGREE OF

MASTER OF SCIENCE

DEPARTMENT OF CIVIL ENGINEERING

WINNIPEG, MANITOBA

APRIL 1981

YIELDING CRITERIA AND LIMIT-STATE IN A WINNIPEG CLAY

BY

KHEW VOON LEW

A thesis submitted to the Faculty of Graduate Studies of
the University of Manitoba in partial fulfillment of the requirements
of the degree of

MASTER OF SCIENCE

ABSTRACT

This thesis investigates the applicability of the concept of yielding to Lake Agassiz clay in the Winnipeg area. Careful sampling and laboratory testing techniques have been used. The test program was designed to examine the limit-state for the blue clay at 11.5 m depth. The study also investigated the time-dependent aspects of the YLIGHT model of soil behaviour, strain energy as a criterion for identifying limit-state, and the threshold energy concept at yielding.

Eighteen 76 mm diameter undisturbed triaxial samples were tested along various stress paths. Drained, stress-controlled tests show that yielding is controlled by the in-situ grain structure of the clay, and by stress-history effects. For the blue clay at 11.5 m depth, a well defined yield envelope has been identified which supports the YLIGHT model concept proposed for Champlain Sea clay. Yield envelopes from different depths in the Winnipeg clay are fairly homothetic, and can be normalized with respect to p'_c.

Undrained, strain-controlled portions of the triaxial testing program were used to examine several aspects of the clay's behaviour. On the basis of the $(\sigma_1-\sigma_3)/2_{max}$ failure criterion, the normally consolidated Coulomb-Mohr strength parameters, c' and ϕ' were found to be 4 kPa and 17.5^o respectively. The average value of s_u/p'_c was found to be 0.22. Porewater pressures at failure depend strongly on the stress levels and stress ratios during laboratory reconsolidation. Values of A_f range between 0.22 to 1.59. The relative stiffness, E_{50}/s_u, lies between 168 and 361. For a tenfold change in strain rate in Winnipeg clays, the change in undrained strength is approximately 11 to 12 percent.

ACKNOWLEDGEMENTS

I am sincerely indebted to my advisor, Dr. J. Graham for his generous and unstinting support during all phases of this work; for his guidance and invaluable advice in the preparation of this thesis; and for the opportunity to work with him.

Helpful discussion with Dr. J.B. Burland, Imperial College of Science and Technology, London, is also gratefully acknowledged.

The author wishes to thank Mr. N. Piamsalee and Mr. J. Clark, the technical staff of Civil Engineering Department, for their assistance during the experimental investigation.

Financial assistance, in the form of support from NSERC grant A3712 is also acknowledged.

The author is deeply indebted to his mother, Madam M. Chai, who has been a constant source of support and encouragement.

Finally, the author owes the deepest gratitude to his wife, Jessamine, for her sacrifice, unending patience, understanding and encouragement during the course of his graduate studies, and for her excellent work in typing the thesis.

TABLE OF CONTENTS

CHAPTER PAGE

LIST OF SYMBOLS

a	-	area of loading piston in the triaxial cell
a_v	-	coefficient of compressibility
A, B	-	porewater pressure parameters (after Skempton, 1954)
A_f	-	value of A at failure
A_ε	-	instantaneous sample area
c'	-	effective cohesion intercept
C_c	-	compression index
c_v	-	coefficient of consolidation
CAD	-	stress-controlled, consolidated anisotropically drained test
CAD(U)	-	strain-controlled, undrained compression test with porewater pressure measurements preceded by CAD test
CAU	-	strain-controlled, consolidated anisotropically undrained compression test
CID	-	stress-controlled, consolidated isotropically drained test
CID(U)	-	strain-controlled, undrained compression test with porewater pressure measurements preceded by CID test
e	-	voids ratio
e_o	-	initial voids ratio
E_{50}	-	elastic modulus to 50% of failure stress
G.W.L	-	groundwater table or phreatic surface

G_s - specific gravity

I_p - plasticity index

k - coefficient of permeability

K_o - coefficient of earth pressure at rest

LSNV - Length of Strain Vector

LSSV - Length of Stress Vector

m_v - coefficient of volume change

OCR - overconsolidation ratio

p' - mean principal stress; = $(\sigma_1' + \sigma_2' + \sigma_3')/3$

p_c' - effective preconsolidation pressure

$(p_c')_{iso}$ - effective preconsolidation pressure in an isotropic compression test

p_o' - effective vertical overburden stress

$(p_{vert}')_{max}$ - maximum effective vertical overburden pressure (approximately equal to p_c')

q - principal stress different; = $(\sigma_1 - \sigma_3)$

s_u - undrained strength; = $(\sigma_1 - \sigma_3)/2_{max}$

u - porewater pressure

w - natural moisture content

w_L - liquid limit

w_p - plastic limit

W - strain energy absorbed per unit volume

W_o - dead load acting at mid-height of sample during consolidation

γ - average unit weight

ε_1, ε_3 - major and minor principal strains (i.e. axial and radial strains in triaxial compression test)

ε_{1c}, ε_{3c} - ε_1 and ε_3 at the end of triaxial consolidation to σ'_{1c}, σ'_{3c}

ε_v - volumetric strain in triaxial compression test

ε_{vc} - ε_v at the end of triaxial consolidation to σ'_{1c}, σ'_{3c}

ε_ρ - average axial strain during relaxation test in undrained compression test

$\dot{\varepsilon}_1$ - axial strain rate

$\rho_{0.1}$ - strain rate effect parameter

σ'_1, σ'_3 - major and minor effective principal stresses

σ'_{1c}, σ'_{3c} - σ'_1 and σ'_3 at the end of triaxial consolidation

σ'_h - effective horizontal stress

σ_{oct} - total octahedral normal stress

σ'_{oct} - effective octahedral normal stress

σ'_{scalar} - effective scalar stress

σ'_v - effective vertical stress

ϕ' - effective angle of shearing resistance

LIST OF TABLES

LIST OF FIGURES

FIGURE PAGE

FIGURE PAGE

CHAPTER 1

INTRODUCTION

Perhaps the most important technical development at the 1979 Canadian Geotechnical Conference was the considerable attention directed for the first time at these conferences to the concept of "yielding" as defined by a limit-state surface in stress space. The limit-state surface in a general stress space is a boundary, or "envelope", at which the compressibility, settlement rate and porewater pressures of undisturbed natural clay all increase markedly as stresses are increased from in-situ stresses to stresses associated with engineering construction. The distinction between limit-state and critical-state surfaces has been carefully examined by Noonan (1980).

Limit-state surfaces or yield envelopes, for post-glacial clays are currently receiving much research attention. Most studies have involved the marine clays of Eastern Canada, (see for example Mitchell, 1970; Tavenas and Leroueil, 1977). Limit-state studies were initiated by Dr. J. Graham in 1976 at the University of Manitoba to examine the applicability of the limit-state concept to the glacio-lacustrine clays of Winnipeg area. The testing program consisted of 76 mm diameter samples, trimmed using equipment specially designed to minimize disturbance, and tested in large diameter, rotating-bush triaxial cells. Samples were taken from 6 m to 12 m depth at the University of Manitoba campus using the block sampler devised by Domaschuk (1977). Preliminary results were presented by Baracos et al.

(1980). Subsequently, further studies have been carried out by Noonan (1980). In concluding his thesis, Noonan drew attention to certain aspects of the clay behaviour which were still unclear. The more important of these may be summarized as follows:

1. Because of the limited number of samples tested, the shape and orientation of the yield envelopes* defined in the earlier tests were tentative. Hence, the details of the YLIGHT model (Tavenas and Leroueil, 1977) could not be confirmed.
2. Verification of the applicability of YLIGHT model to Winnipeg clays required further testing on a larger number of samples from one depth. Isotropic, effective stress paths should be included.
3. The effect of load duration and load increment ratio on the stress-strain time results were not investigated in the earlier tests. They were associated with the time-dependent aspects of YLIGHT model.

---

*There is some confusion in the usage of the terms "Limit-State Envelope" and "yield envelope". Technically, it would appear that "Limit-State Envelope" should be restricted to the locus of yield points in a constant-e plane in (p', q, e) space, as defined for example by undrained tests (Roscoe and Burland, 1968). In contrast, the yield envelopes described in this thesis are derived from tests which start from the same initial p'_o, K_o p'_o, e_o - conditions, but have different voids ratios at yield. The yield envelopes therefore, although shown in Fig. 4.27 for example in (p', q) space, are not in a constant-e plane. The 3-dimensional envelope of the separate limit-state stresses (or yields) found from the individual tests is known as the Limit-State Surface.

4. Strain energy as a yielding criterion needed further investigation.
5. Four 63 mm diameter oedometer samples had been tested in the earlier tests, but there was considerable uncertainty regarding the variation with depth of the preconsolidation pressure p'_c.
6. The samples used in the earlier studies had been stored for more than a year during which time properties of the clay might have been altered significantly. It was suggested that the storage time of samples prior to testing be minimized in the future.

In response to these conclusions, it was considered necessary to carry out further testing, and block samples were taken on July, 1980 and January, 1981 from 11.28 m to 11.66 m depth at the same test site (Baracos et al., 1980). These have now been tested and the results are contained in this thesis. The specific aims of this thesis were as follows:

1. To improve the existing techniques for determining yield envelopes in Lake Agassiz clay.
2. To examine the influence of load duration and load increment ratio on the determination of the yield envelopes in plastic clay.
3. To examine the criteria for defining yield stresses from various stress-strain plots.
4. To investigate the validity of strain energy as a yield criterion and to examine if there is a threshold energy

for yielding which is stress path independent.

5. To improve the techniques for oedometer testing and to determine the distribution of p'_c with depth on the test site.
6. To study the effects of changes of strain rate on undrained shear strength.

The laboratory testing program which will be described in detail in a later chapter, consisted of eighteen large diameter (76 mm), triaxial tests, four oedometer tests and standard classification tests which include sensitivity tests. Both 63 mm and 76 mm diameter oedometer samples were used to determine p'_c. Data were obtained on both drained and undrained triaxial behaviour. Drained stress-controlled triaxial tests were used to examine the limit-state condition along various stress paths. The results were examined with reference to the YLIGHT model proposed by Tavenas and Leroueil (1977), and with regard to the use of different components of stress tensor to define the limit-state condition. In addition, strain energy as a yield criterion was investigated. Samples which were not stressed to rupture during the drained portion of the triaxial test were tested to failure in undrained shear. The undrained part of the test allowed examination of the following characteristics of clay behaviour: the influence of consolidation history on porewater pressure generation and elastic moduli; the effects of changes of strain rate on the undrained shear strength; and the normally consolidated Coulomb-Mohr rupture envelope. In addition, the results of one-dimensional oedometer tests were used to examine the drained compression behaviour of clays along the K_o -

consolidation line.

Before proceeding to the testing program (Chapter 3) and its results (Chapter 4 and 5), the thesis will present in Chapter 2 a brief review of the concept of yielding and the YLIGHT model proposed by Tavenas and Leroueil (1977); and the recent limit-state studies in Lake Agassiz clay (Baracos et al., 1980; Noonan, 1980).

CHAPTER 2

A REVIEW OF LIMIT STATE CONCEPT AS APPLIED TO THE LAKE AGASSIZ CLAYS

2.1 INTRODUCTION

In recent years, considerable attention has been paid to the geotechnical properties and behaviour of soft clays and sensitive clays. Much of the research has focussed on Norwegian quick clays, and on the cemented Leda clays found in Eastern Canada (Bjerrum, 1967; Townsend et al., 1969; Mitchell, 1970; Tavenas and Leroueil, 1977). Excellent reviews of the geotechnical properties and behaviour of the soft post-glacial clays in Canada with respect to embankment and foundation design have recently been presented by Quigley (1980), and by Kenney and Folkes (1979).

Various investigators have shown that the concepts of limit and critical states originally proposed by Roscoe, Schofield and Wroth (1958) and Roscoe and Burland (1968) to describe the behaviour of isotropically consolidated clays could be extended and modified to apply to natural, anisotropic clays. In particular, the existence of limit-state surfaces has been demonstrated by tests on intact lightly overconsolidated clay samples by Graham (1969), Mitchell (1970), Crooks and Graham (1976), and Tavenas and Leroueil (1977). In addition, Baracos et al. (1980) and Noonan (1980) have shown that yield envelopes can be defined in (p', q) stress space for the glacio-lacustrine clays of the Winnipeg area. The practical significance of the limit-state

concept in understanding the behaviour of clay, and in the design of structures on clay foundations has been shown by Tavenas and Leroueil (1977); Tavenas et al. (1978b and 1979); and Tavenas (1979).

Noonan (1980) has given an extensive literature review of the concept of limit-state and critical-state. He discusses its initial development (Roscoe et al., 1958), and the present understanding it provides for the behaviour of natural clays (Tavenas and Leroueil, 1980). Prior to the work by Tavenas and his co-workers at Laval University, an overall picture of the nature of the limit-state envelope for a clay and the factors affecting it was not clear, although yield envelopes for various clays had been found (for example, Mitchell, 1970; Crooks and Graham, 1976).

The following two sections present briefly the YLIGHT model proposed by the Laval workers, and the factors which affect the determination of limit-state envelopes. In view of Noonan's recent review (1980), the presentation will be brief, and restricted to those aspects which relate to the testing program described in this thesis.

2.2 THE YLIGHT MODEL

Tavenas and Leroueil (1977) showed that the shape of the limit-state surface of a natural clay reflects the mineralogy of the deposit, and the stress anisotropy prevailing during deposition and consolidation. It is approximately symmetrical about the $K_o = 0.9 \times (1-\sin\phi')$ line (Jaky, 1944; Tavenas et al., 1977). Its position along the K_o - line, as well as its size, are fixed by local values of the preconsolidation pressure, p'_c. These results were also shown in

preliminary reports by Graham (1969, 1974). On compiling the data available to them, Tavenas and Leroueil (1977) showed that all limit-state surfaces obtained on natural clays have these characteristics and are different from the theoretical shape implied in the Cam Clay model of soil behaviour (Roscoe and Burland, 1968). In addition, they showed that the effect of aging (i.e. the decrease of voids ratio of a clay with time at constant effective stresses due to secondary compression) and strain-rate described by Bjerrum (1967) can be accounted for in their behavioural model known as YLIGHT. This model was initially proposed for Champlain Sea clays (Tavenas and Leroueil, 1977). Its applicability to all natural clays appears promising and is presently being evaluated at the University of Manitoba using Lake Agassiz clay. Detailed examination of the model and the logic behind it have been presented by Noonan (1980). The important features of the YLIGHT model may be summarized as follows:

1. The limit-state envelope of a natural clay has a shape which is approximately elliptical, and centered on the K_o - consolidation line of the normally consolidated clay.
2. The position of the limit-state envelope in stress space is governed by the magnitude of the preconsolidation pressure, p'_c.
3. The limit-state envelope of a natural clay can be qualitatively determined by its effective friction angle, ϕ', which governs the K_o - stress condition of the normally consolidated clay; by its preconsolidation pressure; and by its undrained shear strength.

4. The limit-state envelope can be approximately located in stress space given knowledge of the parameters $(s_u)_{max}$*, $(p'_c)_{iso}$, $(p'_{vert})_{max}$, and the K_o - consolidation line (Fig. 2.1). (All figures are presented at the back of this thesis after the References and Tables). It is also noted that the ratio of $(p'_{vert})_{max}$ to $(p'_c)_{iso}$ is generally in the order of 1.4 to 1.8 (Leroueil and Tavenas, 1977).
5. In a uniform clay which has been deposited in a single unit, the limit-state envelopes at different depths, and thus different p'_c values, are all homothetic, that is, geometrically similar.
6. The critical state line, as used in the model, is identical to the large strain, normally consolidated Coulomb-Mohr strength envelope.
7. The effect of aging of natural clays, as well as the influence of longer loading duration or slower strain-rate can cause the entire limit-state envelope to shrink inwards with time (Tavenas et al., 1978b).

It should be noted that further testing is required to confirm the general validity of this model for all natural clays. In particular, the effect of aging of natural clay, and the influence of loading rate or duration on the characteristics of the yielding of undisturbed natural clays, need further investigation.

---

*See List of Symbols on Page vi

2.3 FACTORS AFFECTING THE DETERMINATION OF YIELD ENVELOPES

A generally accepted definition for the yield envelope of a natural clay is a locus joining a set of yield points in the (p', q) stress space corresponding to the in-situ voids ratio e, inside which strain, strain rates, and porewater pressure generation are low; and outside which all of these parameters are much higher (Baracos et al., 1980; Noonan, 1980). States of stress inside this envelope produce a pseudo-elastic, relatively incompressible and largely recoverable response associated with small-strain, rapid, readjustment of the grain structure of the clay. Non-failing stress states which are outside the yield envelope, in (p', q) space, but on the limit-state surface in (p', q, e) space, produce a more compressible and irreversible response associated with the longer-term, large strain readjustment of the clay structure (Graham, 1974). This behaviour is most easily observed in oedometer tests where it is manifested as the characteristic preconsolidation pressure (p'_c) break in the semi-logarithmic plot of voids ratio versus effective vertical pressure. In undrained triaxial compression tests it is represented by the maximum deviator stress. The concept of the limit-state surface in a clay is simply a generalization of the overconsolidation effect commonly observed in oedometer tests.

Most natural clays appear to have developed an over-competent grain structure (Bjerrum, 1967; Graham, 1974; Crooks and Graham, 1976) which can withstand stresses somewhat higher than their in-situ stress levels without an appreciable breakdown or 'yield' of their grain structure. The causes for this over-competency are many (Graham, 1974).

For example, overconsolidation due to desiccation, groundwater level changes and erosional off-loading cause the clay structure to adjust to stress levels higher than its present in-situ stresses. This leaves the clay with a reserve resistance, above the structural strength it would have at the in-situ stress level if it remained normally consolidated. Bjerrum (1967) showed that an over-competent structure has developed in Norwegian clays by a combination of the following: depositional environment and subsequent geochemical changes; and delayed compression or aging. In addition, cementation has been shown to cause an over-competent structure in some Canadian clays (Sangrey, 1972).

The detailed determination of the yield envelope of a natural clay is difficult because of the natural variability of clay deposits. In order to avoid these difficulties, it is advisable to carry out the entire test program on large samples originating from the same depth*. The use of block sampling techniques is practically mandatory to ensure that all samples have been submitted to the same geological processes and stress history (Leroueil and Tavenas, 1977). Bjerrum and Kenney (1967) showed that the stress-strain behaviour and the strength of sensitive clays are intimately related to the grain structure; that is, to the physical arrangement of soil particles. Eden (1971) demonstrated the reductions in both strengths and preconsolidation pressure caused by various tube samplers in stiff clay from Ottawa. La Rochelle and

---

*Graham (1974), Mesri (1975) and Crooks and Graham (1976), have drawn attention to the usefulness of preconsolidation pressure p_c' in "normalizing" the behaviour of samples from different depths.

Lefebvre (1971) established the influence of tube sampling on the 'strength part' of the yield envelope of the St. Louis clay. More generally, sampling disturbance can induce significant changes in the shape and position of the yield envelope of natural clays by affecting the clay structure.

Tavenas and Leroueil (1977) confirmed that the magnitude of the preconsolidation pressure governs the position of the yield envelope in stress space (Fig. 2.1). Based on their experimental investigation, they further concluded that all the factors which affect the preconsolidation pressure would also affect the entire limit-state envelope. It was in this connection that the work of Bjerrum on the effects of aging and strain rates on preconsolidation pressure was introduced to studies of yield envelopes. Bjerrum (1967) showed that the aging of clays under constant effective stresses causes a reduction in voids ratio due to secondary deformations, and that this reduction in voids ratio results in an increase in the apparent preconsolidation pressure. Tavenas and Leroueil (1977) showed that the aging of a clay results in a homothetic displacement of the entire yield envelope in stress space towards higher pressures and strengths.

Crawford (1964) and Bjerrum (1967) both demonstrated that the apparent preconsolidation pressure of a clay is reduced if the rate of loading is reduced, or if the duration of loading is increased in oedometer tests. Bjerrum showed that this effect was actually another materialization of the secondary consolidation phenomenon caused by aging. With respect to the effects of strain rate, Tavenas and Leroueil (1977) using oedometer tests and triaxial tests, confirmed the effect of rate,

or duration of loading, on the preconsolidation pressure and yield envelope. They showed that the preconsolidation pressure of a clay is reduced if the duration of loading is increased. Similarly, undrained triaxial tests at different strain rates indicate a reduction in strength as strain rate decreases. More importantly, the displacement of the yield envelope indicated a homothetic movement inwards with time. On this basis Tavenas and Leroueil (1977) concluded that the known effects of aging and strain rate on p'_c applied to the entire yield envelope. This hypothesis that the time-dependent behaviour of a clay is completely described by the time-dependent displacement of its limit-state surface is known as the YLIGHT model. It was confirmed in a later paper by Tavenas et al. (1978b). Additional research is required to quantify this time-dependence, particularly for clays other than the Champlain Sea Clays tested by Tavenas and his co-workers.

2.4 YIELD ENVELOPES OF LAKE AGASSIZ CLAY - A REVIEW

The applicability of the limit-state concept is part of a larger investigation by the geotechnical group at the University of Manitoba into the geotechnical properties of the glacial Lake Agassiz clay which underlies the Winnipeg area. Preliminary information was presented by Baracos et al. (1980) and Noonan (1980). Yield envelopes were found from intact overconsolidated clay samples taken from various depths. A summary of the existing information is presented in Fig. 2.2. As proposed by the YLIGHT model, the yield envelopes at different depths were found to be homothetic. However, the trimming and testing techniques in these earlier tests were difficult due to the highly

anisotropic and nonhomogeneous nature of the clay. More importantly, the effects of load duration and load increment ratio on this clay were not clear, and caused considerable delay in Noonan's work. As a result, the shape and orientation of the previously defined yield envelopes were tentative.

As suggested in Chapter 1, further work was considered necessary and forms the test program described in this thesis. In particular, attention has been paid to careful determination of the yield envelope at one depth in the deposit, and to the time effects which form such an integral part of the YLIGHT model.

CHAPTER 3

DESCRIPTION OF SOIL PROPERTIES AND TESTING PROCEDURES

3.1 INTRODUCTION

The soil profile in the Winnipeg area consists mainly of Lake Agassiz deposits of silts and clays, overlying till and Ordovician dolomitic limestone. The formation and geologic features of the Lake Agassiz clays have been described by Elson (1961, 1967), Render (1970) and Teller (1976).

The samples used in the present study were taken from the University of Manitoba campus. This study is part of a larger investigation at the University of Manitoba of the geotechnical properties of the glacial Lake Agassiz clays (Pietrzak, 1979; Baracos et al., 1980; Noonan, 1980). Fig. 3.1 shows the site plan of the test area (Pietrzak, 1979). Boreholes 4 and 5 were drilled on July, 1980 and January, 1981 respectively using a 76 cm diameter power auger. To minimize the sample disturbance during sampling, good quality block samples from depth were obtained using the block sampler devised by Domaschuk (1977). This chapter reviews the general properties of the Lake Agassiz lacustrine clays and presents the testing techniques.

3.2 SOIL PROFILE AND PROPERTIES

An average borehole log for the boreholes from which the samples were taken has been presented by Baracos et al. (1980) and is included in this thesis as Fig. 3.2. Further information from the

present study which is additional to the details given by Baracos et. al . (1980) is shown in Table 1. No major differences result. Improved values for p_c' and C_c will be presented in Section 4.3. Typically, the deposit consists of a layer of brown silty clay approximately 1 m to 2 m thick, a layer of tan-coloured silt generally less than 1 m thick followed in depth by a brown (often mottled brown and blue) clay layer about 3 m thick, and a layer of blue clay 8 m to 10 m thick. The brown and blue clay layers are both thought to be freshwater lacustrine deposits although Teller (1976) has suggested that the depositional environment may have been brackish.

All the test samples used in the present study were taken from block samples at 11.28 m to 11.66 m depth in the blue clay layer. The blue clay is medium to highly plastic (CH), has medium-stiff to stiff consistency, has no visible fissures, and contains numerous pockets or inclusions of grey silt, pebbles, and occasional cobbles.

Standard classification tests (Atterberg limit, moisture content, hydrometer and specific gravity) were performed on the trimmings from each of the block samples. The results of these tests are presented in Table 1 and are in general agreement with the classification results for blue clay described by Baracos et al . (1980). The ranges of index properties were:

Natural moisture content, w	55% - 64%
Liquid limit, w_L	79% - 86%
Plastic limit, w_p	25% - 28%
Plasticity index, I_p	54% - 58%
Average specific gravity, G_s	2.72

Sensitivity tests were performed on clays from 5.5 m (Trainor, 1981); 9.1 m and 11.5 m using a Swedish Fall-cone apparatus. A low sensitivity of only 2.5 to 4 was found. Undisturbed fall-cone strengths of 81 kPa, 67 kPa and 49 kPa were recorded at the respective depths.

Although the deposits in the Winnipeg area have not been subject to any known geologic off-loading they have been found to have overconsolidation ratios varying from 5 at the top of the blue clay to about 2 to 3 deeper in the deposit (Baracos et al., 1980). The overconsolidation is probably due to groundwater level fluctuations, suction pressures associated with desiccation and freezing mechanisms, delayed compression or creep during postdepositional aging, and possibly cementation bonding formed at interparticle contacts by upwards - flowing groundwater with high salt content (Render, 1970). Further attention is directed to consolidation test results in a later section of the thesis.

3.3 SAMPLE PREPARATION AND TESTING PROCEDURES

In order to investigate the applicability of the limit-state concept to the Winnipeg blue clay, it was necessary to examine the strains resulting from applied stress increments up to, and beyond the yield envelope for the clay at a particular depth. All tests were on block samples taken from 11.28 m to 11.66 m depth beneath the ground surface. This section of the thesis outlines the apparatus and techniques used for preparing and testing samples.

3.3.1 Sample Preparation Methods

Methods of sample preparation varied depending on the type of test to be carried out. These methods are described under appropriate headings below.

3.3.1.1 Consolidated-Drained and Undrained Triaxial Samples

Eighteen, 76 mm diameter, triaxial tests (T302 to T319) were performed on carefully trimmed samples from four block samples in the blue clay layer. The testing program placed considerable emphasis on avoiding disturbance of the "structure" or mechanical skeleton of the clay formed by the bond forces between individual soil particles. The importance of this with respect to preserving the field structure of the clay has been emphasized by Graham (1974), and Crooks and Graham (1976). The trimming was done using equipment constructed at the University of Manitoba (Fig. 3.3) which was designed to cause minimum disturbance to the sample. It is similar in principle to equipment described by Landva (1964). An important feature of this equipment is that the sample is supported at all stages during preparation.

The procedure for preparing samples has been described in detail by Noonan (1980). It is similar to that used by Crooks (1973), but was carefully rewritten by Noonan to conform with practice currently in use at the University of Manitoba. A shortened summary of the trimming and building-in procedures is listed in Appendix I. It can be outlined briefly as follows: A roughly trimmed sample was mounted on a trimming platform attached to the base of a triaxial cell. A greased cutting cylinder with a sharp leading edge, was pushed carefully

into the soil for a distance of approximately 1 cm and excess soil round the outside of the cutting edge was removed with a cutting wire. This process was repeated until soil protruded from the top of the cylinder. The ends of the sample were then trimmed across the top and bottom of the cutting cylinder. With the sample fully supported in the cylinder, a filter stone in a holder was attached to one end of the sample. The sample was then lowered on to the cell pedestal, the top cap was located firmly by a central rod, and the cutting cylinder was removed. Drainage was facilitated by lateral filter strips placed longitudinally around the circumference of the sample. Two membranes, separated by a layer of silicone oil, were placed over the sample, together with two o-rings on the top cap and three o-rings on the pedestal. This arrangement was used to minimize leakage during subsequent testing which in some cases lasted more than one month.

With the sample preparation complete, the cell was filled with deaired distilled water and a 2 cm layer of engine oil (SAE 120) added through the top of the cell to reduce leakage of cell water and friction between the piston and bushing.

3.3.1.2 Oedometer Samples

Four oedometer tests (C301 to C304) were performed on block samples from the same depth as the triaxial samples. Both 63 mm and 76 mm diameter samples were tested, the latter in new cells specially made for this testing program. To minimize the sample disturbance, improved trimming techniques were used. Samples were prepared using the same trimming equipment as the triaxial samples, but with some

modification (Fig. 3.4). An important feature of this improved trimming technique is that the cutting ring is held vertically as it is pushed into the sample during preparation.

3.3.2 Test Procedures

This section summaries the procedures adopted during different stages of the various tests. Detailed testing procedures for consolidated-drained stress-controlled tests and undrained shear tests were described by Noonan (1980). Any significant divergence from his procedures in individual cases is discussed in the presentation of test results later in Chapter 4 and 5.

3.3.2.1 Triaxial Consolidation and Drained Stress-Controlled Triaxial Tests

In order to simulate as closely as possible the in-situ behaviour of the clay, careful reconsolidation to in-situ stresses is mandatory. Although careful sampling and laboratory techniques minimize disturbance, changes in effective stresses in the soil samples due to these procedures are inevitable. It is therefore necessary to restress the samples to their in-situ effective stress levels. Crooks and Graham (1976) showed that laboratory reconsolidation strongly influences the stress-strain behaviour and porewater pressure generation during subsequent shearing of a sample.

The first phase of the triaxial compression tests was reconsolidation to the approximate in-situ effective stress levels in three stress increments. (T302, T310, T314 and T318 were non-standard tests

which will be described later). However, difficulty is experienced in defining the in-situ effective overburden stresses. In the Winnipeg area, the groundwater table may vary from ground level during extremely wet seasons, to 6 m or deeper in periods of severe drought (Baracos et al., 1980). For this reason, the value of p_o' is difficult to determine and an average value between these extremes was adopted in this study. This process is identical to that followed by Noonan (1980). The effective overburden stress for each block was calculated assuming the phreatic surface at a depth of 3 m and an average unit weight of 17.5 kN/m^3 both above and below the phreatic surface. The difficulties associated with deciding on the value of horizontal stress to use have been discussed by Graham (1974). Baracos et al. (1980) found that at stresses below p_o' the stress ratio required to keep sample area constant was approximately 0.65. A stress ratio of 0.65 was therefore adopted during the reconsolidation phase of the present study. Corresponding lateral strains were small, averaging 0.36% (compression).

The consolidation stages of the undrained triaxial tests and the drained stress-controlled tests were both carried out on a steel test frame, the general arrangement of which is shown in Fig. 3.5. Up to three rotating bush cells could be used at one time. The sample diameters were 76 mm in all tests.

The height changes of the samples were measured using a dial gauge fixed to the top of the cell and resting on an arm attached to the piston. Volume changes were measured using burettes with the water level maintained at the mid-height of the sample. Before each loading increment, water was flushed through the drainage leads to remove air

which might have been trapped between the membrane and sample, together with any gas released by the sample (Noonan, 1980). This procedure was repeated daily. Air bubbles were observed only irregularly.

Cell pressure was applied through water in the cell, using compressed air to pressurize an external air-water tank. The cell pressures and porewater pressures were both monitored by pressure transducers and were re-zeroed to atmospheric pressure daily at mid-height of sample. Axial loading was applied by dead loads on a hanger which rested freely on the piston. The load P required to give a predetermined axial stress σ_1' was calculated at the mid-height of the sample using the expression:

$$\sigma_1' = \sigma_3' (1 - a/A_\varepsilon) + \left(\frac{W_o + P}{A_\varepsilon}\right)$$

Where

a = piston area

A_ε = instantaneous sample area = $\frac{V}{H}$

W_o = dead load acting at mid-height of sample during consolidation

P = extra loading on hanger

All the anisotropically consolidated-drained stress-controlled tests were reconsolidated to $\sigma_{1c}' = p_o'$, $\sigma_{3c}' = 0.65\ p_o'$ before proceeding along predetermined stress paths. For each stress increment thereafter, the cell pressure and the required axial loads were calculated separately and added simultaneously. After the application of the stresses, axial dial gauge and burette readings were taken using standard 'doubling' time intervals (i.e. 1, 2, 4, 8, 15, 30 min; 1, 2, 4 hr etc.). Stress increments in triaxial consolidation, oedometer and drained stress-

controlled tests were added at approximately 24-hour intervals, with the exception of T312 and T315 where 5-day intervals were used.

Oedometer tests were carried out using the standard method outlined by Bowles (1978), except that initial vertical stresses of about 65 kPa were used to prevent swelling at low pressures. In general a load increment ratio of 1.6 was chosen to give at least 3 stress points on the reload section of the curve preceding the pre-consolidation pressure p'_c . In test C303 a constant load increment of 1.36 kg (3 lbs) was adopted.

3.3.2.2 Undrained Shearing

After triaxial consolidation, samples which were to be subjected to undrained strain-controlled shearing were moved carefully from the consolidation frame to a 10 t compression frame. Fig. 3.6 shows the arrangement used for shearing in consolidated-undrained tests. The piston was clamped before the axial load and hanger were removed but the cell pressure, burettes, dial gauge and transducer lines were all kept in place. The axial load was reapplied in the compression frame using a proving ring (sensitivity $\simeq$ 4.156 N/div), taking into account the change in dead load on the mid-height of the sample. In general, this process was accompanied by axial and volumetric strains of less than 0.05% which can be considered unimportant.

Prior to back-pressuring, the sample drainage system was flushed to remove any air which had collected during the last consolidation increment. A back-pressure of approximately 210 kPa was applied in seven increments of 30 kPa each. At each increment, the external

cell pressure and the internal porewater pressure were increased by the same amount, and the proving ring reading was increased appropriately to counteract the cell pressure increase against the bottom of the piston.

The sample was usually allowed to remain in this condition for a few hours or overnight, before checking for saturation. In most cases, values of the porewater parameter B were greater than 98% (Table 6). At this stage, the drainage valve was closed and the sample was allowed to stand for a short period of time to reduce the effects of any pressure surges in the system before undrained shearing was commenced.

Undrained shearing was normally carried out at an initial strain rate of about 1%/hour. Readings of axial deflection, proving ring, porewater pressure and cell pressure were taken at 10 minute intervals for the first hour and at 20 minute intervals thereafter until the maximum proving ring load was obtained. After reaching the peak proving ring load, the sample was strained for a further 2 to 3 percent axial strain, at which point a "relaxation test" was carried out to examine the effect of strain rate variation on the undrained strength. This procedure, developed by Kenney (1966), involves switching off the compression machine and noting changes with time in the axial deflection, proving ring, porewater pressure and cell pressure. Stopping the compression machine in this manner allows the sample to continue straining at a decreasing rate due to the stored energy in the proving ring. Relaxation tests were usually continued overnight. On the following morning, the compression machine was switched on again and shearing continued at various strain rates to axial strains of 14% to 18% in

special testing procedures which will be described later.

Undrained shear tests provided information on several aspects of the soil's behaviour, such as the stress-strain and porewater pressure generation characteristics. In particular, the porewater pressure parameter, A_f, the strain rate parameter, $\rho_{0.1}$ and the elastic modulus, E_{50}, for each test were examined. In addition, the failure stresses found in the test permitted an evaluation of the normally consolidated Coulomb-Mohr envelope for the clay at this depth. These will be presented in detail in Chapter 5.

Test T317 was a consolidated-drained, strain-controlled test with an initial strain rate of about 1%/day.

A simple computer program called Triaxial Test Program was developed to process the raw data collected from undrained shear tests. The calculated stress-strain values are printed in tabular form. Details of the program and instruction notes are given by Lew (1981), and are included in this thesis as Appendix II. It should be pointed out that no correction was made to allow for the restraining effect of the membranes and filter strips.

Subsequent to undrained shearing, the failed samples were removed from the triaxial cell and cut longitudinally. One-half of the sample was stored in moist condition for further study such as electron microscope examination of its failure planes. The other half was used to determine the final moisture content of the sample (Table 1).

CHAPTER 4

TEST RESULTS OF OEDOMETER TESTS AND CONSOLIDATED-DRAINED COMPRESSION TESTS

4.1 INTRODUCTION

In the course of the present investigation into the applicability of the limit-state concept to the Lake Agassiz lacustrine clay, consolidated-drained and undrained tests, and oedometer tests were carried out on samples recovered from 11.28 m to 11.66 m in boreholes 4 and 5 at the University of Manitoba campus (see Fig. 3.1). This chapter presents the testing program and a detailed quantitative presentation of the test results for oedometer tests and consolidated-drained stress-controlled tests.

A considerable effort was made in the present study to minimize the disturbance during sampling and laboratory preparation of samples because the grain structure of a soil can have an important influence on its strength and deformation behaviour (Crooks and Graham, 1976; Leroueil and Tavenas, 1977). The tests were designed to investigate several aspects of the limit-state concept and shearing behaviour of the soil (see Chapter 1), and to verify the conclusions of the previous study by Noonan, (1980). The results have been examined with reference to the YLIGHT model (Tavenas and Leroueil, 1977), and with regard to the use of different components of stress tensor to define the limit-state conditions.

Standard classification tests (Atterberg limits, specific

gravity, natural moisture content, and hydrometer) were performed on the trimmings taken from the triaxial compression samples. These are listed along with sampling depths and test types in Table 1. It is considered that the consistency limits from triaxial trimmings also apply to oedometer samples because each oedometer sample was trimmed from clay immediately adjacent to a triaxial sample.

4.2 TESTING PROGRAM

The drained triaxial testing comprised the largest and most important part of the investigation. With respect to preserving the field structure of the clay, the first phase of most of the triaxial compression tests were reconsolidation of the sample to its approximate in-situ stress levels (Crooks and Graham, 1976), using the procedures described in Chapter 3. (Samples T302 and T314 were consolidated along an isotropic effective stress path). Once the triaxial samples were reconsolidated to approximate in-situ stresses, the shape of the yield envelope in (p', q) stress space was explored by a series of stress paths chosen to define limit-state stresses in various regions of the stress space. Fig. 4.1 shows the proposed stress paths for the present study and Fig. 4.2 shows the stress paths which were actually followed during the investigation. The complete stress-strain results for the drained, stress-controlled portion of this study are tabulated in Appendix III and are shown in Figs. 4.5 - 4.24 in this chapter. In addition, the triaxial consolidation results at the end of the drained portion of the tests are summarized in Table 4. The axial strains, ε_1, and the volumetric strains, ε_v, for the drained portion of the tests were

calculated using the original sample dimensions, and the recorded drainage burette and axial dial gauge readings. Graphs of σ_1' vs ε_1 and $(\sigma_1-\sigma_3)$ vs ε_1 are given in Figs. 4.5 - 4.8a and Figs. 4.9a - 4.12 respectively. Graphs of σ'_{oct} vs ε_v are shown in Fig. 4.8b and Figs. 4.13 - 4.16. σ_3' vs ε_3 plots are presented in Fig. 4.9b and Figs. 4.17 - 4.19. Finally, graphs of strain energy* per unit volume (W) versus Length of Stress Vector (LSSV)† are shown in Figs. 4.20 - 4.26. These will be presented in more detail in Section 4.4.2.2.

The stress paths chosen for the present study can be divided generally into the following categories:

1. T302, T314 (Figs. 4.5, 4.9a, 4.13, 4.17 and 4.20)
   - "Isotropic" effective stress path. However, a small 2 kPa excess axial stress was used to ensure constant contact between the piston and the sample, so that the height changes of the sample could be monitored at all times.
2. T303 (Figs. 4.5, 4.9a, 4.13, 4.17 and 4.21)
   - Stress path of increasing effective octahedral normal stress and constant shear stress of $p_o'\ (1-K_o)$.
3. T304, T315 (Figs. 4.8, 4.9 and 4.24)
   - Stress path of constant effective octahedral normal stress of $p_o'\ (\frac{1 + 2K_o}{3})$ and increasing shear stress.

---

*At a late stage in preparing this thesis it was realized that the units of W - the strain energy per unit volume - should be written as kilo Joules per cubic metre, kJ/m^3. The numerical values do not change.

†See Section 4.4.2.1.

4. T305, T316 (Figs. 4.8, 4.9 and 4.24)
   - Stress path of decreasing effective octahedral normal stress and increasing shear stress.
5. T307, T309 (Figs. 4.5, 4.6, 4.10, 4.14, 4.17, 4.18 and 4.21)
   - Stress path of increasing both effective octahedral normal stress and shear stress.
6. T308, T311, T312, T313 (Figs. 4.6, 4.7, 4.11, 4.12, 4.15, 4.16, 4.18, 4.19, 4.22 and 4.23)
   - Approximate K_o - consolidation.
7. T317 (Fig. 4.26 and Fig. 5.7a)
   - Anisotropically consolidated strain-controlled drained stress path.
8. T306, T310, T318, T319 (Figs. 4.25, 5.3, 5.4 and 5.7b)
   - Anisotropically consolidated strain-controlled undrained stress path.

It should perhaps be explained here why test T301 was deleted from the test program. Test T301 was trimmed from a block sample unused in the previous study by Noonan (1980). The sample was from the blue clay layer, but from a different depth than the present test series. The author used T301 to practice trimming, building-in, and testing techniques before the actual test program was started.

The stress increments along each drained stress-controlled stress path were equal in magnitude, and were initially chosen to give 4 to 6 stress points between the in-situ stress level and the limit-state level predicted on the basis of the yield envelopes determined

by Noonan (1980) (see Fig. 4.1). The stress increments along the stress paths for T302 and T303 were chosen on this basis, but it was realized almost immediately that they were too large for the clay used in the present study (see Fig. 4.2). This will be discussed in more detail in Section 4.4.2.2. Subsequently, the stress increments for all remaining stress paths were chosen on the basis of 4-6 stress increments before reaching the yield envelope determined by Baracos et al. (1980) (see Fig. 4.1).

Some anxiety developed in the earlier work of Noonan (1980) as to whether complete dissipation of excess porewater pressures (i.e. consolidation) was occurring in 24-hour period following the application of each new stress increment. Noonan (1980) showed that at high stresses, and load increments less than 1.4, there was a reduced tendency for the rate of volume change to decrease when plotted against log(time). (See Noonan, 1980 Fig. 3.11). This is contrary to the traditional 'S-shape' curve which is predicted by Terzaghi consolidation theory when a sample has consolidated fully under a load increment. He further speculated with reference to earlier work on the effects of load duration and load increment ratio in one-dimensional consolidation (Lo, 1961; Leonards et al., 1964), that pore pressure generation and dissipation would not follow standard Terzaghi consolidation theory in his tests because of the small load increment ratios applied. As a consequence the volume change versus log time plot would not give any indication of the end of the consolidation period, and there was no way of differentiating between end of consolidation period and the beginning of creep. Based on their test results, Tavenas et al. (1978b)

confirmed that the relative importance of primary consolidation was greatly diminished, and the observed behaviour was essentially representative of secondary consolidation or creep, when the stress increment ratios were less than 1.3.

Previous investigators (for example Graham, 1974; Crooks and Graham, 1976; Tavenas et al., 1978b) have used the standard 24-hour load duration successfully in defining yield envelopes. The assumption inherent in their work is that the majority of the strains occurring in the first 24 hours are due to creep (not consolidation) and that the majority of these movements occur during this 24-hour period. In view of Noonan's work (1980), it was decided that the present study would follow the standard methodology used by Baracos et al. (1980) and others, (for example Graham, 1974; Crooks and Graham, 1976; Tavenas et al., 1978b) where a standard 24-hour load duration was applied.

Test T317 was restressed to in-situ stress levels and sheared under drained conditions at an initial strain rate of about 1%/day. Tests T306 and T319 were consolidated to approximate in-situ stresses and then put directly into undrained shear in order to obtain information on the undrained behaviour of the clay in-situ. Tests T310 and T318 were respectively consolidated anisotropically to high stresses past yield; and to low stresses before yield, and were then sheared to failure under undrained conditions. They provided additional stress-strain information for the clay during undrained shearing. The undrained stress-strain results for this study will be presented in detail in Chapter 5.

4.3 ONE-DIMENSIONAL CONSOLIDATION

In addition to the triaxial compression tests, four oedometer tests were carried out using 63 mm and 76 mm diameter samples to confirm the preconsolidation pressure for the blue clay at this depth. The results of these tests are summarized in Table 2. The graphs of e vs log σ'_v and e vs σ'_v are shown in Fig. 4.3 and Fig. 4.4 respectively. More importantly, the preconsolidation pressures from these tests are used for 'normalizing' the behaviour of samples from different depths (Graham, 1974; Mesri, 1975; Crooks and Graham, 1976). This section reports only the results of the oedometer tests.

Samples were trimmed from the same block samples used in the triaxial compression portion of the testing program and were designated by C301 to C304. All samples were prepared such that the compressibility of the clay in the direction of the in-situ effective vertical stress was measured. Trimming and testing procedures were described in Chapter 3.

Fig. 4.3 shows the e vs log σ'_v curves for all four tests. They showed quite clear changes in slope at the apparent preconsolidation pressures p'_c. At p'_c the soil structure began to break down or yield, and the compressibility and axial strain rates of the soil increased significantly. "Virgin" sections of the consolidation curves were very steep, with compression index values C_c ranging from 0.94 to 1.10. These C_c values are listed in Table 2 and are similar to earlier values presented by Baracos et al. (1980). Other consolidation parameters such as c_v, m_v, a_v and k have not been calculated for these tests because they are not fundamental to this thesis study. They are

all pressure-dependent parameters, and therefore not fundamental soil properties.

The values of p'_c were determined using the Casagrande construction. Points of minimum radius of curvature were difficult to locate due to the roundness of the e vs log σ'_v curves. In addition, the virgin consolidation lines were slightly concave upwards, and cause some difficulty in estimating the values of p'_c. The p'_c-values are tabulated in Table 2.

In view of the difficulty of locating the point of minimum radius of curvature and determining p'_c using Casagrande construction, graphs of e vs σ'_v were plotted for all four oedometer tests (Fig. 4.4). Values of p'_c are listed in Table 2, and are similar to values obtained from the e vs log σ'_v plots. Further attention has been paid to curve-fitting and interpretation of data like those shown in Figs. 4.3 - 4.4 in a Technical Note currently in preparation for submission to the Canadian Geotechnical Journal by Graham, Pinkney, Lew and Trainor (1981), (Appendix V).

All the graphs of e vs σ'_v (Fig. 4.4) revealed an initial straight section of low compressibility of the clay which changed to a higher compressibility at p'_c. At high pressures, strain-hardening behaviour was observed which might explain the upwards concavity of the virgin consolidation lines in the e vs log σ'_v plots. Yielding in this case was defined by the intersection of the bi-linear plot which joined the initial linear behaviour of the clay to the more compressible behaviour after yield. The p'_c break is usually better defined by the e vs σ'_v curves in Fig. 4.4 than by the e vs log σ'_v curves in Fig. 4.3.

The rounded curve in Fig. 4.3 for test T303 is possibly an indication of sample disturbance. It is further noted that the sample thickness for this test was less than 15 mm. This is usually considered inadequate for high quality research testing (Leonards and Girault, 1961). As a consequence, the value of p_c' obtained from test C301 will not be used for normalizing purposes which will be discussed later in this thesis.

To improve the quality of the oedometer test results, 76 mm diameter consolidation rings and caps were specially made for this study. Test C303 and C304 were performed on 76 mm diameter samples. Samples were prepared using improved trimming technique (see Section 3.3.1.2) and trimmed to at least 19 mm in thickness. The e vs log σ_v' curves are shown in Fig. 4.3 and the results are tabulated in Table 2. It is considered that the test results were improved significantly by these improved techniques. The curves are less rounded, and a more distinct p_c' break can be observed. The p_c' values were 250 kPa and 245 kPa for tests C303 and C304 respectively. The corresponding compression indexes were 1.10 and 1.05.

From the test curves of e vs σ_v' and e vs log σ_v', the average value of p_c' determined from tests C302, C303 and C304 is 218 kPa. This average value will be used in Chapter 6 for normalizing test results.

4.4 TRIAXIAL CONSOLIDATION

4.4.1 Reconsolidation to In-Situ Stresses

The limit-state envelope of a clay is controlled by the in-situ grain structure of a soil and by its post-depositional stress

history. In order to examine the field behaviour of a soil, careful laboratory reconsolidation to its approximate in-situ stresses is mandatory (Graham, 1974; and Crooks and Graham, 1976). Stressing to higher stresses changes the measured properties of the clay in a significant way. The problem of determining the in-situ effective stresses of clays in the Winnipeg area was discussed in Chapter 3. For the samples in this study they were estimated to range from 116.9 kPa to 118.5 kPa. On the basis of the previous test program (Baracos et al., 1980), a ratio of horizontal to vertical effective stress during restressing was taken as 0.65. The estimated in-situ stresses were applied in three equal increments, with at least 24 hours between increments.

The stress-strain results of reconsolidating the samples to the estimated in-situ stresses are tabulated in Table 3. For samples T303 to T313, the axial strains at in-situ stress levels were less than 2.5% with the exception of T303, T306 and T307 where the axial strains were 2.98%, 3.32% and 2.71% respectively. The corresponding lateral strains on restressing ranged from 0.22% to 0.66%. These were samples taken from borehole 4 in July, 1980.

The strains on restressing to in-situ stress levels were much smaller for the fresher, second series of samples, T315 to T319 which were taken from borehole 5 in January, 1981. The axial strains to in-situ stresses ranged from 1.39% to 1.75%. The lateral strains to in-situ stresses were varied from 0.06% to 0.28%.

The amount of straining which occurs during restressing is in part a measure of the amount of sample disturbance. Crooks (1973)

stated that axial strains below 2% at p_o' result when a small degree of disturbance occurs during sample preparation. He worked with less plastic clays than the Winnipeg clays in this study. With regards to this statement, the axial strain of about 2.5% to p_o' for samples T303 to T313 are not very good. On the other hand, the axial strain of less than 1.75% to p_o' for samples T315 to T319 may be the result of the relatively short storage time prior to testing. In general, it should be noted that the axial strains to p_o' are influenced by the stress ratio used during restressing, and by changes in the clay during storage.

4.4.2 Drained Compression Results

4.4.2.1 Criteria for Defining Yield Stresses

In order to examine the applicability of the limit-state concept to the Lake Agassiz clays, reconsolidated samples were tested under drained stress-controlled conditions along various stress paths. The proposed and actual effective stress paths for this testing program are shown in Fig. 4.1 and Fig. 4.2 respectively. The development of stresses and strains during each test is summarized in tabular form in Appendix III. Limit-state conditions were examined using a variety of stress-strain relationships for a bi-linear behaviour which could be used to distinguish pre-limit-state from post-limit-state behaviour. Stress-strain curves for these tests are presented in Fig. 4.5 to Fig. 4.19.

In previous studies (Graham, 1974; Crooks and Graham, 1976; Tavenas et al., 1977; Baracos et al., 1980 and Noonan, 1980), yield

or limit-state stresses were identified by stress-strain criteria which depended on the stress path of the test. Clearly for example, no yield stress can be obtained from a plot of $(\sigma_1 - \sigma_3)$ versus ε_1 for a test carried out at constant shear stress, or from a plot of σ'_{oct} versus ε_v from a test at constant octahedral normal stress. Yield stresses have had to be defined in a number of ways depending on the stress paths in question. In general they have been taken as the intersection of straight approximations of the initial stiff section and to the subsequent more flexible response to applied loading. Baracos et al. (1980) and Noonan (1980) showed that limit-state in tests involving generally increasing shear stresses can be most easily defined by plotting σ'_1 versus ε_1, whereas tests with increasing cell pressures required graphs of σ'_3 versus ε_3, or σ'_{oct} versus ε_v. However, in the case of a stress path between these two extremes, no unique stress-strain criterion is best for defining the yield stresses.

In addition to using stress-strain plots to identify limit-state, and following an earlier suggestion by Graham (1974), Tavenas et al. (1979) showed that the scalar, 'strain energy absorbed per unit volume', plotted against octahedral normal stress can provide a useful limit-state criterion, which is applicable to all stress paths, except those at constant σ'_{oct}. Assuming a linear stress-strain relationship between any two stress increments along a stress path, the total strain energy absorbed per unit volume from in-situ stress levels to the end of each stress state is given by:

$$W = \Sigma \left(\left(\frac{\sigma'_{1(j+1)} + \sigma'_{1(j)}}{2} \right) \left(\varepsilon_{1(j+1)} - \varepsilon_{1(j)} \right) + 2 \left(\frac{\sigma'_{3(j+1)} + \sigma'_{3(j)}}{2} \right) \right.$$

$$\left. x \left(\varepsilon_{3(j+1)} - \varepsilon_{3(j)} \right) \right) \qquad j = 1, M$$

By plotting the strain energy absorbed per unit volume, W, against effective octahedral normal stress, all components of the strain tensor were combined into a single limit-state criterion. Noonan (1980) introduced a more fundamental stress term called σ'_{scalar} instead of using σ'_{oct} (as suggested by Tavenas et al., 1979), because there are stress paths along which σ'_{oct} is constant. Along these stress paths a plot of W versus σ'_{oct} does not provide a useful limit-state criterion. σ'_{scalar}' is found by summing the changes in σ'_{scalar} between successive stress levels. The value of σ'_{scalar} at any stress level is the length of the stress path on a plot of (q/2) versus p'. The change in σ'_{scalar} between two stress levels is given by:

$$\Delta\sigma'_{scalar} = \left((\Delta p')^2 + \Delta (q/2)^2 \right)^{1/2}$$

It is noted that the σ'_{scalar} term is not a true 'scalar' quantity in stress space. The term is used by Noonan (1980) to identify an empirical parameter which has proved useful in defining limit-state.

It is for this reason that the author, following the idea of Crooks (1980), substituted for Noonan's σ'_{scalar} an even more fundamental scalar quantity, 'LSSV' that is the Length of Stress Vector. LSSV is the length of the stress vector in (p', q) stress space, from in-situ

stress levels to each successive stress state in turn. It is calculated from the expression:

$$LSSV = \left(\left(\sigma'_{1(j)} - p'_o \right)^2 + \left(\sigma'_{3(j)} - K_o \, p'_o \right)^2 \right)^{1/2}$$

$$j = 1, N$$

Results have indicated that the W vs LSSV plot is applicable to all stress paths. Graphs of W vs LSSV are presented in Figs. 4.20 - 4.26. Values of W and LSSV are tabulated in Appendix III. In addition, the author has used strain energy plotted against LSNV (i.e. the Length of Strain Vector defined in the same way as LSSV), to determine limit-state. Preliminary results showed that plots of W vs LSNV are not useful. The values of LSNV and the algorithm for calculating it are presented in Appendixes III and IV respectively.

A simple computer program called Energy Calculation Program was developed by the author to calculate the strain energy absorbed by a triaxial clay sample during drained triaxial testing or undrained shear; and the Length of Stress Vector (LSSV). Results are printed in well-organized, tabular form. Details of the program and instruction notes are given by Lew (1981), and are included in this thesis as Appendix IV.

The remaining sections of Chapter 4 examine the stress-strain data for each test in turn to determine their limit-state stresses.

4.4.2.2 Stress-Strain Results

In the course of examining and defining the limit-state for each stress path shown in Fig. 4.2, yield points were identified where possible using the following plots:

1. σ_1' vs ε_1
2. $(\sigma_1-\sigma_3)$ vs ε_1
3. σ'_{oct} vs ε_v
4. σ_3' vs ε_3
5. W vs LSSV

Yield points are shown on each graph (Figs. 4.5 - 4.26) and the yield stresses defined from the various plots are summarized in Table 5. The results for the yield stress from the various plots have been presented in Table 5 as the interpolated σ'_{oct}. The range of possible yield stress along each stress path is illustrated in Fig. 4.27.

As was pointed out earlier in Section 4.2, the stress increments used along stress paths T302 and T303 (Fig. 4.2), predicted on the basis of the yield envelope determined by Noonan (1980), were too large for the clay used in the present study. Trainor (1981) has performed oedometer tests using samples from the same depth as Noonan (1980), namely 8-10 m. His tests show an average p_c' value of about 400 kPa. However, for the present study at 11.5 m depth, the average p_c' value for the clay is only 218 kPa (Table 2). If the position of yield envelope in stress space is governed by the magnitude of preconsolidation pressure as implied by the YLIGHT model (Tavenas and Leroueil, 1977), the yield envelope for the clay in the present study should be

situated closer to the in-situ stress levels in stress space, but homothetic to the yield envelope determined by Noonan (1980) (Fig. 4.1). For this reason, it was decided that the stress increments for all remaining stress paths would be chosen on the basis of the yield envelope determined by Baracos et al. (1980) (see Fig. 4.1).

Tests T302 and T314 followed the isotropic stress path (Fig. 4.2), with a constant shear stress of about 2 kPa to ensure contact between the piston and the sample during the test, so that height changes of the sample could be monitored. These isotropic stress paths were designed to examine the limit-state during isotropic consolidation. The yield stress along the isotropic stress path is termed $(p'_c)_{iso}$ (Tavenas and Leroueil, 1977).

To determine the limit-state condition along T302 and T314, all of the various available yield criteria were examined. In this case, a plot of $(\sigma_1-\sigma_3)$ vs ε_1 (Fig. 4.9a) is linear and provides no information about limit-state. However, both σ'_{oct} vs ε_v (Fig. 4.13) and σ'_3 vs ε_3 (Fig. 4.17) plots are revealing. A distinct bilinear behaviour can be identified, with the second section having a flatter slope than the first. The yield stresses are indicated on the figures, and the equivalent σ'_{oct} values at yield are given in Table 5.

A plot of σ'_1 vs ε_1 for these two tests (Fig. 4.5) can be interpreted in a bilinear manner, but the yield stresses are not well defined. In contrast, the graphs W vs LSSV (Fig. 4.20) show a clear bi-linear behaviour which can be identified as yield. The range of possible yield stresses along the stress path is shown in Fig. 4.27. It should be pointed out specifically for tests T302 and T314 that the

strain energy and LSSV are calculated starting from zero stresses. This is different from the procedure for samples that have been restressed to in-situ stress levels (Appendix IV).

Test T303 followed a stress path of almost constant principal stress difference of about 41 kPa after being restressed to the in-situ stress levels. For this reason, the plot of $(\sigma_1-\sigma_3)$ vs ε_1 (Fig. 4.9a) is linear and not useful. In this test, graphs of σ_1 vs ε_1 (Fig. 4.5), σ'_{oct} vs ε_v (Fig. 4.13), σ'_3 vs ε_3 (Fig. 4.17) and W vs LSSV (Fig. 4.21) indicate a distinct bilinear behaviour where yield stresses are well defined (Fig. 4.27).

The stress paths followed by samples T304, T305, T315 and T316 are shown in Fig. 4.2. Samples T304 and T315 were consolidated anisotropically to the in-situ stress levels and sheared at constant octahedral normal stress of about 91 kPa. A 5-day loading duration was used for T315, instead of the standard 24-hour interval used for most tests. Tests T305 and T316 had stress paths of decreasing octahedral normal stress and increasing principal stress difference. Graphs of σ'_1 vs ε_1, σ'_{oct} vs ε_v, σ'_3 vs ε_3, $(\sigma_1-\sigma_3)$ vs ε_1 and W vs LSSV are presented in Fig. 4.8, Fig. 4.9 and Fig. 4.24. All these samples failed abruptly in drained shear. The interpretation of limit-state for these tests is difficult and requires a careful examination of strain rate effects along these stress paths. This will be discussed in more detail in Chapter 6. However, using $(\sigma_1-\sigma_3)$ vs ε_1 plots, the author has proposed ranges of possible yield stresses in terms of $(\sigma_1-\sigma_3)$ as shown in Fig. 4.9a and Fig. 4.27.

Fig. 4.2 shows that tests T307 and T309 followed a stress

path in (p', q) stress space which has both effective octahedral normal stress and principal stress difference increasing. Sample T307 failed abruptly after the application of the 7th stress increment, whereas, sample T309 was still stable at the end of consolidation. Stress-strain plots and graphs of W vs LSSV are given in Figs. 4.5 - 4.6, Fig. 4.10, Fig. 4.14, Figs. 4.17 - 4.18 and Fig. 4.21. Distinct bilinear behaviour which is defined as yielding in this thesis can be observed on each of the stress-strain and W vs LSSV plots.

Samples T308, T311, T312 and T313 were tested along the approximate K_o - consolidation line given by $\sigma_1'/\sigma_3' = 0.65$. T312 was a 5-day duration test with about 4 stress increments before yield, whereas, T313 is a 24-hour duration test with about 12 stress increments to yield. On the other hand, T308 and T311 were standard 24-hour tests with about 4 stress increments to yield. Together with T304 and T315, these tests were designed to examine the effect of load duration and load increment ratio on yielding. The test results will be examined with reference to the YLIGHT model in Chapter 6.

Figs. 4.6 - 4.7 show the plots of σ_1' vs ε_1, for these tests. Limit-state is easily defined by the intersection of two straight sections of the test results. For T308 and T311, strain hardening behaviour was observed after axial strains of about 14%. This type of behaviour has been noted in the previous study by Baracos et al. (1980) and Noonan (1980). Graphs of $(\sigma_1-\sigma_3)$ vs ε_1, σ'_{oct} vs ε_v, and W vs LSSV are shown in Figs. 4.11 - 4.12, Figs. 4.15 - 4.16 and Figs. 4.22 - 4.23 respectively. Distinct bilinear behaviour is observed on each plot, followed by strain hardening behaviour at large strains.

Figs. 4.18 and 4.19 show the plot of σ_3' vs ε_3 for T308, T311, T312 and T313. The relationship between σ_3' and ε_3 does not indicate the usual bilinear behaviour for most samples, but it does show that the samples had yielded. These samples compressed laterally as they were loaded up to a certain pressure, and then changed to lateral expansion (or dilation) behaviour at higher pressure. Stresses at which the behaviour changed from compression to expansion (i.e. point of constant radial strain, ε_3) were taken as limit-states.

Sample T317 was restressed to in-situ stress levels and then sheared at about 1%/day under drained condition. Tests T306, T310, T318 and T319 were consolidated strain-controlled undrained shear tests. The stress-strain results of these tests will be presented in detail in Chapter 5. Plots of W vs LSSV for T306, T317 and T319 are shown in Figs. 4.25 and 4.26.

On the basis of the limit-state stresses defined using various yield criteria (Table 5) for this test program, it has been possible to propose a 1-day yield envelope for the blue clay at 11.5 m depth. This envelope is shown in Fig. 4.27. This yield envelope is slightly different in shape from those identified by Baracos et al. (1980) and Noonan (1980) as shown in Fig. 4.1, but remains fairly symmetrical about the K_o - consolidation line. The number of tests performed, and the relatively small scatter in the results, suggest that this is the best-defined envelope which has been identified to date in the Winnipeg clay.

The section of the yield envelope in the overconsolidated region is difficult to define and requires the examination of the effect of strain rate along the stress path. On the other hand, the yield

envelope is well defined for stress paths with increasing effective octahedral normal stress σ'_{oct} in the normally consolidated region. Details of the yield envelope will be further discussed in Chapter 6. The results of the undrained portion of the triaxial tests are described in the following chapter.

CHAPTER 5

RESULTS OF UNDRAINED SHEAR TESTS

5.1 INTRODUCTION

Samples which had not failed during the drained stress-controlled portion of the test were transferred to a 10 t strain-controlled compression frame for undrained shearing to rupture (Fig. 3.6). To ensure that the samples were fully saturated prior to shearing, a back-pressure, usually in the order of 210 kPa, was applied in the manner described in Chapter 3. Values of porewater pressure parameter B are tabulated in Table 6 for each test. Normalized undrained stress-strain curves are presented in Figs. 5.1 - 5.7b. A summary of the undrained test results is given in Table 6.

Undrained shear tests provided information on several aspects of the soil's behaviour during shearing under undrained conditions. They allowed the examination of stress-strain and porewater pressure generation characteristics of each sample. These include the porewater pressure parameter, A_f, the strain-rate parameter, $\rho_{0.1}$, and the elastic modulus, E_{50}. In addition, the undrained shear results permitted an evaluation of the normally consolidated Coulomb-Mohr rupture envelope for the blue clay (Fig. 5.8). The failure stresses from the undrained tests on the overconsolidated samples (T306, T318 and T319) were used, in conjunction with the results from the drained stress-controlled tests, to identify the yield envelope in the overconsolidated region (Fig. 4.27).

The following section will present the undrained results in more detail. A discussion of the results is given in Chapter 6.

5.2 UNDRAINED SHEARING RESULTS

5.2.1 Stress-Strain Relationship

The stress-strain conditions for each sample prior to undrained shearing are summarized in Table 4. Graphs of $(\sigma_1-\sigma_3)/2\sigma'_{1c}$, σ'_1/σ'_3 and $\Delta u/\sigma'_{1c}$ versus ε_1 are shown in Figs. 5.1 - 5.7b. The effective stress paths in (p', q) stress space are shown in Fig. 5.8 for each test and the complete shear test results are summarized in Table 6. For tests T302, T303 and T310, the stress-strain curves (Figs. 5.1 - 5.3) appear broken and stepped. This is due to experimental procedures used to investigate the strain-rate effect. This will be reported in Section 5.2.5.

For those samples (T306, T319) in which the field structure had been essentially preserved by anisotropic consolidation to the in-situ stresses, i.e. CAU*, $\sigma'_{1c}/p'_o \simeq 1$, the maximum deviator stress was attained at low axial strains. Values of $(\sigma'_1-\sigma_3)_{max}$ for T306 and T319 are 77.8 kPa and 107.7 kPa respectively. Crooks (1973) demonstrated that the amount of straining which occurs during restressing is in part a measure of the amount of sample disturbance, and axial strains below 2% at p'_o result when a small degree of disturbance occurs during

---

*The following abbreviations are used in the thesis: C = Consolidated, A = Anisotropic, I = Isotropic, D = Drained, U = Undrained.

sample preparation. With regard to this, it should be pointed out that a axial strain of 3.32% (see Table 3) to p_o' for sample T306 is not good, and possibly an indication of more disturbance than normal during preparation. In contrast, the axial strain to p_o' for sample T319 is only 1.39%. Fig. 5.4 shows the stress-strain behaviour during undrained shearing for samples T306 and T319. The stress-strain curve of T319 rises quickly to the maximum deviator stress, drops abruptly after reaching this peak, and eventually levels off at higher strains. On the other hand, the stress-strain curve for T306 is more rounded. T306 and T319 reached the maximum deviator stress at axial strains of 2.82% and 1.6% respectively, while the maximum stress ratio occurred at 2.82% and 1.33% axial strain.

Samples consolidated below the in-situ stresses also reached the peak deviator stress at small strain. Fig. 5.7b shows the stress-strain behaviour of sample T318 which had been anisotropically consolidated to low stresses (Fig. 4.2). Both the maximum deviator stress and the maximum stress ratio occurred at axial strains less than 1.75%.

Samples T308, T309 and T311 were anisotropically consolidated well past limit-state stresses before being put into undrained shearing. The stress-strain behaviour of these samples is shown in Fig. 5.5. The deviator stress rises quickly to a peak value, and then gradually decreases with increasing axial strain. The in-situ grain structure of these samples is completely modified in CAU tests with $\sigma_{1c}'/p_c' > 1$, and the resulting laboratory-formed structure is without the reserve resistance developed during overconsolidation in the field. As a result, $((\sigma_1-\sigma_3)/2\sigma_{1c}')_{max}$ is reduced below the corresponding value from

CAU tests with $\sigma'_{1c}/p'_o \simeq 1$, (Table 6). However, the stress-strain behaviour of these normally consolidated samples is more brittle, with axial strains lower than 0.57% at maximum deviator stress (Fig. 5.5) with the exception of T309 where maximum deviator stress occurs at 1.88%. The maximum stress ratio occurs at axial strains of 6.39%, 3.91% and 6.91% for samples T308, T309 and T311 respectively.

Fig. 5.6 shows the stress-strain behaviour of sample T314 which is isotropically consolidated to high stresses. In this test, the deviator stress rises gradually to the maximum value at which point it remains relatively constant for the rest of the test. Sample T314 reached the maximum deviator stress and the maximum stress ratio at an axial strain of 9.13% and 12.77% respectively. It can be seen that CAU samples (Figs. 5.4 - 5.5) have lower strains to maximum deviator stress than the CIU sample (Fig. 5.6). This is due to different consolidation histories.

Finally, Fig. 5.7a shows the stress-strain curve of test T317 which is a strain-controlled CAD test. The maximum deviator stress and the maximum stress ratio occur simultaneously at 3.37% axial strain.

5.2.2 Effective Stress Paths

The effect of consolidation history on undrained shearing behaviour is shown clearly by the effective stress paths during shearing. Fig. 5.8 shows the effective stress paths plotted in terms of stress parameters, $(\sigma_1-\sigma_3)$ and $(\sigma'_1+2\sigma'_3)/3$ for all undrained shear samples (Figs. 5.1 - 5.7b). Porewater pressures generated during the

initial stages of shearing in CAU samples with $\sigma'_{1c}/p'_c > 1$, are substantially linear with respect to changes in total octahedral normal stress (see Section 5.2.3 Fig. 5.12a). As a result the effective stress paths are almost linear up to a large percentage of the maximum shear stress. After this point shear strains begin to have a significant influence on the porewater pressures and the stress paths move sharply to the left. For CIU samples, the effective stress paths curve to the left from the outset because of higher porewater pressures resulting from the structural changes during reconsolidation. It is noted that sample T303 behaves more like an isotropically consolidated sample, although it has been restressed to in-situ stress levels. This is possibly because sample T303 followed a stress path (Fig. 4.1) of increasing octahedral normal stress at a constant principal stress difference, which tends to produce a more isotropic structure.

The influence of overconsolidation is clearly demonstrated by the effective stress paths of the CAU tests with $\sigma'_{1c}/p'_o \leq 1$, namely T318 and T319 (Fig. 5.8). The initial sections of these stress paths are almost straight and cross the Coulomb-Mohr rupture envelope. Because the porewater pressure decreases slightly after about 75% of the shear strength has been applied, the stress paths curve to the right before reaching the maximum shear stress. After reaching this peak stress, the samples tend to dilate on further straining. This is accompanied by a decrease in porewater pressure, and the shear stress drops abruptly, drawing the effective stress paths vertically downward. The non-typical behaviour of sample T306 is thought to be due to sample disturbance (see Section 5.2.1).

Using the undrained shear strengths of this test program (Table 6) and the previous information from Noonan (1980), a normally consolidated Coulomb-Mohr envelope for the blue clay has been identified. Fig. 5.8 shows the failure envelope predicted on the basis of $(\sigma_1-\sigma_3)/2_{max}$ criterion. The correlation coefficient of this line is 0.996. During the process of linear regression, five assumed data points (0, 0) and an additional five data points (0, 5) in (p', q) space were used along with other measured undrained shear strengths to ensure that the effective cohesion intercept lay between zero and 5 kPa. The effective angle of shearing resistance determined from this line is 17.5^{o} and the effective cohesion intercept is 4 kPa. This compares with a ϕ' value of approximately 20^{o} and an effective cohesion intercept of 2 kPa for the 76 mm diameter samples in previous study by Baracos et al. (1980).

5.2.3 Porewater Pressure Generation

The study of porewater pressure generation as a result of loading is important because effective stress analyses require a knowledge of pore pressures before an estimate of the stability of earth structures such as embankments can be made.

The relationship between $\Delta u/\sigma'_{1c}$ and ε_1 for all the undrained shear samples is given in Figs. 5.1 - 5.7b. Porewater pressures during undrained shearing (Figs. 5.1 - 5.3 and Figs. 5.5 - 5.6), rose quickly during the period up to the maximum deviator stress after which they rose more slowly. Porewater pressures in the overconsolidated samples, with $\sigma'_{1c}/p'_o \leq 1$, tended to fall off after reaching the $\{(\sigma_1-\sigma_3)/2\sigma'_{1c}\}_{max}$ (see Figs. 5.4 and 5.7b), with the exception of T306. Changes in strain-

rate are seen to influence the porewater pressures (Figs. 5.1 - 5.3), but only in a minor way.

The porewater pressure parameter $A = \Delta u/\Delta(\sigma_1-\sigma_3)$ (Skempton, 1954), designated 'A_f' for failure conditions, is often used in practice. Values of A_f for the undrained tests are tabulated in Table 6. Fig. 5.9 and Fig. 5.10 show the relationship of A_f plotted against $(1/\sigma'_{1c})$ (see Baracos et al., 1980) and overconsolidation ratio respectively. The values of A_f for overconsolidated samples range between 0.22 and 0.67. For normally consolidated CAU samples and CIU samples, the values of A_f range from 0.7 to 1.13 and 1.16 to 1.59 respectively. The value of the A_f parameter depends to a large extent on the stress history of the soil and particularly on the degree of overconsolidation. These results will be further discussed in the following chapter.

The previous study by Baracos et al. (1980) revealed that a linear relationship exists between the change in porewater pressure and the change in total octahedral normal stress in the initial stages of testing. Figs. 5.11 - 5.12 show the normalized values of $\Delta u/\sigma'_{1c}$ versus $\Delta\sigma_{oct}/\sigma'_{1c}$ for all undrained strain-controlled tests. For overconsolidated samples (i.e. $\sigma'_{1c}/p'_o \leq 1$) where the in-situ grain structure is essentially preserved, the relationship is approximately linear up to a high percentage of the maximum shear stress. The gradients of the linear section, m, are summarized in Table 6 and are in the range 1.27 - 1.92. Thereafter the porewater pressures are more significantly affected by yielding of the grain structure and the relationship becomes distinctly non-linear. The same behaviour

is observed in normally consolidated CAU samples, $\sigma'_{1c}/p'_c > 1$, except that the slopes of the linear relationships are greater than those obtained from overconsolidated samples. In both cases, the initial response in porewater pressure changes, Δu, is greater than the changes in total octahedral normal stress. This contrasts with the previously observed behaviour by Graham (1969, 1974) in lightly overconsolidated sensitive clays where overconsolidation resulted in porewater pressure changes less than the changes in total octahedral normal stress. This once again reflects the highly compressible nature of the Winnipeg clay. Once the structure of the clay begins to respond nonlinearly, however, the behaviour is very different in the two cases. Overconsolidated samples produce strongly decreasing porewater pressures, whereas normally consolidated samples give increasing porewater pressures.

For CIU samples (Fig. 5.12b), the relationship of $\Delta u/\sigma'_{1c}$ versus $\Delta\sigma_{oct}/\sigma'_{1c}$ is curvilinear and the porewater pressures are considerably higher than in CAU tests. Note that the scales are significantly different in Figs. 5.12a and 5.12b.

The cause of the non-typical behaviour in sample T306 (Fig. 5.11) is unknown. The axial strain to p'_o is 3.32% which is considered high (Crooks, 1973). It should be pointed out that a slickenside surface was observed in this sample. The clay for this study is highly anisotropic and heterogeneous with many silt-sized inclusions. Fig. 5.13 shows a typical example of the samples used.

5.2.4 'Elastic' Parameters

The use of finite element analysis for predicting stresses and deformation prior to local failure requires the measurement of elastic or 'pseudo-elastic' parameters in laboratory testing programs. In the present study, the non-linearity of the $(\sigma_1-\sigma_3)$ vs ε_1 curves from triaxial compression tests has been approximated by a secant modulus E_{50} from the end of consolidation to 50% of the reserve resistance (Graham, 1974). Values of E_{50} have been normalized by dividing by the undrained strength $s_u = (\sigma_1-\sigma_3)/2_{max}$ to give what is known as the relative stiffness, E_{50}/s_u. Table 6 summarizes all values of E_{50} and E_{50}/s_u. The results vary considerably with test type, and show significant scatter.

Fig. 5.14 shows a plot of relative stiffness versus over-consolidation ratio (OCR) for the undrained tests. No clear relationship is observed, but a general conclusion can be drawn that values from CAU samples are generally somewhat higher than the corresponding values from CIU samples. Relative stiffness ranges from 183 - 361 MPa for CAU samples and between 168 - 251 MPa for CIU samples.

5.2.5 Strain Rate Effect

Bjerrum, Clausen and Duncan (1972) have drawn attention to the large variations in undrained shear strength $(\sigma_1-\sigma_3)/2_{max}$ which accompany changes in straining rate during the testing of carefully sampled natural clays. Crooks and Graham (1976) demonstrated that an axial strain-rate effect is important for Belfast soft clays. In the present study, the strain-rate effect was examined by two

procedures. The first was to step-change the rate of testing periodically during the course of a single test and then piece together the resulting stress-strain curve, as shown in Fig. 5.1 - 5.3, (Richardson and Whitman, 1963). A second method was the 'relaxation' procedure described by Kenney (1966) which involves switching off the compression machine motor at a given strain, and then taking readings of stress and strain with time. When the motor is stopped the sample continues to strain at a continuously decreasing rate due to the stored energy in the proving ring. The strain-rate effect can be represented by a parameter $\rho_{0.1}$, which gives the percentage change in shearing resistance produced by a tenfold change in strain rate, referred to the shearing resistance at a strain rate of 0.1%/hour.

In this testing program, the strain-rate effect was investigated using samples T302, T303 and T310, as shown in Figs. 5.1 - 5.3. Values of $\rho_{0.1}$ along with the average axial strain during the relaxation period, ε_ρ, are given in Table 6. These values are consistently higher than values from the previous study by Noonan (1980), and range from 11% to 12.2%. One possible explanation is that the relaxation tests for the present study were performed at axial strains closer to the failure strains (that is, ε_1 at $(\sigma_1-\sigma_3)_{max}$), and therefore show higher strain-rate effects. This agrees with the earlier work by Crooks (1973) which showed that strain-rate effect decreases with increasing axial strains. The average undrained strength versus the axial strain-rate, from relaxation test data, is shown in Fig. 5.15.

The effect on the stress-strain behaviour of step-changing the strain-rate has already been indicated in Figs. 5.1 - 5.3. The

curves of $(\sigma_1-\sigma_3)/2\sigma'_{1c}$ versus axial strain have been reconstructed approximately for each strain rate and projected to the strain at which the relaxation tests were performed. Values of $(\sigma_1-\sigma_3)/2$ have been plotted against the corresponding strain-rate in Fig. 5.15. Also, values of $\rho_{0.1}$ have been calculated at different axial strains and are summarized in Table 7. From these results, two general conclusions can be drawn. The $\rho_{0.1}$ values determined by step-changing tests are approximately 11 to 12 percent, and are comparable to values obtained from the relaxation tests. Secondly, the $\rho_{0.1}$ value seems to decrease with increasing axial strains (see T310 in Table 7). Similar results have been reported by Graham (1969), and Crooks (1973).

Previous work summarized by Graham (1979) has suggested that the $\rho_{0.1}$ parameter is related to the plasticity index of a clay. The value of $\rho_{0.1}$ versus plasticity index for these tests has been plotted along with other data from Graham (1979) and is shown in Fig. 5.16. This data suggests that no simple relationship exists between $\rho_{0.1}$ and I_p.

CHAPTER 6

DISCUSSION OF RESULTS

6.1 INTRODUCTION

The previous studies by Baracos et al. (1980) and Noonan (1980) showed that the Winnipeg clays have an in-situ grain structure which governs its initial stress-strain response to applied stresses. Tentative yield envelopes were identified for clays at different depths (Fig. 6.1). The purpose of the present research was to further investigate the concept of yielding as it applies to the Winnipeg clays. In general, the test results reported in this thesis sustain the previous interpretations.

Yield envelopes have been found for a number of natural clays. With the exception of the work on Belfast estuarine clays (Crooks and Graham, 1976), most limit-state studies have been involved with sensitive and cemented clays (Mitchell, 1970; Graham, 1974; Tavenas and Leroueil, 1977), and represent the extreme examples of the effect of grain structure. Because of the low sensitivity of the Winnipeg clays, the extension of the limit-state concept to include these clays is a significant step towards verifying the concept of yielding to all natural clays.

The present study was specifically designed to examine the limit-state for the blue clay at 11.5 m depth. The yield envelope identified in this test program is shown in Fig. 4.27 and Fig. 6.1. In this chapter, results will be compared with those of the previous

studies (Baracos et al., 1980; Noonan, 1980); and examined with reference to the YLIGHT model (Tavenas and Leroueil, 1977). In addition, strain energy as a yielding criterion is also investigated.

6.2 DRAINED COMPRESSION BEHAVIOUR

6.2.1 Interpreting Yield Stresses

As described in Section 4.4.2.1, the major problem in determining the yield envelope of a clay is to establish a criterion by which the limit-state stresses can be identified. The present study has involved the acquisition and interpretation of data such as those shown in Figs. 4.5 - 4.26. Yielding along various stress paths (Fig. 4.2) was interpreted in a number of ways. In general, yield stresses have been taken as the intersection of straight approximations of the initial stiff section and to the subsequent more flexible response to applied stresses. Fig. 6.2 shows the various yield criteria for defining limit-state in Test T312 which was tested along the approximate K_o - consolidation line (Fig. 4.2). In this case, limit-state stresses were well defined in all five plots. With the exception of σ_3' vs ε_3 plot (see Section 4.4.2.2), distinct bilinear behaviour is observed in each plot. Table 5 shows that the limit-state stresses are rather similar, although there is some variation in the values found by the different criteria. Tavenas et al. (1979) suggested that the limit-state stresses defined by the various strain components are frequently not identical. Similar observations were reported by Crooks (1973).

Table 5 reveals that all five of the yield criteria were

useful in defining limit-state for stress paths which generally had increasing effective octahedral normal stress and principal stress difference. For stress paths which had σ_1' and σ_3' increasing at about the same rate, at least four of the five criteria were useful. However, the limit-state along stress paths in the overconsolidated region is more difficult to define. These include Tests T304, T305, T315 and T316 (Fig. 4.27) which failed abruptly after the application of the last stress increment. Graphs of various stress-strain relationships and W vs LSSV are presented in Figs. 4.8 - 4.9. It is thought that the magnitude of the load increments used had a considerable effect on the observed behaviour of these samples. A careful examination of the strain rates in the 5th and 6th stress increments in Test T312 (Fig. 6.3) shows clearly that the sample is in fact accelerating towards failure at the final stress level, and that the strain rate parameter, $\rho_{0.1}$, may be applicable. Fig. 6.3 shows that for the first four load increments, the axial strain rate, $\dot{\varepsilon}_1$, averaged over the 5-day loading interval was essentially constant. For the fifth increment the 5-day average strain rate (point 6) was rather higher. After the 6th increment was added the strain-rate decreased for the first two hours (points 7, 8 and 9), but then accelerated to rupture (point 10). Informal discussion with Dr. Graham suggested that the sample had in fact begun to yield at low strain rates during the fifth increment, and that the extra shearing resistance shown in the sixth increment simply reflected the influence of the strain rate parameter, $\rho_{0.1}$. It is interesting to note that if points are joined which represent in the fifth and sixth increments, the shearing resistance and strain-rate

in the same time interval after loading (for example points 1, 7; 2, 9; 3, 8), then the strength increase corresponds to an average $\rho_{0.1}$ value of about 13%. This is similar to the average value obtained from relaxation tests on strain-controlled undrained samples. It is appreciated that this discussion is speculative and is inadequately proved by the present series of tests. The author recommends further testing in the future.

Noonan (1980) used an empirical graphical bilinear curve-fitting procedure for determining yield stresses. It was subsequently the subject of some further discussion and study. The question is whether the procedure is rational, repeatable, and free from the influence of the person using it. It was suggested that the use of mini-computer and automatic curve-fitting techniques would reduce personal influences, and therefore provide more rational, repeatable results.

In view of its attractiveness for computer application, a simple bilinear curve-fitting program was developed by Pinkney (1980). Leong (1981) has investigated the potential of using this bilinear curve-fitting program to data like those shown in Figs. 4.20 - 4.26. The curve-fitting process was automatic once the basic data had been read into the computer. The program worked well with most sets of test data, and it appeared that a reliable, impersonal procedure had been developed. It was possible to proceed trustingly from the tabulated laboratory data, to a numerical prediction of yield stresses without visually examining the detailed shape of the stress-strain curve or exercising discretionary judgement. Graham et al. (1981) advise against this procedure in a Technical Note currently in

preparation for submission to the Canadian Geotechnical Journal (Appendix V). It is always necessary to be fully aware of the general shape of the stress-strain relationship which is being fitted. The present study has returned to Noonan's practice of graphical curve-fitting.

Fig. 6.4 shows a representative graph of W vs LSSV in which discretionary judgement is necessary to define the limit-state. This is test data from T313 of the present study. The data points have been shown as open circles in the initial and final linear sections, and as solid circles in the transition section. As programmed, the computer cannot exercise judgement to identify the data points on the transition section, and fits two straight lines through all the data points as shown by the dashed lines. If discretionary judgement is used then the solid points are ignored and the curve-fitting is shown by solid lines in the figure. The two estimates of the limit-state condition can be significantly different.

Finally, graphs of σ_1' vs ε_1 and W vs LSSV which have been plotted in terms of 'engineering' strain and 'natural' strain are shown in Fig. 6.5. It can be seen that the slope of the straight line section after yield (or at large strain) can be significantly different. Although all stress-strain data presented in this thesis is in terms of engineering strain, the author recognizes that plotting in terms of natural strain can be useful in some circumstances. Graham et al. (1981) show that the upward concavity of the virgin consolidation line in one-dimensional consolidation can be reduced somewhat by plotting in terms of natural strain rather than engineering strain.

6.2.2 Yield Envelopes

The range of limit-state stresses defined by various yield criteria (Table 5) were illustrated on the stress path of each test, and joined to form a yield envelope in (p', q) space (Fig. 4.27), inside which small strain behaviour applies, and outside which more compressible, larger strain conditions apply.

With regard to finding the limit-state envelope for an undisturbed natural clay (that is, the locus of yield points in a (p', q) plane at constant e), it should be pointed out that an assumption inherent in all previous work is that the in-situ voids ratio of the clay does not change significantly prior to the clay reaching the limit-state envelope corresponding to its in-situ voids ratio. If, however, voids ratio changes occur and are more significant along certain stress paths than others, the yield envelope defined by drained stress probing would be skewed to the constant e-plane limit-state envelope.

The yield envelope established in this study and the yield envelopes determined in previous studies by Baracos et al.(1980) and Noonan (1980) are shown in Fig. 6.1. Although the present yield envelope is slightly different in shape from those identified in earlier studies, the nature of this envelope may be compared with the details of the YLIGHT model described in Chapter 2. Considering the number of tests performed, and the quality of the test results, it can be argued that this is the best-defined envelope which has been identified thus far in Winnipeg clay.

The YLIGHT model proposes that the limit-state envelope of a natural clay has a shape which is approximately elliptical, and

centered on the K_o - consolidation line of the normally consolidated clay. Based on a normally consolidated, effective angle of shearing resistance, ϕ', of 17.5^o and $K_o = 0.9\ (1-\sin\phi')$ (Jaky, 1944; Tavenas et al., 1977), a K_o - consolidation line has been shown in Fig. 6.1. This yield envelope is fairly symmetrical about the K_o - consolidation line, but the shape is somewhat semi-circular rather than elliptical.

The yield envelope in this study is found to be fairly homothetic (that is, geometrically similar) to the yield envelopes at different depths that were previously defined by Baracos et al. (1980) from a preliminary test series, and by Noonan (1980) (Fig. 6.1). This tends to support the YLIGHT model which states that the limit-state envelopes at different depths are all homothetic.

The YLIGHT model also states that the position of the limit-state envelope in stress space is governed by the magnitude of the preconsolidation pressure, p'_c. In this regard, the YLIGHT model links the limit-state envelope defined by drained, triaxial stress probing, to the preconsolidation pressure defined by one-dimensional consolidation tests. According to the YLIGHT model, the p'_c line* should just intersect the K_o - consolidation line at the limit-state envelope for the clay at that depth (see Fig. 2.1). Based on the oedometer test results for this study (Table 2), the p'_c line is shown in Fig. 6.1 for an average value of p'_c of 218 kPa for the clay at 11.5 m. This p'_c line

*A line representing all the possible states of stress in (p', q) space of the oedometer sample at its preconsolidation pressure, including the extreme values of σ'_h which are possible, namely $\sigma'_h = p'_c$, and $\sigma'_h = 0$.

intersects the K_o - consolidation line slightly outside the yield envelope identified in this study. In addition, it is noted that the ratio of $(p'_{vert})_{max}$ to $(p'_c)_{iso}$ (see Fig. 2.1) is between 1.4 and 1.5. Similar results in the range 1.4 to 1.8 have been reported by Leroueil and Tavenas (1977).

An important consideration in the YLIGHT model is the influence of strain rate on the limit-state envelope. Tavenas and Leroueil (1977) were the first to recognize that the strain rate effects need to be considered in the determination of the limit-state of a natural clay. They proposed that a reduction of the rate of loading or an increase in the duration of load will lead to a reduction of not only the oedometer p'_c value, but of the entire limit-state envelope.

In this study, the effects of strain rate were investigated along various stress paths. The results are presented in Fig. 6.6. In CID tests (see T302 and T314 in Fig. 4.27), average σ'_{oct} yield stresses were 156 kPa and 150 kPa for tests taking 4 days and 8 days to yield respectively. Along the approximate K_o - consolidation line, sample T311 was tested using 1-day load duration, and a 5-day load duration was used for sample T312. A reduction of average σ'_{oct} yield stresses from 151 kPa (4 days to yield) to 144 kPa (20 days to yield) was observed. Similarly, T304 and T315 were tested using 1-day and 5-day load duration respectively. The range of possible yield stresses are shown in Fig. 6.6. Additional results on strain-rate effects were obtained by undrained, strain-controlled tests. After applying an average strain-rate correction to make the undrained results more comparable with the duration and the strain-rates in the stress-controlled

tests, (that is, $\rho_{0.1}$ = 11%), these undrained strength were plotted in Fig. 6.6. Based on these results, the displacement of the yield envelope towards reduced preconsolidation pressure and shear strength is clearly defined, and agrees with the YLIGHT model.

6.2.3 Normalized Yield Envelope

Crooks (1973, 1980) showed that the yield stresses when normalized with respect to p'_c form a unique envelope, which demonstrates the dependence of yield behaviour on overconsolidation. Because of the uncertainty regarding the variation with depth of the preconsolidation pressure p'_c, Baracos et al. (1980) had difficulty normalizing their results with p'_c from different depths in Winnipeg.

The present study has placed considerable effort on improving the techniques for oedometer testing in the University of Manitoba. The quality of the results has improved significantly (see Section 4.3). Trainor (1981) has also performed oedometer testing on samples from various depths from the site of the Physical Education Building on the University of Manitoba campus. The distribution of p'_c with depth from both test programs is shown in Fig. 6.7. This figure also includes the p'_c values from K_o - consolidation triaxial tests.

Yield envelopes which have been identified to date in Winnipeg clay at different depths were shown in Fig. 6.1. If the yield stresses used to determine these yield envelopes are normalized with the appropriate value of p'_c from their respective depths (Fig. 6.7), a probable zone of yield can be identified in normalized (p', q) space as shown in Fig. 6.8. This normalized yield envelope is the first to be presented for

the Lake Agassiz clay, and perhaps only the third or fourth in the literature. While there is some scatter in the data, the shape of this normalized yield envelope is approximately elliptical and symmetric about the K_o - line. It is also interesting to note that the ratio of p'_c to $(p'_c)_{iso}$ is about 1.6 which is the average value for 23 natural clays reported by Tavenas and Leroueil (1979).

6.2.4 Strain Energy as a Yielding Criterion

There are some stress paths along which the σ'_{oct} vs ε_v plot is not useful for identifying the limit-state condition. In these cases, Crooks and Graham (1976) suggested using components of the stress tensor other than σ'_{oct}. They also pointed out that strain energy is a good yield criterion in connection with the concept of limit-state. They noted that the limit-state corresponds to a discontinuity of the relationships between stress and strain energy absorbed per unit volume, and that contours of the total strain energy developed along various stress paths assume shapes similar to those of the limit-state surfaces. Consequently, they were led to suggest the existence of a threshold energy level which defined the limit-state, and was independent of the stress path.

After proposing the YLIGHT model, Tavenas et al. (1979) decided to investigate this hypothesis of a correlation between the strain energy and limit-state. They examined the use of strain energy as a limit-state and creep criterion in Leda clay. They found that the strain energy could be used to define the limit-state envelope because a clear discontinuity exists in the energy-stress relationship along

all stress paths in their studies, except when the effective octahedral normal stress is constant. However, their study did not find a distinct threshold energy at which all samples reached limit-state, as was proposed by Graham (1974). Their results showed that strain energy is a function of the stress state at the limit-state. In addition, they demonstrated that strain energy is also a good indicator for the creep behaviour of overconsolidated clays. In particular, the rate of dissipation of the strain energy was shown to depend essentially on the relative position of the applied effective creep stresses to the limit-state surface of the clay.

In this study, strain energy as a yielding criterion is further investigated in Winnipeg clays. Following an idea by Crooks (1980), the author has used the relationship of strain energy versus Length of Stress Vector to examine the limit-state along various stress paths. Graphs of W vs LSSV were presented in Figs. 4.20 - 4.26. Test results show that strain energy provides a useful yielding criterion which is independent of stress path. Clear discontinuities were observed in all W vs LSSV plots, where limit-state is clearly defined. Anisotropically consolidated drained, and undrained, strain-controlled test samples tend to give lower strain energy at yield (Figs. 4.25 - 4.26).

Following careful examination of the strain energy at limit-state, it can be stated that all samples reached limit-state at different strain energy depending on stress paths. It is of interest to note that sample T316 which followed a stress path of decreasing σ'_{oct} and increasing $(\sigma_1-\sigma_3)$, had a negative strain energy at yield (Figs. 4.2 and 4.24). This is an example where the sample feeds out its energy to the

surrounding as it tends to swell. For this reason, the author supports the view of Tavenas et al. (1978b) that there is no threshold energy at the yield envelope, and that the strain energy at yield is stress path dependent.

6.3 UNDRAINED SHEARING BEHAVIOUR

6.3.1 Undrained Shear Strength

Samples which had not failed during the drained, stress-controlled portion of the testing program were sheared to rupture in undrained conditions. The undrained shear results were presented in Chapter 5. The results show that there is a difference in shearing behaviour between isotropically and anisotropically consolidated samples because of different consolidation histories. The difference in behaviour is evident in the strains required to attain $(\sigma_1-\sigma_3)/2_{max}$. The failure strain, ε_f, was greater in CIU test than in CAU tests (see Fig. 5.5 - 5.6).

Samples which were anisotropically consolidated with $\sigma'_{1c}/p'_c > 1$, gave lower values of $((\sigma_1-\sigma_3)/2\sigma'_{1c})_{max}$ than CAU samples with $\sigma'_{1c}/p'_o \simeq 1$. This is because the reserve resistance of the grain structure, developed during overconsolidation in the field is exceeded during the consolidation stage of the former tests. Furthermore, values of relative stiffness, E_{50}/s_u, obtained from CAU samples are generally somewhat higher than the corresponding values from CIU samples (Fig. 5.14).

The relationship between $(\sigma_1-\sigma_3)/2_{max}$ and σ'_{1c} (or p'_c) for consolidated-undrained tests in Winnipeg clays is given in Fig. 6.9. It can be approximated fairly well by a straight line passing through

the origin with slope $s_u/\sigma'_{1c} = 0.22$. Fig. 6.10 shows a plot of normalized undrained shear strength versus plasticity index which has been prepared by combining data of this study with that in recent papers by Trak et al. (1980) and Larsson (1980). Using the USALS method (Lefebvre, 1980), Trak et al. (1980) demonstrated that the average value of $s_u(\text{USALS})/\sigma'_{1c}$ for clays from Quebec is 0.22. Based on data obtained from reported failures of embankments, foundations and large-scale loading tests, Larsson (1980) showed that there is a trend of increasing normalized undrained shear strength with increasing plasticity, except for the organic clays for which the trend is uncertain. He further pointed out that the relation $s_u = 0.22\ \sigma'_{1c}$ corresponds to an average for all the clays, but will overestimate the undrained shear strength in very low-plastic clays and underestimate in high-plastic clays. It is of interest to note that a value of $s_u/\sigma'_{1c} = 0.22$ for the Winnipeg clays is comparable to the average value reported by Larsson (1980) and Trak et al. (1980).

6.3.2 Normally Consolidated Coulomb-Mohr Envelope

A normally consolidated Coulomb-Mohr envelope for the blue clay has been identified on the basis of $(\sigma_1-\sigma_3)/2_{max}$ failure criterion (Fig. 5.8), using the undrained shear strength of this test program and results from Noonan (1980). The effective angle of shearing resistance, ϕ', is 17.5^o and the effective cohesion intercept, c', is 4 kPa. The failure envelope predicted using $(\sigma'_1/\sigma'_3)_{max}$ criterion, which is not presented in this thesis, is similar to the one predicted on the basis of $(\sigma_1-\sigma_3)/2_{max}$ criterion.

The effective stress paths for the overconsolidated samples (that is, T306, T318, T319) are plotted along with the Coulomb-Mohr envelope in Fig. 5.8. It is of interest to note that the post-peak strengths (that is, the 'USALS' strengths) of these samples are close to the failure envelope. It should be pointed out that the post-peak strengths for Test T318 and T319 were taken at axial strains of about 4% (see Figs. 5.4 and 5.7b) which is considered rather too small in other clays (Lefebvre, 1980). However, Fig. 5 of Baracos et al. (1980) showed that after reaching the peak strengths at axial strains of about 2%, the shearing resistance of overconsolidated samples in Winnipeg clay decreased sharply with further straining to axial strains of about 4%, and then levelled off to approximately constant shearing resistance. On this basis, the results of this study tend to agree with the work of Lefebvre (1980) on Champlain Sea clay.

6.3.3 Porewater Pressure Generation

It was noted in Figs. 5.5 - 5.6 that CIU sample produced a higher normalized pore pressure increase, $\Delta u/\sigma'_{1c}$, than CAU samples. It was further observed that there was a considerable difference in the effective stress paths for samples with different consolidation histories (Fig. 5.8). This was caused by differences in porewater pressure generation.

Skempton's (1954) parameter 'A' is one of the most widely known and used porewater pressure parameters, and is known to be considerably affected by stress history. Henkel (1956) showed that the A-value at failure (A_f), is highly dependent on the overconsolidation

ratio in general. Crooks (1973) confirmed this for the Belfast estuarine clays.

Fig. 5.10 showed the variation of A_f with overconsolidation ratio for the Winnipeg clays. Also included in that figure are results obtained by Henkel (1956) and Crooks (1973) for remoulded Weald clay, and Belfast estuarine clay at the Kinnegar and Holywood sites respectively. The variation of A_f with OCR from the present study follows the expected pattern, that is the value of A_f decreases with increasing degree of overconsolidation. However, the A_f values for Winnipeg clays are consistently higher than results obtained by Henkel (1956) and Crooks (1973). Furthermore as Noonan (1980) also discovered, values of A_f greater than unity can be measured in the Winnipeg clays (Table 6). This is quite unusual. This can be contributed to the high compressibility of the Winnipeg clay (Table 2). Values of A_f published in the literature seldom exceed 1.0.

In previous studies by Baracos et al. (1980) and Noonan (1980), A_f values were plotted against $(1/\sigma'_{1c})$ because of some uncertainty associated with the measured oedometer p'_c values. A plot of A_f versus $(1/\sigma'_{1c})$ is presented in Fig. 5.9. The results support the trend proposed by Baracos et al. (1980).

Fig. 6.11 shows the relationship between the porewater pressure parameter, A_f, and the stress ratio, $\sigma'_{3c}/\sigma'_{1c}$, at the end of consolidation before undrained shear. These results show that as the stress ratio during consolidation increases from about 0.63 to 1.0, the A_f values also increase. This is an indication that the porewater pressure generation during undrained shearing is closely related to the in-situ grain

structure of the soil. It is further noted that normally consolidated samples generate higher pore pressure than overconsolidated samples during undrained shear. Therefore, it can be argued that careful anisotropic reconsolidation of samples using stress ratio in the same order of magnitude as those in the field, hence preserving the grain structure, is practically mandatory if porewater pressures are to be predicted accurately. Similar results have been reported by Crooks (1973).

CHAPTER 7

CONCLUSIONS AND SUGGESTIONS FOR FURTHER RESEARCH

7.1 CONCLUSIONS

1. Drained stress-controlled tests confirm the earlier conclusions from previous studies by Baracos et al. (1980) and Noonan (1980) that a limit-state can be determined at which a distinct change takes place from an initial "small-strain" behaviour to a subsequent "large-strain" behaviour. The limit-state is controlled by the in-situ grain structure of the clay, and by stress-history effects (Fig. 6.1).

2. In the present study, a well defined yield envelope was identified for the Lake Agassiz clay at 11.5 m depth (Fig. 4.27). This envelope supports the YLIGHT model concept proposed by Tavenas and Leroueil (1977) for Champlain Sea clay. The results show clearly that the yield envelope is displaced towards reduced preconsolidation pressure and shear strength as the load duration increases, that is with decreasing strain rate (Fig. 6.6). This again agrees with the YLIGHT model.

3. A limited zone of yielding can be identified in normalized (p', q) space when the yield stresses used to determine the yield envelopes at various depths are normalized by dividing by appropriate p'_c values (Fig. 6.8). That is, yield envelopes from different depths are homothetic, and can be normalized with respect to p'_c.

4. Strain energy absorbed per unit volume provides a useful limit-state criterion which is not stress path dependent and includes

all components of the strain tensor. Strain energy per unit volume (W) should be plotted against Length of Stress Vector (LSSV) to generalize its applicability to any stress path.

5. The present study supports the view of Tavenas et al. (1978b) that there is no threshold energy at the yield envelope, and that the strain energy at yield is stress path dependent.

6. Based on the $(\sigma_1-\sigma_3)/2_{max}$ failure criterion, the normally consolidated Coulomb-Mohr strength parameters, c' and ϕ' were 4 kPa and 17.5^{o} respectively, for the blue clay (Fig. 5.8).

7. The quality of the one-dimensional consolidation results has been improved significantly by using improved oedometer sample preparation and testing techniques (see Section 4.3).

8. Stress levels and stress ratio during laboratory reconsolidation influence strongly the behaviour of samples during subsequent shearing, particularly with respect to stress-strain behaviour and porewater pressure generation. Careful field sampling, storage and sample preparation techniques must be adopted if the in-situ grain structure of the soil is to be preserved, and its properties are to be measured. Anisotropic reconsolidation to in-situ stresses is recommended where possible.

9. In samples which have been anisotropically consolidated, porewater pressures in the laboratory are greater than, and linearly proportional to, octahedral normal stress changes up to a high percentage of the maximum shear stress (Figs. 5.11 - 5.12a).

10. The porewater pressure parameter, A_f, depends strongly on the consolidation stress ratio and the degree of overconsolidation

(Figs. 5.9, 5.10 and 6.11).

11. The shear strength determined from strain-controlled tests depends on the rate of straining. For example, a tenfold change in strain-rate in Winnipeg clays produces a change in undrained strength of between 11% and 12% (Fig. 5.15).

7.2 SUGGESTIONS FOR FURTHER RESEARCH

1. The time-dependent aspects of the YLIGHT model on yielding has been investigated in this study (Fig. 6.6), using drained stress-controlled tests. Although preliminary results show that the yield envelope shrinks inwards with time, the author recommends further testing to confirm the general validity of the concept in Lake Agassiz clay.

2. Time effects on the preconsolidation pressure, p'_c, should be examined by means of non-standard oedometer tests like those performed by Tavenas et al. (1977). The procedure involves step-loading oedometer samples (say 6 samples) in one increment to predetermined stress levels, ranging from about 3/4 p'_o to stresses higher than p'_c. The development of vertical strains is monitored for a period of at least 30 days. The tests should be done under temperature controlled conditions. This would allow the plotting of the e vs σ'_v curves for the clay at various times. The effect of time on p'_c could be observed from these curves.

3. Strain-controlled oedometer testing (Bell, 1977) should also be used to investigate the strain rate effects on p'_c. The procedure would be similar to the step-changing test in triaxial testing. It

involves varying the strain-rate during the course of a single test, and subsequent piecing together the stress-strain curves for different strain-rates.

4. As described in Section 6.2.1, the limit-state in the overconsolidated region is difficult to define and requires a careful examination of the strain-rate effects. The author suggests using CAU strain-controlled tests at various strain-rates to examine the effect of time on the overconsolidated branch of the yield envelope. This would provide another means of verifying the strain-rate effects from relaxation tests.

5. The low stress strength envelope shown by Baracos et al. (1980) has not been investigated in the present study. It is known qualitatively in Winnipeg, that Lake Agassiz clay often fails in embankments, riverbanks and excavations at strengths significantly lower than "peak strengths, but higher than "residual" strengths. Further research on the low stress envelope is recommended, using strain-controlled CAU tests on undisturbed samples, fully softened samples, and samples which have been subjected to freeze-thaw degradation.

6. It would also be of great interest to further examine the undrained strength at large strains in Lake Agassiz clay using the USALS method described by Lefebvre (1980), and by implication by Rivard and Lu (1978).

7. After the last paragraphs were written, the author had the benefit of discussions with Dr. J.B. Burland, Imperial College, London. On the basis of those discussions, the author proposes that

further attention should be paid to the anisotropy and elasticity of the soil before yield. Preliminary examination suggests that the Bulk Modulus K is largely independent of stress path. Further work should be done to examine this in detail, and also the nature of the Shear Modulus G. Any result which suggests the uniqueness of the Bulk and Shear Moduli before yield has major significance in terms of the elasticity of the clay.

REFERENCES

Baracos, A., J. Graham, and L. Domaschuk. 1980. "Yielding and Rupture in a Lacustrine Clay". Canadian Geotechnical Journal, Vol. 17, pp. 559-573.

Bell, A. 1977. "A Geotechnical Investigation of Post Glacial Estuarine Deposits at Kinnegar, Belfast Lough". Ph.D. Thesis, Queen's University, Belfast, Northern Ireland.

Bjerrum, L. 1967. "Engineering Geology of Norwegian Normally Consolidated Marine Clays as Related to Settlements of Buildings". Geotechnique, Vol. 17(2), pp. 83-119.

Bjerrum, L., C.J.F. Clausen, and J.M. Duncan. 1972. "Stability of Flexible Structures". Fifth European Conference on Soil Mechanics and Foundation Engineering, Madrid. General Report, Session IIIa.

Bjerrum, L., and T.C. Kenney. 1967. "Effect of Structure on the Shear Behaviour of Normally Consolidated Quick Clays". Proceedings, Geotechnical Conference on Shear Strength Properties of Natural Soils and Rocks, Oslo, Norway, Vol. 2, pp. 19-27.

Bowles, J.F. Engineering Properties of Soils and Their Measurement. Toronto: McGraw-Hill Book Company, 1978.

Crawford, C.B. 1964. "Interpretation of the Consolidation Test". ASCE Journal of Soil Mechanics and Foundation Engineering Div., Vol. 90, No. SM5, pp. 87-102.

Crooks, J.H.A. 1980. Panel Discussion, Session 2, Data Reduction and Applications for Analytical Modelling. ASTM SYMPOSIUM, Chicago, Illinios.

Crooks, J.H.A. 1973. "Laboratory Studies of Belfast Estuarine Deposits". Ph.D. Thesis, Queen's University of Belfast, Northern Ireland.

Crooks, J.H.A., and J. Graham. 1976. "Geotechnical Properties of the Belfast Estuarine Deposits". Geotechnique, Vol. 26(2), pp. 293-315.

Domaschuk, L. 1977. "Soil Block Sampler". Canadian Geotechnical Journal, Vol. 14, pp. 262-265.

Eden, W.J. 1971. "Sampler Trials in Overconsolidated Sensitive Clays". Am. Soc. Test. Mat., S.T.P. 483, pp. 132-142.

Elson, J.A. 1967. "Geology of Glacial Lake Agassiz". Life, Land and Water, occasional papers, No. 1, Dept. of Anthropology, University of Manitoba, Winnipeg, Manitoba.

Elson, J.A. 1961. "Soils of the Lake Agassiz Region". In Soils of Canada. Edited by R.F. Legget. Royal Society of Canada, Special Publication No. 3, University of Toronto Press, Toronto, Ontario, pp. 51-79.

Graham, J. 1979. "Embankment Stability on Anisotropic Soft Clays". Canadian Geotechnical Journal, Vol. 16, pp. 295-308.

Graham, J. 1974. "Laboratory Testing of Sensitive Clay from Lyndhurst, Ontario". Civil Engineering Research Report CE 74-2, Royal Military College, Kingston, Ontario.

Graham, J. 1969. "Laboratory Results from Mastemyr Quick Clay After Reconsolidation to In-Situ Stresses". Internal Report F372-5, Norwegian Geotechnical Institute, Oslo, Norway.

Graham, J., R.B. Pinkney, K.V. Lew, and P.G.S. Trainor. 1981. "On Curve-Fitting and Laboratory Data". In preparation.

Henkel, D.J. 1956. "The Effect of Overconsolidation on the Behaviour of Clays During Shear". Geotechnique, Vol. 6(4), pp. 139-150.

Jaky, J. 1944. "The Coefficient of Earth Pressure at Rest". Jnl. Soc. Hung. Architects and Engrs, pp. 355-358.

Kenney, T.C. 1966. "Shearing Resistance of Natural Quick Clays". Ph.D. Thesis, University of London.

Kenney, T.C., and D.J. Folkes. 1979. "Mechanical Properties of Soft Soils". State-of-the-Art Report, Session 2, Proceedings, 32nd Canadian Geotechnical Conference, Quebec City, Canada, pp. 1-51.

Landva, A. 1964. "Equipment for Cutting and Mounting Undisturbed Specimens of Clay in Testing Devices". Norwegian Geotechnical Institute Publications No. 56, Oslo, Norway.

LaRochelle, P., and G. Lefebvre. 1971. "Sampling Disturbance in Champlain Clays". Am. Soc. Test. Mat., S.T.P. 483, pp. 143-163.

Larsson, R. 1980. "Undrained Shear Strength in Stability Calculation of Embankments and Foundations on Soft Clays". Canadian Geotechnical Journal, Vol. 17, pp. 591-602.

Leonards, G.A., and P. Girault. 1961. "A Study of the One-Dimensional Consolidation Test". Proc. 5th Int. Conf. Soil Mech. and Found. Eng. (Paris) 1:213-218.

Leonards, G.A., and A.G. Altschaeffl. 1964. "Compressibility of Clay". ASCE Journal of the S.M.F.E. Division, Vol. 90, SM5, pp. 133-155.

Leong, W.C. 1981. "Interpreting Yield Stress Using Bilinear Curve-Fitting Technique". B.Sc. Graduation Project, University of Manitoba, Winnipeg, Manitoba.

Leroueil, S., and F. Tavenas. 1977. "Discussion of Geotechnical Properties of Belfast Estuarine Deposits". Geotechnique, Vol. 27(3), pp. 441-446.

Lew, K.V. 1981. "Triaxial Test Program". Internal Report, Department of Civil Eng., University of Manitoba, Winnipeg, Manitoba.

Lew, K.V. 1981. "Energy Calculation Program". Internal Report, Department of Civil Eng., University of Manitoba, Winnipeg, Manitoba.

Lo, K.Y. 1961. "Secondary Compression of Clays". ASCE Journal of the S.M.F.E. Division, Vol. 87, SM4, pp. 61-87.

Mesri, G. 1975. "Discussion on New Design Procedure for Stability of Soft Clays". ASCE Journal of the Geotechnical Division, 101(GT4), pp. 409-412.

Mitchell, R.J. 1970. "On the Yielding and Mechanical Strength of Leda Clays". Canadian Geotechnical Journal, Vol. 7, pp. 297-312.

Noonan, M.L. 1980. "Limit-State Studies in Winnipeg Clays". M.Sc. Thesis, University of Manitoba, Winnipeg, Manitoba.

Pinkney, R.B. 1980. "Least-Squares Bilinear Curve Fit and Plot". Unpublished Computer Program, Dept. of Civil Eng., University of Manitoba, Winnipeg, Manitoba.

Quigley, R.M. 1980. "Geology, Mineralogy, and Geochemistry of Canadian Soft Soils: A Geotechnical Perspective". Canadian Geotechnical Journal, Vol. 17, pp. 261-285.

Render, F.W. 1970. "Geohydrology of the Metropolitan Winnipeg Area As Related to Groundwater Supply and Construction". Canadian Geotechnical Journal, Vol. 7, pp. 243-274.

Richardson, A.M. and R.V. Whitman. 1963. "Effect of Strain Rate upon Undrained Shear Resistance of a Saturated Remoulded Fat Clay". Geotechnique, Vol. 13(4), pp. 310-324.

Rivard, P.J. and Y. Lu. 1978. "Shear Strength of Soft Fissured Clays". Canadian Geotechnical Journal, Vol. 15, pp. 382-390.

Roscoe, K.H., A.N. Schofield, and C.P. Wroth. 1958. "On the Yielding of Soils". Geotechnique, Vol. 8(1), pp. 22-53.

Roscoe, K.H., and J.B. Burland. 1968. "On the Generalized Stress-Strain Behaviour of Wet Clay". Engineering Plasticity, ed. J. Weyman and F.A. Leckic. Cambridge University Press, pp. 535-609.

Sangrey, D.A. 1972. "Naturally Cemented Sensitive Soils". Geotechnique, Vol. 22(1), pp. 139-152.

Skempton, A.W. 1954. "The Porepressure Coefficients A and B". Geotechnique, Vol. 4(4), pp. 143-147.

Tavenas, F. 1979. "The Behaviour of Embankments on Clay Foundations". State-of-the-Art Report, Session 3, Proceedings, 32nd Canadian Geotechnical Conference, Quebec City, Canada.

Tavenas, F., and S. Leroueil. 1980. "The Behaviour of Embankments on Clay Foundations". Canadian Geotechnical Journal, Vol. 17, pp. 236-260.

Tavenas, F., and S. Leroueil. 1979. "Clay Behaviour and the Selection of Design Parameters". Proceedings of the Fifth European Conf. on Soil Mechanics and Found. Eng., Brighton, Vol. 1, pp. 281-292.

Tavenas, F., and S. Leroueil. 1977. "The Effects of Stresses and Time on Yielding of Clays". Proceedings, 9th International Conference on S.M.F.E., Tokyo, Japan, Vol. 1, pp. 319-326.

Tavenas, F., J.P. Des Rosiers, S. Leroueil, P. La Rochelle, and M. Roy. 1979. "The Use of Strain Energy as a Yield and Creep Criterion for Lightly Overconsolidated Clays". Geotechnique Vol. 29, pp. 285-303.

Tavenas, F., S. Leroueil, P. LaRochelle, and M. Roy. 1978b. "Creep Behaviour of an Undisturbed Lightly Overconsolidated Clay". Canadian Geotechnical Journal, Vol. 15, pp. 402-423.

Teller, J.T. 1976. "Lake Agassiz Deposits in the Main Offshore Basin of Southern Manitoba". Canadian Journal of Earth Sciences, Vol. 13, No. 1, pp. 27-43.

Townsend, D.L., D.A. Sangrey, and L.K. Walker. 1969. "The Brittle Behaviour of Naturally Cemented Soils". Proc. 7th Int. Conf. on Soil Mechanics and Foundation Eng., Mexico, Vol. 1, pp. 411-417.

Trainor, P.G.S. 1981. M.Sc. Thesis, In Preparation. University of Manitoba, Winnipeg, Manitoba.

Trak, B., P. LaRochelle, F. Tavenas, S. Leroueil, and M. Roy. 1980. "A New Approach to the Stability Analysis of Embankments on Sensitive Clays". Canadian Geotechnical Journal, Vol. 17, pp. 526-544.

TABLE 1 BASIC SOIL PROPERTIES

Test Number	T302	T303	T304	T305	T306	T307	T308	T309	T310
Test Type	CID(U)	CAD(U)	CAD	CAD	CAU	CAD	CAD(U)	CAD(U)	CAU
Borehole Number	4	4	4	4	4	4	4	4	4
Block Sample Number	6	6	6	6	6	6	6	6	7
Depth (m)	11.58	11.58	11.58	11.58	11.38	11.38	11.38	11.38	11.56
Initial Moisture Content (%)	58.5	62.8	63.1	63.8	60.2	60.6	59.9	59.8	63.1
Final Moisture Content (%)	47.0	46.6	64.3	63.9	56.0	53.8	46.2	45.4	50.7
Liquid Limit (%)	-	81.8	-	-	-	-	-	-	-
Plastic Limit (%)	-	26.8	-	-	-	-	-	-	-
Plasticity Index (%)	-	55.0	-	-	-	-	-	-	-
Clay Content (%)	-	72	-	-	-	-	71	-	-
Specific Gravity	-	2.71	-	-	-	-	-	-	-
Unit Weight (kN/m^3)	16.1	16.1	16.1	16.1	16.4	16.2	16.1	16.3	16.4

Test Number	T311	T312	T313	T314	T315	T316	T317	T318	T319
Test Type	CAD(U)	CAD	CAD	CID(U)	CAD	CAD	CAD	CAU	CAU
Borehole Number	4	4	4	4	5	5	5	5	5
Block Sample Number	7	7	7	5	5	5	5	5	5
Depth (m)	11.56	11.56	11.57	11.57	11.57	11.57	11.57	11.37	11.37
Initial Moisture Content (%)	60.5	59.0	61.3	62.1	56.1	54.9	56.4	60.5	58.2
Final Moisture Content (%)	39.2	46.4	50.0	42.5	60.4	55.8	58.6	61.9	60.9
Liquid Limit (%)	82.4	-	-	86.4	-	78.8	-	-	85.0
Plastic Limit (%)	25.3	-	-	27.3	-	25.0	-	-	28.1
Plasticity Index (%)	57.1	-	-	59.1	-	53.8	-	-	56.9
Clay Content (%)	73	-	-	77	-	71	-	-	76
Specific Gravity	2.72	-	-	2.72	-	-	-	-	-
Unit Weight (kN/m^3)	16.4	16.5	16.4	16.3	16.5	17.0	16.4	16.5	16.4

- Not obtained for this test

TABLE 2 ONE-DIMENSIONAL CONSOLIDATION TEST RESULTS

Test Number	C301	C302	C303	C304
Borehole Number	4	4	5	5
Block Sample Number	6	6	5	5
Depth (m)	11.47	11.47	11.47	11.47
$*p_c'$	153	170	250	245
$**p_c'$	150	170	240	230
C_c	0.94	1.04	1.10	1.05

$*p_c'$ obtained from voids ratio vs. log σ_v' plot

$**p_c'$ obtained from voids ratio vs. σ_v' plot

TABLE 3 TRIAXIAL CONSOLIDATION RESULTS FOR RESTRESSING TO IN-SITU STRESSES

Test Number	T303	T304	T305	T306	T307	T308	T309	T311	T312	T313	T315	T316	T317	T319
$p_o'^*$ (kPa)	118.5	118.5	118.5	116.9	116.9	116.9	116.9	118.3	118.3	118.3	118.4	118.4	118.4	116.9
σ_{1c}' (kPa)	118.9	119.3	118.7	116.7	117.1	117.2	116.7	118.3	118.5	118.2	118.7	118.3	118.2	116.9
σ_{3c}' (kPa)	77.2	77.6	77.0	75.7	76.1	76.3	75.6	76.7	76.9	76.6	77.1	76.8	76.7	76.0
$p_c'^{**}$ (kPa)	218	218	218	218	218	218	218	218	218	218	218	218	218	218
σ_{1c}'/p_o'	1.0	1.01	1.0	1.0	1.0	1.0	1.0	1.0	1.0	1.0	1.0	1.0	1.0	1.0
p_c'/σ_{1c}'	1.83	1.83	1.84	1.87	1.86	1.86	1.87	1.84	1.84	1.84	1.84	1.84	1.84	1.86
$\sigma_{3c}'/\sigma_{1c}'$	0.65	0.65	0.65	0.65	0.65	0.65	0.65	0.65	0.65	0.65	0.65	0.65	0.65	0.65
ε_{1c} (%)	2.98	2.11	2.26	3.32	2.71	2.47	2.36	2.31	2.14	2.19	1.66	1.54	1.75	1.39
ε_{3c} (%)	0.34	0.66	0.40	0.22	0.36	0.44	0.42	0.53	0.55	0.50	0.28	0.08	0.16	0.06
ε_{vc} (%)	3.65	3.41	3.06	3.76	3.42	3.35	3.20	3.36	3.24	3.18	2.22	1.70	2.06	1.51

*Based on G.W.T. at 3 metres and γ_{sat} = 17.5 kN/m^3

**From one-dimensional consolidation tests (see Table 2)

TABLE 4 TRIAXIAL CONSOLIDATION RESULTS AT THE END OF STRESS-CONTROLLED TESTING

Test Number	T302	T303	T304#	T305#	T306†	T307#	T308	T309	T311	T312#	T313#	T314	T315#	T316#	T317†	T319†
p_o'* (kPa)	118.5	118.5	118.5	118.5	116.9	116.9	116.9	116.9	118.3	118.3	118.3	118.4	118.4	118.4	118.4	116.9
σ_{1c}' (kPa)	444.0	442.8	161.7	134.4	116.7	211.6	404.7	420.4	594.2	295.9	447.8	588.6	166.0	66.8	118.2	116.9
σ_{3c}' (kPa)	442.1	400.8	56.3	45.2	75.7	102.3	256.3	314.2	378.6	189.5	289.9	587.3	53.3	9.2	76.7	76.0
$\sigma_{3c}'/\sigma_{1c}'$	0.996	0.995	0.35	0.34	0.65	0.48	0.63	0.75	0.64	0.64	0.65	0.998	0.32	0.14	0.65	0.65
ε_{1c} (%)	8.31	11.95	4.95	3.99	3.32	11.18	20.73	14.11	26.15	12.0	16.76	9.02	3.75	8.67	1.75	1.39
ε_{3c} (%)	4.51	3.11	-0.48	-0.52	0.22	-1.88	-1.40	1.20	-2.08	0.10	-2.06	5.65	-0.82	-4.89	0.16	0.06
ε_{vc} (%)	17.33	18.17	3.99	2.95	3.76	7.42	17.93	16.51	21.99	12.20	12.64	20.33	2.12	-1.10	2.06	1.51

*Based on G.W.T. at 3 metres and γ_{sat} = 17.5 kN/m^3

**p_c' = 218 kPa (see Table 2)

#Sample failed in drained shear at the value shown

†Sample consolidated to in-situ stresses only

TABLE 5 YIELD STRESSES FROM DIFFERENT YIELD CRITERIA

Plotted Parameter	Test Number	T302	T303	T304	T305	T307	T308	T309	T311	T312	T313	T314	T315	T316	T317†
	σ_1' vs ε_1	200*	154	-	-	126	152	154	153	143	153	180*	-	-	-
	$(\sigma_1-\sigma_3)$ vs ε_1	-	-	98-105.4#	82-89.2#	129	151	160	151	144	154	-	102-106#	57.6-59#	104-116#
	σ'_{oct} vs ε_v	172	152	-	-	130	152	160	152	142	152	150	-	-	-
	σ_3' vs ε_3	143	160	-	-	126	133*	173	136*	149	151	144	-	-	-
	W vs LSSV	153	163	-	-	122	148	160	149	143	148	155	-	-	-

Note: The yield (or limit-state) stresses presented in this table have been put in terms of σ'_{oct} along the stress path for the test, with the exception of data points marked by #

#Yield stress in terms of $(\sigma_1-\sigma_3)$

*Not included in averaging

†Strain-controlled CAD test

TABLE 6 SUMMARY OF UNDRAINED SHEAR TEST RESULTS

Test Number	T302	T303	T306	T308	T309	T310	T311	T314	T318	T319
Test Type	CID(U)	CAD(U)	CAU	CAD(U)	CAD(U)	CAU	CAD(U)	CID(U)	CAU	CAU
Borehole Number	4	4	4	4	4	4	4	4	5	5
Block Sample Number	6	6	6	6	6	7	7	5	5	5
Depth (m)	11.58	11.58	11.38	11.38	11.38	11.56	11.56	11.57	11.37	11.37
p_o'* (kPa)	118.5	118.5	116.9	116.9	116.9	118.3	118.3	118.4	116.9	116.9
σ_{1c}' (kPa)	444.0	442.8	116.7	404.7	420.4	301.7	594.2	588.6	40.3	116.9
$\sigma_{3c}'/\sigma_{1c}'$	0.996	0.995	0.65	0.63	0.75	0.70	0.64	0.998	0.65	0.65
σ_{1c}'/p_o'	3.75	3.74	1.0	3.46	3.60	2.55	5.02	4.97	0.34	1.0
σ_{1c}'/p_c'**	2.04	2.03	0.54	1.86	1.92	1.38	2.73	2.70	0.18	0.54
$(\sigma_1-\sigma_3)/2_{max}$ (kPa)	80#	85#	38.9	94.1	83.5	68.9	130.6	101.2	36.5	53.8
$(\sigma_1-\sigma_3)/2\sigma_{1c\ max}'$	0.18#	0.192#	0.333	0.232	0.199	0.229	0.219	0.172	0.907	0.460
σ_{oct}' at $(\sigma_1-\sigma_3)/2_{max}$ (kPa)	265#	250#	76.5	285.4	287.9	208.2	427.1	292.6	39.6	87.7
ε_1 at $(\sigma_1-\sigma_3)/2_{max}$ (%)	x	x	2.82	0.57	1.88	1.43	0.55	9.13	1.75	1.6
$(\sigma_1'/\sigma_3')_{max}$	x	x	2.54	1.91	1.78	2.18	1.85	2.00	6.24	3.17
ε_1 at $(\sigma_1'/\sigma_3')_{max}$ (%)	x	x	2.82	6.39	3.91	4.17	6.91	12.77	1.22	1.33
E_{50} (MPa)	18.4	21.3	9.9	24.5	30.2	24.1	43.6	17.0	8.3	9.8
$E_{50}/(\sigma_1-\sigma_3)/2_{max}$	230	251	254	260	361	350	334	168	228	183
A_f	1.16	1.28	0.67	0.70	1.13	0.87	0.75	1.59	0.22	0.36
B (%)	100	98	98	-	102	100	-	-	99	100
$m = \Delta u/\Delta\sigma_{oct}'$	x	x	1.67	1.92	1.86	1.86	1.75	x	1.27	1.6
$\rho_{0.1}$ at ε_ρ	12.2	11.7	x	x	x	11.0	x	x	x	x
ε_ρ (%)	3.58	4.21	x	x	x	5.35	x	x	x	x
Initial Strain Rate $\dot{\varepsilon}_1$ (%/hr)	0.95	1.0	0.93	1.11	1.02	0.99	1.19	0.96	0.87	0.89

*Based on G.W.T. at 3 metres and γ_{sat} = 17.5 kN/m^3

**p_c' = 218 kPa

- Assumed to be satisfactory

#Values obtained by extrapolation from stress-strain curve

x Not obtained for the test

TABLE 7 VALUES OF STRAIN RATE PARAMETER $\rho_{0.1}$ FOR VARIOUS AXIAL STRAINS

ε_1 (%)		2	5	7	8	9.5	10.5	11	12	15.5
T302	$\rho_{0.1}$ at ε_1 (%)	-	-	-	11.2	-	11.6	-	-	-
T303	$\rho_{0.1}$ at ε_1 (%)	-	-	11.3	-	11.7	-	-	-	-
T310	$\rho_{0.1}$ at ε_1 (%)	12.7	11.5	-	9.5	-	-	9.4	-	7.5

- Not calculated at this strain

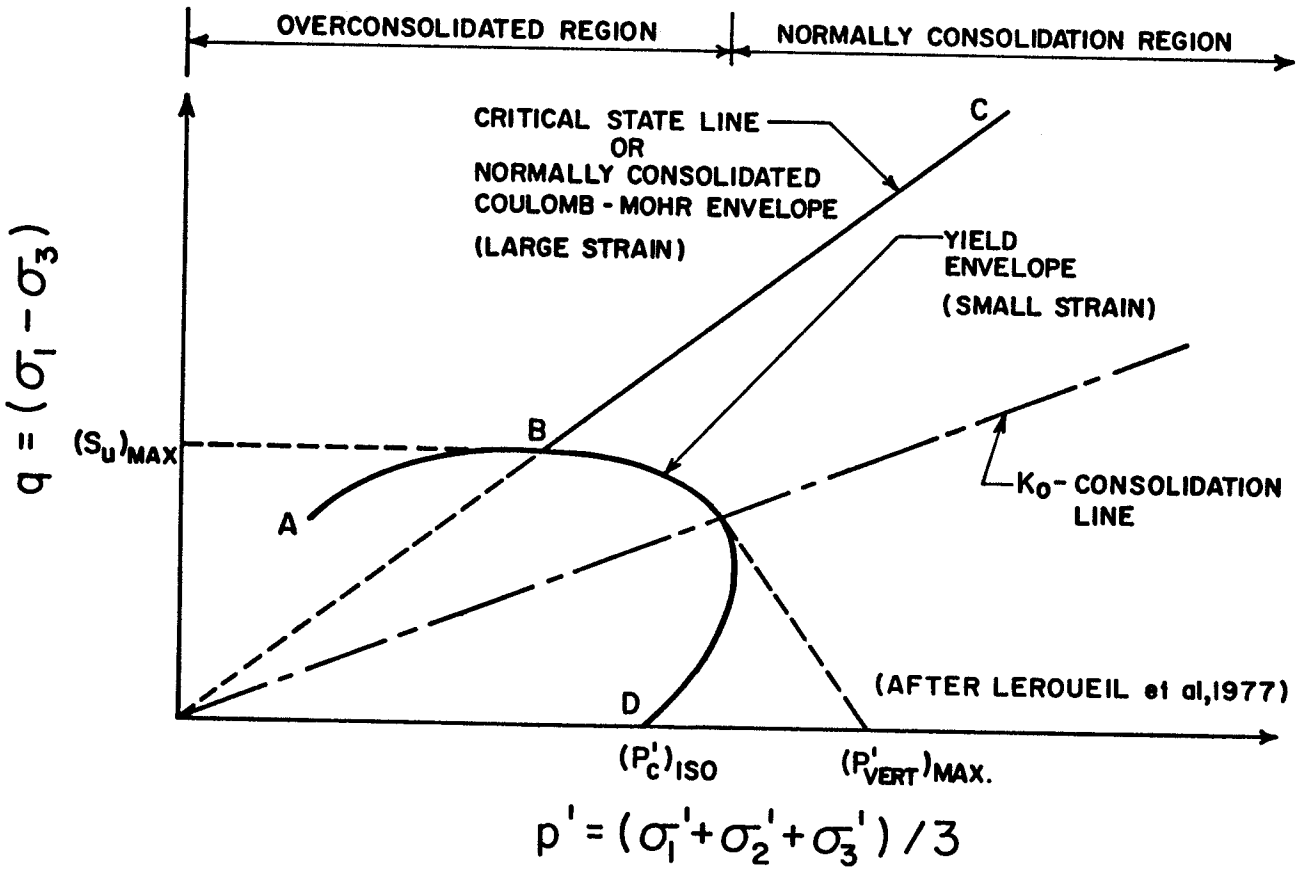

FIG. 2.1 TYPICAL CRITICAL STATE LINE, YIELD ENVELOPE, AND ASSOCIATED PARAMETERS

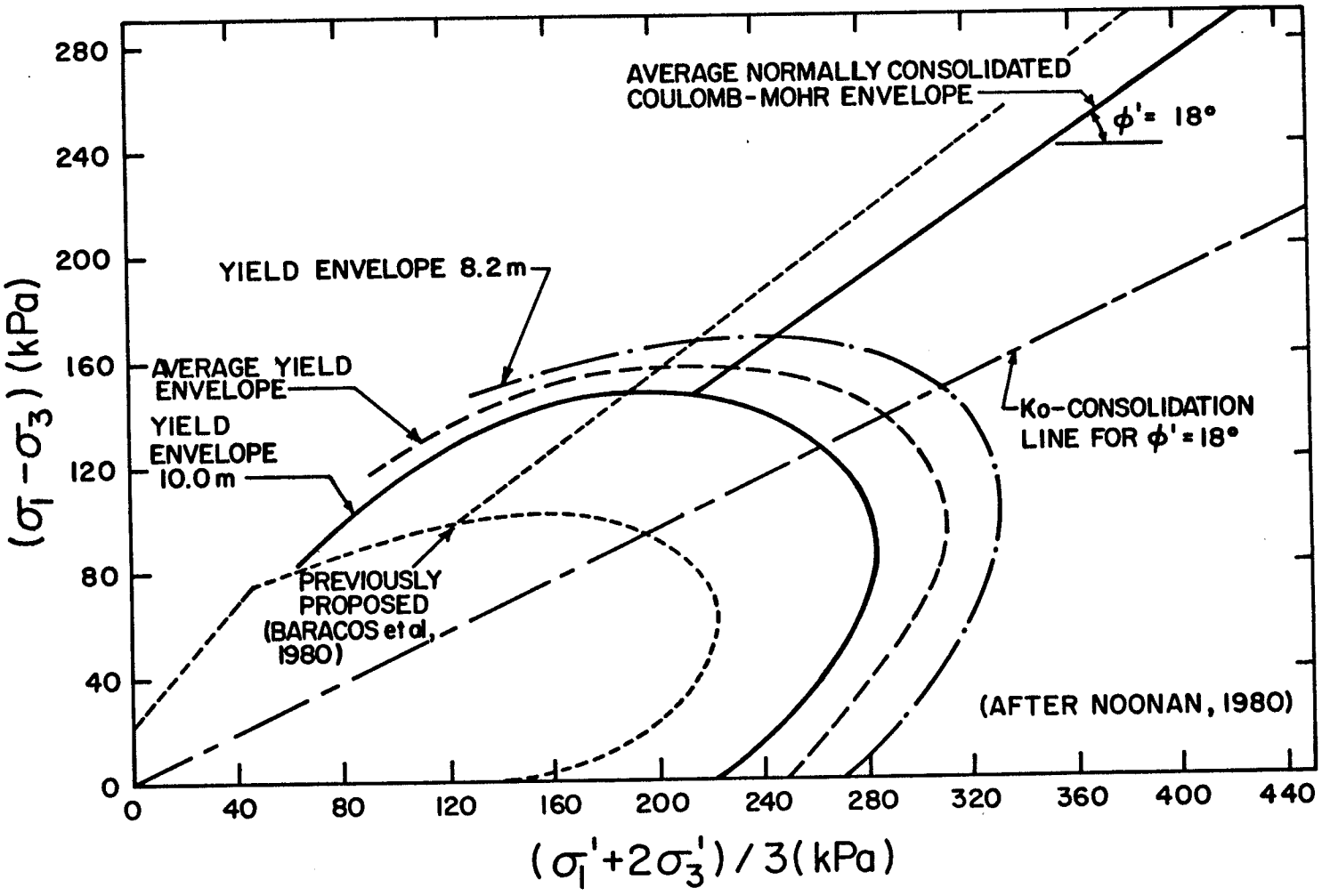

FIG. 2.2 YIELD ENVELOPES AND COULOMB-MOHR LINE (NOONAN, 1980)

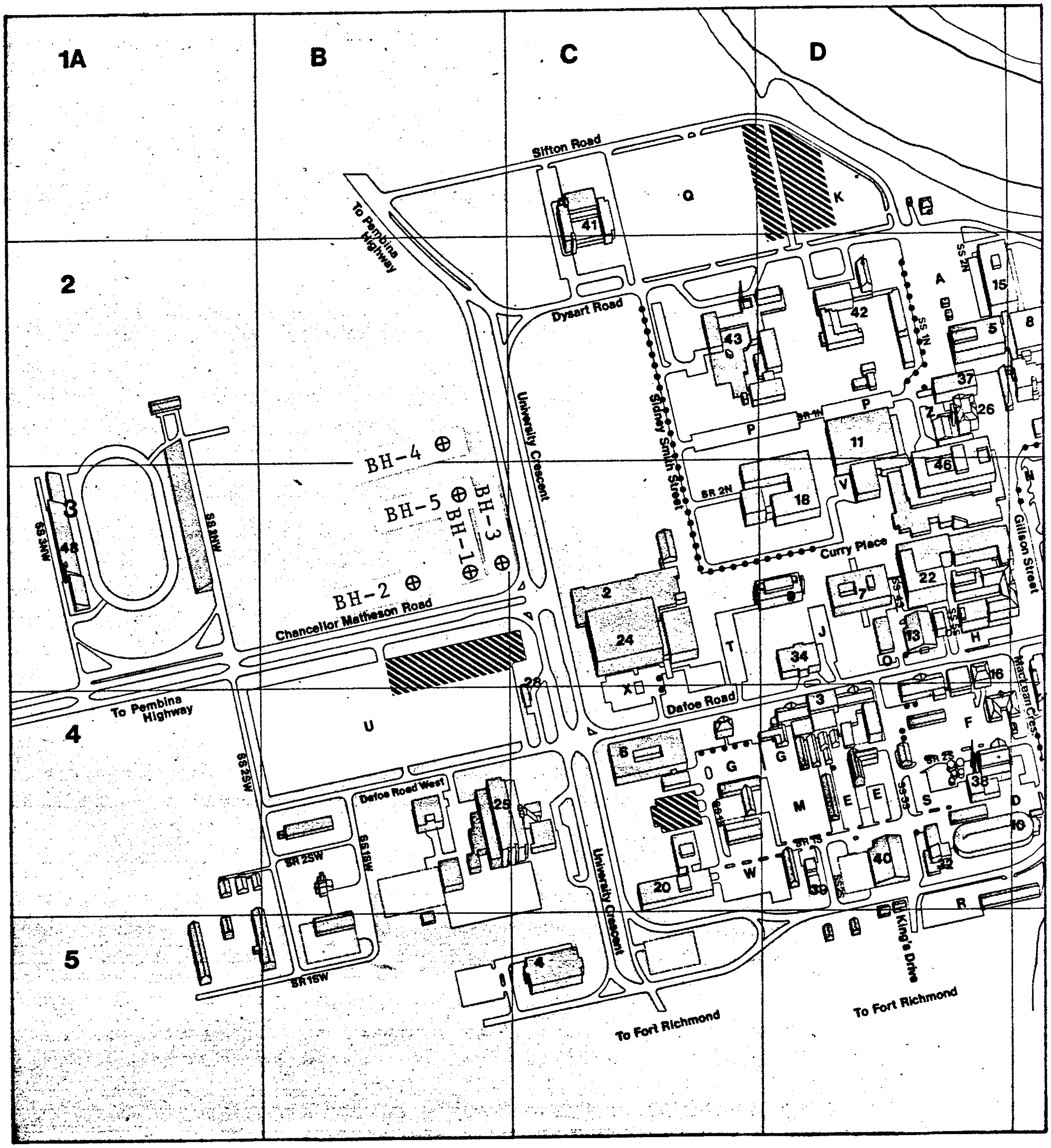

FIG. 3.1 SITE PLAN AND LOCATION OF BOREHOLES

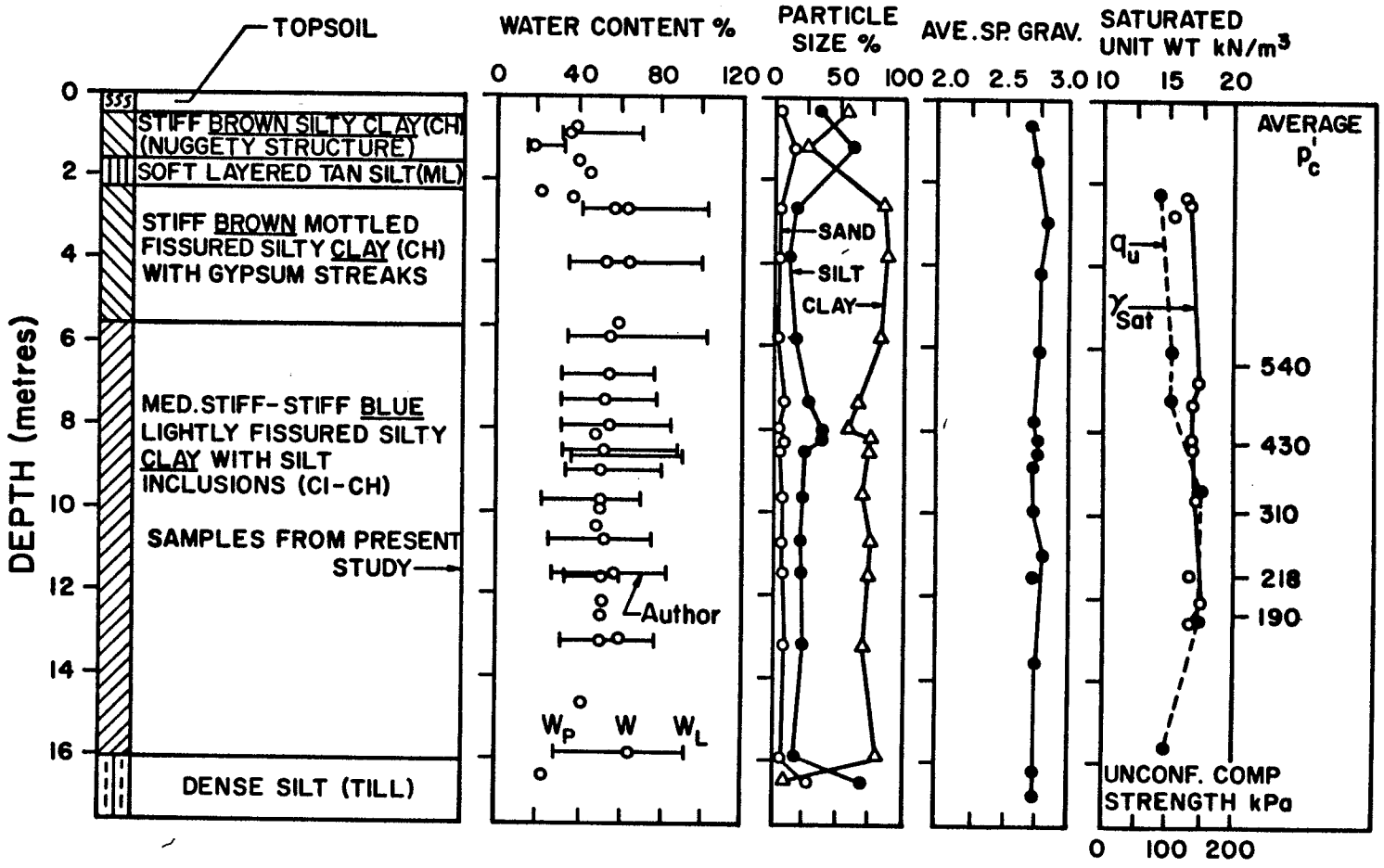

FIG. 3.2 AVERAGE BOREHOLE LOG INFORMATION, UNIVERSITY OF MANITOBA CAMPUS (BARACOS et al., 1980)

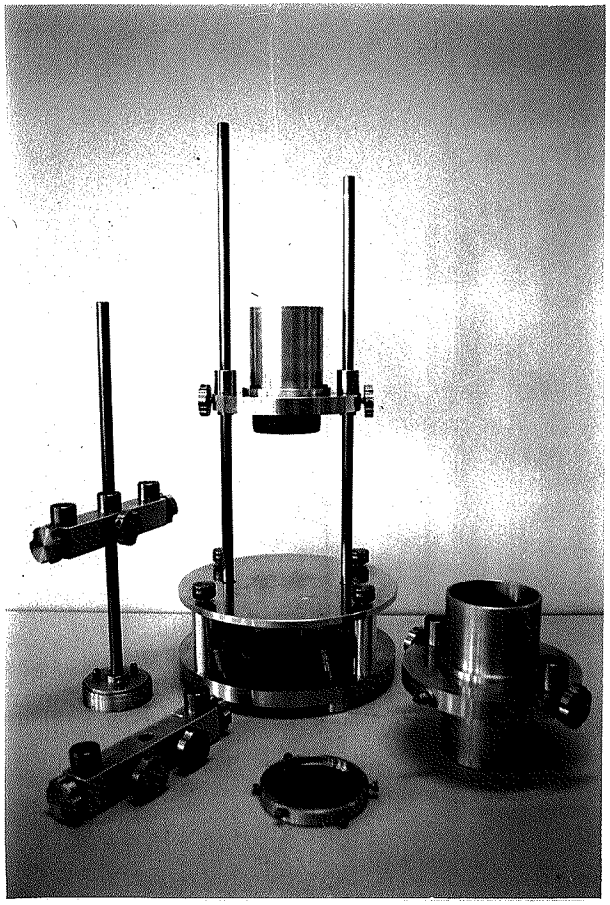

FIG. 3.3 TRIMMING AND BUILDING-IN EQUIPMENT FOR TRIAXIAL TESTS

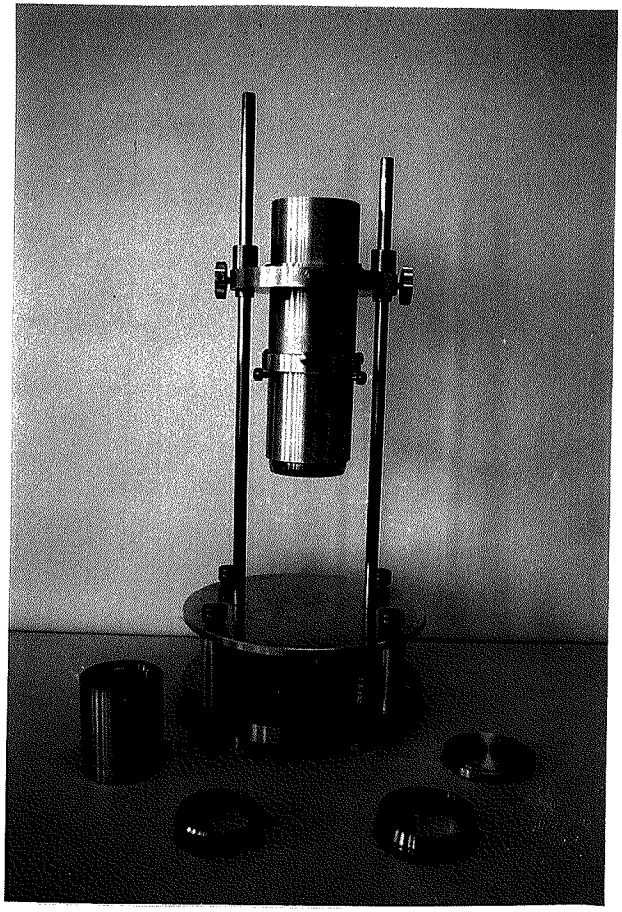

FIG. 3.4 TRIMMING EQUIPMENT FOR OEDOMETER TESTS

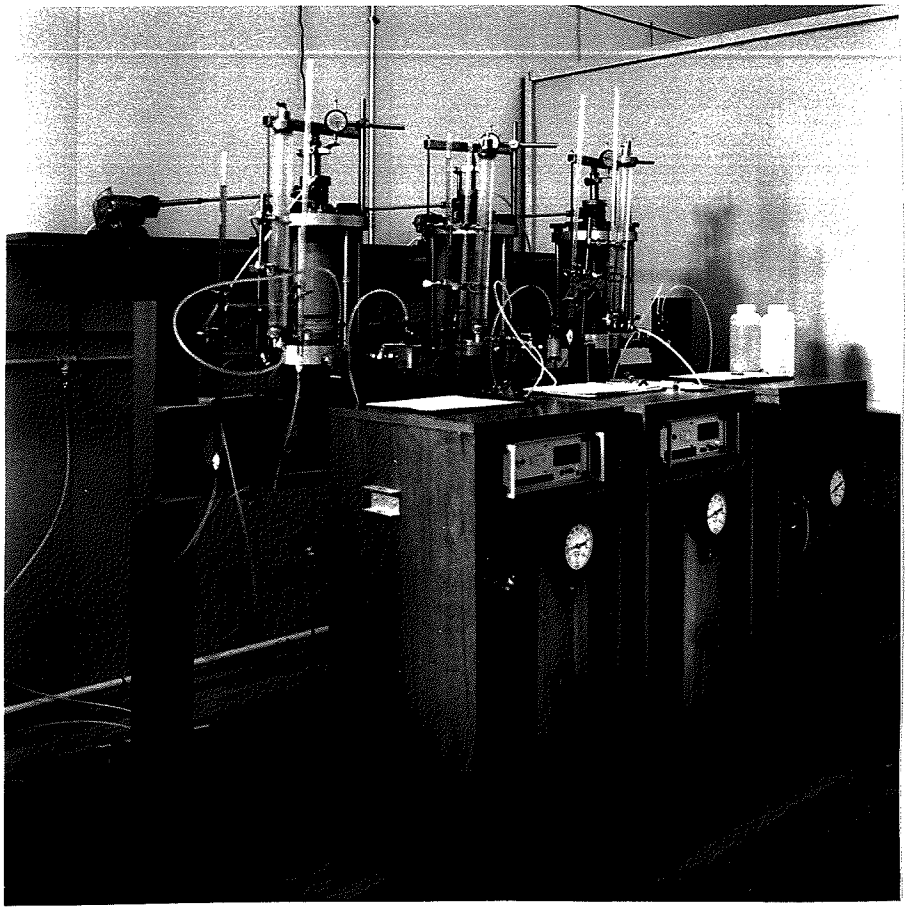

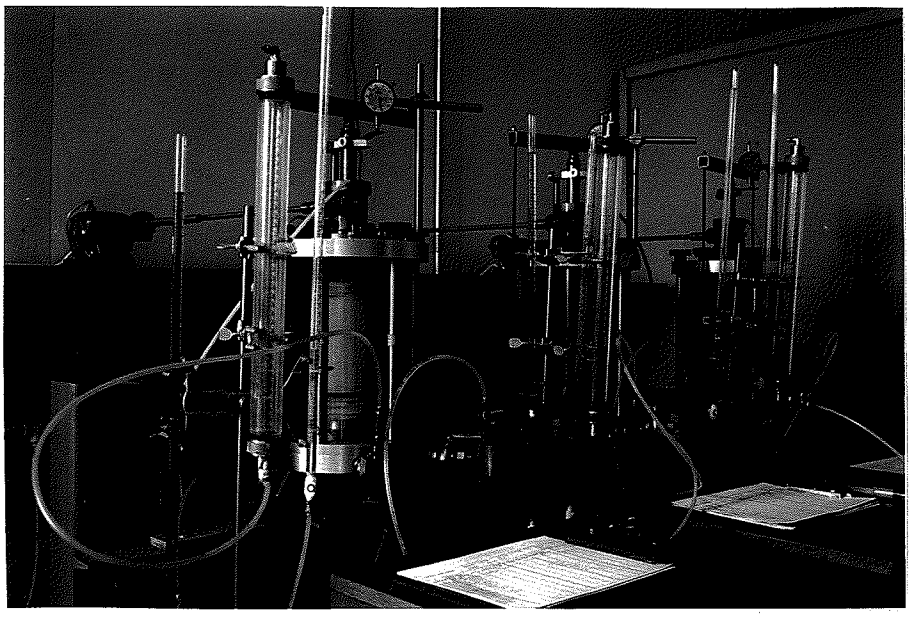

FIG. 3.5 TRIAXIAL SET-UP DURING DRAINED STRESS-CONTROLLED TESTS

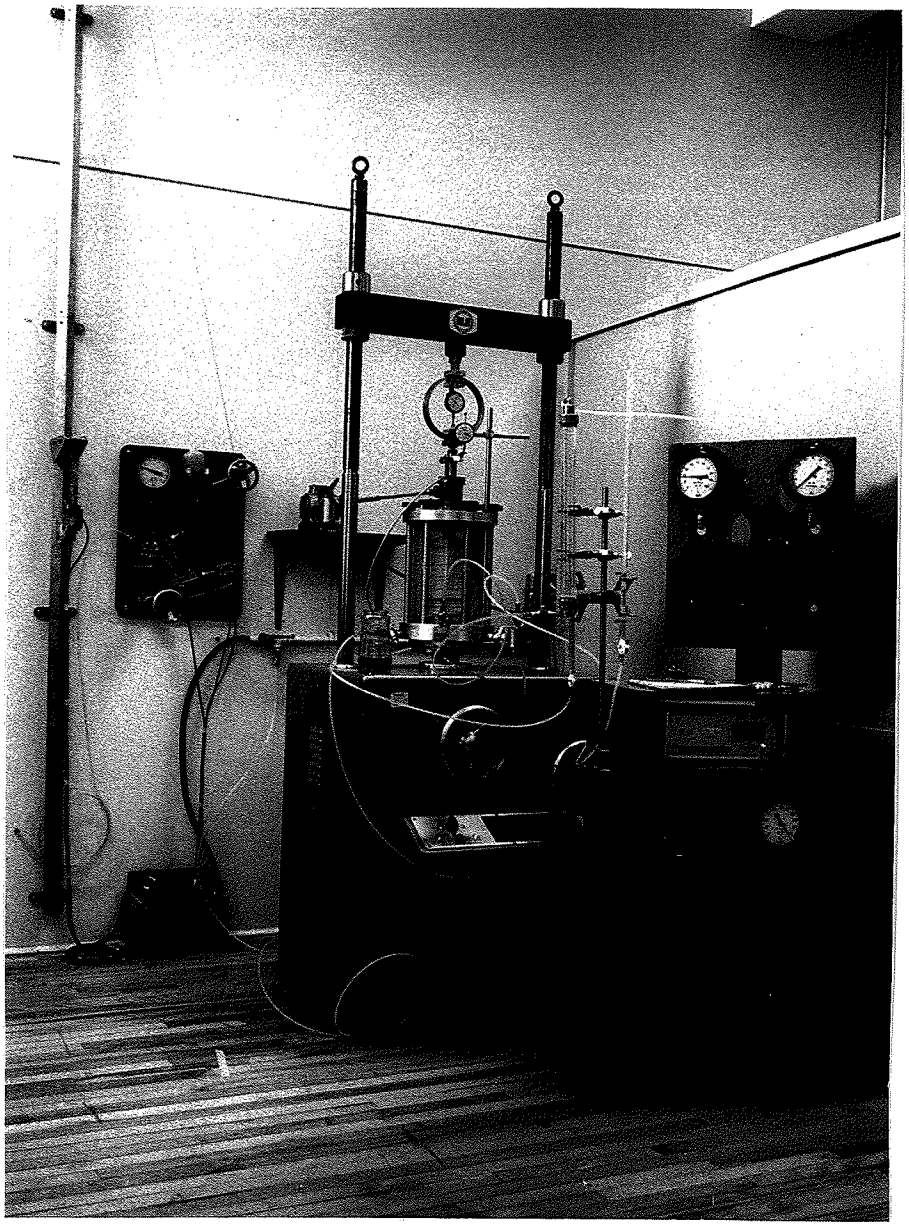

FIG. 3.6 TRIAXIAL SET-UP DURING CONSOLIDATED-UNDRAINED SHEAR TESTS

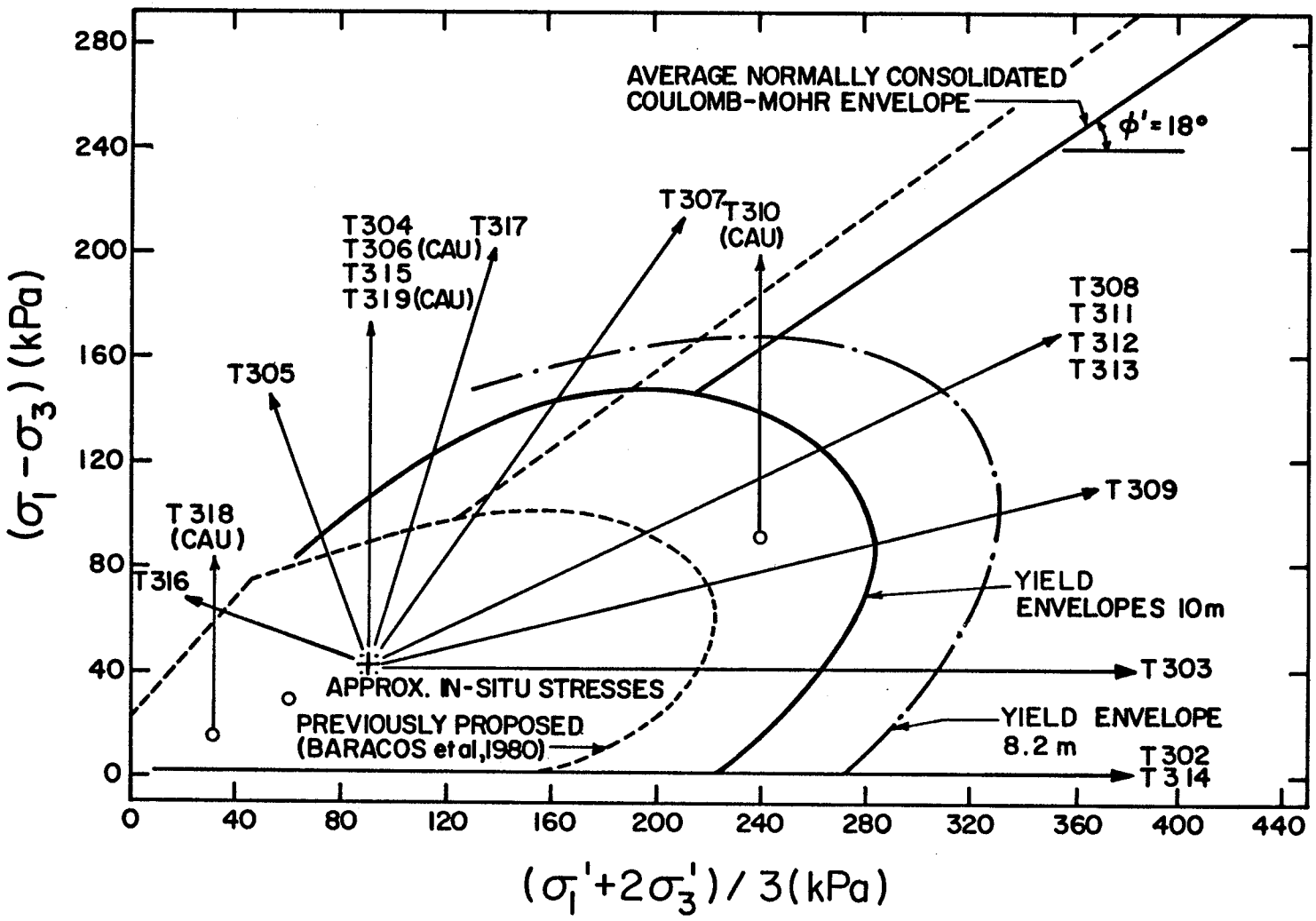

FIG. 4.1 PROPOSED STRESS PATHS AND EXISTING YIELD ENVELOPES

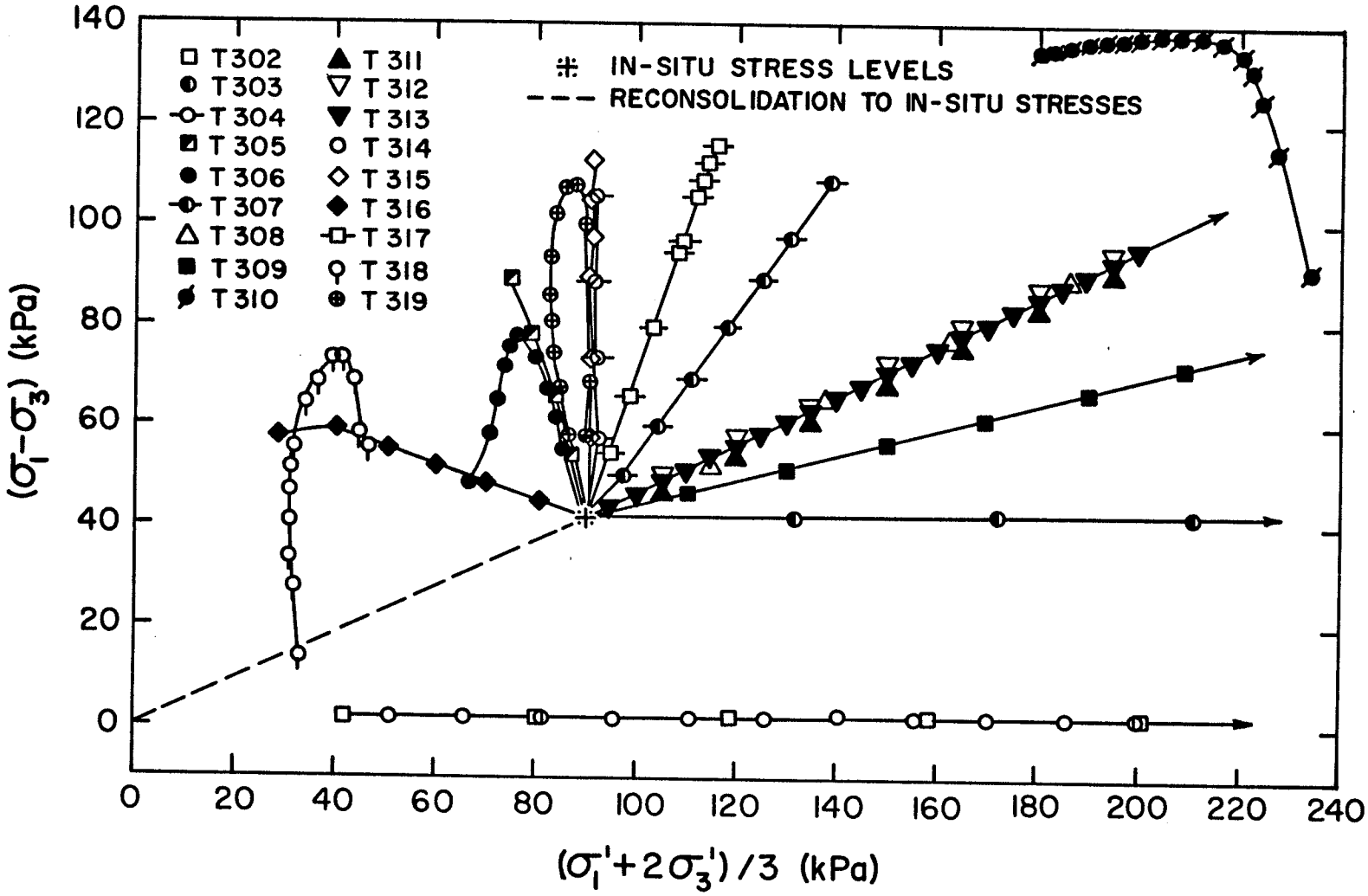

FIG. 4.2 STRESS PATHS FOLLOWED DURING TEST PROGRAM

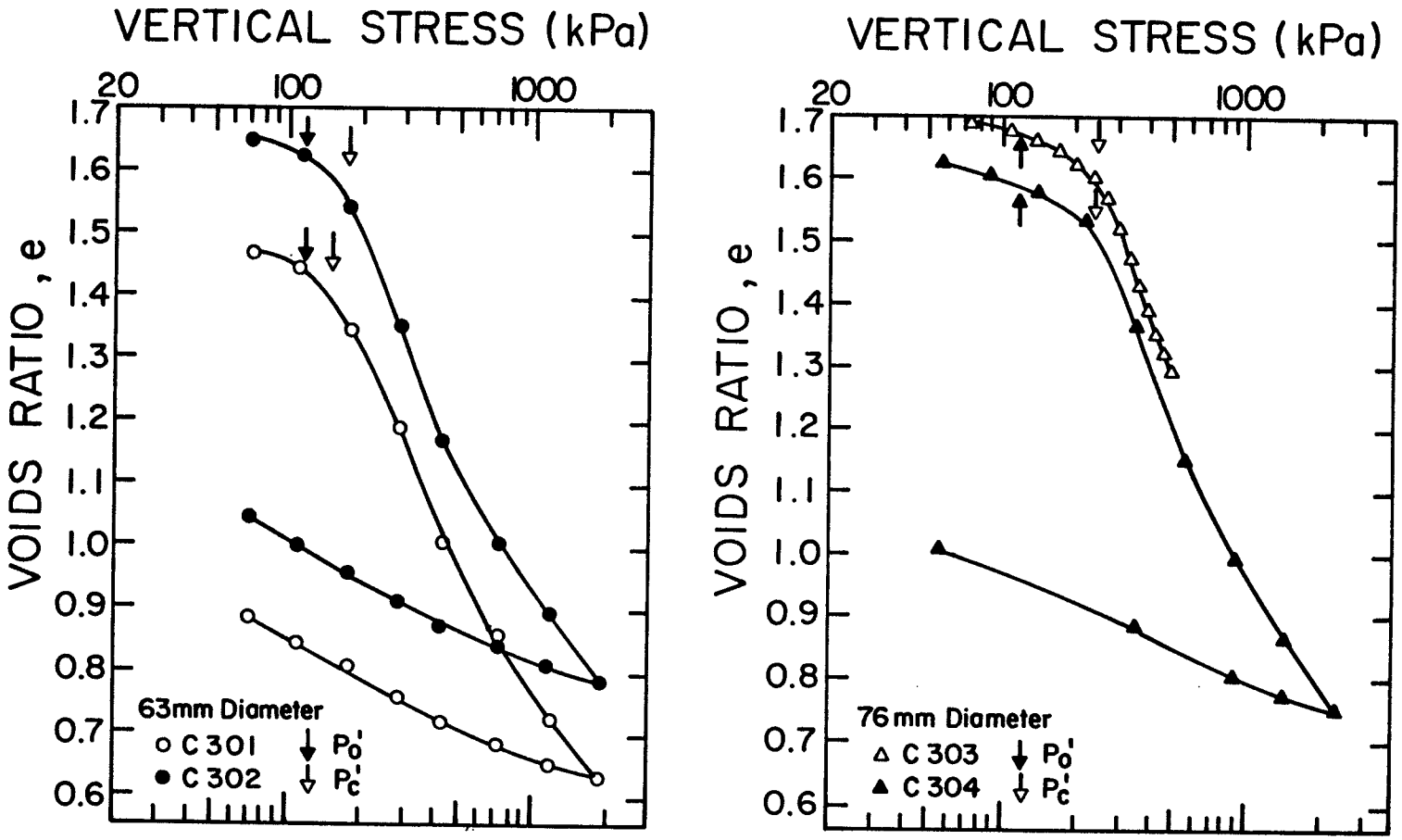

FIG. 4.3 OEDOMETER TESTS, e vs log σ_v' RESULTS

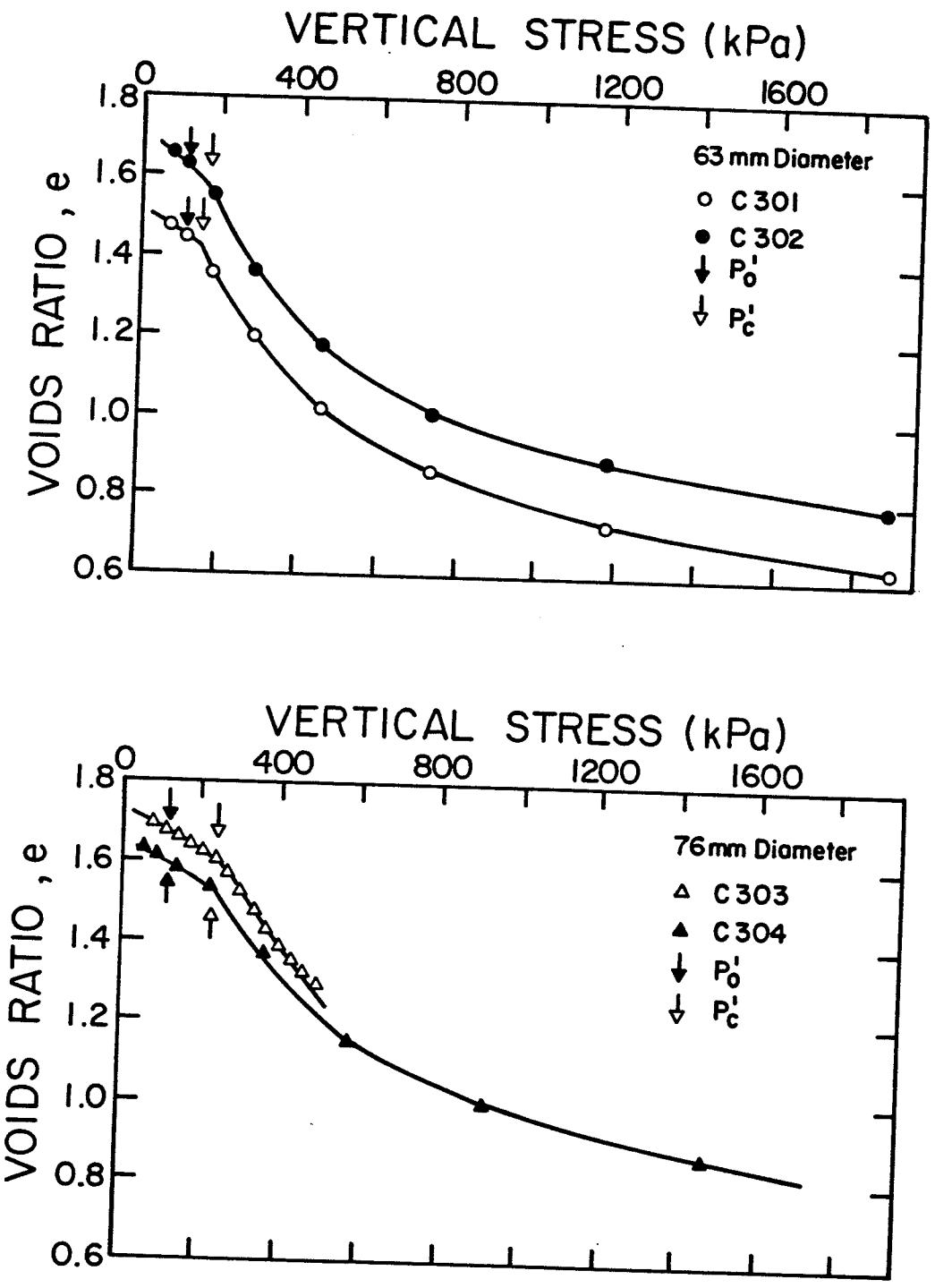

FIG. 4.4 OEDOMETER TESTS, e vs σ_v' RESULTS

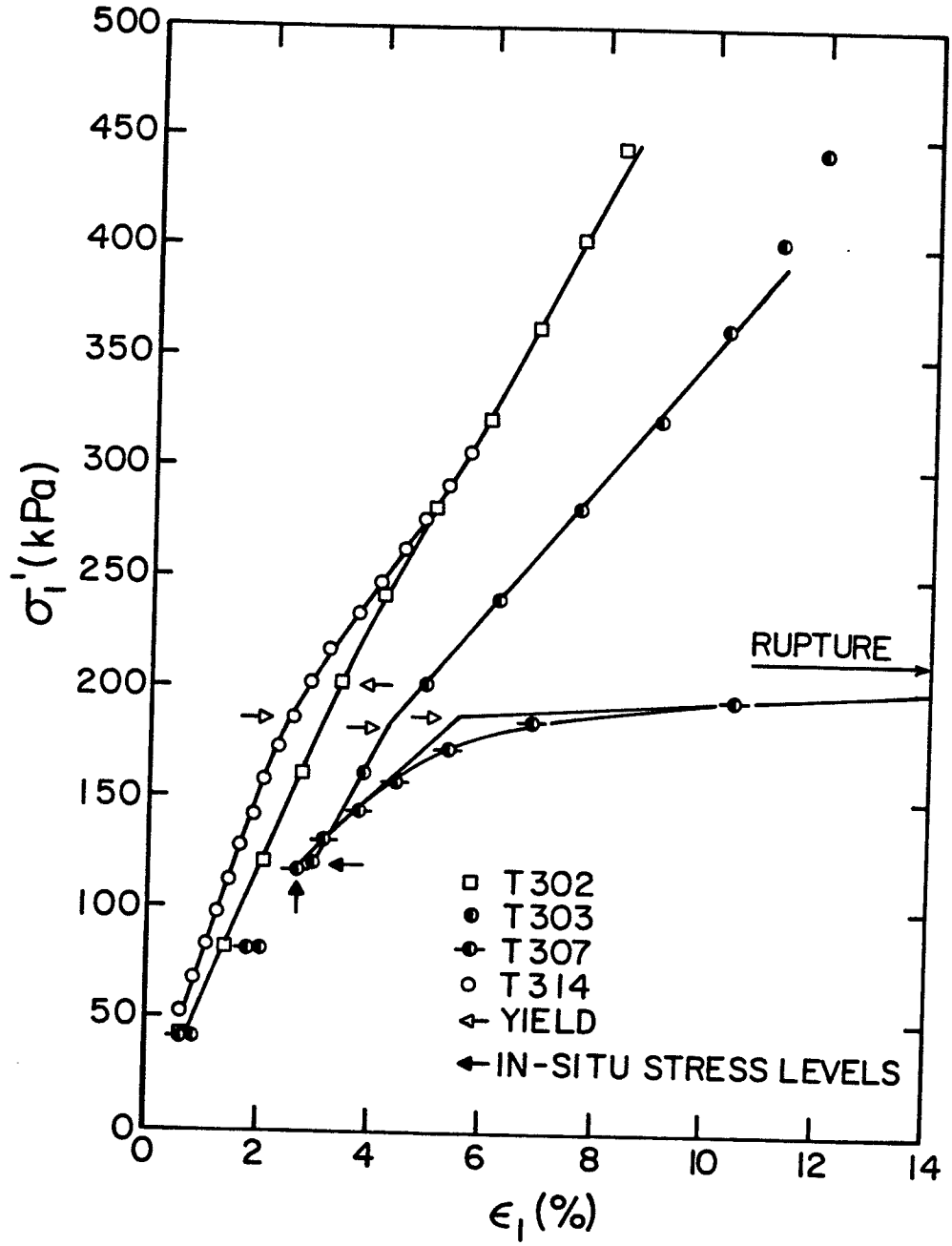

FIG. 4.5 YIELD DETERMINATION, σ_1' vs ε_1; T302,T303,T307,T314

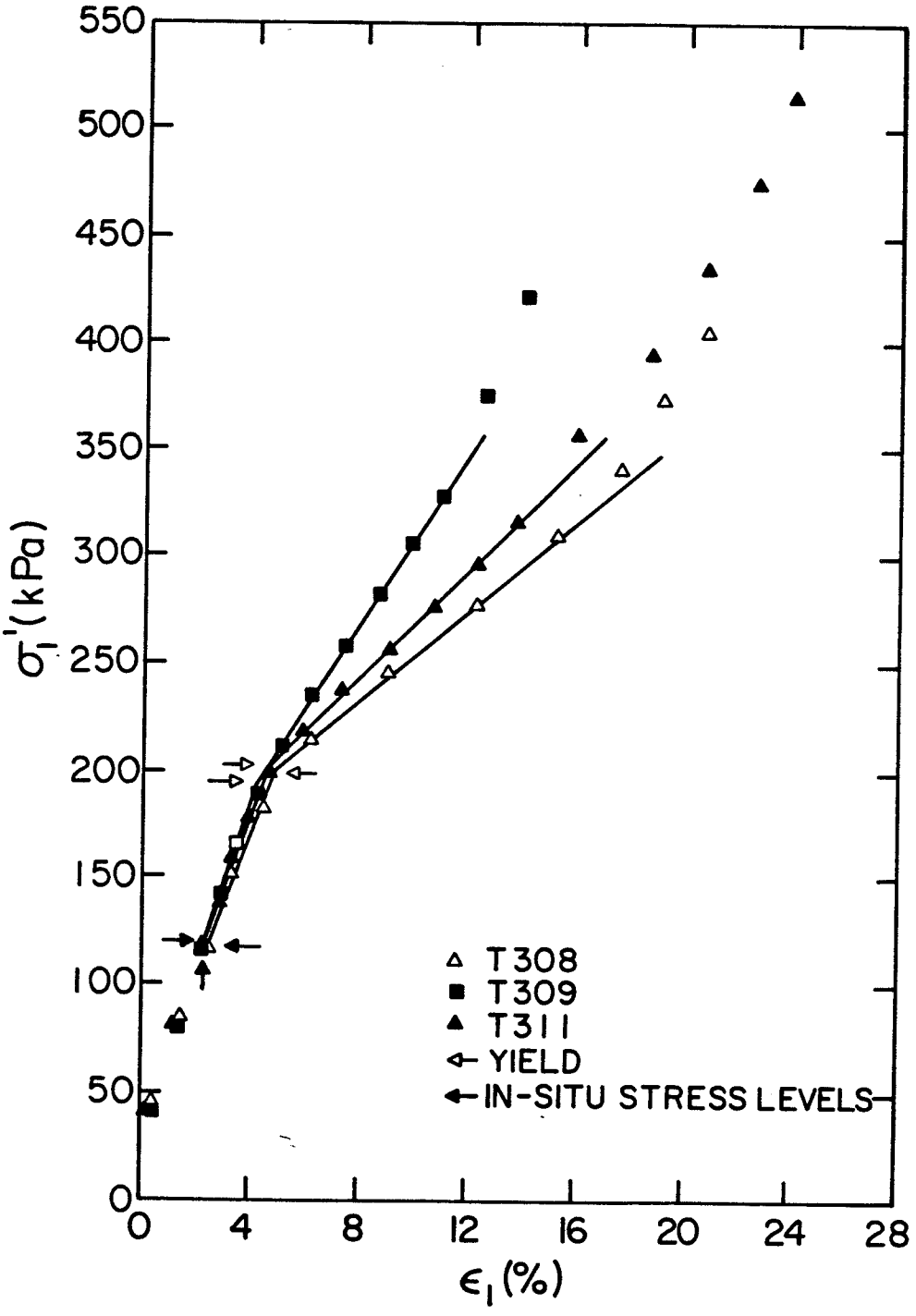

FIG. 4.6 YIELD DETERMINATION, σ_1' vs ε_1; T308,T309,T311

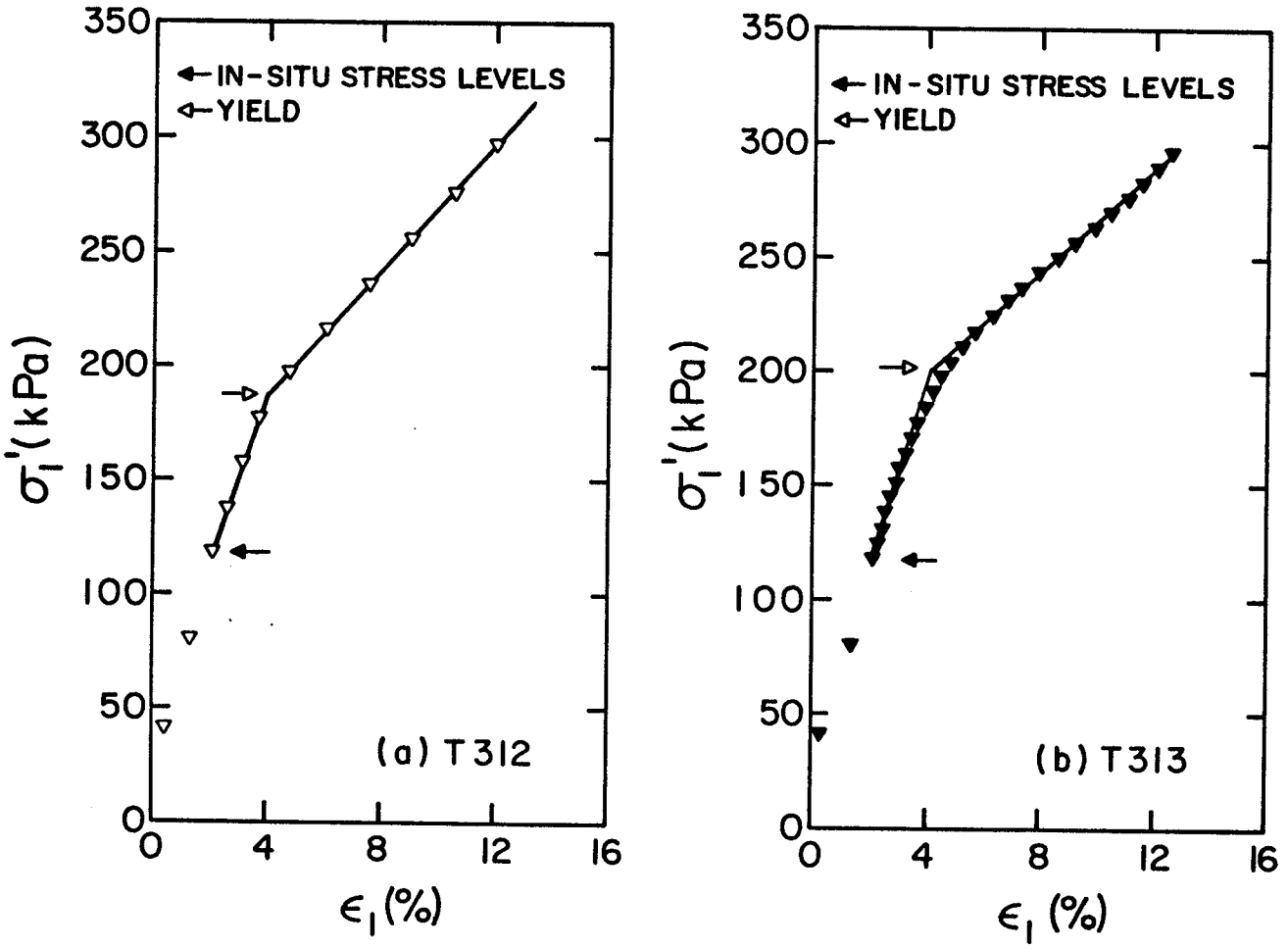

FIG. 4.7 YIELD DETERMINATION, σ_1' vs ϵ_1; T312,T313

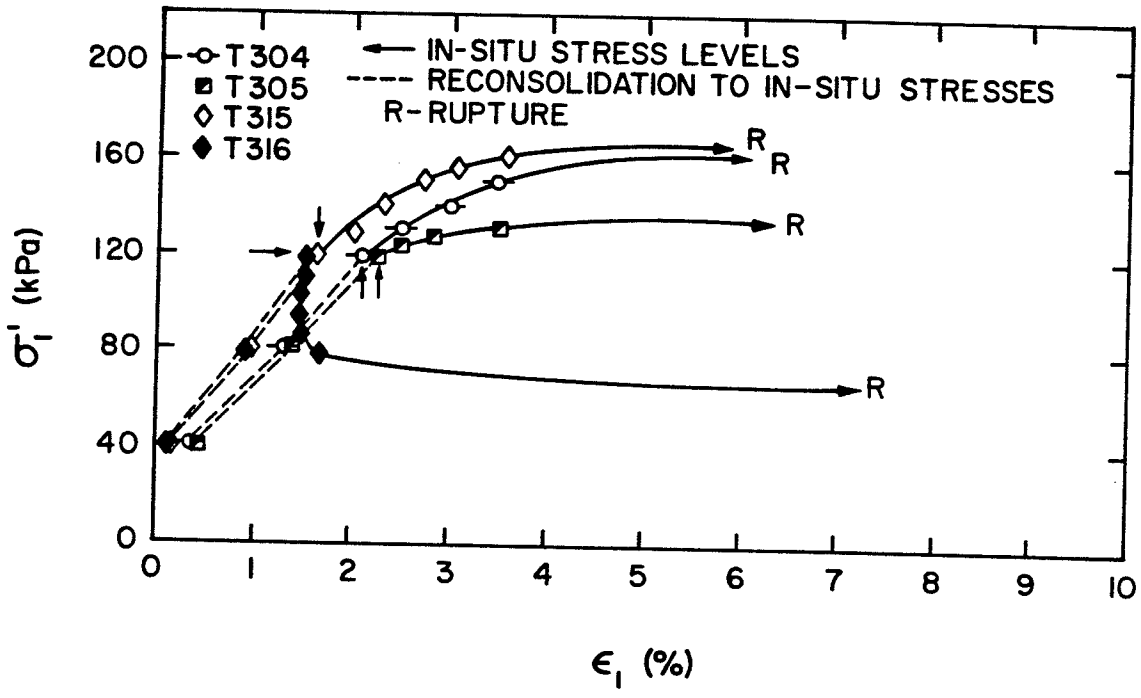

FIG. 4.8a YIELD DETERMINATION, σ_1' vs ε_1; T304,T305,T315,T316

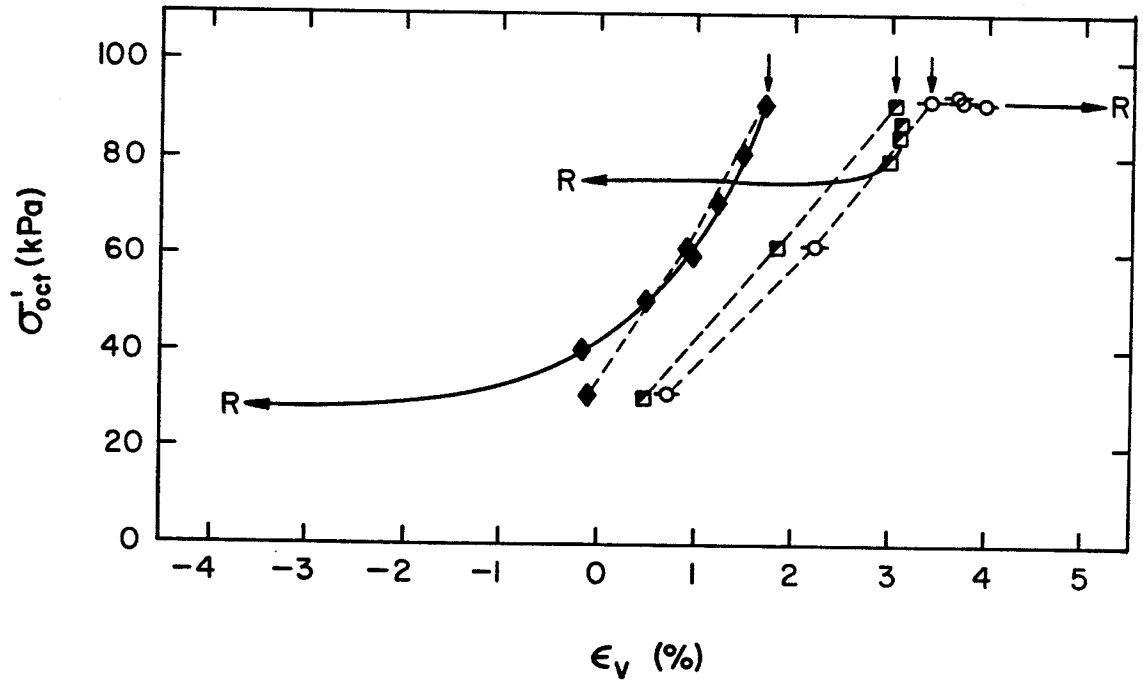

FIG. 4.8b YIELD DETERMINATION, σ_{oct}' vs ε_v

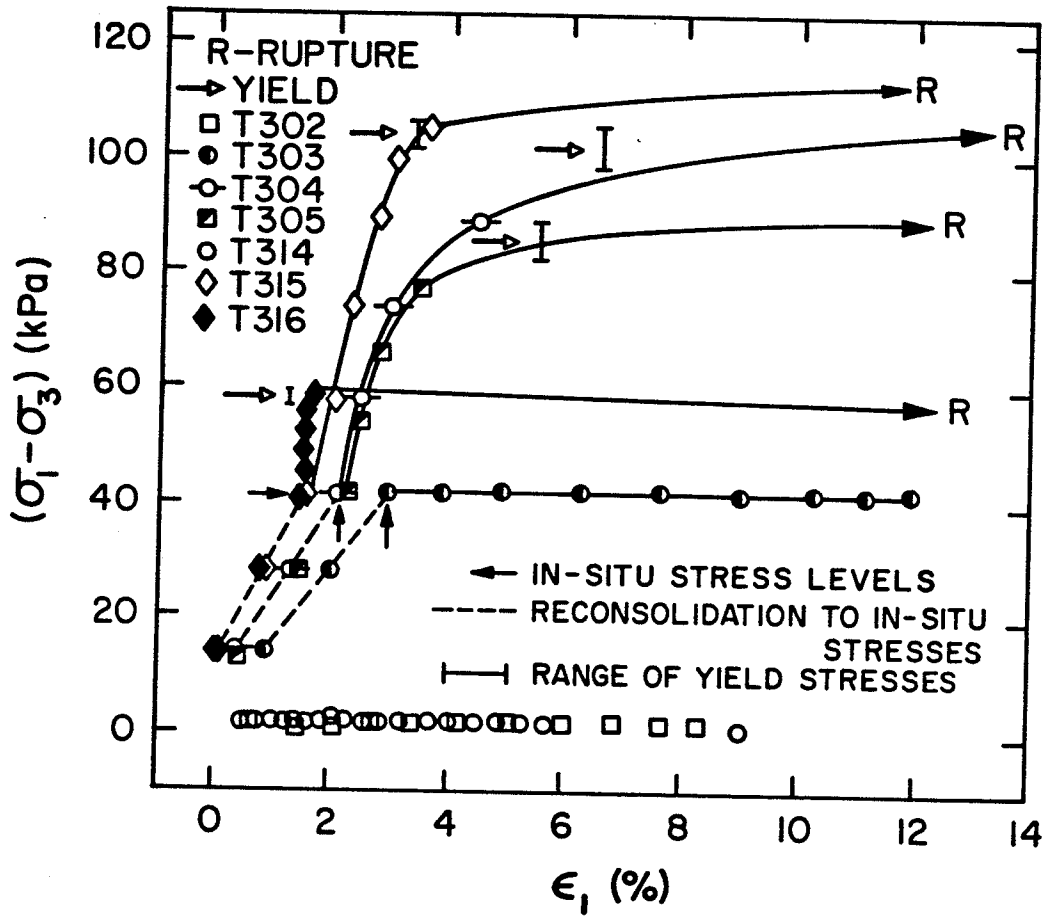

FIG. 4.9a YIELD DETERMINATION, $(\sigma_1-\sigma_3)$ vs ε_1; T302,T303,T304,T305,T314,T315,T316

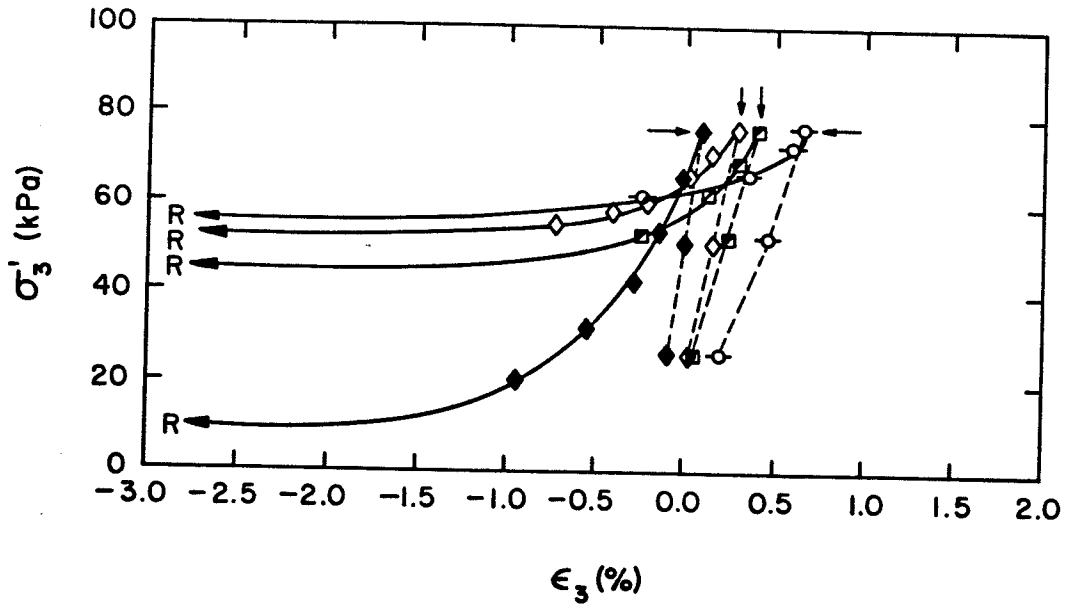

FIG. 4.9b YIELD DETERMINATION, σ_3' vs ε_3

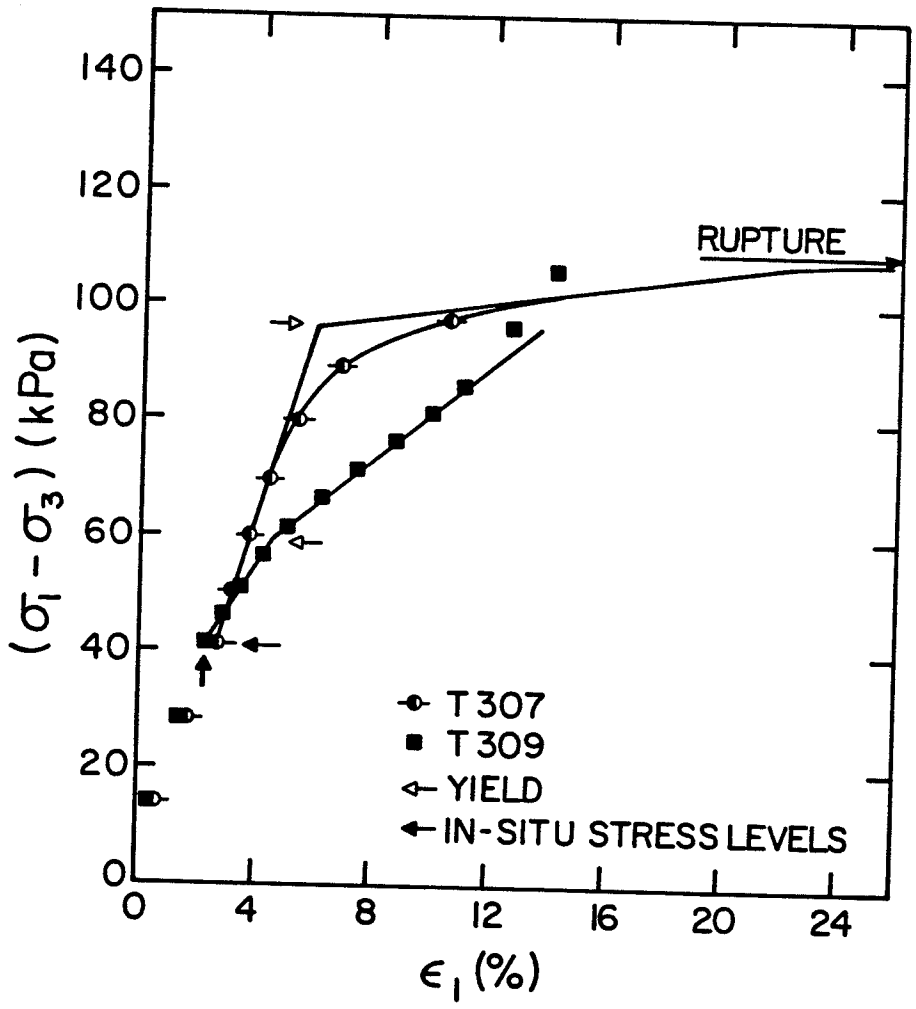

FIG. 4.10 YIELD DETERMINATION, $(\sigma_1-\sigma_3)$ vs ε_1; T307,T309

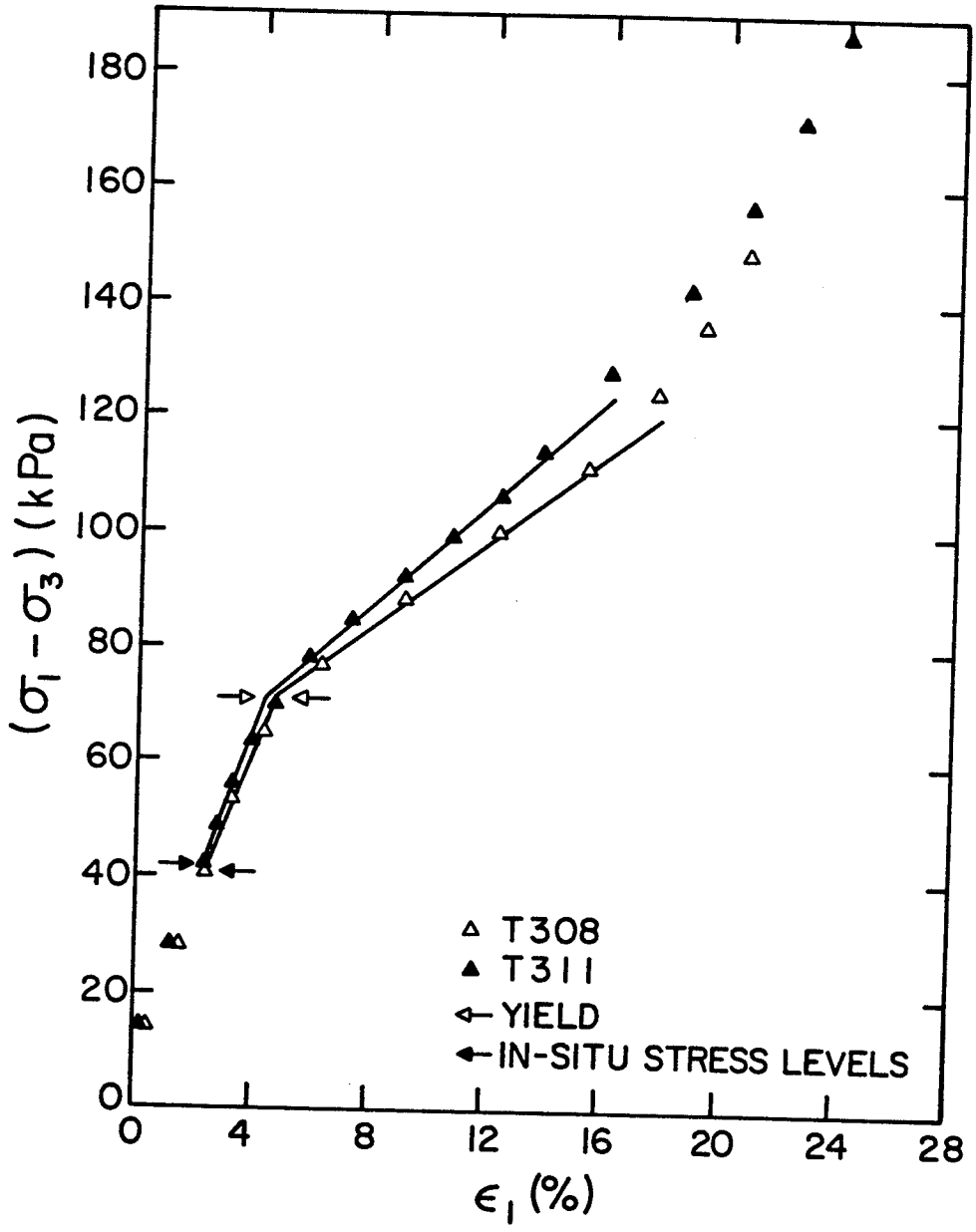

FIG. 4.11 YIELD DETERMINATION, $(\sigma_1-\sigma_3)$ vs ϵ_1; T308,T311

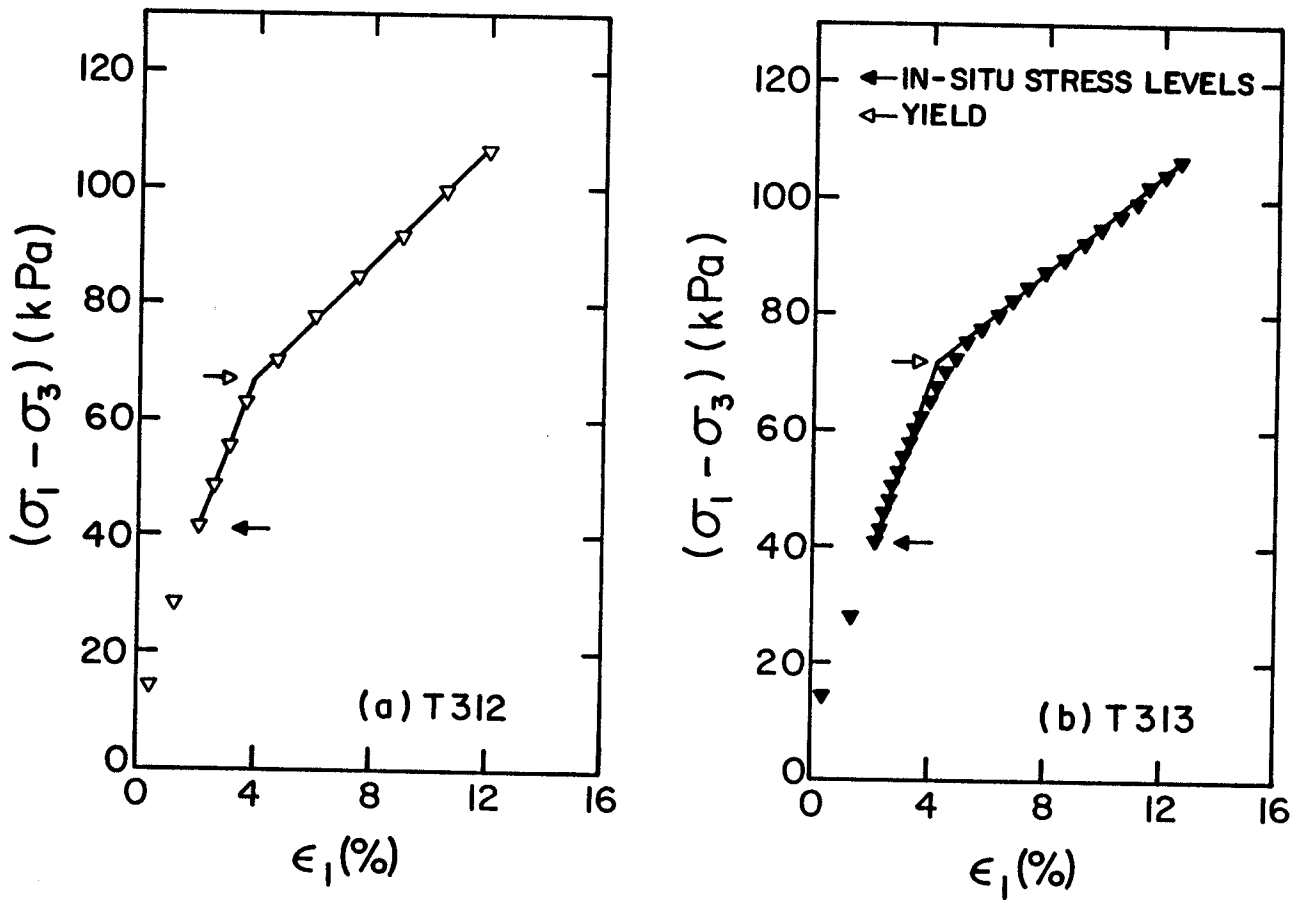

FIG. 4.12 YIELD DETERMINATION, $(\sigma_1-\sigma_3)$ vs ϵ_1; T312,T313

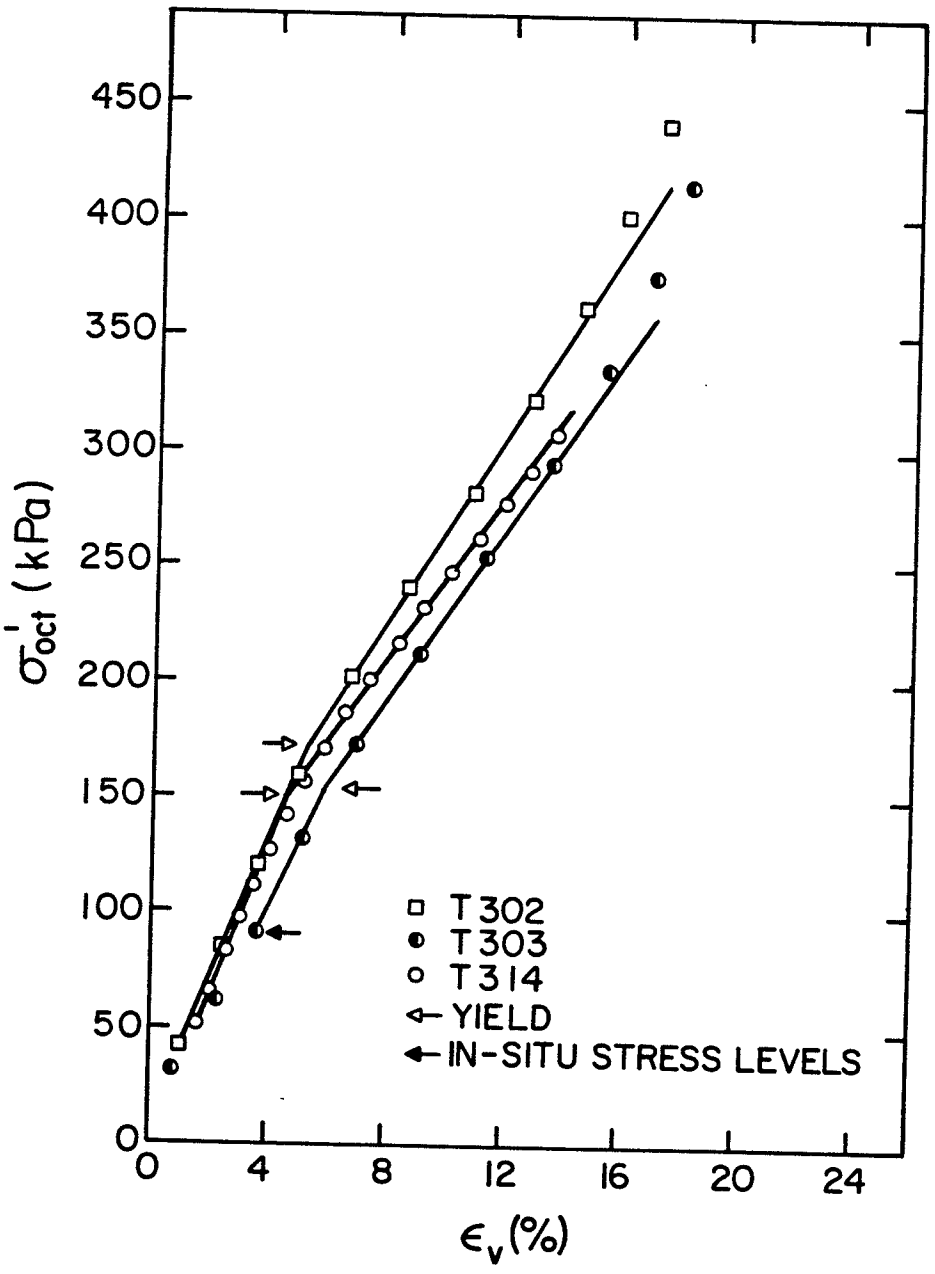

FIG. 4.13 YIELD DETERMINATION, σ'_{oct} vs ϵ_v; T302,T303,T314

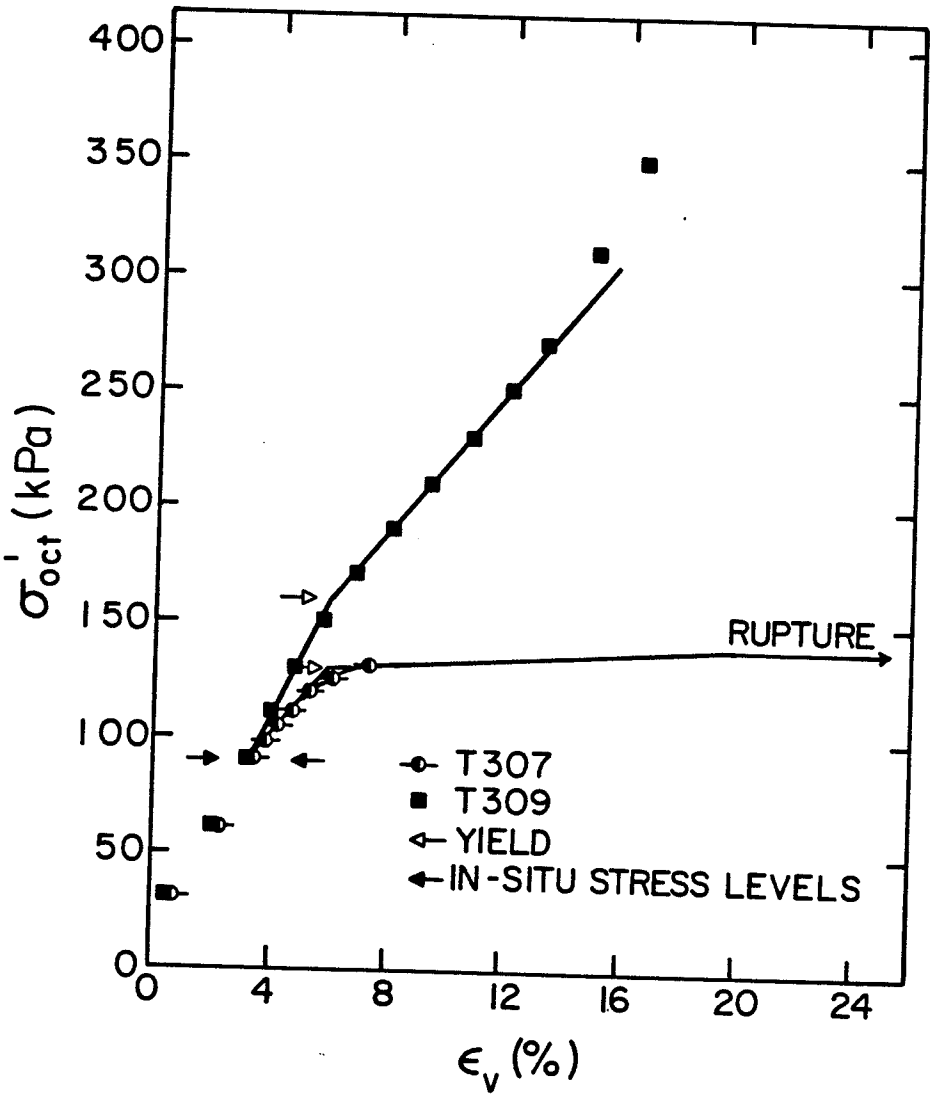

FIG. 4.14 YIELD DETERMINATION, σ'_{oct} vs ϵ_v; T307,T309

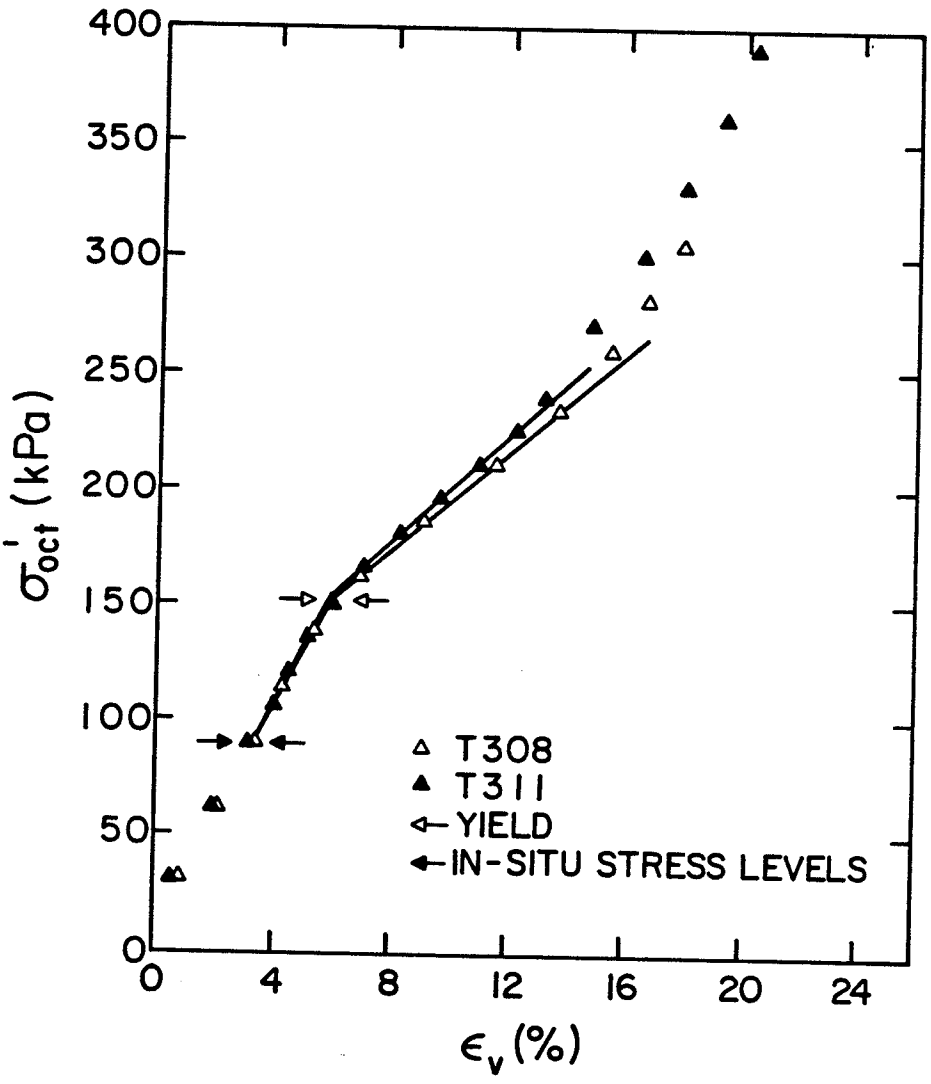

FIG. 4.15 YIELD DETERMINATION, σ'_{oct} vs ϵ_v; T308,T311

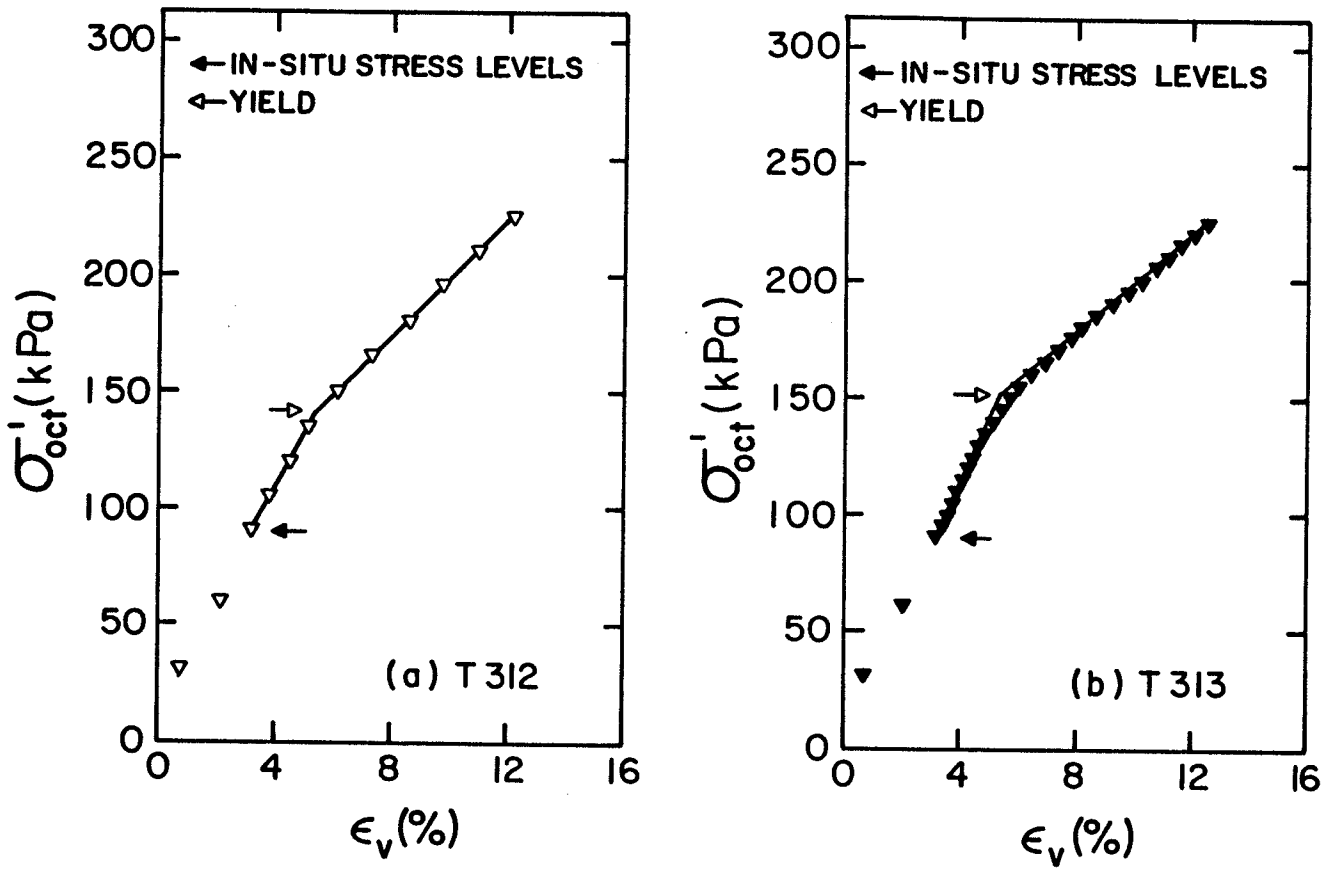

FIG. 4.16 YIELD DETERMINATION, σ'_{oct} vs ϵ_v; T312,T313

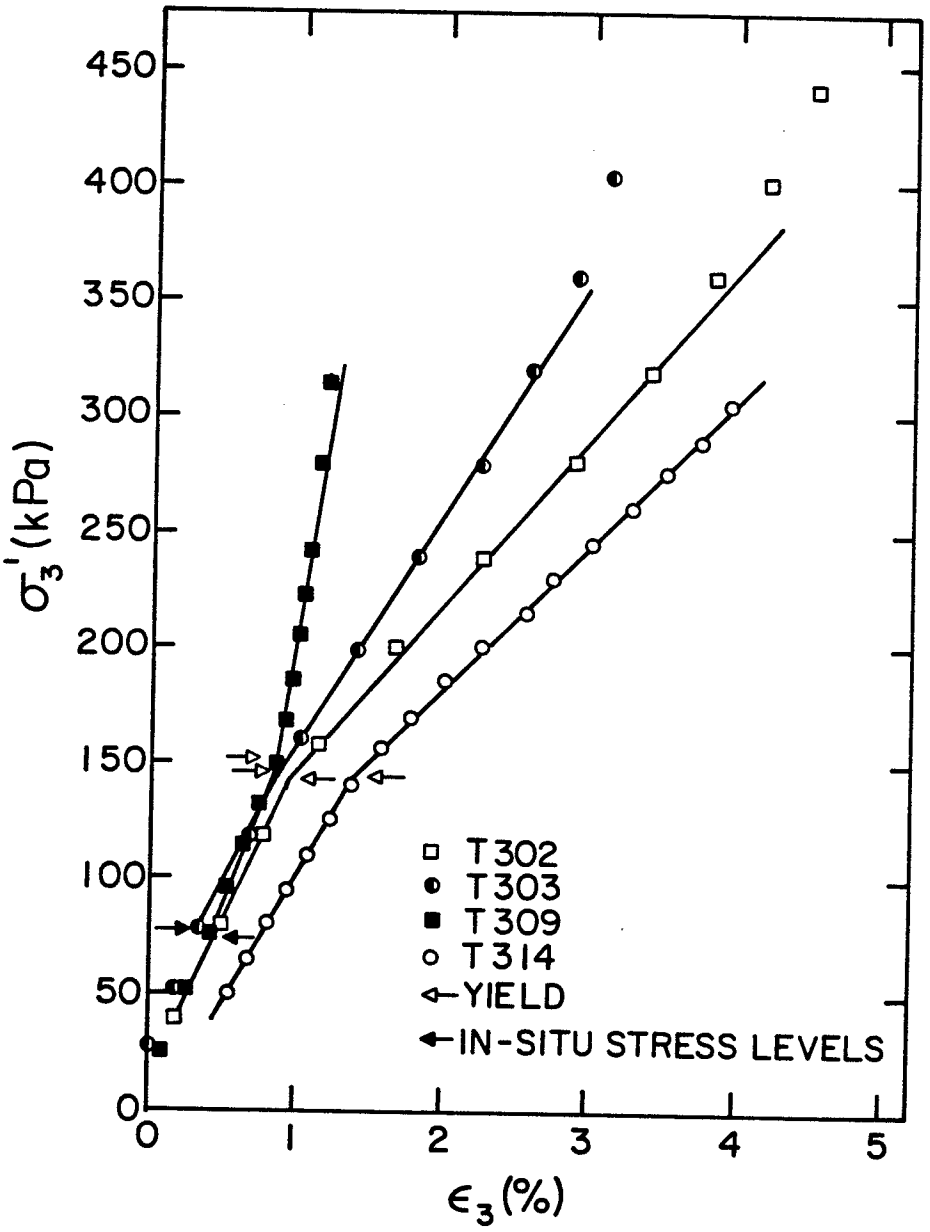

FIG. 4.17 YIELD DETERMINATION, σ_3' vs ϵ_3; T302, T303,T309,T314

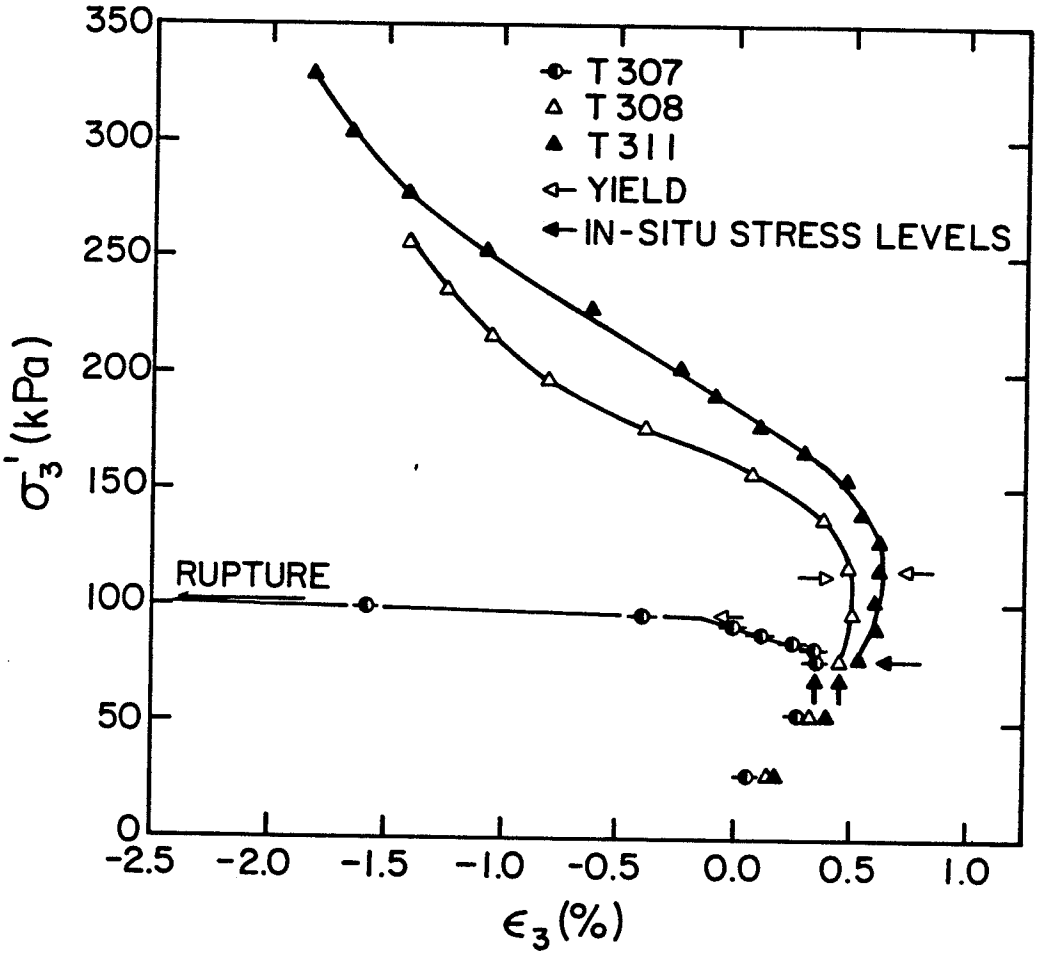

FIG. 4.18 YIELD DETERMINATION, σ_3' vs ε_3; T307,T308,T311

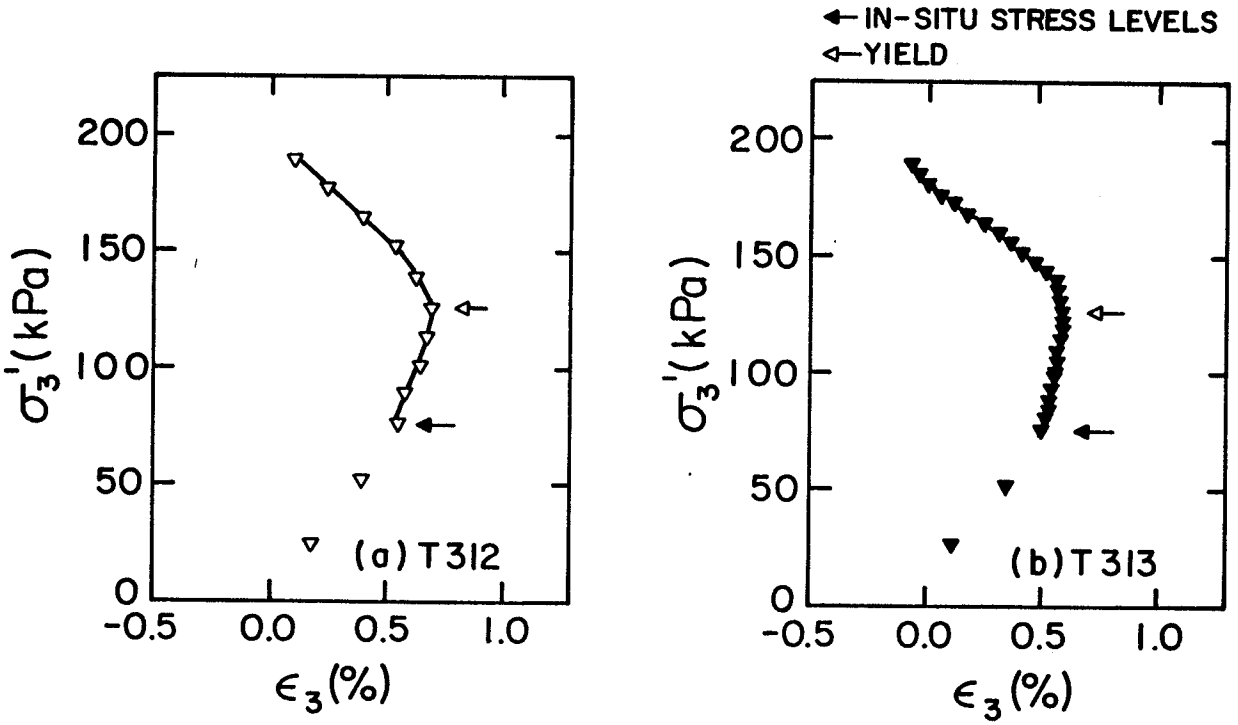

FIG. 4.19 YIELD DETERMINATION, σ_3' vs ϵ_3; T312,T313

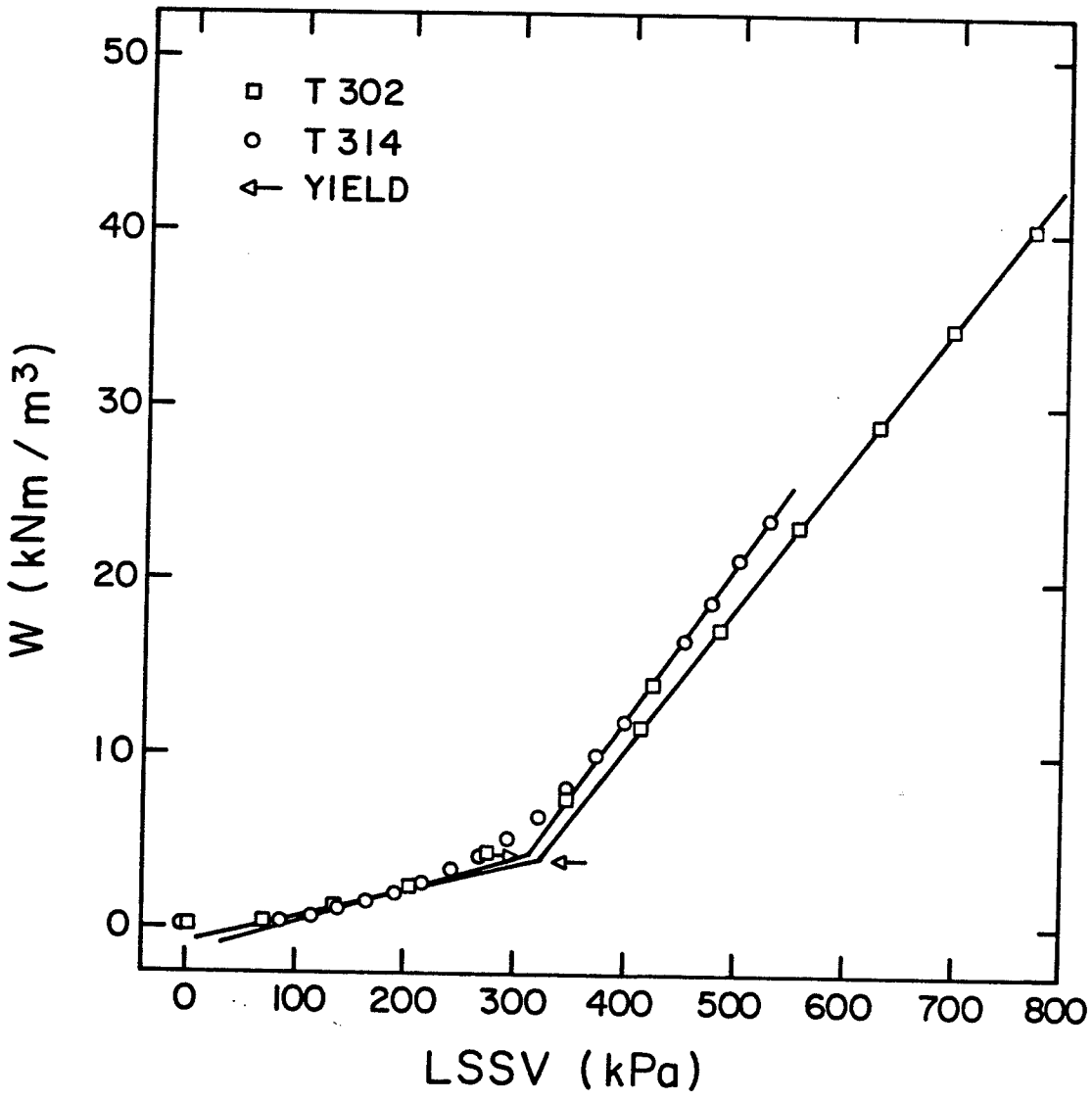

FIG. 4.20 YIELD DETERMINATION, W vs LSSV; T302,T314

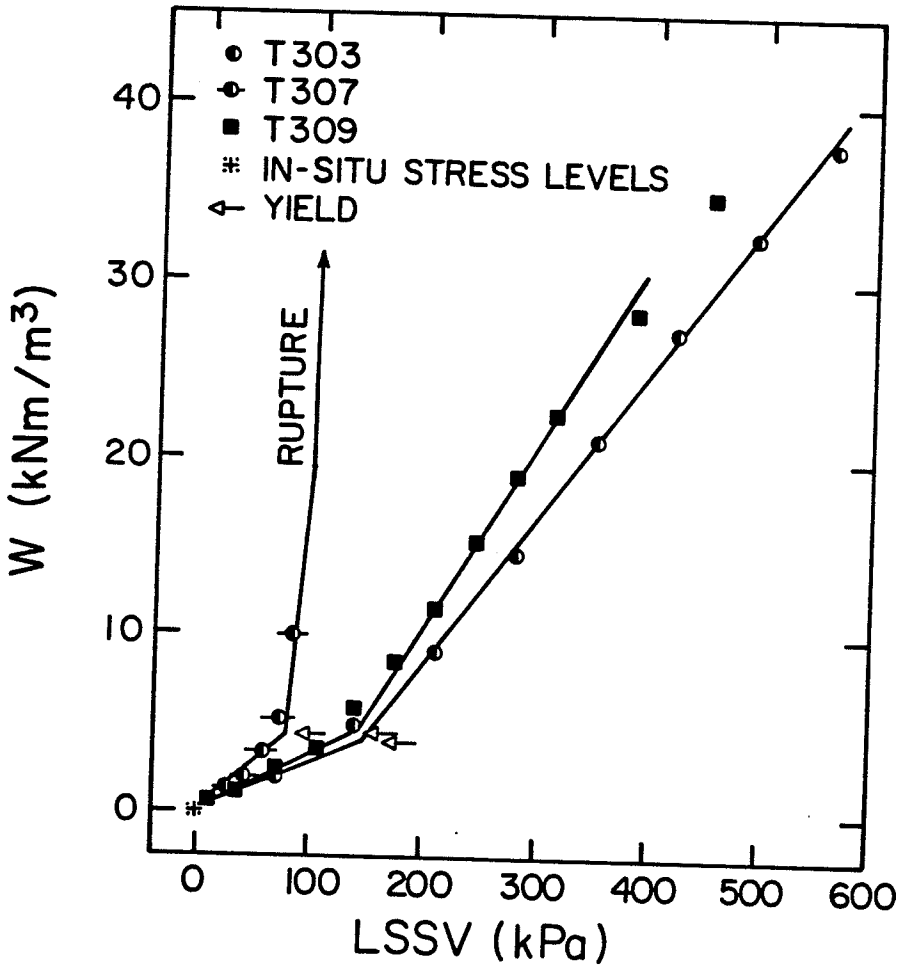

FIG. 4.21 YIELD DETERMINATION, W vs LSSV; T303,T307,T309

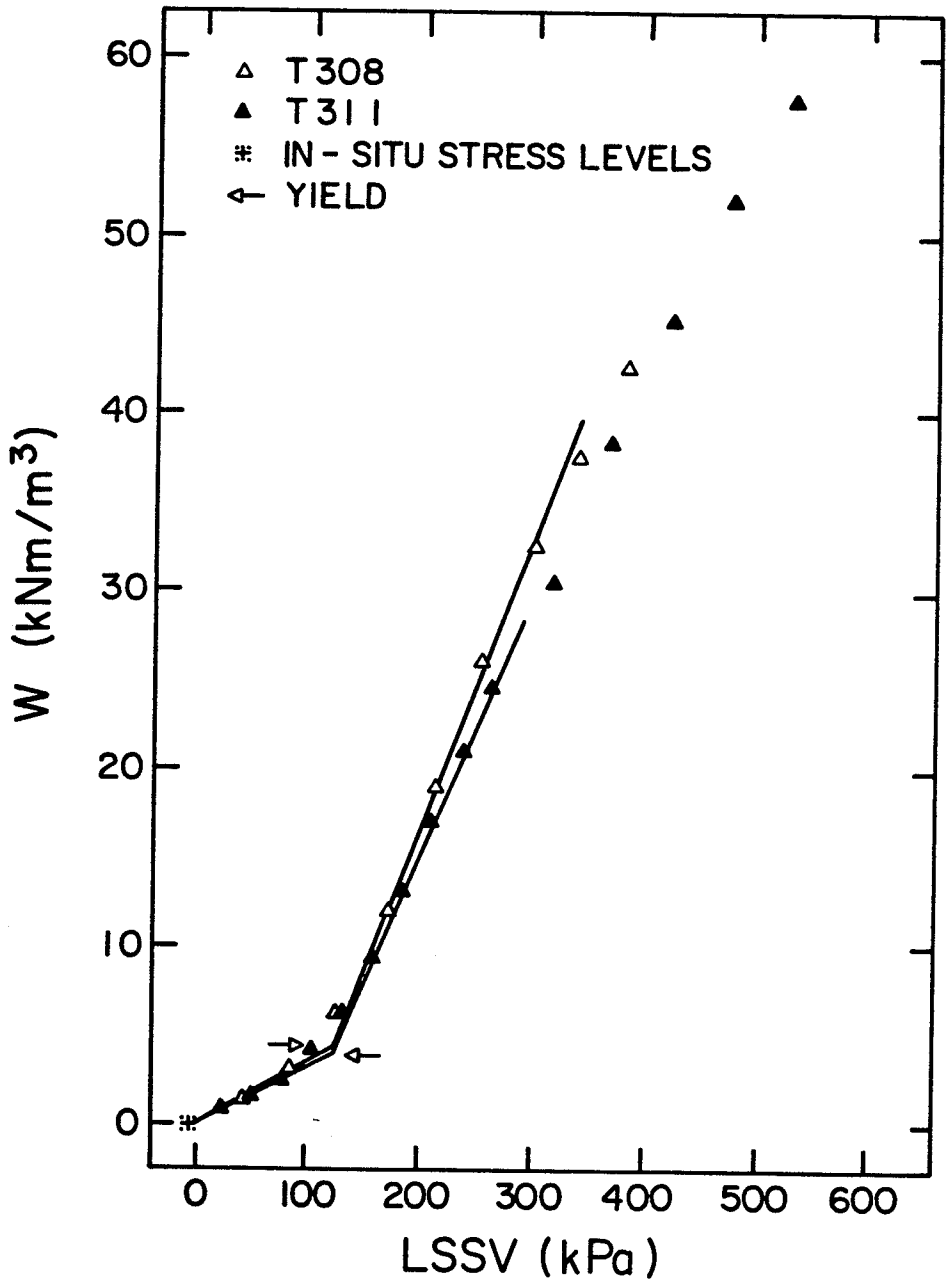

FIG. 4.22 YIELD DETERMINATION, W vs LSSV; T308,T311

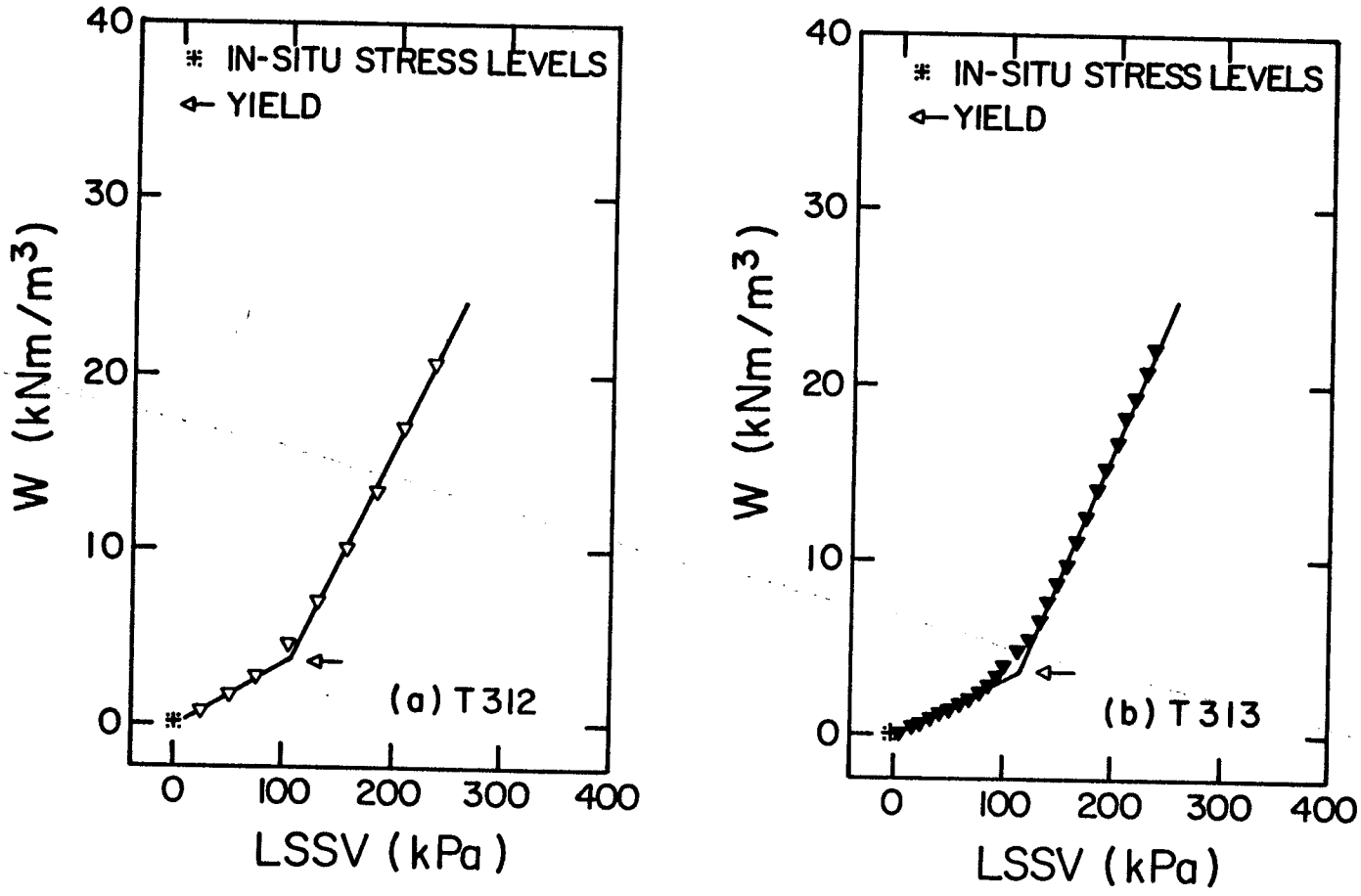

FIG. 4.23 YIELD DETERMINATION, W vs LSSV; T312,T313

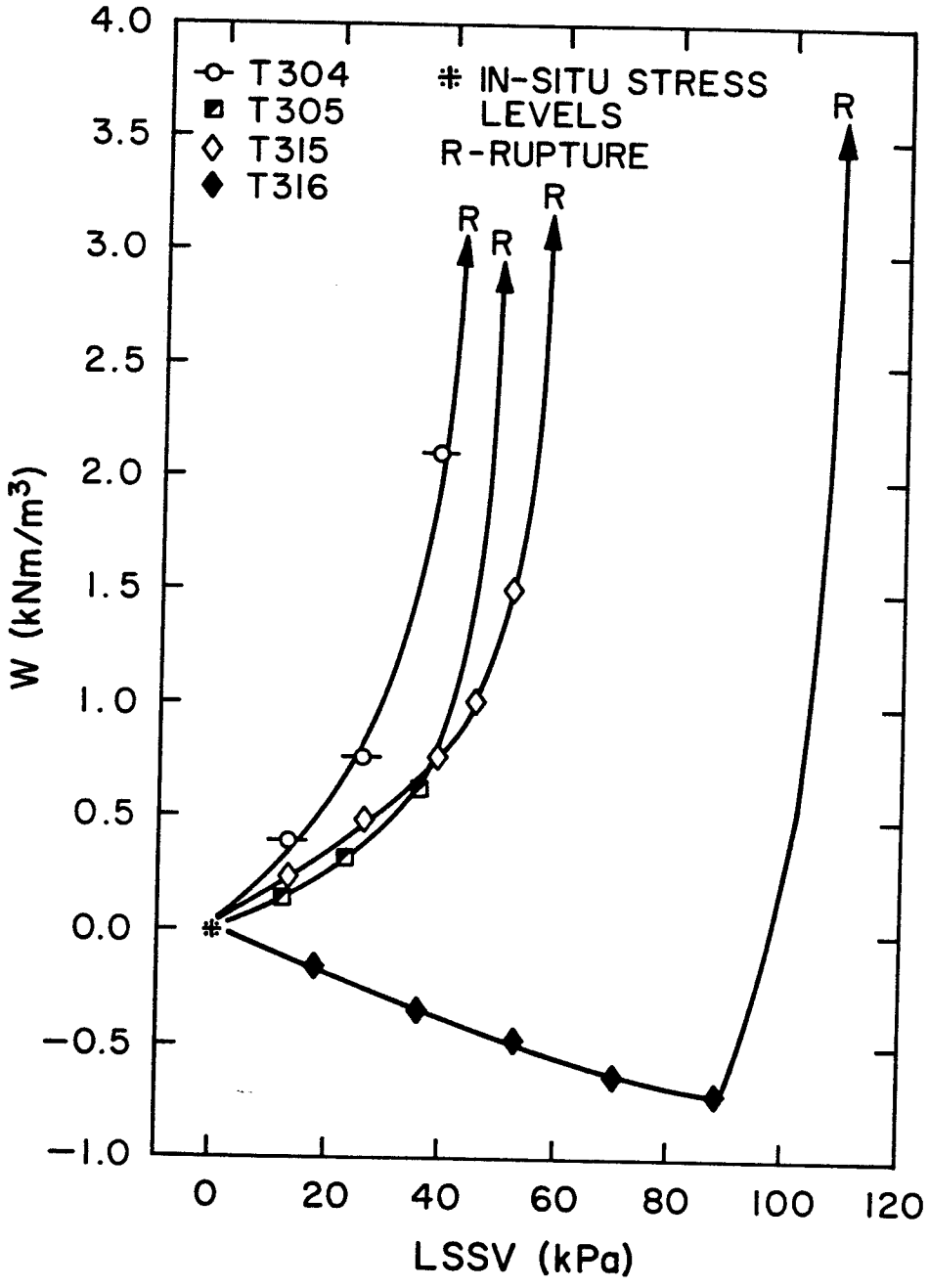

FIG. 4.24 YIELD DETERMINATION, W vs LSSV, T304,T305,T315,T316

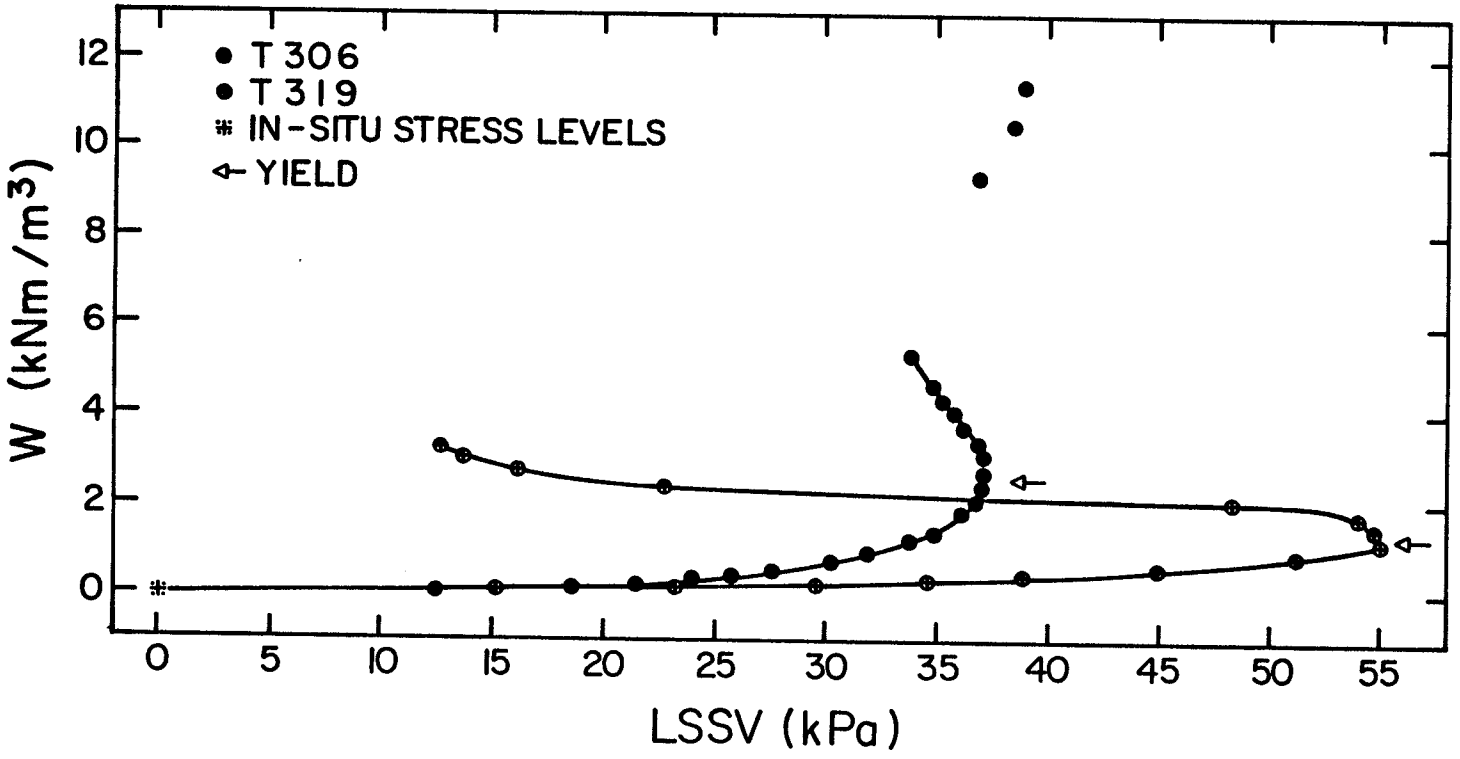

FIG. 4.25 YIELD DETERMINATION, W vs LSSV; T306,T319

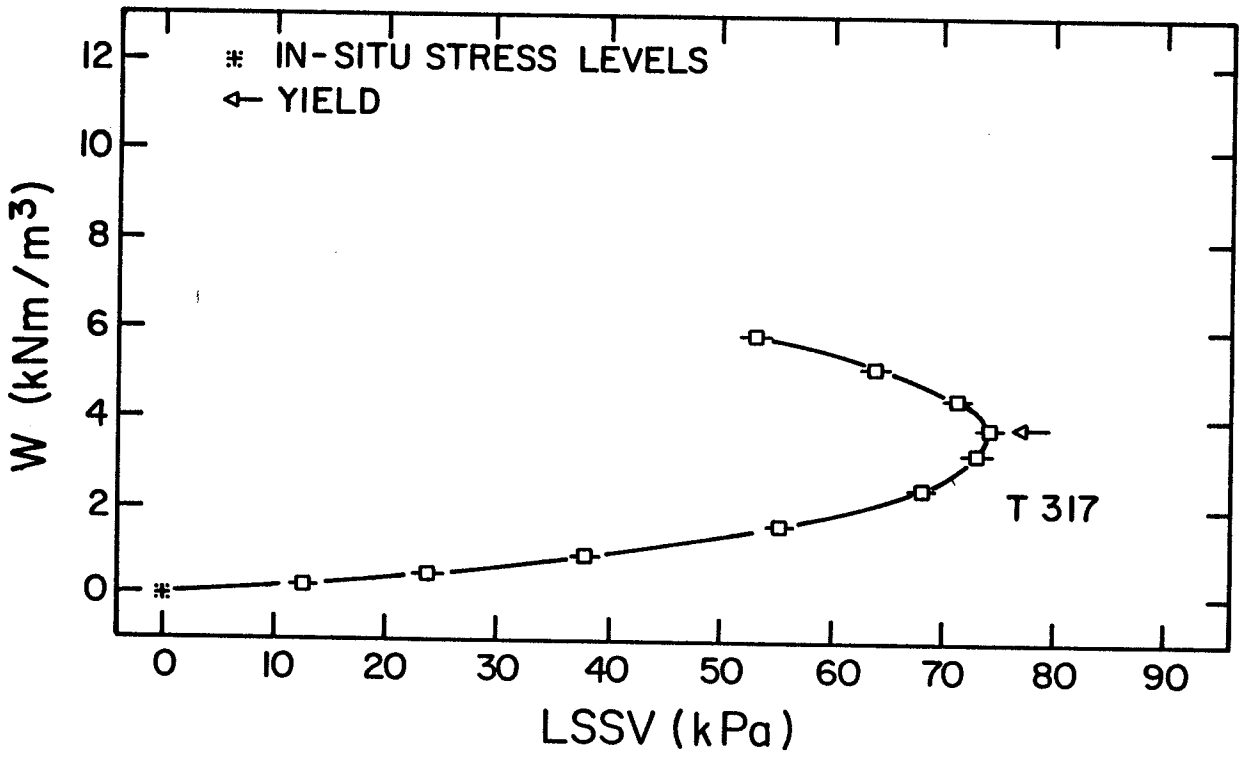

FIG. 4.26 YIELD DETERMINATION, W vs LSSV; T317

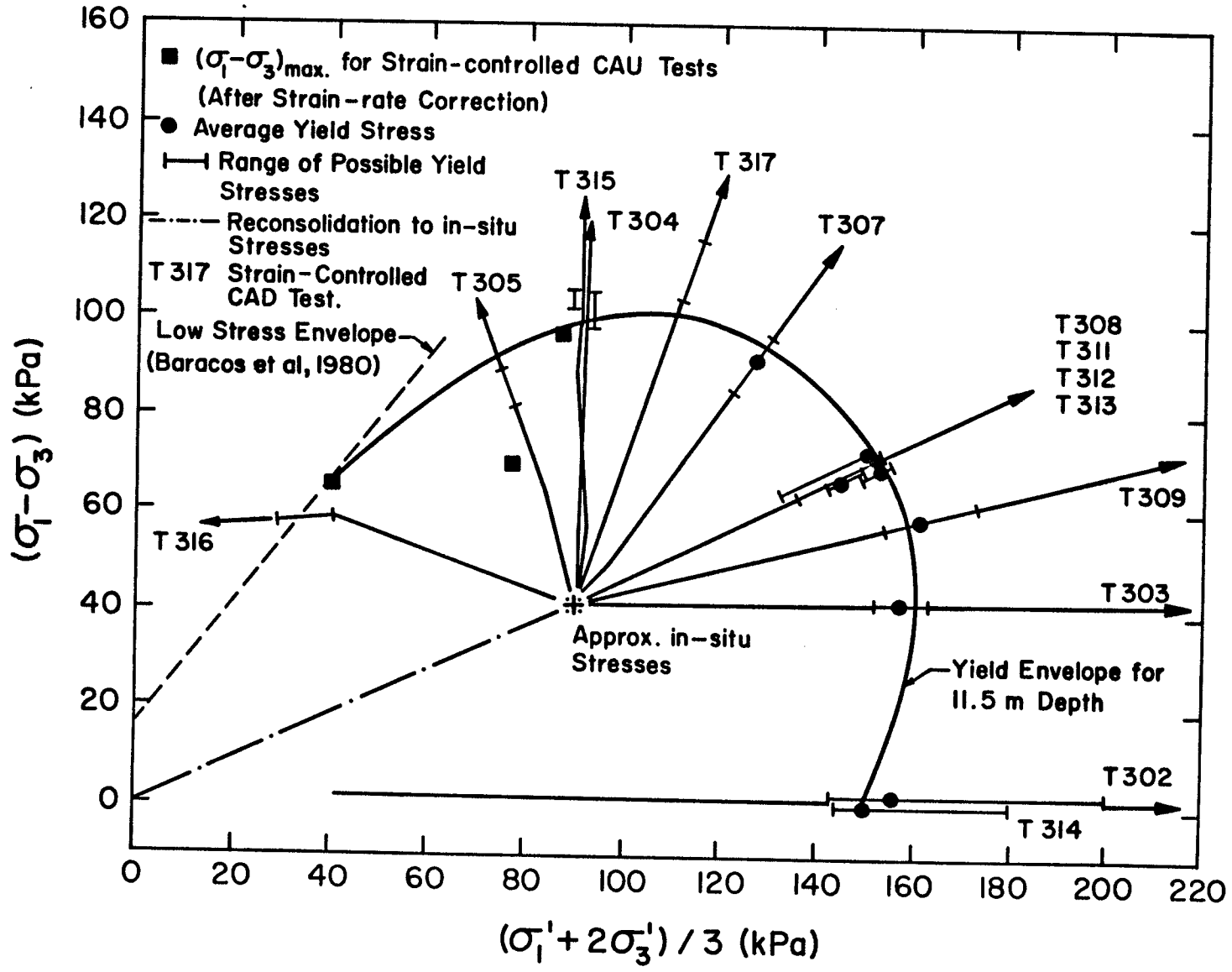

FIG. 4.27 YIELD ENVELOPE FROM TESTS ON CLAYS FROM 11.5 m

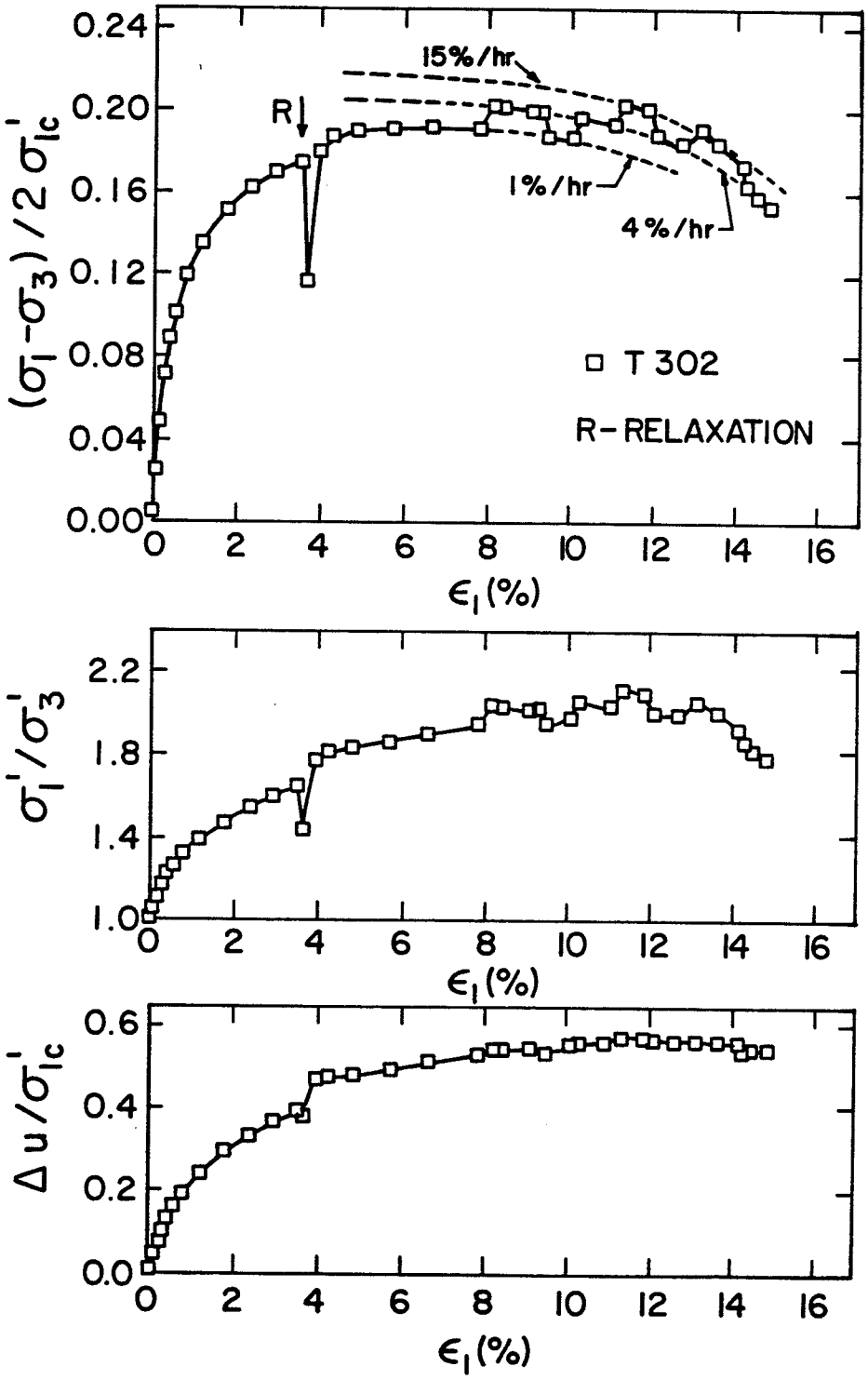

FIG. 5.1 UNDRAINED STRESS-STRAIN-POREWATER PRESSURE RESULTS, T302

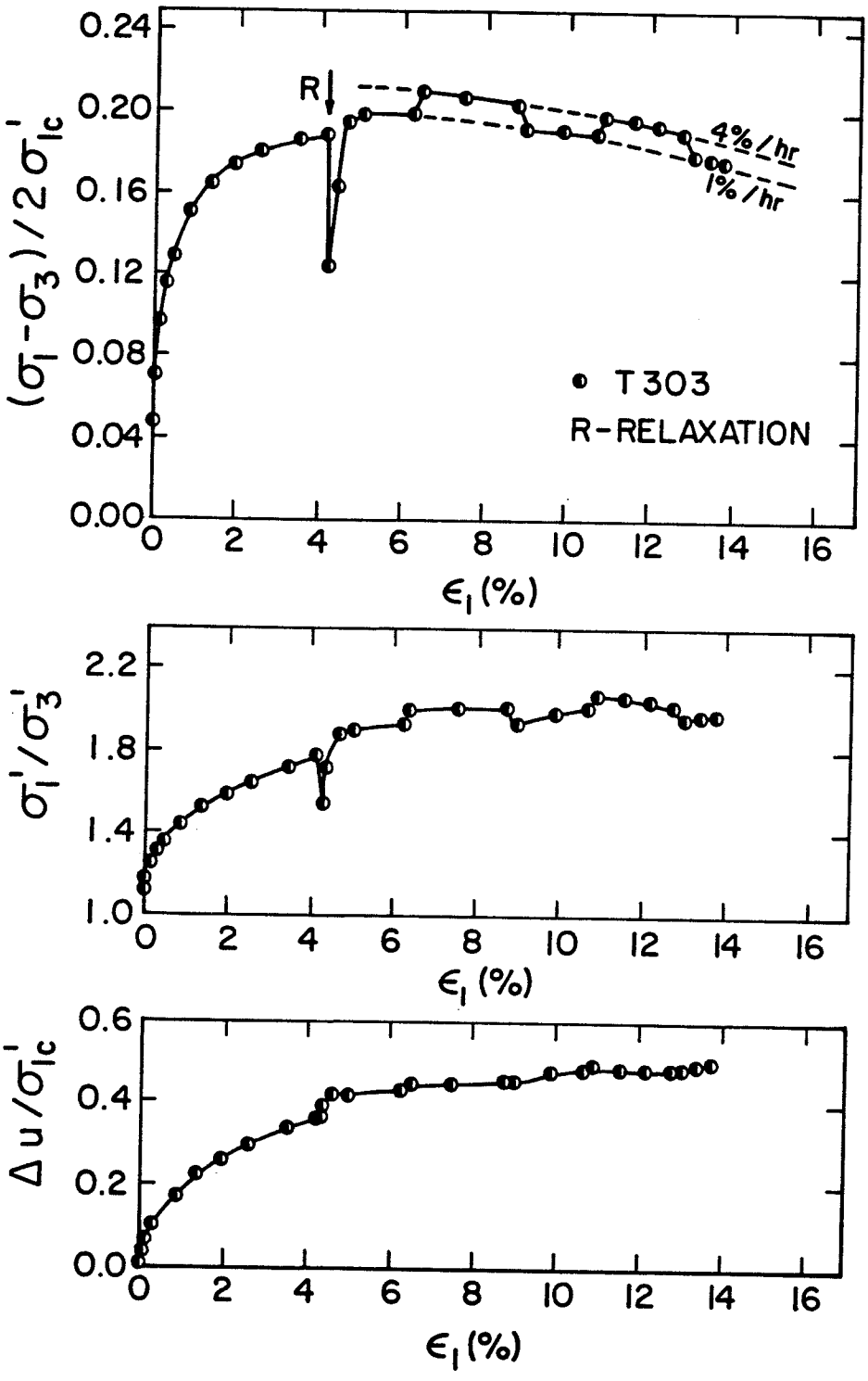

FIG. 5.2 UNDRAINED STRESS-STRAIN-POREWATER PRESSURE RESULTS, T303

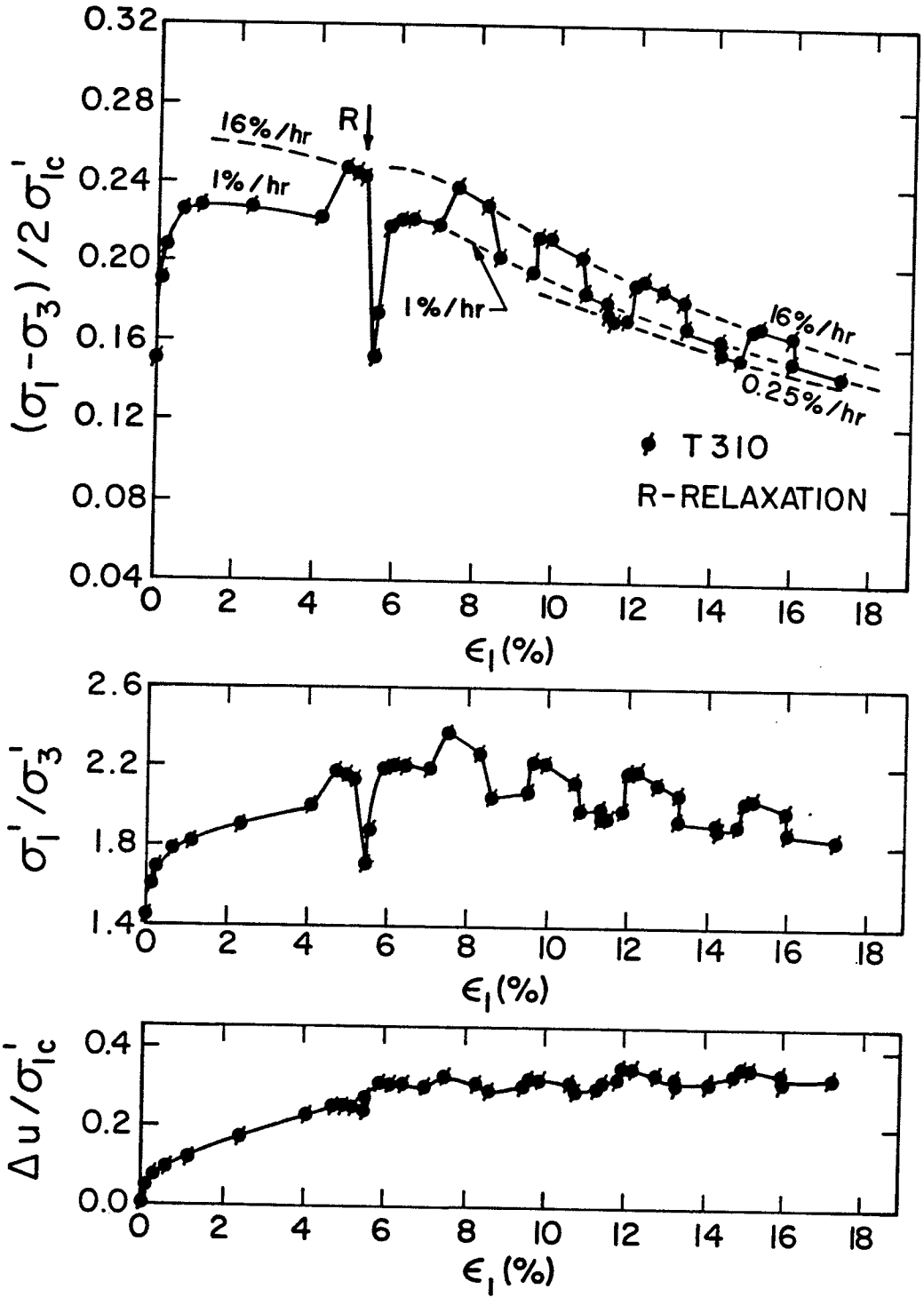

FIG. 5.3 UNDRAINED STRESS-STRAIN-POREWATER PRESSURE RESULTS, T310

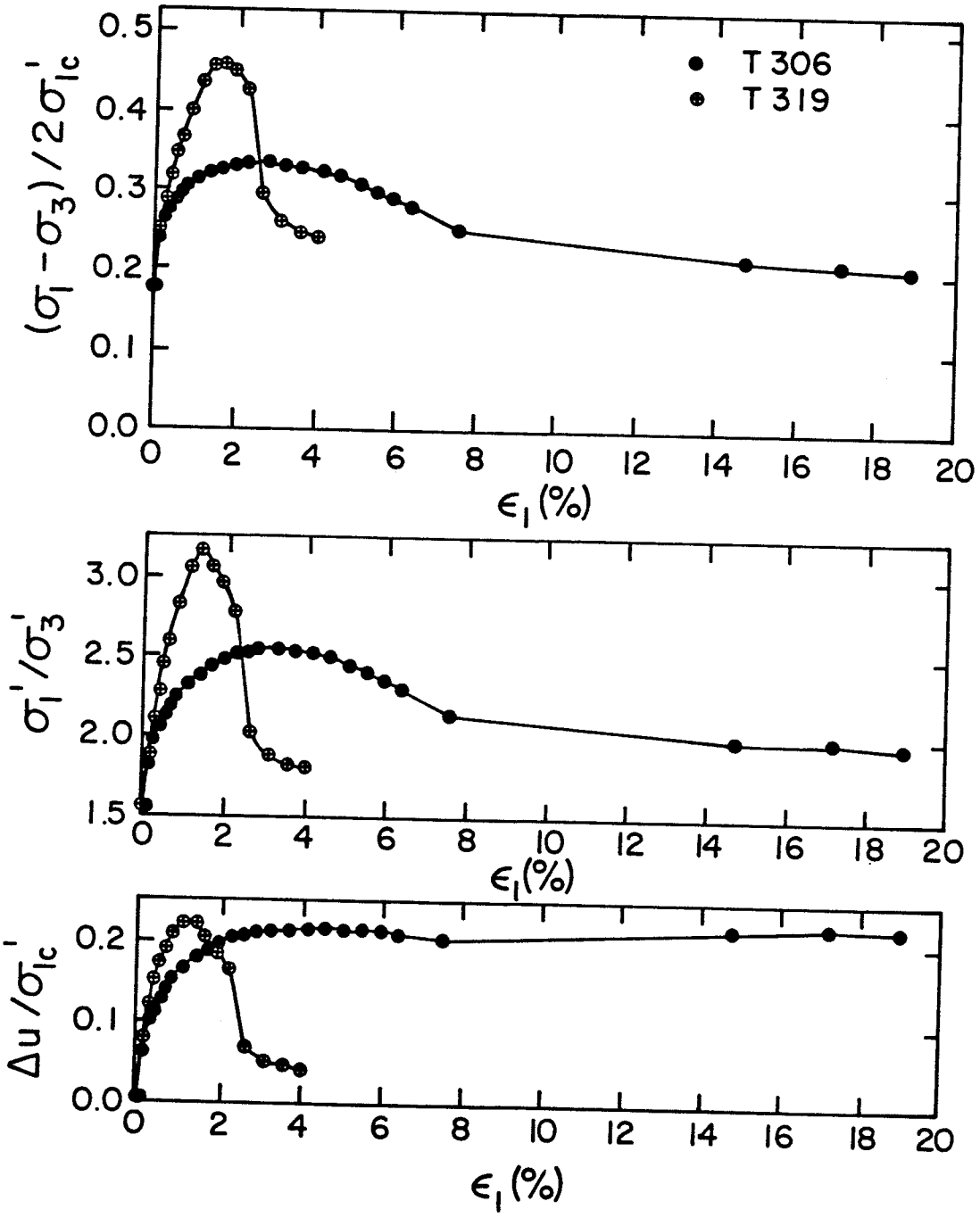

FIG. 5.4 UNDRAINED STRESS-STRAIN-POREWATER PRESSURE RESULTS, T306,T319

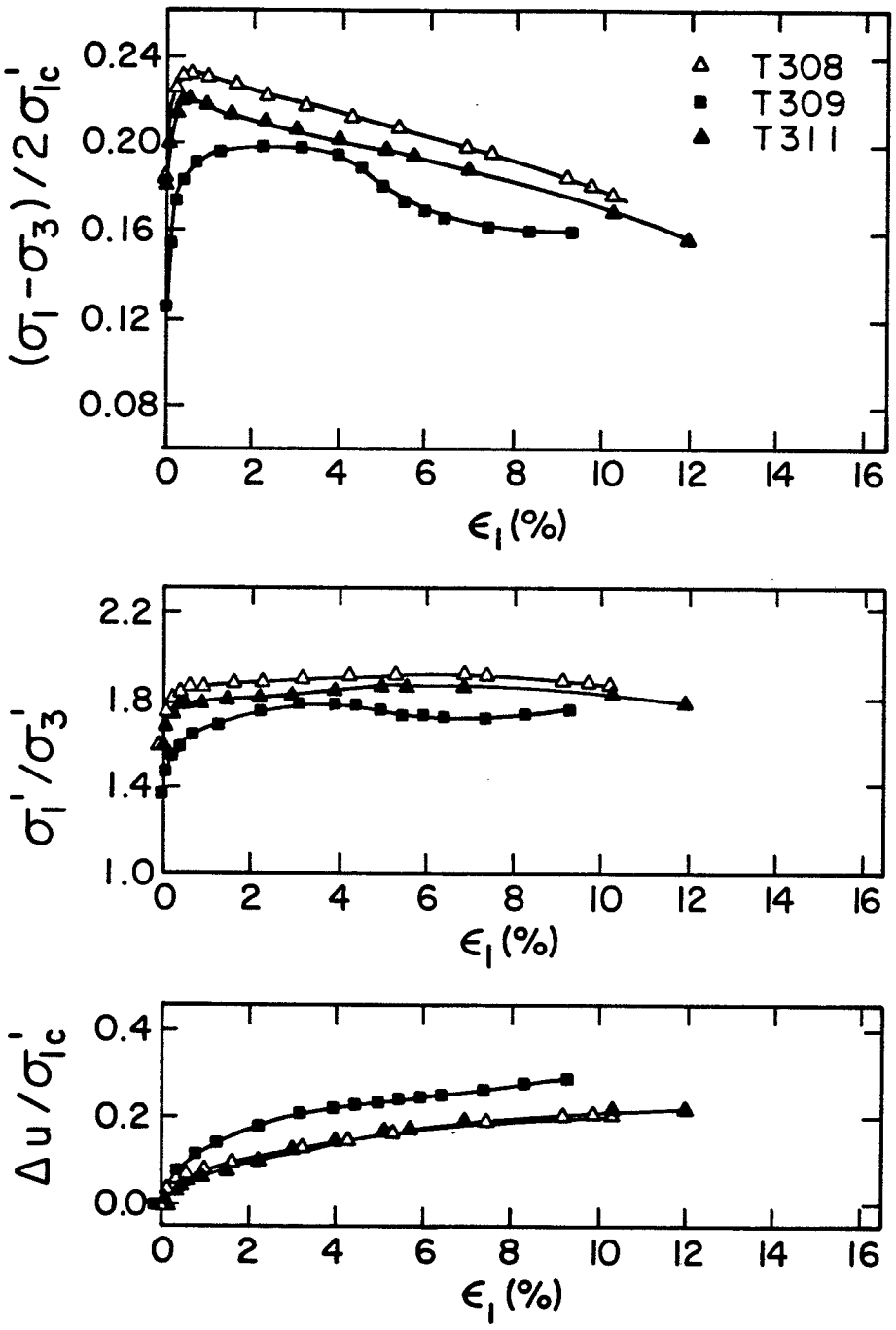

FIG. 5.5 UNDRAINED STRESS-STRAIN-POREWATER PRESSURE RESULTS, T308,T309,T311

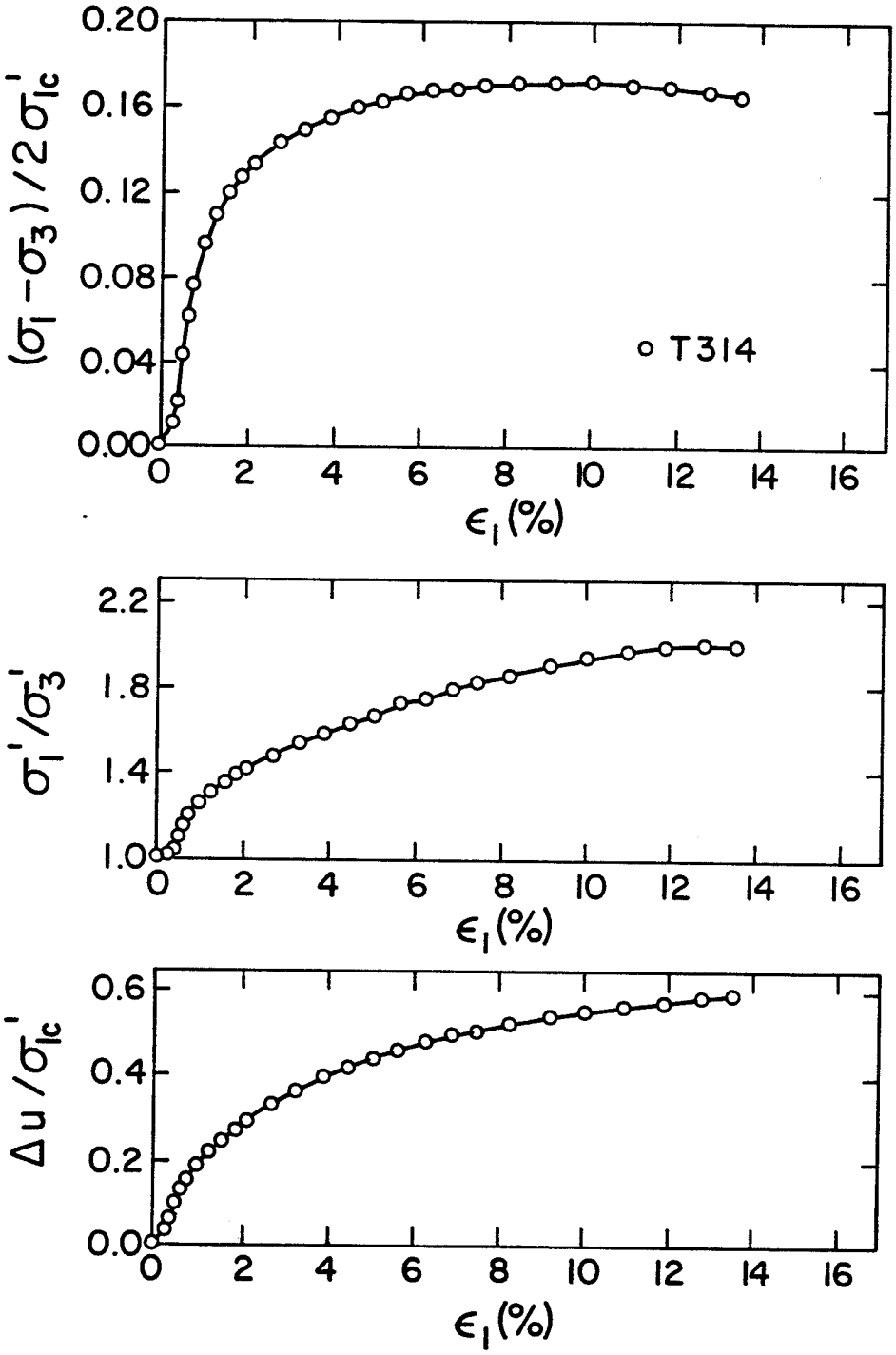

FIG. 5.6 UNDRAINED STRESS-STRAIN-POREWATER PRESSURE RESULTS, T314

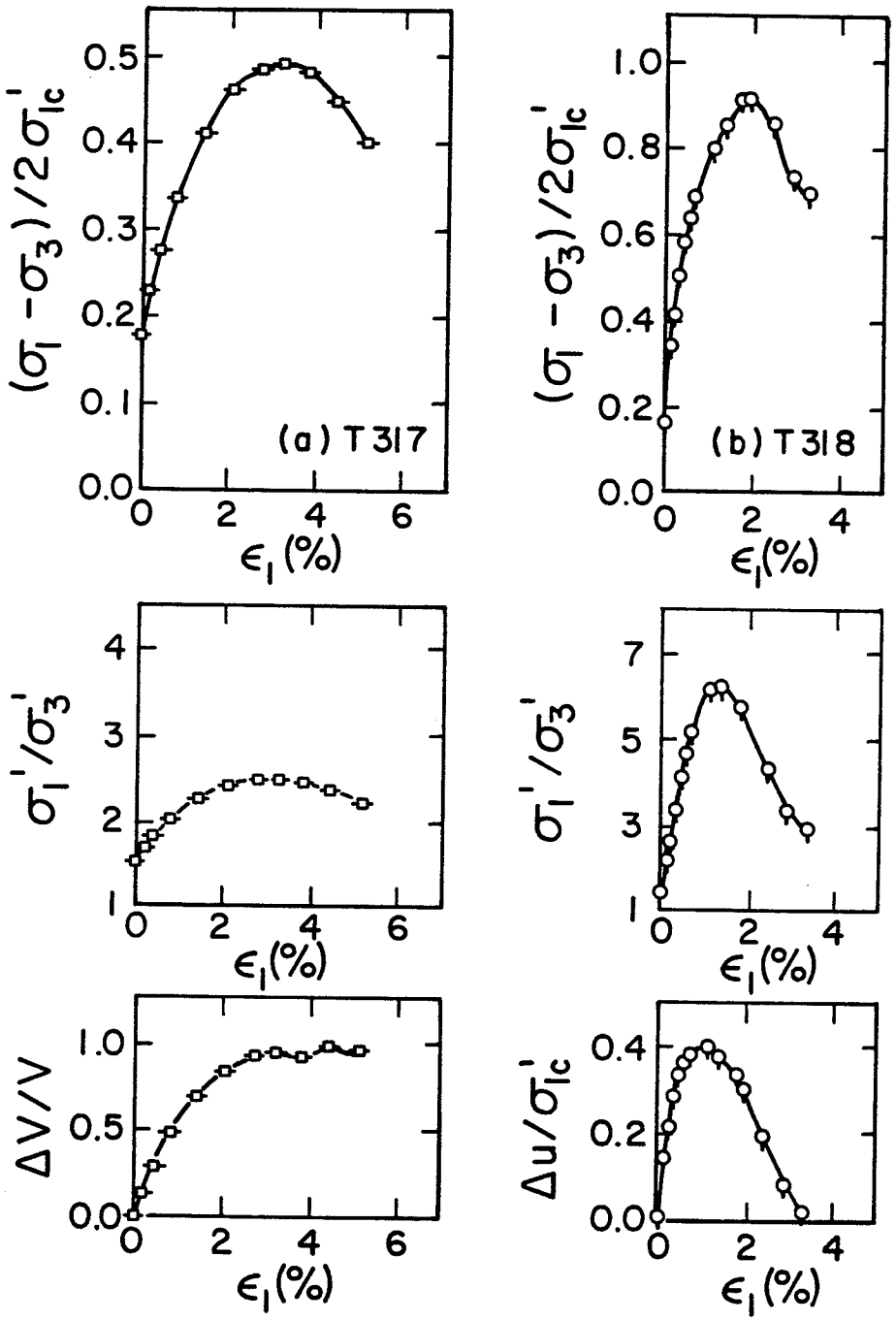

FIG. 5.7 (a) DRAINED STRESS-STRAIN RESULTS, T317
(b) UNDRAINED STRESS-STRAIN RESULTS, T318

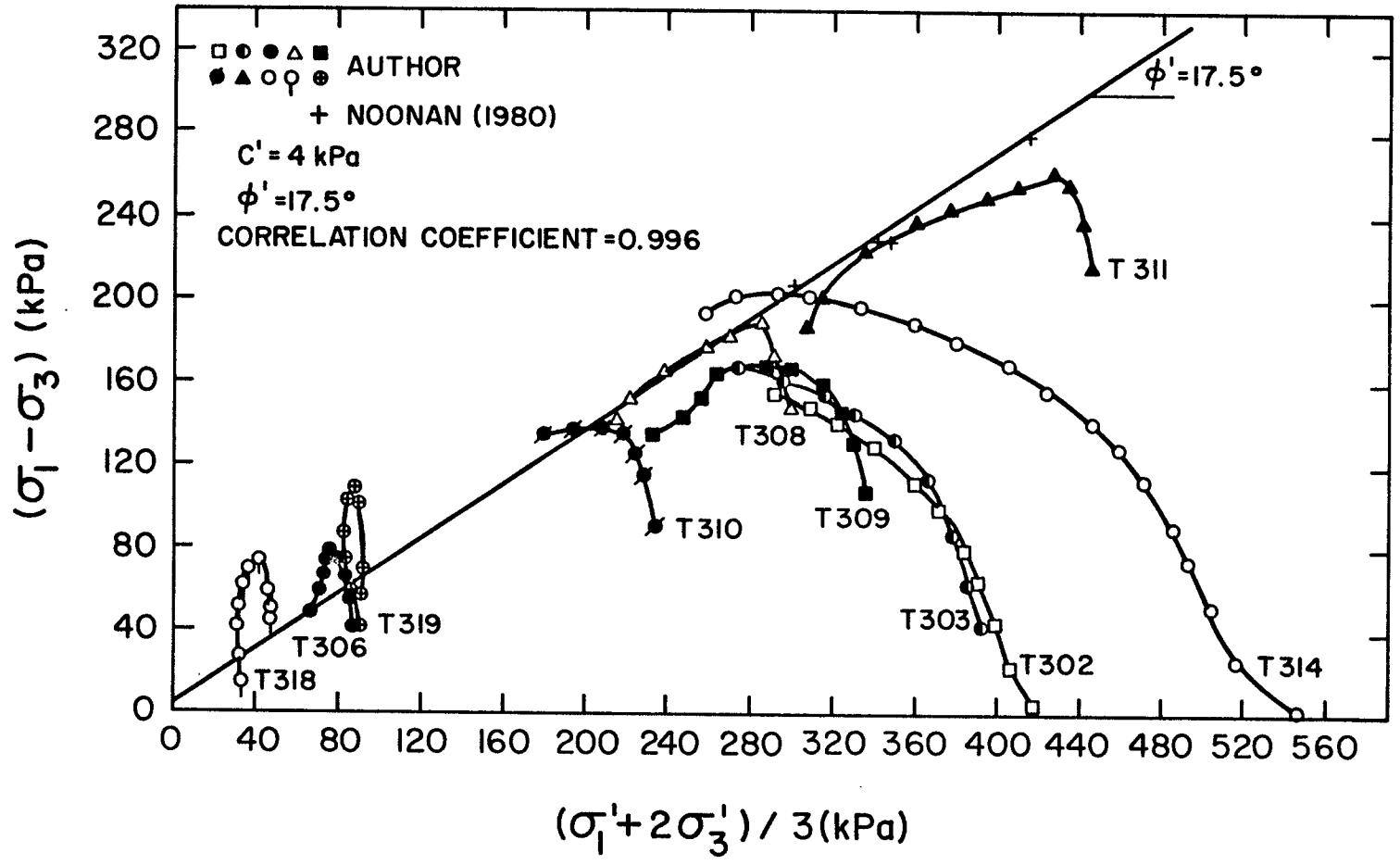

FIG. 5.8 EFFECTIVE STRESS PATHS AND COULOMB-MOHR ENVELOPE FROM UNDRAINED TESTS

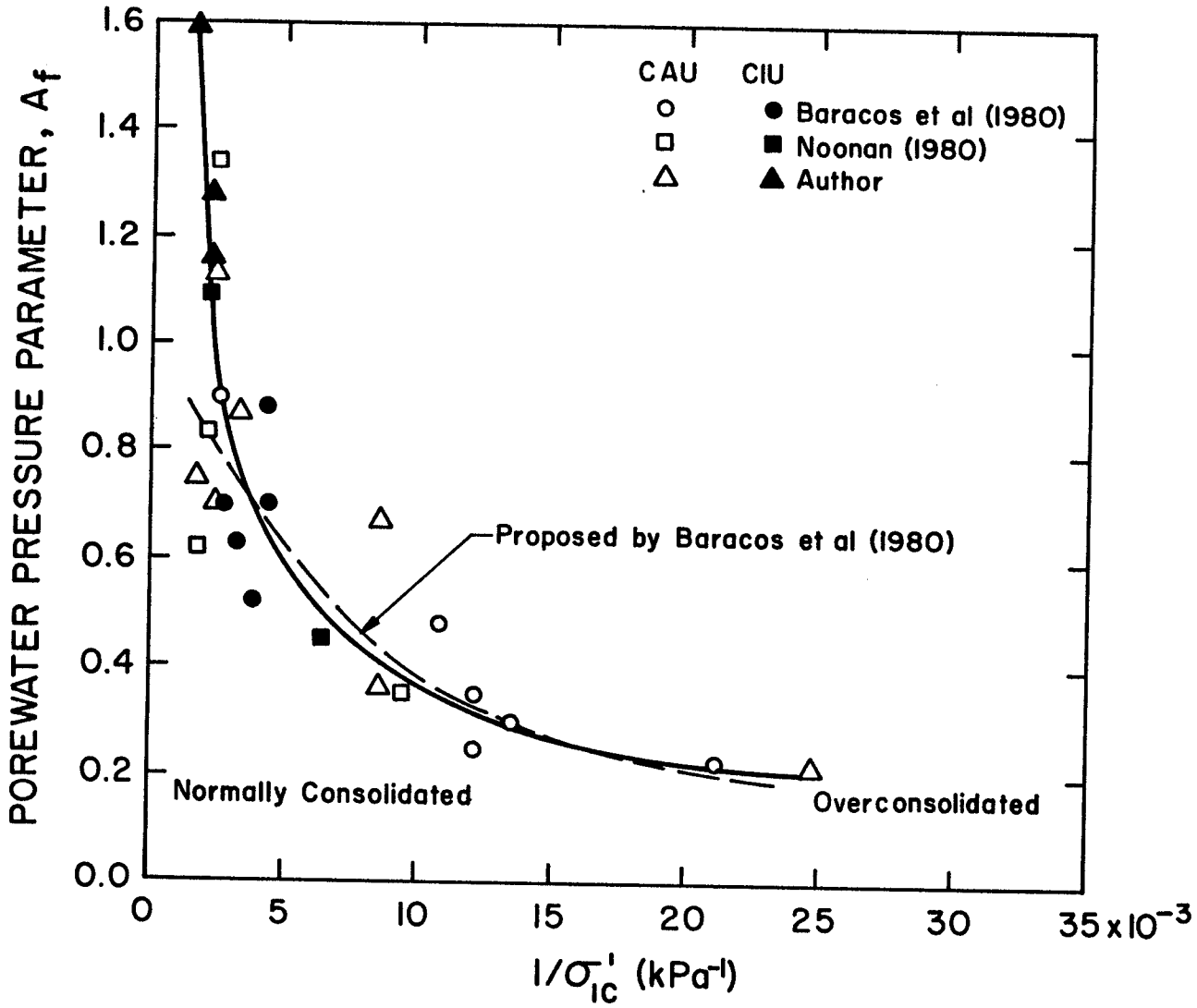

FIG. 5.9 GRAPH OF POREWATER PRESSURE PARAMETER A_f VERSUS $1/\sigma'_{1c}$ FOR WINNIPEG CLAY

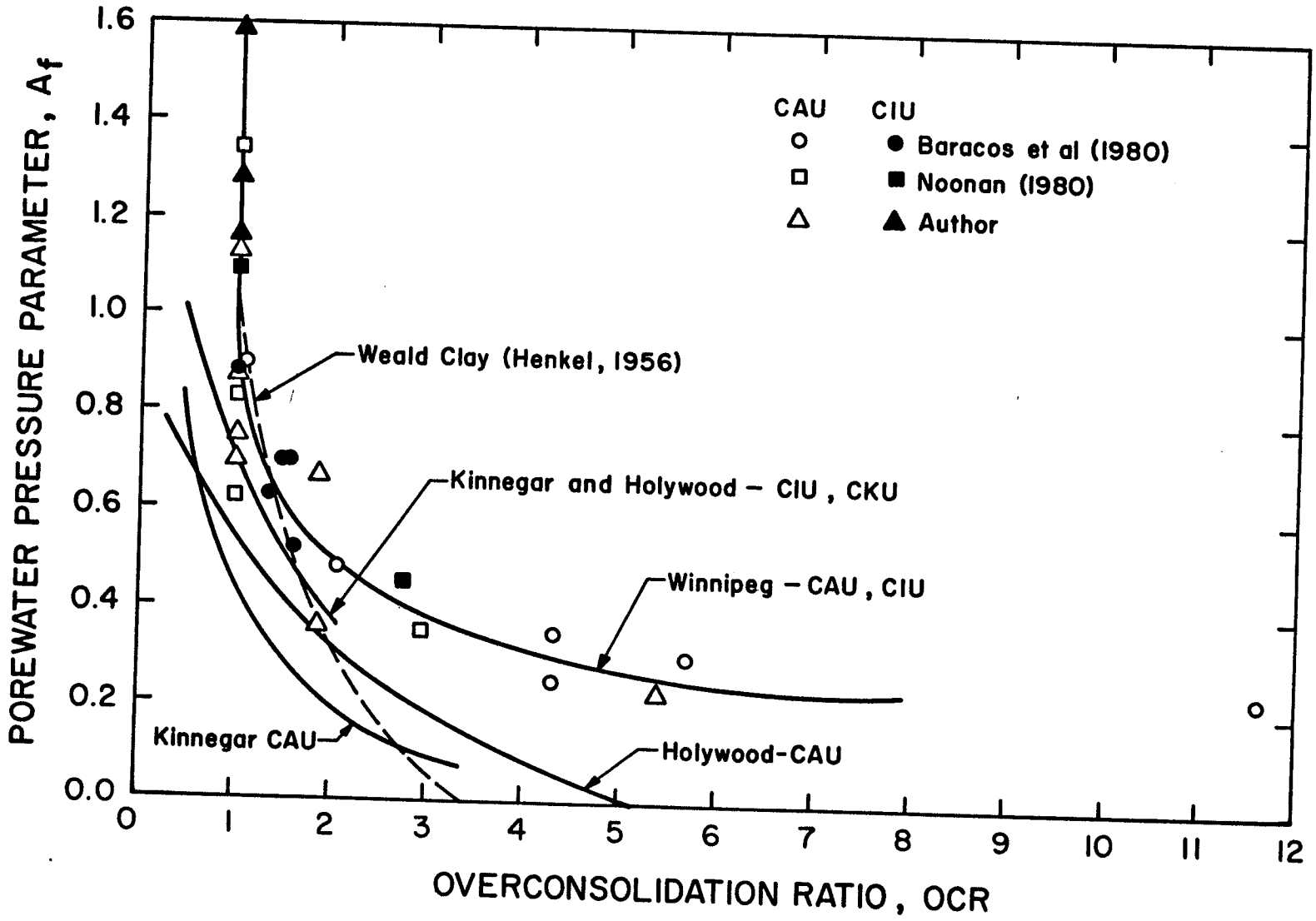

FIG. 5.10 SUMMARY GRAPH OF POREWATER PRESSURE PARAMETER A_f VERSUS OVERCONSOLIDATION RATIO

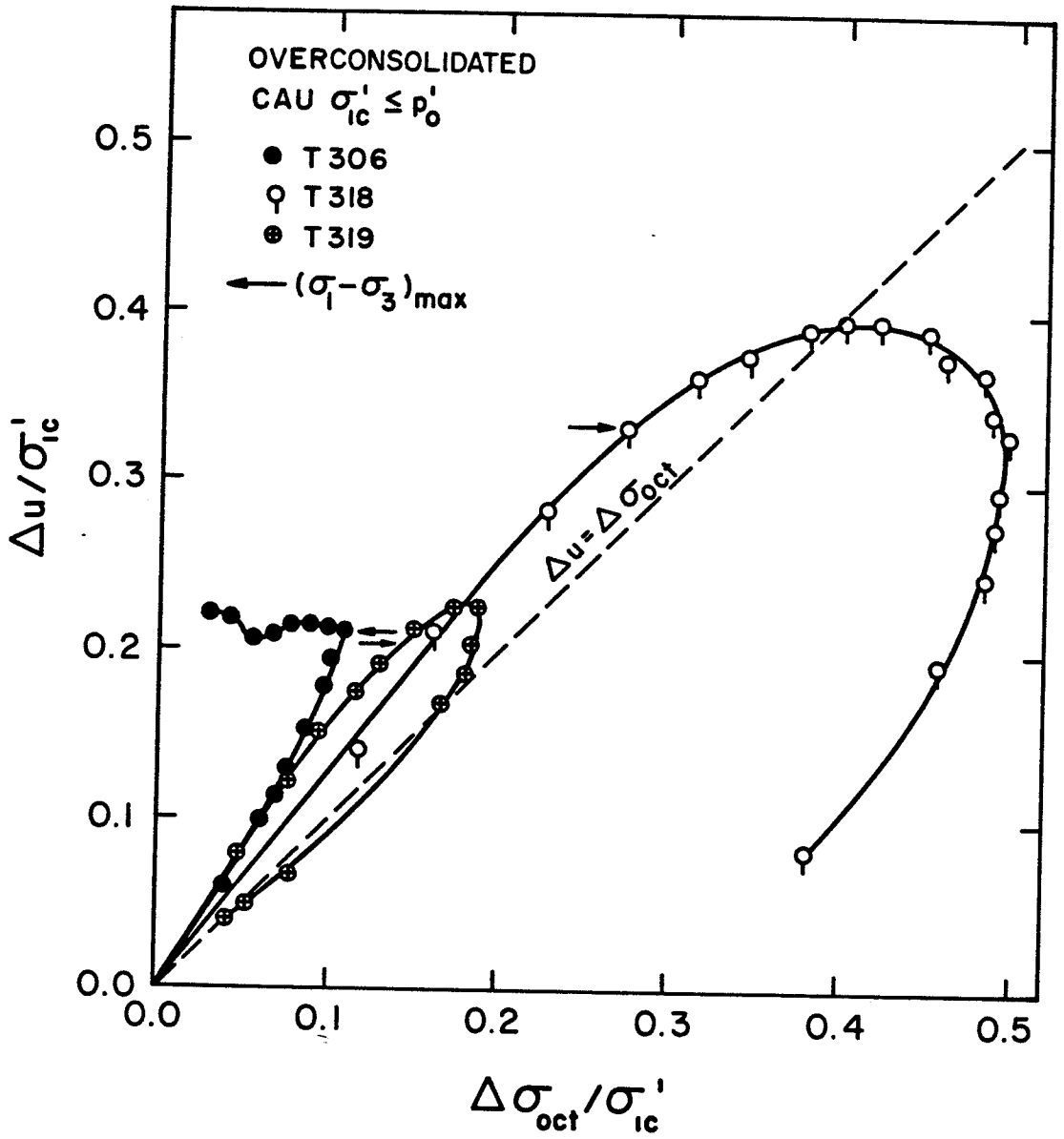

FIG. 5.11 POREWATER PRESSURE BEHAVIOUR,
$\Delta u/\sigma'_{ic}$ vs $\Delta \sigma_{oct}/\sigma'_{ic}$; T306,T318,T319

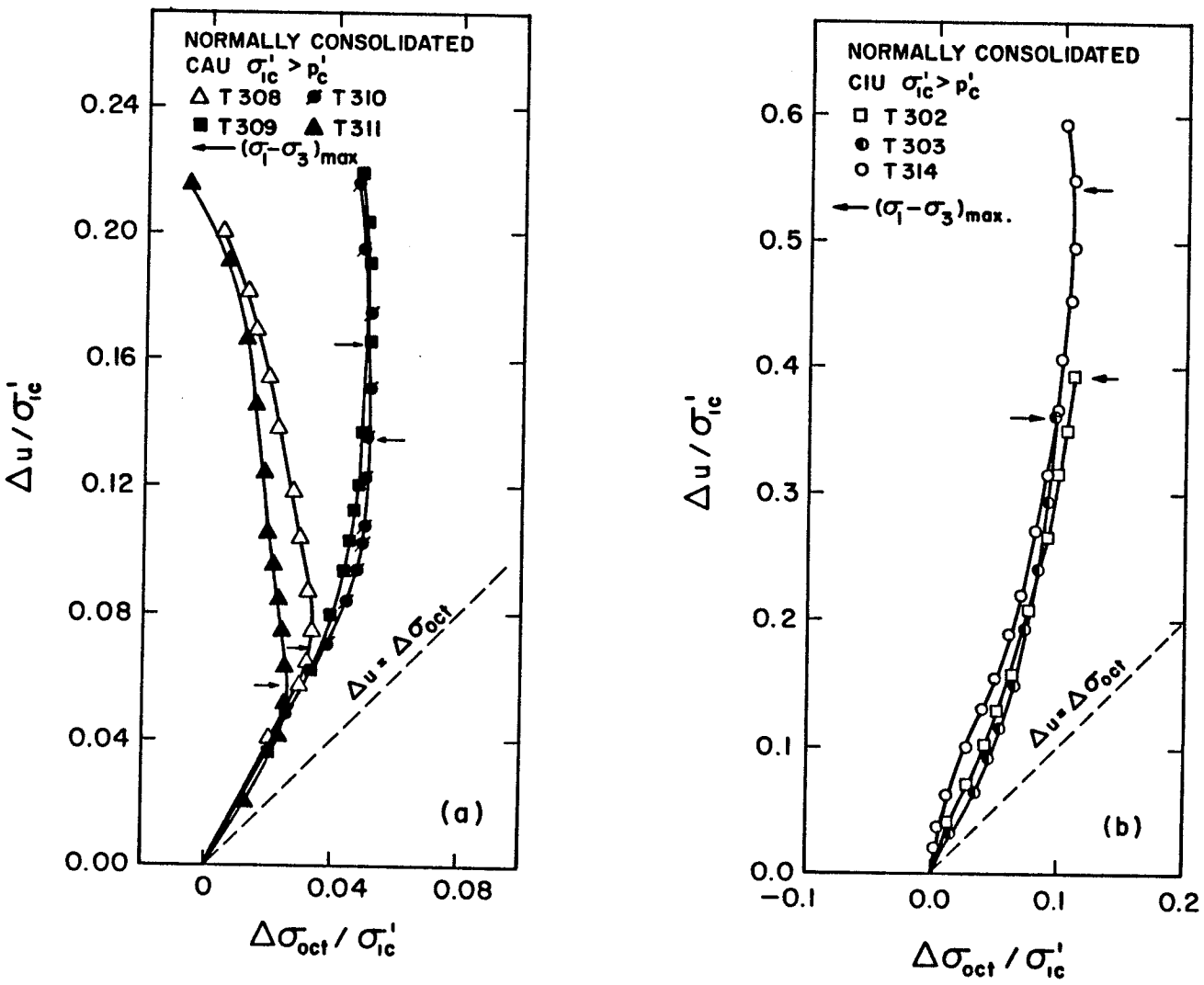

FIG. 5.12 POREWATER PRESSURE BEHAVIOUR, $\Delta u/\sigma'_{1c}$ vs $\Delta\sigma_{oct}/\sigma'_{1c}$

(a) T308,T309,T310,T311

(b) T302,T303,T314

FIG. 5.13 SAMPLES T305, T306, T319

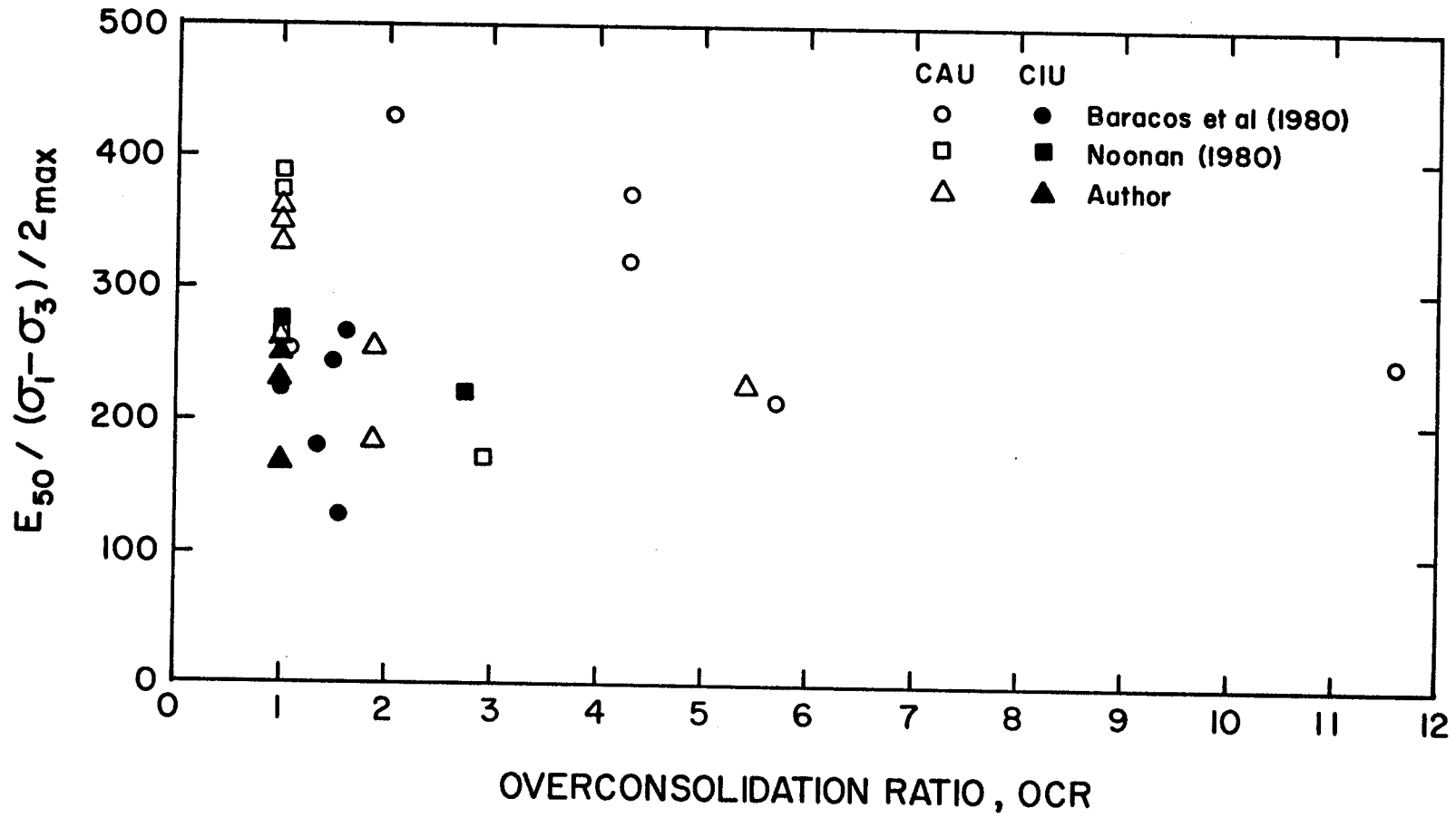

FIG. 5.14 RELATIVE STIFFNESS E_{50}/s_u VERSUS OVERCONSOLIDATION RATIO

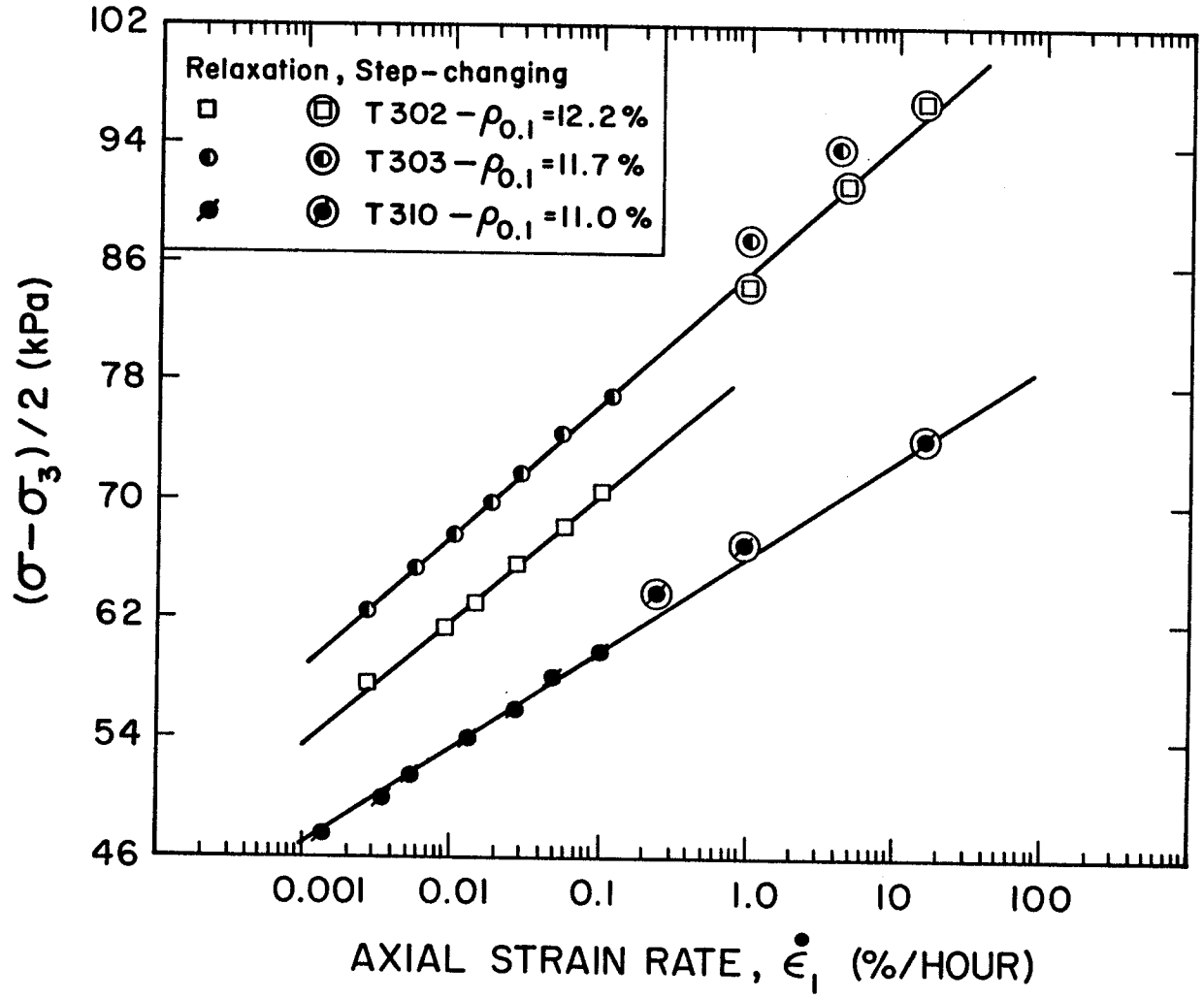

FIG. 5.15 STRAIN-RATE EFFECTS FROM RELAXATION AND STEP-CHANGING TESTS, T302,T303,T310

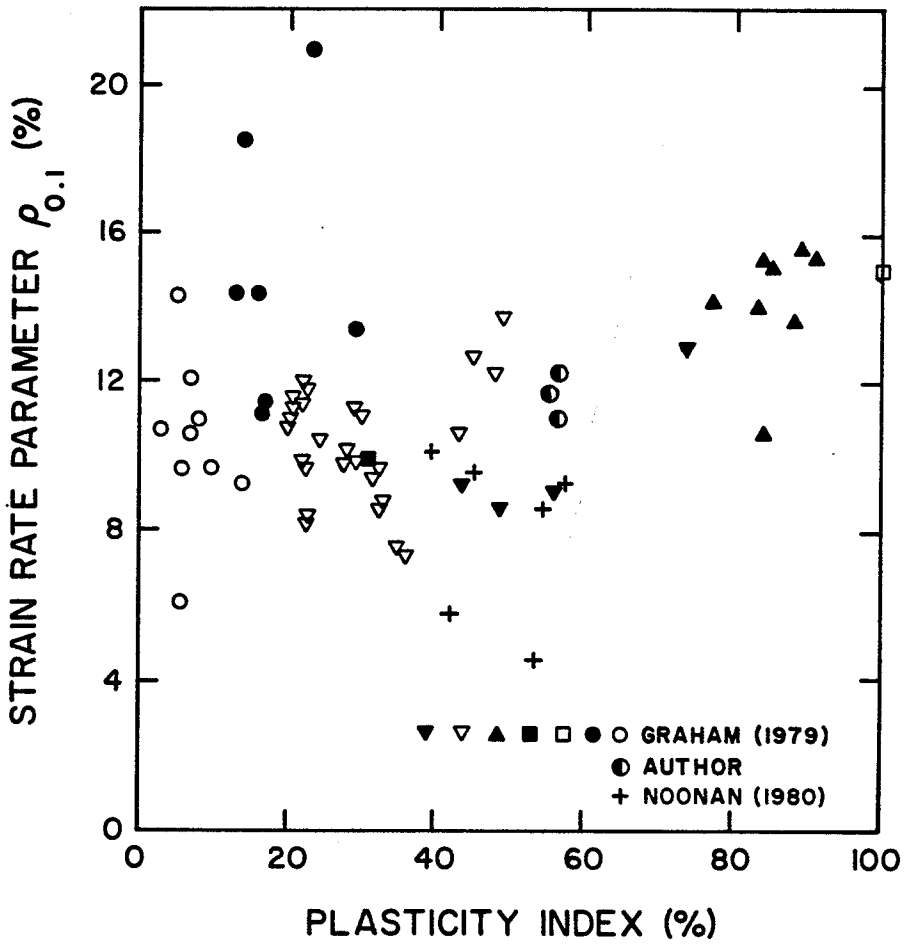

FIG. 5.16 SUMMARY GRAPH OF $\rho_{0.1}$ PARAMETER VERSUS PLASTICITY INDEX

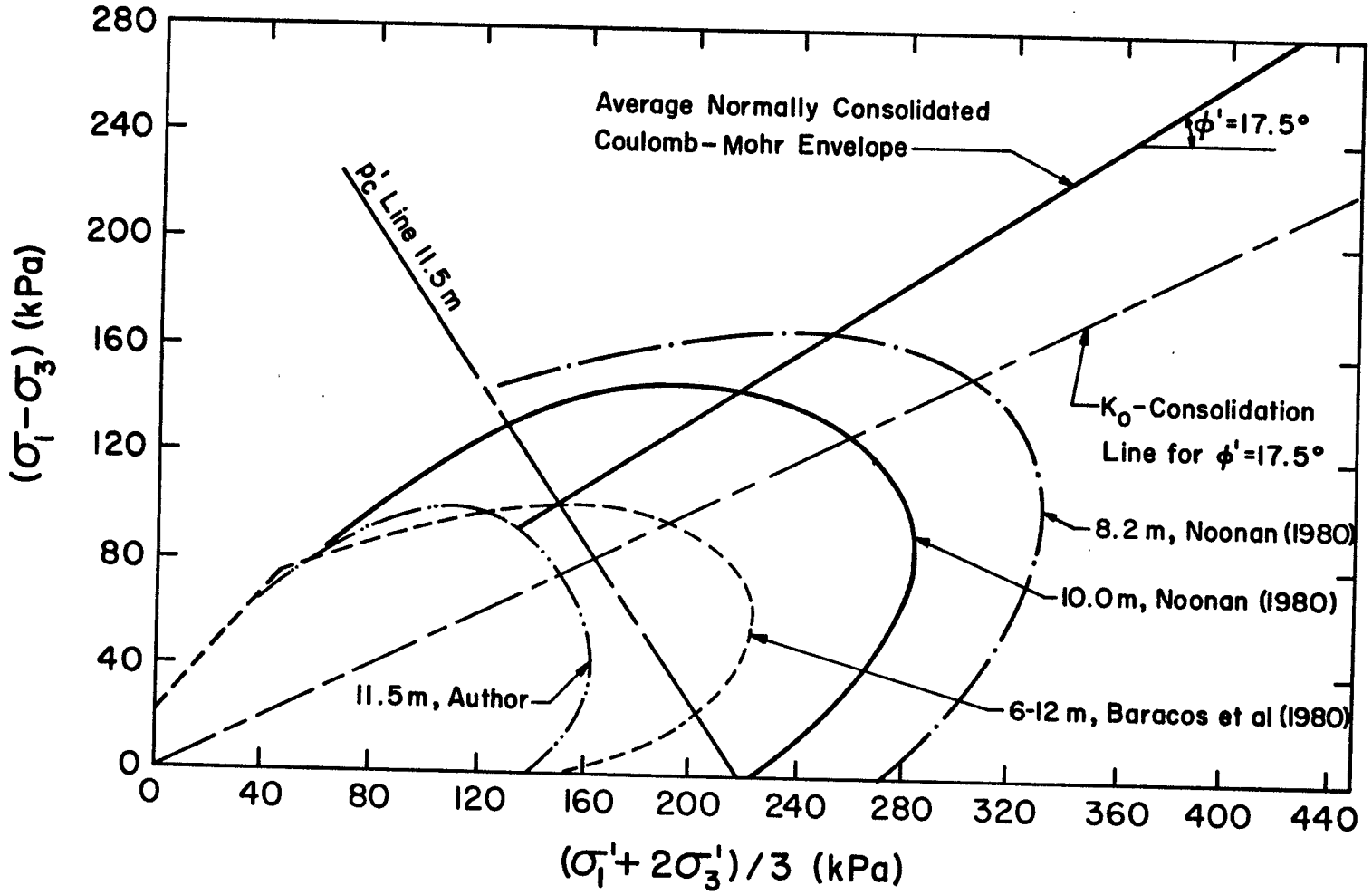

FIG. 6.1 SUMMARY OF ALL AVAILABLE YIELD ENVELOPES FOR WINNIPEG CLAY

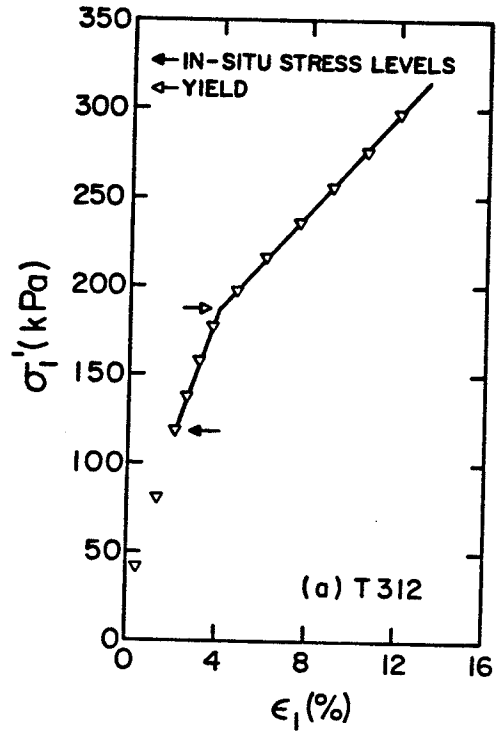

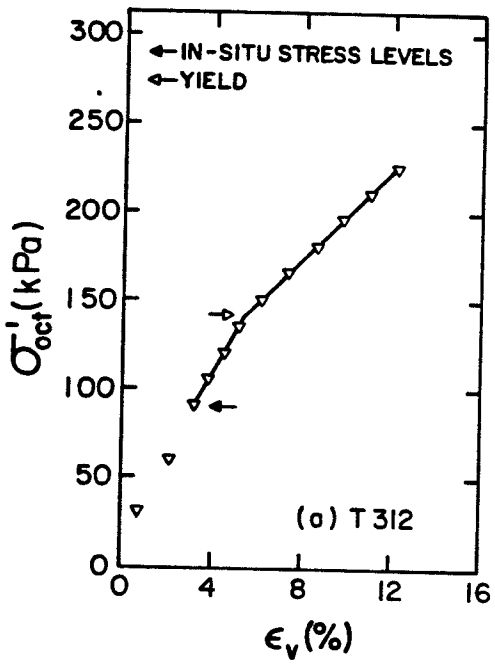

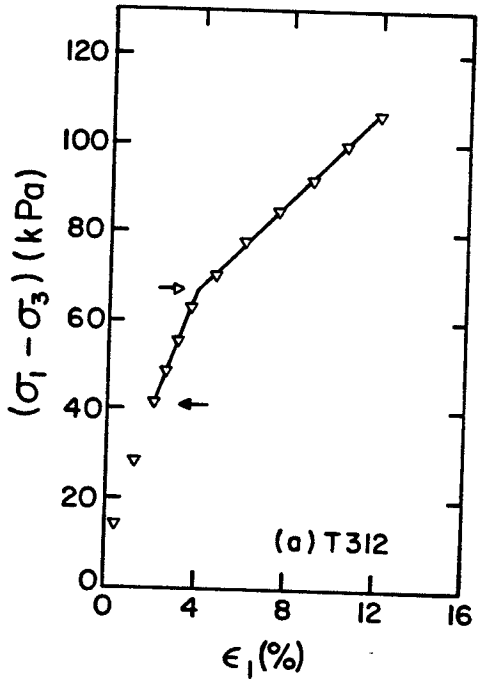

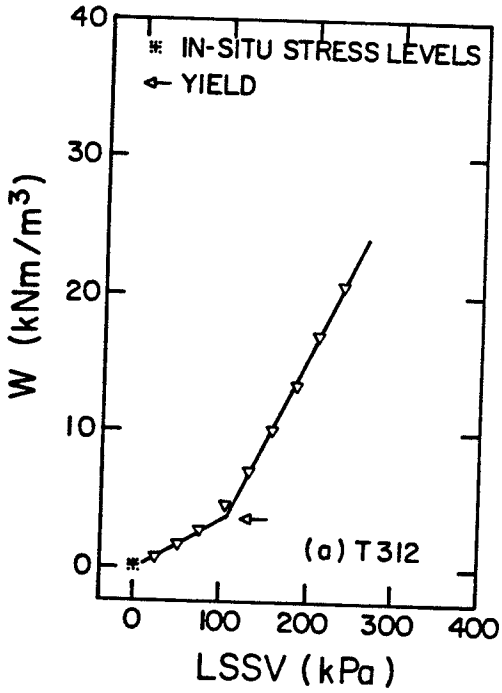

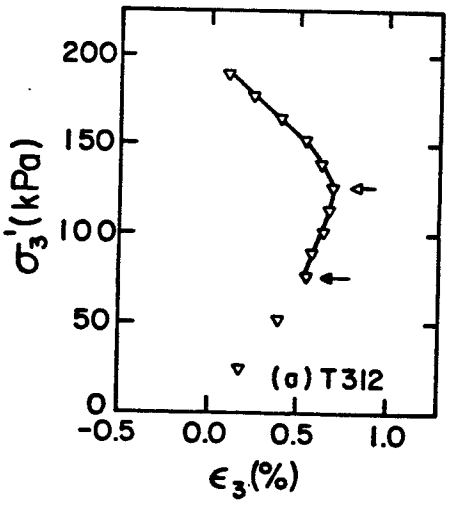

FIG. 6.2 ESTIMATION OF YIELD STRESSES FROM DIFFERENT CRITERIA

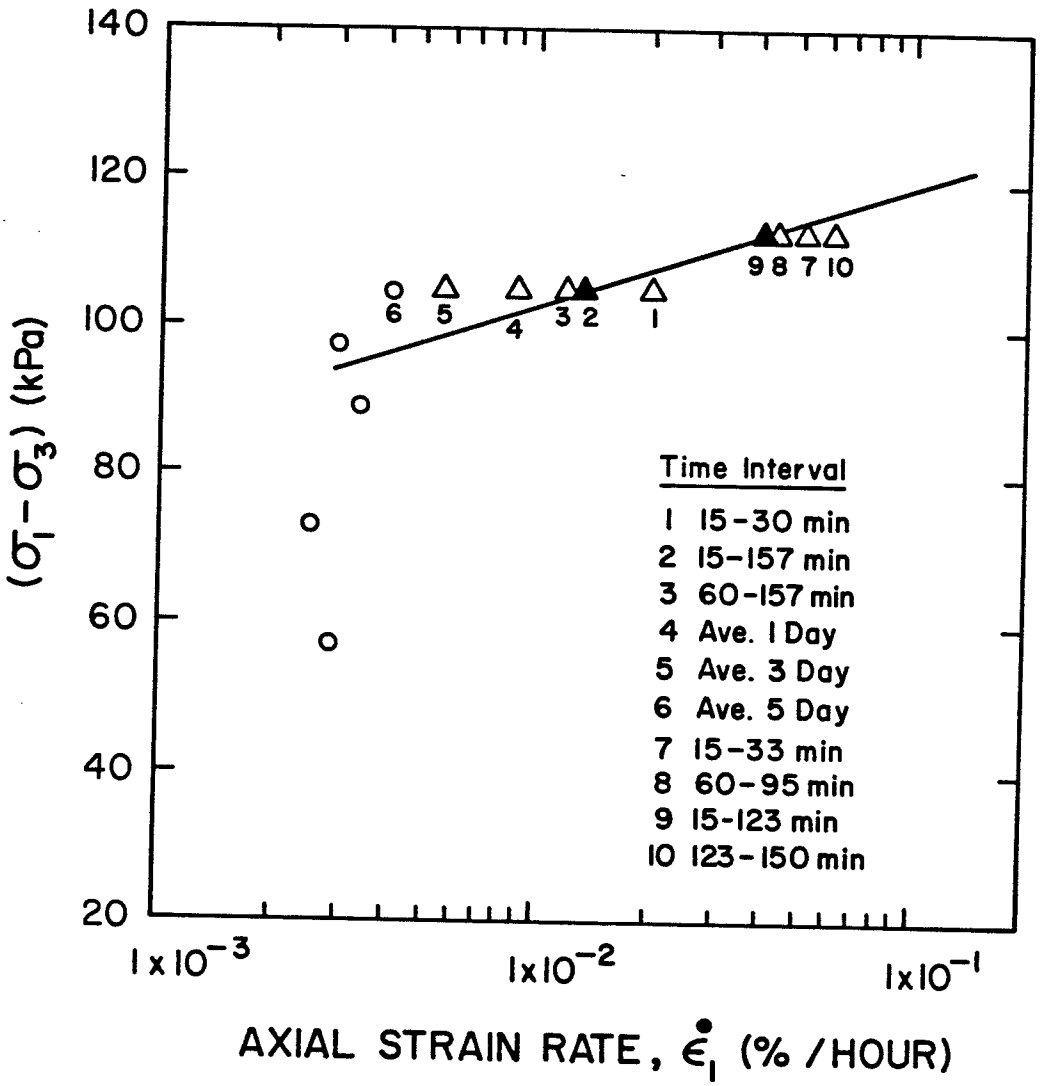

FIG. 6.3 STRAIN RATE STUDIES AT YIELD, FROM STRESS-CONTROLLED TEST T312

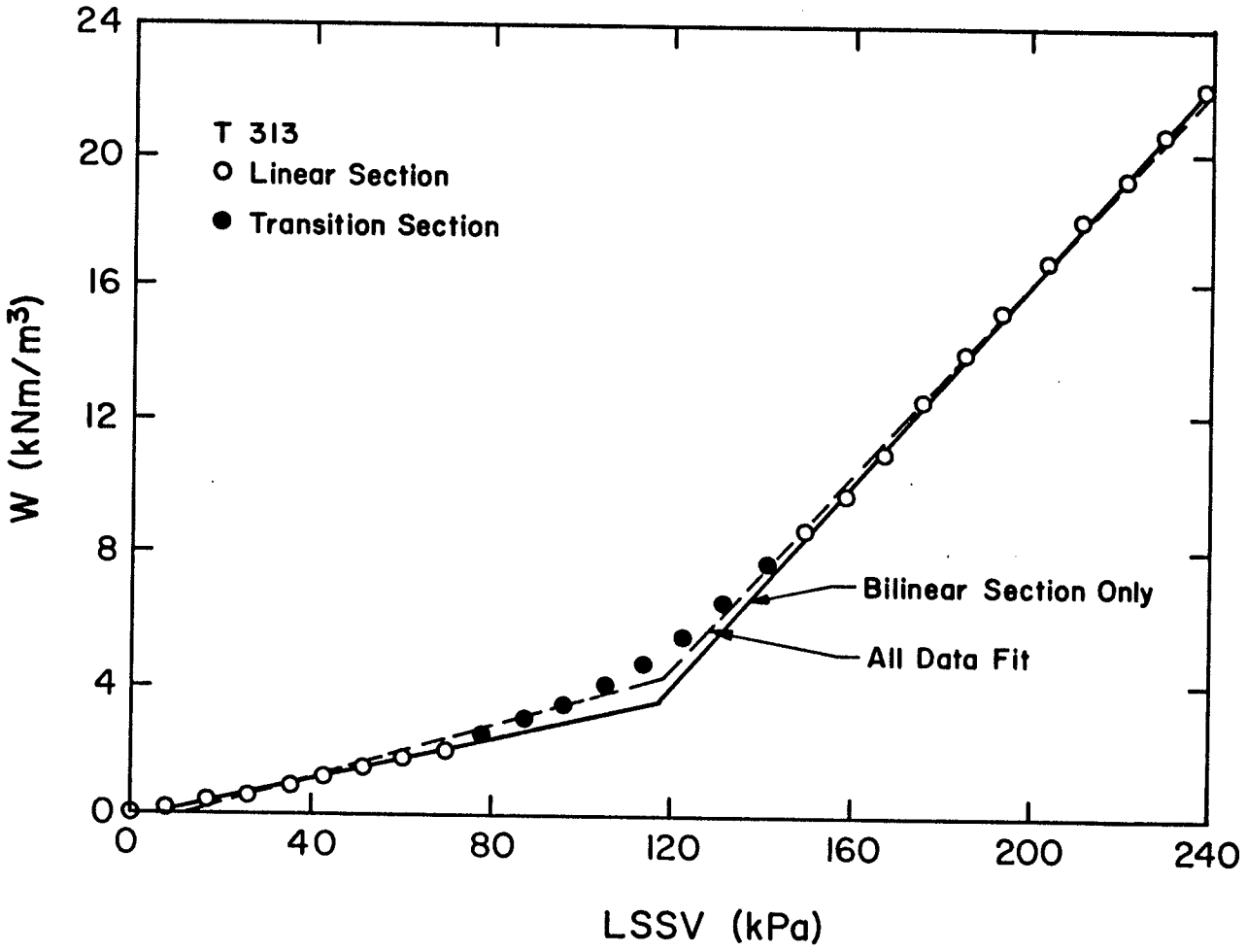

FIG. 6.4 EXAMPLE OF CURVE FITTING TECHNIQUES FOR DETERMINING YIELD STRESSES

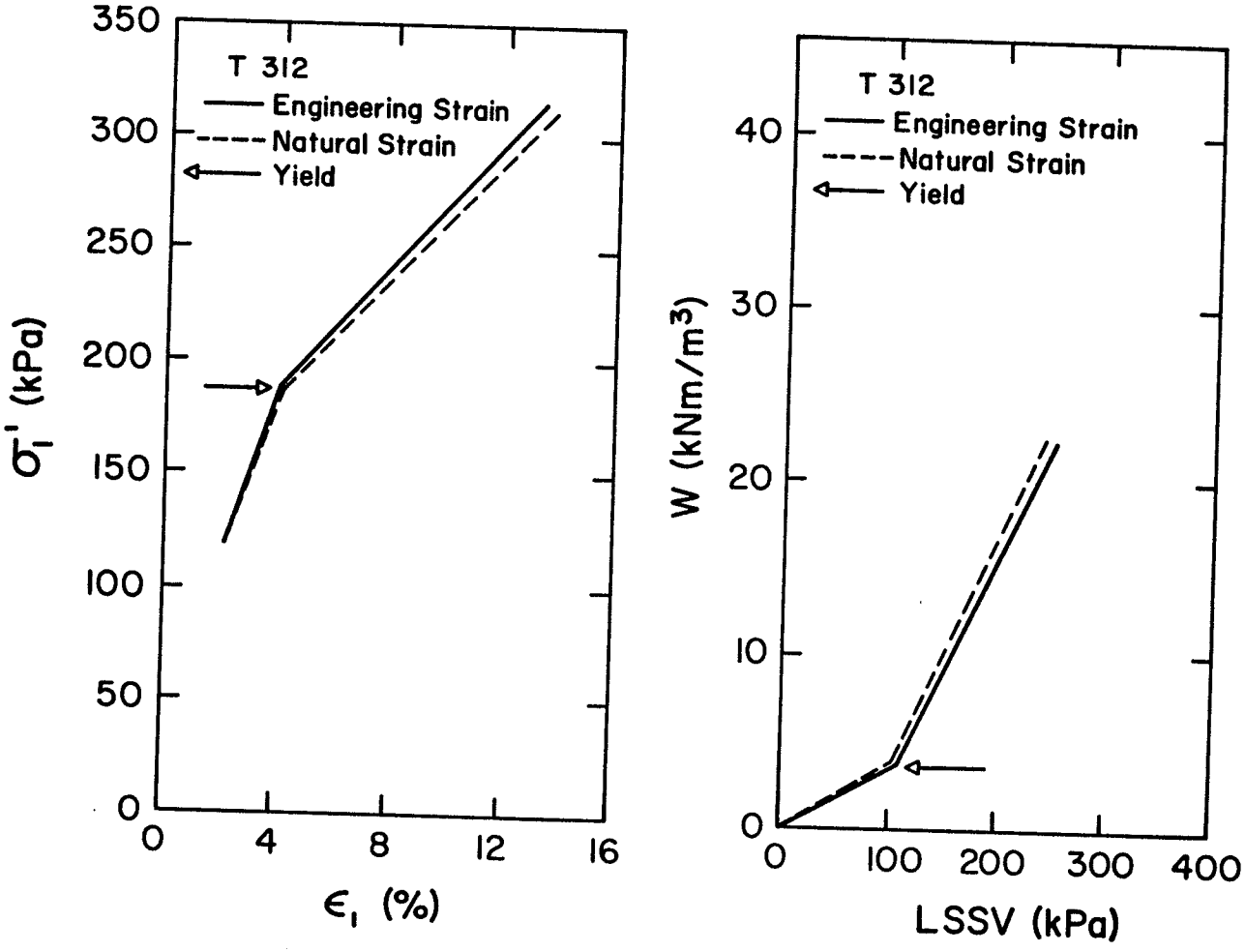

FIG. 6.5 YIELD STRESS DETERMINATION IN TERMS OF ENGINEERING STRAINS AND NATURAL STRAINS

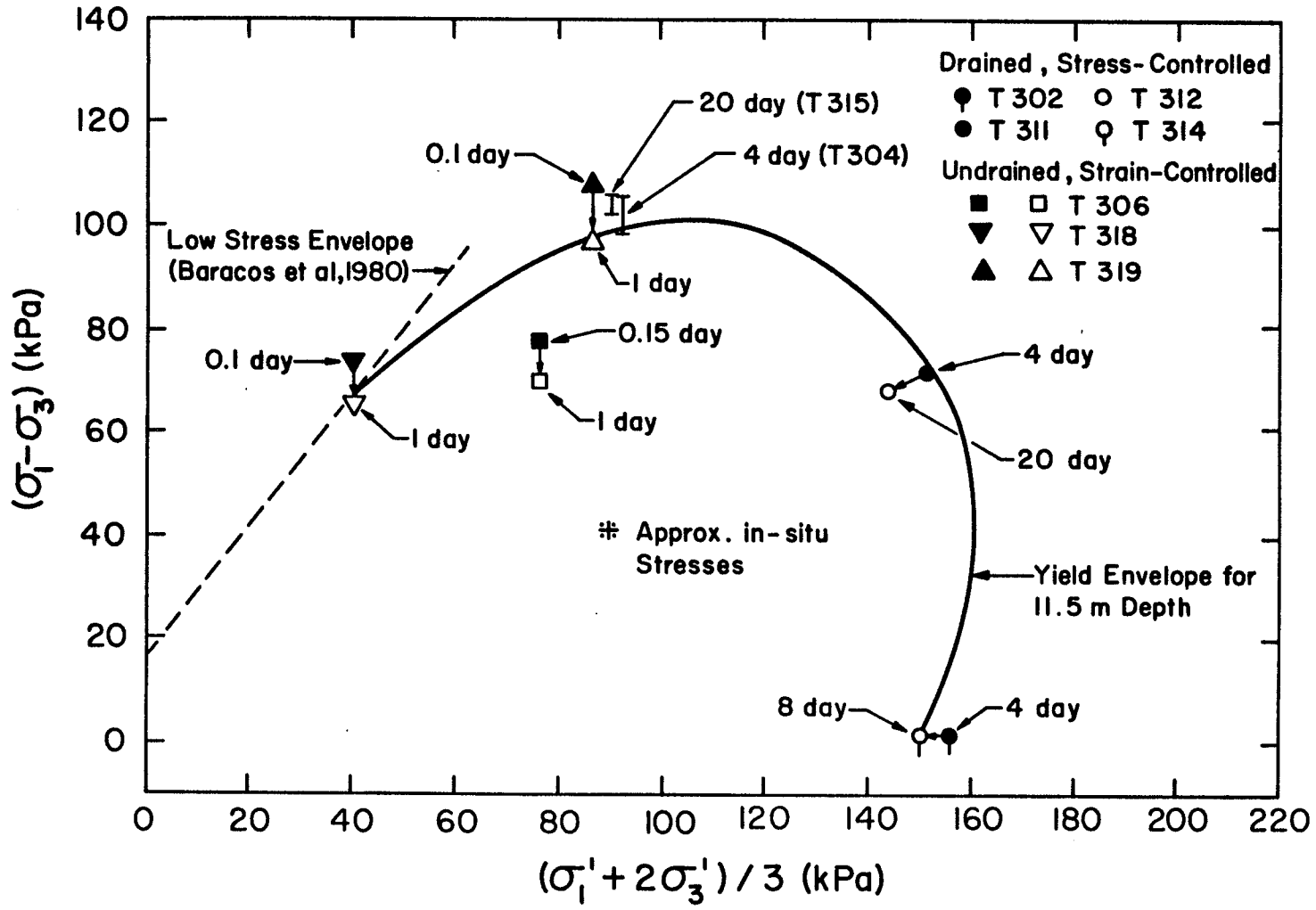

FIG. 6.6 STRAIN RATE AND TIME EFFECTS ON THE YIELD ENVELOPE AT 11.5 m DEPTH

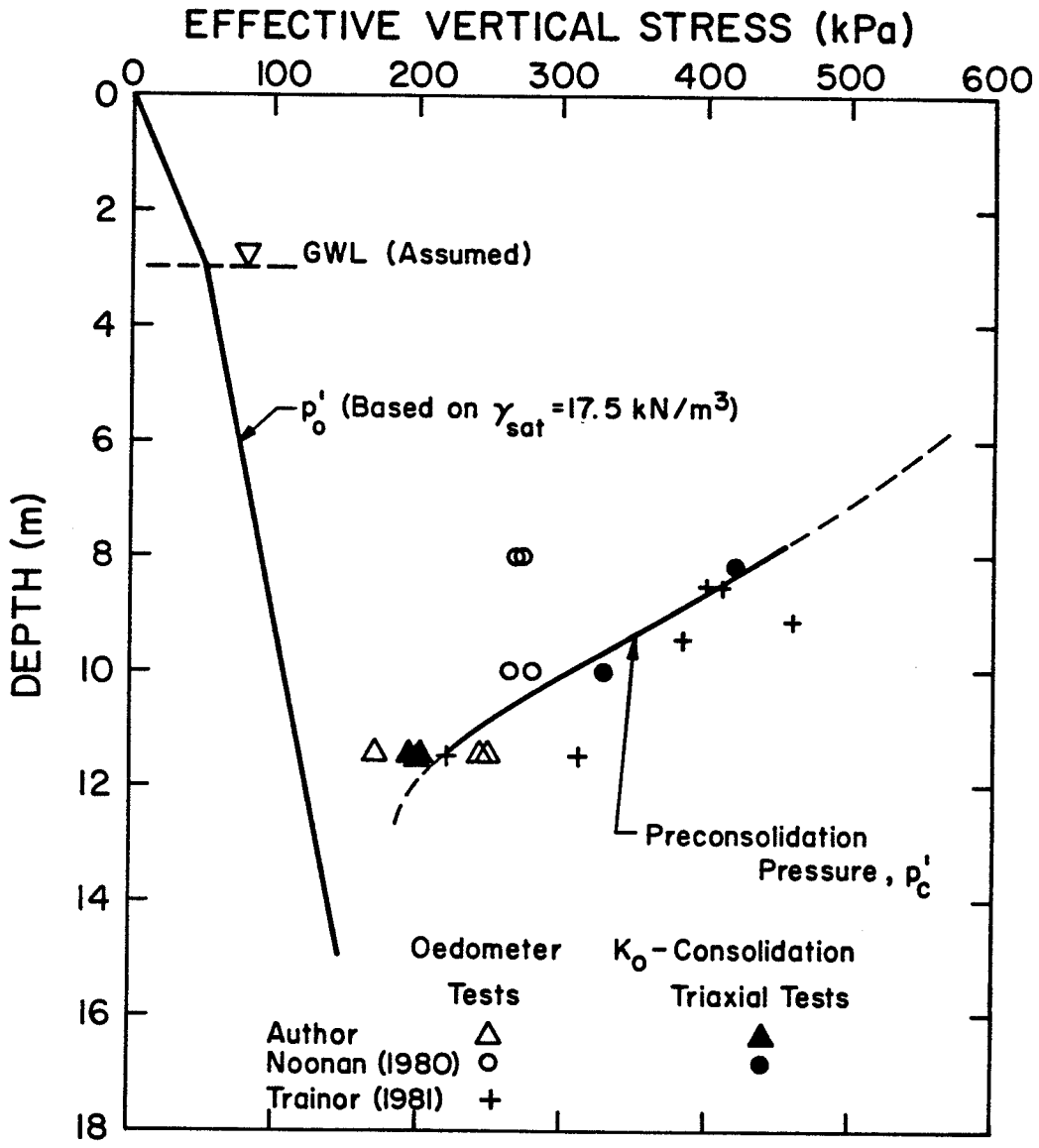

FIG. 6.7 VARIATION OF PRECONSOLIDATION PRESSURE p_c' WITH DEPTH, PHYSICAL EDUCATION BUILDING, UNIVERSITY OF MANITOBA

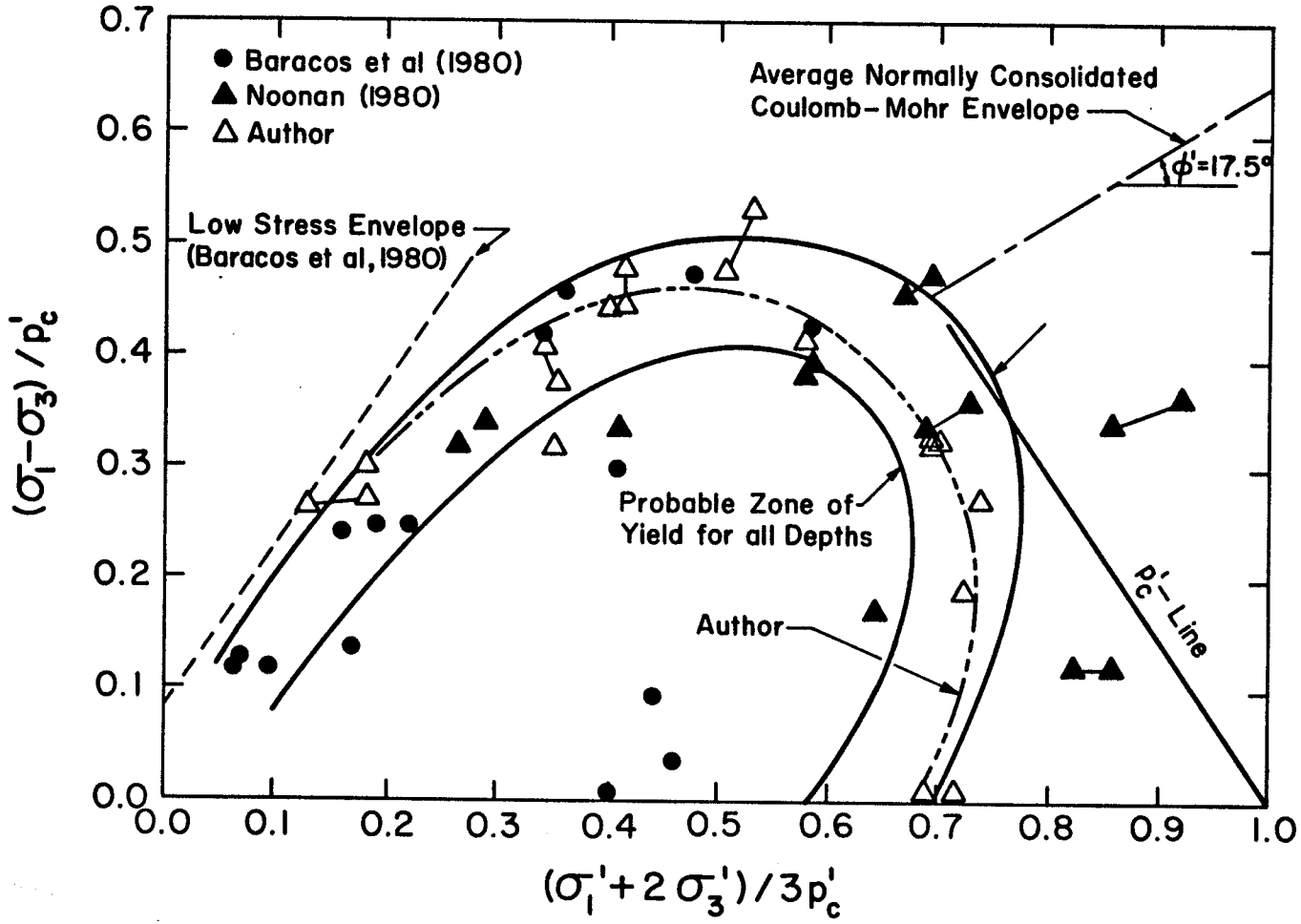

FIG. 6.8 NORMALIZED YIELD ENVELOPE INCORPORATING ALL AVAILABLE DATA

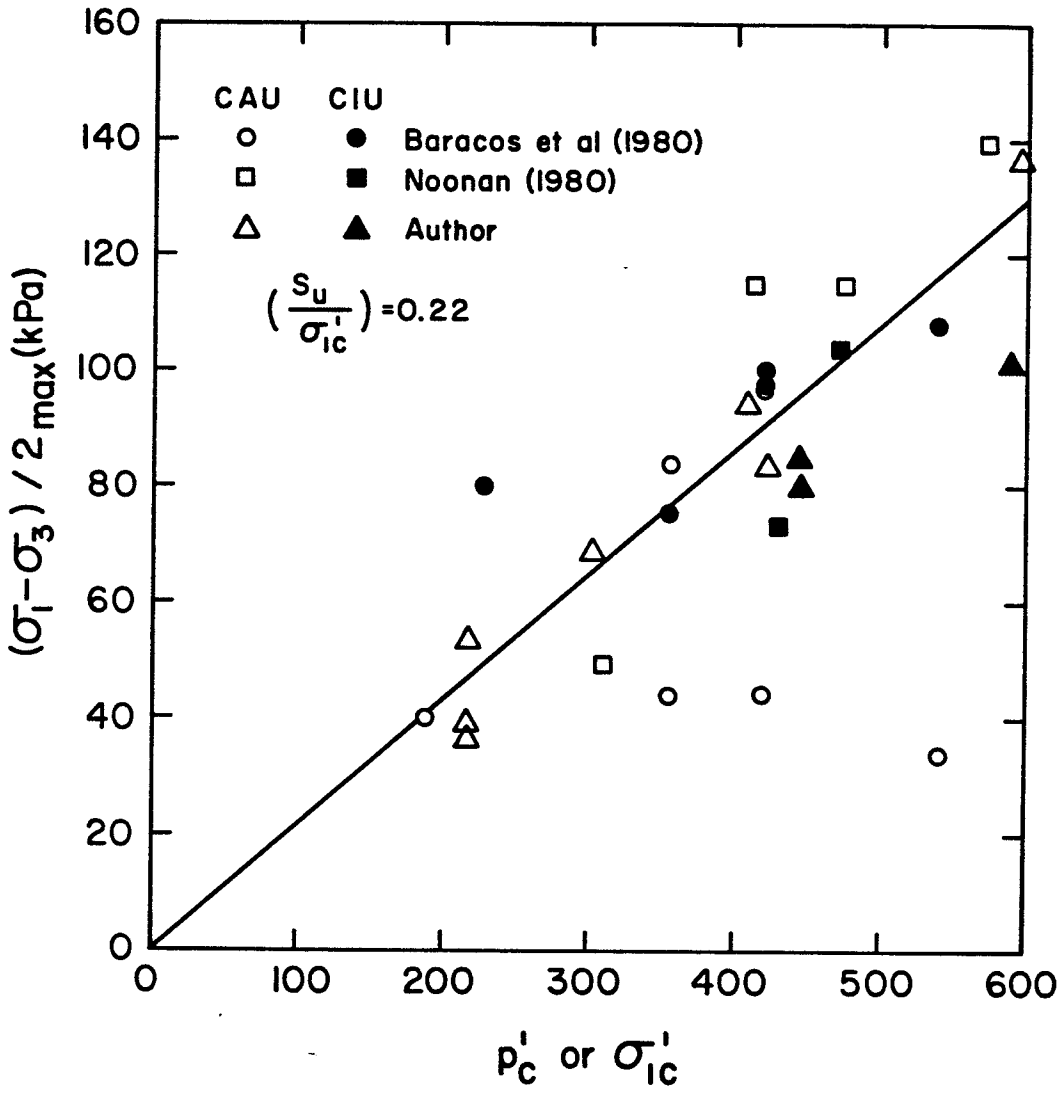

FIG. 6.9 RELATIONSHIP BETWEEN UNDRAINED SHEAR STRENGTH AND MAXIMUM CONSOLIDATION PRESSURE

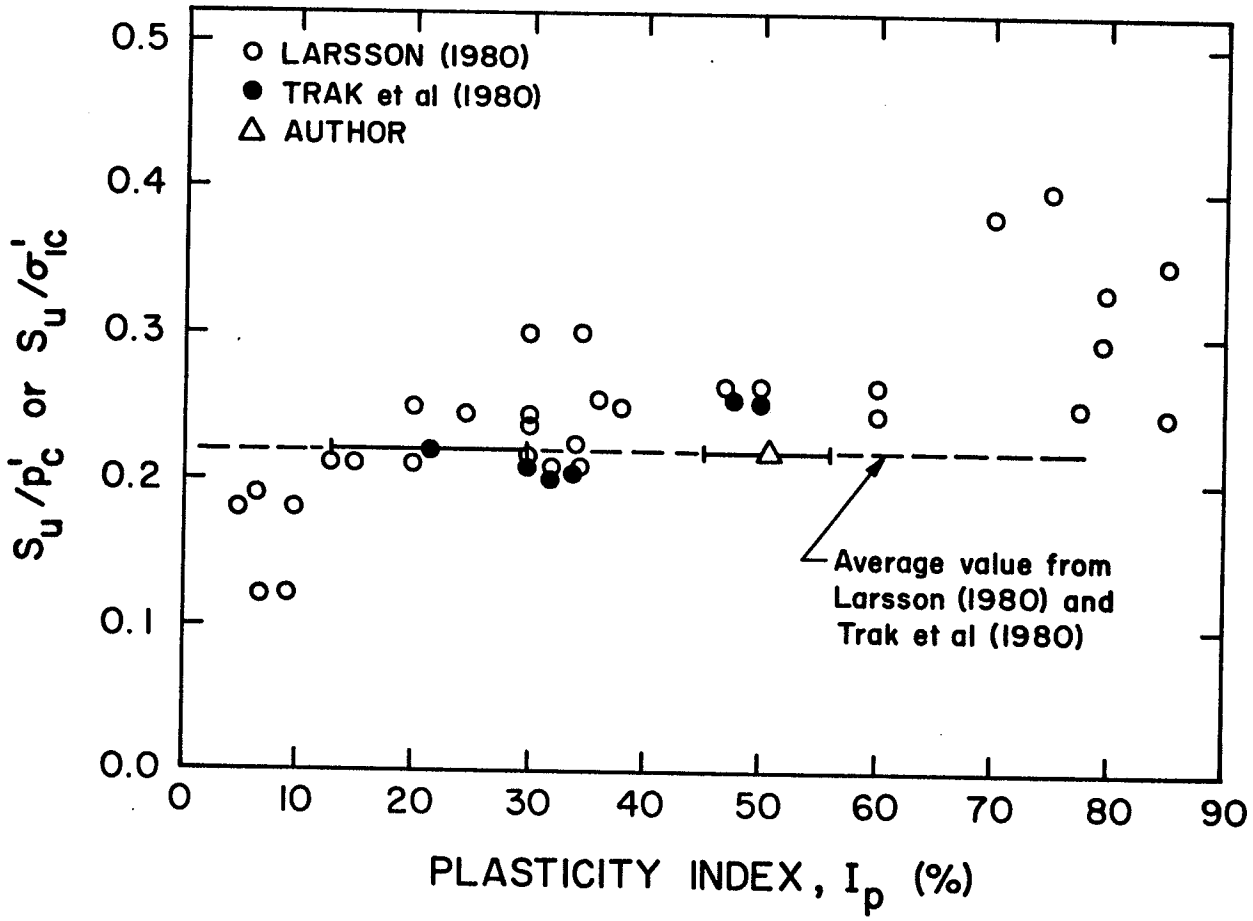

FIG. 6.10 SUMMARY GRAPH OF UNDRAINED SHEAR STRENGTH RATIO s_u/p'_c VERSUS PLASTICITY INDEX I_p

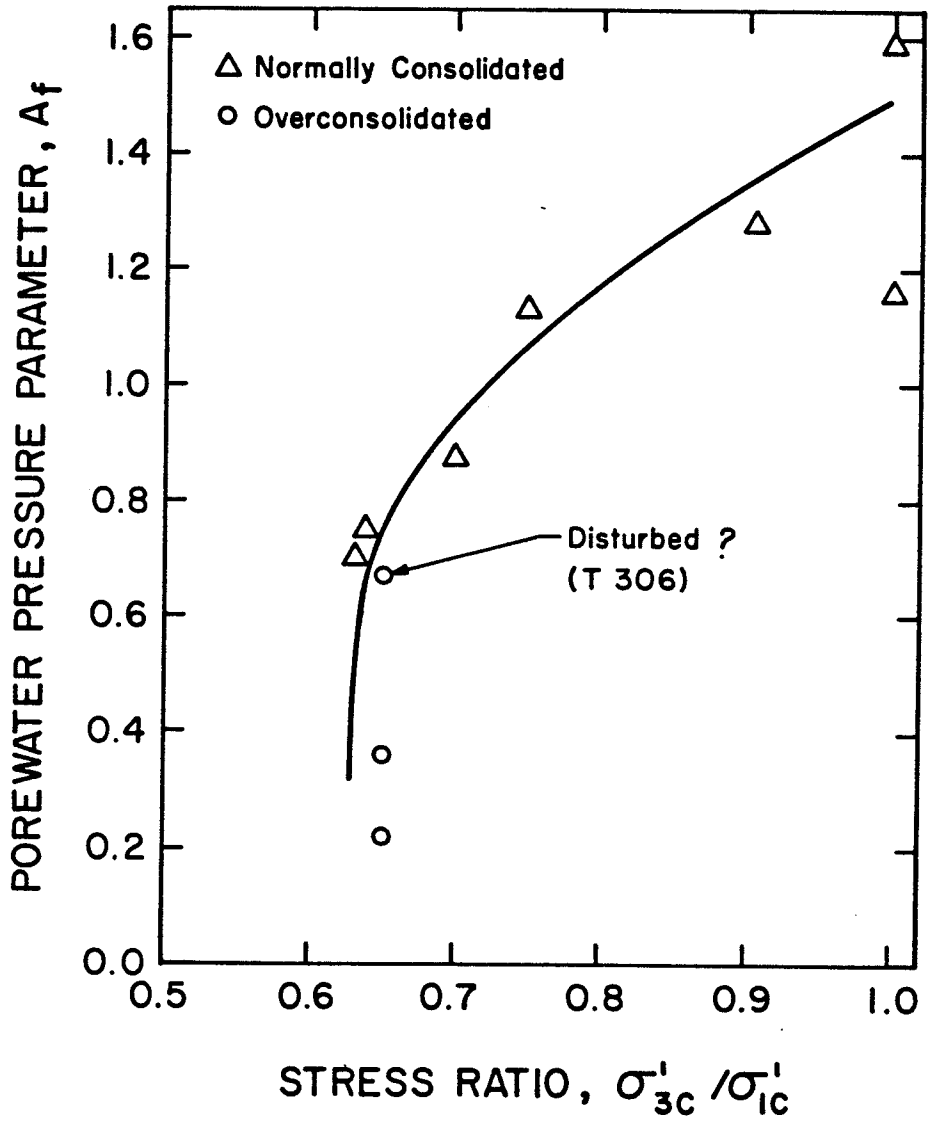

FIG. 6.11 DEPENDENCE OF POREWATER PRESSURE PARAMETER A_f ON STRESS LEVELS AND STRESS RATIO DURING CONSOLIDATION

A P P E N D I X I

SAMPLE TRIMMING AND BUILDING-IN PROCEDURES

SAMPLE TRIMMING AND BUILDING-IN PROCEDURES

1. Prepare deaired water. Deair all water. Deair the filter stone in its holder. Deair the cell pedestal.

2. A roughly cut sample should be ready (bottom end should be squared off).

3. Place the base plate of the trimming equipment loosely on the cell base with the cutting cylinder in position on the upright.

4. Adjust until the cutting cylinder is accurately centered over the pedestal.

5. Attach the trimming table to the base plate.

6. Place the roughly cut sample on the trimming table so that it lies within the projection of the cutting cylinder for its full length.

7. Force the cutting cylinder (cutting edge down) slowly into the clay to a depth of slightly less than the full length of the cutting edge.

8. Remove the excess clay outside the cutting edge using a piece of cutting wire (or a sharp knife).

   NOTE: Particular attention must be paid to avoid undercutting the leading edge.

9. Using the technique described above, the cutting cylinder is gradually pushed in steps towards the trimming table.

10. Collect two moisture content samples (one from near the top and one near the bottom).

11. Collect the remainder of the trimmings in a tare (or plastic bag) for standard classification tests.

12. Continue the trimming process until approximately 1 cm of clay protrudes from the top of the cutting cylinder.

13. Remove the cutting cylinder from the upright.

    NOTE: Support the soil in the cylinder with care and place (cutting edge down) on a glass plate.

14. Trim off the excess clay from the non-cutting edge of the cylinder.

15. Invert the cylinder and carefully press the loading cap approximately 1 cm into the bottom of the cylinder. The clay is then trimmed flush with the cutting edge of the cylinder.

16. Remove the top loading cap, clean the cutting cylinder, and weigh it with the wet clay.

17. Place the cutting cylinder (cutting edge down) on a glass plate and attach the saturated filterstone and its holder to the top of the cutting cylinder.

    NOTE: Care should be taken to ensure that the filter stone remains saturated during this process - use an extra spacer, and deair whole assembly beforehand.

18. Remove the trimming platform and form a meniscus of water on the pedestal.

19. Slide the two pieces of split clamp to the bottom of the uprights.

    NOTE: This step is important, and should not be forgotten.

20. Invert the cutting cylinder (filter stone and its holder on bottom), place on the uprights and slide down the uprights to the pedestal. Unclamp the filter stone from its holder.

21. Place the top loading cap, its holder and the top clamp in the uprights.

22. Secure the clamp in place and lower the top loading cap until contact is made with the top of the sample.

23. Secure the top loading cap in this position by tightening the center screw of the clamp and then carefully slide the cutting cylinder and filter stone holder up the uprights until they are about 8 cm clear of the top loading cap and secure in this position.

24. Bring the split clamp up from the bottom of the uprights and clamp in place just above the loading cap.

    NOTE: At this stage, the sample is standing on the pedestal base with its top supported.

25. Remove the top clamp and the cutting cylinder from the uprights.

26. Measure the height and diameter of the sample and record on data sheet 1. (see Noonan, 1980)

27. Grease the side of the pedestal and the top loading cap with a thin layer of silicone stopcock grease.

28. Provide lateral drains by applying saturated filter strips longitudinally around the circumference of the sample.

    NOTE: Care must be taken to ensure that the filter strips overlap the filter stone at the bottom of the sample.

29. Put one rubber membrane on the membrane stretcher along with five o-rings on the bottom half of the stretcher.

30. Place the membrane stretcher on the uprights and lock in position above the split clamp. Place the top clamp on the uprights to lock the top cap in place.

31. Unlock and lower the split clamp below the sample.

32. Lower the membrane stretcher and place the first membrane over the sample with one o-ring at the bottom just below the filter stone.

33. Raise the membrane stretcher above the sample and lock in place. Slide the split clamp above the sample and lock the top cap.

34. Remove the membrane stretcher and the top clamp from the uprights.

35. With the first membrane on, water is passed through the pedestal from one of the pedestal drainage burettes. Venting between the top cap and the membrane allows the region between the membrane and the sample to become saturated.

    NOTE: Care should be taken to ensure that most of the air bubbles between the sample and the first membrane are eliminated.

36. Apply a layer of silicone oil to the outside of the first membrane and using the same procedures as in step 29-32, put a second membrane over the sample.

37. Place 4 additional o-rings on the sample.

    NOTE: (1) Two o-rings are put on the pedestal and two on the loading cap at this stage, plus the one o-ring which was placed earlier in step 32.

    (2) Care must be taken not to pinch the sample when rolling the sealing rings onto the pedestal and the loading cap.

38. After placing the second membrane and its o-rings, the membrane stretcher is secured above the sample so that the split clamp can be brought above the sample and locked in place.

39. Remove the top clamp and the membrane stretcher. Remove the three top cap screws carefully. Slacken the clamping screws in the split clamp, and raise the top cap holder. Reclamp.

40. Remove the base plate plus the split clamp and the top cap holder carefully as a unit, leaving the sample free-standing on the pedestal.

41. Fit the cell top to the cell base carefully and screw down.

    NOTE: Care must be taken to ensure the loading piston is clamped and out of the way, and the bushing drive lines up with the bushing.

42. Lower the loading piston until contact is made with the sample and then lock the piston in place to provide support for the sample.

43. Fill the cell with deaired water to a level just above the top cap. Pump a layer of engine oil about 2 to 3 cm thick into the cell through connection in the top of the cell.

44. Continue to fill the cell through the cell base until some of the engine oil begins to come out the top connection which is then sealed off.

45. Remove the air trapped in the pedestal and drainage leads by passing water between two burettes attached to the pedestal drainage leads.

    NOTE: (1) This is accomplished by establishing a gradient between the two burettes and alternately flushing in one direction or the other.

    (2) The process is continued until flushing produces no more air bubbles, and all air bubbles are removed from the drainage lines.

46. Seal off the drainage lead which does not have a pressure transducer. Leave the other open and set the water level in this burette to the mid-height of the sample.

    NOTE: Additionally, a drainage lead and burette is attached to the cell pressure transducer connection. The water level in this burette is also set at mid-height of the sample.

47. Attach the rotating bush drive coupling and place the torque arm against the thrust post.

48. Zero the vertical dial gauge. Place the ball bearing and the loading hanger in position on top of the loading piston.

49. The sample is now ready for its first load increment.

50. Finally, the trimming equipment should be cleaned and lightly oiled with silicone oil and set aside for the next sample.

A P P E N D I X II

TRIAXIAL TEST PROGRAM

Data Preparation Instructions

(FREE-FORMAT VERSION)

SUMMARY

The FORTRAN program TRIAXIAL TEST will reduce the data collected from Consolidated Undrained Triaxial Tests. Details of the input and output information are described. A listing of the program and an example showing the output format are given.

PREPARATION OF INPUT INFORMATION

The program is written in WATFIV and "Free Format" input is used. Input should be presented in the order shown below as Integer or Real. Real number data require decimal points. Data should be separated by commas, or at least two spaces.

The order of the input information is as follows:

Card Type			Format
1.	JSAMP	Sample No.	Integer
	NHOLE	Hole No.	Integer
	TDPTHM	Depth of Sample (Top)	Real
	BDPTHM	Depth of Sample (Bottom)	Real
2.	SHGHTM	Sample Height after Consolidation	Real
	SVOLM	Sample Volume after Consolidation	Real
	SAREAM	Sample Area after Consolidation	Real
	RDILOM	Initial Dial Reading	Real

Card Type			Format
3.	AA	Scale factor for dial gauges not read in units of 0.01 mm	Real
	Note:	(1) AA = 1.0 for dial gauges read in units of 0.01 mm	
		(2) AA is positive for dial gauges giving decreasing readings for sample compression	
		(3) AA is negative for dial gauges giving increasing readings for sample compression	
4.	CLOADM	Constant Load (Dead Load)	Real
	PFCTRM	Proving Ring Factor	Real
	APISTM	Piston Area	Real
5.	CONAXM	Consolidation Axial Stress	Real
	PCONPM	Pre-consolidation Stress	Real
	PWPOM	Initial Porewater Pressure	Real
6.	M	Counting Index (Total No. of points in test series)	Integer
	Note:	Test points for Relaxation Test should not be included	
7.	JDATES	Starting Date of Shear Test	Integer
	JDATEE	Ending Date of Shear Test	Integer

Card Type			Format
8.	JTIME	Time when reading is taken	Integer
	RDIAL	Dial Reading	Real
	PRING	Proving Ring Reading	Real
	PWP	Porewater Pressure during Shear	Real
	CELLPR	Cell Pressure	Real
	JPT	Point where reading is taken	Integer

Note: (1) If (PWP) is negative

- Relaxation Test

(2) If (PWP) is positive

- Consolidated Undrained Triaxial Test

9. Control Cards — Integer

Note: (1) For a single set of data, the control cards are as follows:

(Program Card Deck)

(Data Cards)

(-1 0 0 0 0 0) indicates end of data pack

(0) prints calculated results

(0) searches for new data

(-1 0 0 0) stops program

Note: (2) For multiple sets of data, the control cards are as follows:

(Program Card Deck)

(Data Cards)

(-1 0 0 0 0 0) indicates end of data pack

(0) prints calculated results

(0) searches for new data

(Data Cards)

(-1 0 0 0 0 0) indicates end of data pack

(0) prints calculated results

(0) searches for new data

(-1 0 0 0) stops program

OUTPUT INFORMATION

1. The program will first print out the following input data, i.e.,

Sample No.	JSAMP
Hole No.	NHOLE
Depth of Sample (Top)	TDPTHM
Depth of Sample (Bottom)	BDPTHM
Sample Height after Consolidation	SHGHTM
Sample Volume after Consolidation	SVOLM
Sample Area after Consolidation	SAREAM

Dead Load	CLOADM
Proving Ring Factor	PFCTRM
Piston Area	APISTM
Initial Dial Reading	RDILOM
Starting Date of Shear Test	JDATES
Ending Date of Shear Test	JDATEE
Consolidation Axial Stress	CONAXM
Pre-consolidation Pressure	PCONPM
Normalizing Stress	XNRMSM

2. PRINTOUT OF RESULTS

(i) The Calculated Results are printed in a form of a well organized table which consists of the following:

Point where reading is taken	JPT
Time when reading is taken	JTIME
Dial Reading	RDIAL
Proving Ring Reading	PRING
Porewater Pressure during Shear	PWPRM
Percent (%) Strain	PCSTR
Effective Axial Stress (Eff. Sigma 1.)	EFSTRM
Effective Cell Pressure (Eff. Sigma 3.)	ECELPM
Half Deviator Stress	HDVSTR
Deviator Stress	DVSTRM

Effective Normal Octahedral Stress	OCTSTM
Effective Principal Stress Ratio	RATIO
Porewater Pressure Parameter	A

(ii) A table which consists of Normalized stresses is also printed, i.e.,

Normalized Half Deviator Stress	HDVSTN
Normalized Deviator Stress	DEVSNM
Normalized Effective Normal Octahedral Stress	OCTSNM
Normalized Change in Porewater Pressure	DCTONM

OPERATIONAL PROCEDURE

The program is written in WATFIV and can be operated on the system currently in operation at the 5th Floor Computer Terminal, Engineering Building, University of Manitoba. The control cards are as follows:

```
//jobname[1] JOB 'XXXX,YYYY,,L=2,T=10,C=Ø,CO=1','username'
  (Note XXXX denotes the users' 4-digit    account number,
   and YYYY their security code).
// EXEC WATFIV
//SYSIN DD *
$JOB  WATFIV   username,NOEXT
  (PROGRAM CARD DECK)
$ENTRY
  (DATA CARDS)
/*
```

[1]Maximum 8 characters commencing with a letter

CONCLUSION

A FORTRAN program has been developed for computer in use at University of Manitoba in 1981, which will reduce the raw data collected from Consolidated Undrained Triaxial Test. The calculated results are printed in tabular form.

ACKNOWLEDGEMENT

The author would like to acknowledge Dr. J. Graham for his supervision and useful comments.

```
$JOB  WATFIV   LEW,NOEXT
C*****************************************************************************C
C                                                                             C
C       *             *                                                       C
C      **TRIAXIAL TEST** ( FREE FORMAT VERSION )                              C
C       *             *                                                       C
C     *********************                                                   C
C                                                                             C
C      THIS PROGRAM WILL REDUCE DATA COLLECTED FROM                           C
C                                                                             C
C                              CONSOLIDATED DRAINED TRIAXIAL TESTS            C
C*****************************************************************************C
C                                                                             C
C      TERMS AND DEFINITIONS                                                  C
C      *********************                                                  C
C                                                                             C
C      NOTE: (1) IN THIS VERSION OF THE PROGRAM                               C
C                                                                             C
C                  (1) SAMPLE DIMENSIONS ARE READ IN CENTIMETRES              C
C                                                                             C
C                  (2) SAMPLE DEPTHS ARE READ IN METRES                       C
C                                                                             C
C                  (3) PRESSURES ARE READ IN KPA                              C
C                                                                             C
C                  (4) CONSTANT (DEAD) LOAD IS READ IN NEWTONS                C
C                                                                             C
C                  (5) PROVING RING FACTOR IS READ IN N/DIV                   C
C                                                                             C
C                  (6) DIAL GAUGE READING IS READ IN UNITS OF 0.01 MM         C
C                                                                             C
C      NOTE: (2) FOR SINGLE SET OF TEST DATA                                  C
C                                                                             C
C                  CONTROL CARDS ARE AS FOLLOWS:                              C
C                                                                             C
C                    **********************                                   C
C                    *                    *                                   C
C                    *       PROGRAM      *                                   C
C                    *                    *                                   C
C                    **********************                                   C
C                                                                             C
C                    **********************                                   C
C                    *                    *                                   C
C                    *         DATA       *                                   C
C                    *                    *                                   C
C                    **********************                                   C
C                                                                             C
C                    **********************                                   C
C                    *                    *                                   C
C      CONTROL CARDS *  -1  0  0  0  0  0 *   INDICATES END OF DATA PACK      C
C                    *                    *                                   C
C                    *--------------------*                                   C
C                    *                    *                                   C
C                    *   0                *   PRINTS CALCULATED RESULTS       C
C                    *                    *                                   C
C                    *--------------------*                                   C
C                    *                    *                                   C
C                    *   0                *   SEARCHES FOR NEW DATA           C
C                    *                    *                                   C
C                    *--------------------*                                   C
C                    *  -1  0  0  0       *   STOPS PROGRAM                   C
C                    *                    *                                   C
C                    **********************                                   C
```

NOTE: (3) FOR MULTIPLE SETS OF TEST DATA

CONTROL CARDS ARE AS FOLLOWS:

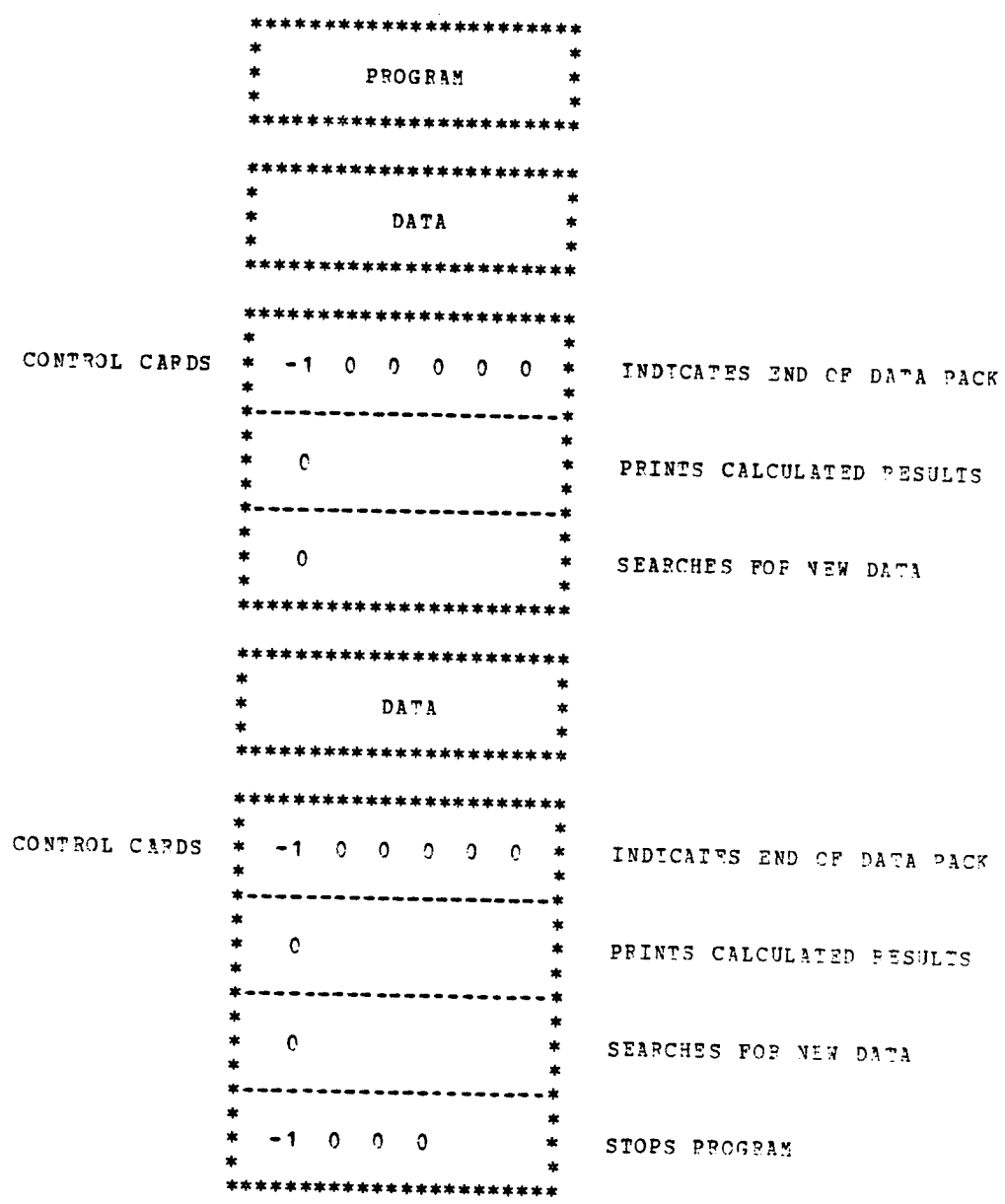

A = POREWATER PRESSURE PARAMETER
AA = SCALE FACTOR FOR DIAL GAUGES NOT READ IN UNITS OF 0.01MM
APISTM = PISTON AREA
AREAM = CURRENT SAMPLE AREA AT ANY STAGE OF THE TEST

B = COUNTING INDEX (CONTROL CARD)
BDPTHM = DEPTH OF SAMPLE (BOTTOM)

CELLPR = CELL PRESSURE
CLOADM = CONSTANT LOAD (DEAD LOAD)
CONAXM = CONSOLIDATION AXIAL STRESS

DEVSNM = NORMALIZED DEVIATOR STRESS
DEVSNO = INITIAL DEVIATOR STRESS (NORMALIZED)
DLTAUM = CHANGE IN POREWATER PRESSURE
DLTUNM = NORMALIZED CHANGE IN POREWATER PRESSURE
DVSTRM = DEVIATOR STRESS

```
C
C     ECELPM  =  EFFECTIVE CELL PRESSURE ( EFF. SIGMA 3 )
C     EFSTRM  =  EFFECTIVE AXIAL STRESS (EFF. SIGMA 1 )
C
C     F       =  ( 1-APISTM/AREAM )
C
C     HDVSTN  =  NORMALIZED HALF DEVIATOR STRESS
C     HDVSTR  =  HALF DEVIATOR STRESS
C
C     I       =  COUNTING INDEX
C
C     JDATEE  =  ENDING DATE OF SHEAR TEST
C     JDATES  =  STARTING DATE OF SHEAR TEST
C     JPT     =  POINT WHERE READING IS TAKEN
C     JPTX    =  POINT WHERE READING IS TAKEN
C     JSAMP   =  SAMPLE NO.
C     JTIME   =  TIME
C
C     M       =  COUNTING INDEX ( TOTAL NO. OF POINTS IN TEST SERIES )
C
C     NHOLE   =  HOLE NO.
C
C     OCTSNM  =  NORMALIZED EFFECTIVE NORMAL OCTAHEDRAL STRESS
C     OCTSTM  =  EFFECTIVE NORMAL OCTAHEDRAL STRESS
C
C     PCONPM  =  PRE-CONSOLIDATION STRESS
C     PCSTR   =  PERCENT (%) STRAIN
C     PCSTRN  =  PERCENT (%) STRAIN
C     PFCTRM  =  PROVING RING FACTOR
C     PRING   =  PROVING RING READING
C     PWP     =  POREWATER PRESSURE DURING SHEAR
C     PWPOM   =  INITIAL POREWATER PRESSURE
C     PWPPM   =  POREWATER PRESSURE DURING SHEAR
C
C     RATIO   =  EFFECTIVE PRINCIPAL STRESS RATIO
C     RDIAL   =  DIAL READING
C     RDILOM  =  INITIAL DIAL READING
C
C     SAREAM  =  SAMPLE AREA AFTER CONSOLIDATION
C     SHGHTM  =  SAMPLE HEIGHT AFTER CONSOLIDATION
C     STRAIN  =  AXIAL STRAIN
C     STRESM  =  TOTAL AXIAL STRESS ( SIGMA 1 )
C     SVOLM   =  SAMPLE VOLUME AFTER CONSOLIDATION
C
C     TDPTHM  =  DEPTH OF SAMPLE (TOP)
C
C     X       =  AXIAL STRESS INCREASE DUE TO CHANGE IN CELL PRESSURE
C     XLOAD   =  AXIAL LOAD
C     XNPMSM  =  NORMALIZING STRESS
C
C     Y       =  AXIAL STRESS DUE TO PROVING RING AND DEAD LOADS
C*************************************************************************
C
C
C     START READING IN ESSENTIAL INFORMATION
C     ======================================
C
1       DIMENSION JPTX(90),STRAIN(90),PCSTRN(90),DEVSNM(90),A(90),
       1OCTSNM(90),DLTUNM(90),HDVSTN(90)
2     1 READ    ,JSAMP,NHOLE,TDPTHM,BDPTHM
3       IF (JSAMP)2,3,3
4     2 CALL EXIT
5     3 PRINT 60
6       PRINT 61
7       READ    ,SHGHTM,SVOLM,SAREAM,RDILOM
8       READ    ,AA
9       READ    ,CLOADM,PFCTRM,APISTM
10      READ    ,CONAXM,PCONPM,PWPOM
11      PRINT 630,JSAMP,NHOLE,TDPTHM,BDPTHM,SHGHTM,SVOLM,
       1SAREAM,CLOADM,PFCTRM,APISTM,RDILOM
```

```
12          9 I=0
13            READ    ,M
14            IF(M) 1,1,10
15         10 READ    ,JDATES,JDATEE
16            PRINT 165,JDATES,JDATEE
17            PRINT 64
18            PRINT 65
19            PRINT 69
20            PRINT 70
21            PRINT 710
22            PRINT 720
C
C
C       INPUT DATA FROM SHEAR TEST
C      ============================
C
23          4 READ    ,JTIME,RDIAL,PRING,PWP,CELLPR ,JPT
24            IF (JTIME)6,5,5
25          5 PWPRM=PWP
26            IF (PWPRM)8,7,7
27          7 I=I+1
C
C
C       STRESS - STRAIN CALCULATION
C      ============================
C
C       NOTE:
C
C       (1) IF ( PWP ) IS NEGATIVE --- RELAXATION TEST
C
C       (3) IF ( PWP ) IS POSITIVE --- CONSOLIDATED UNDRAINED TRIAXIAL TEST
C
C
28            STRAIN(I)=(RDILOM-RDIAL)/(1000.*SHGHTM)*AA
29            PCSTR=STRAIN(I)*100
30            PCSTRN(I)= PCSTR
31            JPTX(I)=JPT
32            AREAM=SAREAM/(1.-STRAIN(I))
33            F=1-APISTM/AREAM
34            X=F*CELLPR
35            XLOAD=PRING*PPCTRM+CLOADM
36            Y=XLOAD/AREAM*10
37            STRESM=X+Y
38            EFSTRM=STRESM-PWPRM
39            ECELPM=CELLPR-PWPRM
40            DVSTRM=(STRESM-CELLPR)
41            HDVSTR=DVSTRM/2
42            OCTSTM=(EFSTRM+2*ECELPM)/3
43            RATIO=EFSTRM/ECELPM
C
C
C       NORMALIZATION OF STRESSES
C      ===========================
C
44            XNRMSM=CONAXM
45            DEVSNM(I)=DVSTRM/XNRMSM
46            HDVSTN(I)=HDVSTR/XNRMSM
47            OCTSNM(I)=OCTSTM/XNRMSM
48            DLTAUM=PWPRM-PWPOM
49            DLTUNM(I)=DLTAUM/XNRMSM
50            IF ( I.EQ.1 ) GO TO 106
51            GO TO 107
52       106  DEVSNO=DEVSNM(1)
53            GO TO 108
54       107  A(I)=DLTUNM(I)/(DEVSNM(I)-DEVSNO)
C
C
```

```
C
C     PRINT CALCULATED RESULTS
C     ========================
C
  108 PRINT980,JPT,JTIME,RDIAL,PRING,PWPRM,PCSTR,
     1EFSIRM,ECELPM,HDVSTR,DVSTRM,OCTSTM,RATIO,A(I)
      GO TO 4
    8 PRINT 81,JPT     ,JTIME,RDIAL,PRING
      GO TO 4
    6 READ    ,B
      IF (B) 13,13,1
   13 PRINT 99
      PRINT 163,JSAMP,NHOLE,TDPTHM,BDPTHM,CONAXM,PCONPM,
     1YNRMSM
      PRINT 265,JDATES,JDATEE
      PRINT 860
      DO 50 I=1,M
      PRINT 82,JPTX(I),PCSTRN(I),HDVSTN(I),DEVSNM(I),OCTSNM(I),
     1DLTUNM(I)
   50 CONTINUE
      PRINT 99
      GO TO 9
   60 FORMAT (1H1,////,23H UNIVERSITY OF MANITOBA)
   61 FORMAT (26H SOIL MECHANICS LABORATORY//)
   64 FORMAT(37H CONSOLIDATED UNDRAINED TRIAXIAL TEST )
   65 FORMAT(37H ::::::::::::::::::::::::::::::::::::    ///)
  163 FORMAT(15H SAMPLE NO. = T,I4,5X,11H HOLE NO. = ,I4,5X,
     1  9H DEPTH = ,F6.2,11H METRES TO ,F6.2,8H METRES  //
     1        37H CONSOLIDATION AXIAL STRESS        = ,F7.2,
     15H KPA /
     1        37H PRECONSOLIDATION PRESSURE         =  ,F7.2,
     15H KPA /
     1        37H NORMALIZING STRESS                =  ,F7.2,
     15H KPA /)
  165 FORMAT(28H SHEAR TEST RESULTS    START,  I10,5H     ,
     13HEND, I10          //)
  265 FORMAT(/  ,39H NORMALIZED SHEAR TEST RESULTS    START,
     1I10,8H     END,I10        //)
   69 FORMAT(46H  PT  TIME      DISPL   PRING   PORE    PEF    ,
     162H  EFFECT   EFFECT   HALF     DEV      EFFECT   PATIO OF      A)
   70 FORMAT(46H                 DIAL    DIAL    PRESS   CENT   ,
     157H  SIGMA1   SIGMA3   DEV      STRESS   OCT      EFF SIGMA1)
  980 FORMAT(I4,2X,I4,3X,F7.1,4X,F5.1,2X,F6.1,2X,F5.2,4X,
     1F5.1,4X,F5.1,4X,F5.1,4X,F5.1,4X,F5.1,5X,F6.3,4X,F7.2)
   81 FORMAT(I4,2X,I4,3X,F7.1,4X,F5.1,3X,15HRELAXATION TEST)
   82 FORMAT(I4,3X,F5.2,5X,F6.3,4X,F6.3,3X,F6.3,4X,F6.3)
  630 FORMAT(15H SAMPLE NO. = T,I4,5X,11H HOLE NO. = ,I4,5X,
     1  9H DEPTH = ,F6.2,11H METRES TO ,F6.2,8H METRES  //
     1 37H SAMPLE HEIGHT AFTER CONSOLIDATION = ,F7.3,
     112H CENTIMETRES /
     1        37H SAMPLE VOLUME AFTER CONSOLIDATION =  ,F7.3,
     118H CUBIC CENTIMETRES  /
     1 38H SAMPLE AREA AFTER CONSOLIDATION   =  ,F6.3,
     1 19H SQUARE CENTIMETRES //
     137H CONSTANT LOAD                      = ,F7.2,5H  N ./
     1 37H PROVING RING FACTOR                = ,F7.4,
     1 9H  N ./DIV /
     1 37H PISTON AREA                        = ,F7.4,
     119H SQUARE CENTIMETRES  //
     1 37H INITIAL DIAL READING               = ,F7.2,
     110H DIVISIONS //)
  710 FORMAT (46H                        RDG     RDG      KPA      STRAIN
     1,57H  KPA       KPA       STRESS   KPA       STRESS   EFF SIGMA3)
  720 FORMAT (45H
     149H                        KPA                  KPA          ,
     1                                                          /)
  860 FORMAT(53H  PT    PER        NRMLZD    NRMLZD    NRMLZD    NRMLZD  /
     1       53H        CENT       HALF      DEV       OCT       CHANGE  /
     1       53H        STRAIN     DEV       STRESS    STRESS    IN PWP  /
     1       53H                   STRESS    KPA       KPA       KPA     /
     1       52H                   KPA                                   /)
   99 FORMAT(1H1,////)
      END
$ENTRY
```

SAMPLE NO. = T 310 HOLE NO. = 4 DEPTH = 11.28 METRES TO 11.66 METRES

SAMPLE HEIGHT AFTER CONSOLIDATION = 12.104 CENTIMETRES
SAMPLE VOLUME AFTER CONSOLIDATION = 538.120 CUBIC CENTIMETRES
SAMPLE AREA AFTER CONSOLIDATION = 44.458 SQUARE CENTIMETRES

CONSTANT LOAD = 14.03 N .
PROVING RING FACTOR = 4.1560 N ./DIV
PISTON AREA = 5.0600 SQUARE CENTIMETRES

INITIAL DIAL READING = 3400.00 DIVISIONS

SHEAR TEST RESULTS START 19801025 END 19801026

CONSOLIDATED UNDRAINED TRIAXIAL TEST

PT	TIME	DISPL DIAL RDG	PRING DIAL RDG	PORE PRESS KPA	PER CENT STRAIN	EFFECT SIGMA1 KPA	EFFECT SIGMA3 KPA	HALF DEV STRESS KPA	DEV STRESS KPA	EFFECT OCT STRESS KPA	RATIO OF EFF SIGMA1 EFF SIGMA3	A
1	1050	3400.0	145.1	217.1	0.00	294.4	203.5	45.5	90.9	233.8	1.447	UUUUUU
2	1100	3388.0	171.0	231.6	0.10	303.9	188.9	57.5	115.0	227.2	1.609	0.60
3	1110	3373.4	182.0	238.2	0.22	307.6	182.5	62.6	125.1	224.2	1.686	0.62
4	1120	3357.2	188.5	242.1	0.35	309.4	178.4	65.5	131.0	222.1	1.735	0.62
5	1130	3337.5	192.1	245.2	0.52	309.6	175.4	67.1	134.2	220.1	1.765	0.65
6	1140	3320.8	194.0	247.6	0.65	308.7	172.9	67.9	135.8	218.2	1.785	0.68
7	1150	3302.8	195.2	249.4	0.80	307.7	171.0	68.3	136.7	216.6	1.799	0.71
8	1210	3264.9	196.7	253.8	1.12	304.0	166.3	68.8	137.7	212.2	1.828	0.79
9	1230	3227.5	197.4	257.9	1.43	300.1	162.2	68.9	137.9	208.2	1.850	0.87
10	1250	3189.0	197.9	262.3	1.74	295.9	158.0	68.9	137.9	204.0	1.873	0.96
11	1310	3152.1	198.1	265.9	2.05	292.1	154.5	68.8	137.6	200.4	1.891	1.05
12	1330	3115.5	198.2	269.5	2.35	288.2	150.9	68.6	137.3	196.7	1.910	1.13
13	1350	3076.6	198.3	272.8	2.67	284.3	147.3	68.5	137.0	193.0	1.930	1.21
14	1410	3038.5	198.3	276.0	2.99	280.7	144.2	68.3	136.5	189.7	1.947	1.29
15	1430	3000.7	198.1	279.2	3.30	276.8	140.9	67.9	135.9	186.2	1.964	1.38
16	1450	2962.5	198.0	282.0	3.61	273.5	138.1	67.7	135.4	183.2	1.980	1.46
17	1510	2924.8	197.9	284.8	3.93	270.2	135.4	67.4	134.8	180.3	1.996	1.54
18	1520	2906.3	197.8	285.7	4.08	269.0	134.5	67.3	134.5	179.3	2.000	1.57
19	1523	2830.0	215.5	293.6	4.71	275.9	126.5	74.7	149.4	176.3	2.181	1.31
20	1524	2801.5	214.0	293.0	4.94	274.7	127.0	73.9	147.7	176.2	2.163	1.34
21	1525	2770.0	213.5	292.7	5.20	274.3	127.4	73.4	146.9	176.4	2.153	1.35
101	1527	2749.5	200.5	RELAXATION TEST								
102	1528	2748.5	195.5	RELAXATION TEST								
103	1530	2747.0	188.5	RELAXATION TEST								
104	1534	2746.0	185.5	RELAXATION TEST								
105	1541	2744.8	181.0	RELAXATION TEST								
106	1556	2743.5	176.5	RELAXATION TEST								
107	1626	2741.8	172.0	RELAXATION TEST								
108	1726	2740.0	168.1	RELAXATION TEST								
109	2028	2738.0	162.1	RELAXATION TEST								
110	2226	2737.3	160.0	RELAXATION TEST								
111	26	2736.9	158.3	RELAXATION TEST								
112	1109	2735.5	152.2	RELAXATION TEST								
22	1140	2735.5	151.9	291.2	5.49	221.3	129.4	46.0	91.9	160.0	1.711	72.92
23	1145	2731.5	166.5	299.9	5.52	225.9	121.1	52.4	104.8	156.0	1.865	5.98
24	1150	2725.3	178.0	305.5	5.57	230.2	115.3	57.4	114.9	153.6	1.996	3.69
25	1200	2710.5	191.0	309.5	5.70	237.4	111.2	63.1	126.2	153.3	2.135	2.62
26	1210	2693.0	197.1	310.6	5.84	241.6	110.2	65.7	131.4	154.0	2.192	2.31
27	1230	2656.3	200.7	310.1	6.14	244.7	110.6	67.1	134.1	155.3	2.213	2.15
28	1250	2619.0	201.3	309.4	6.45	245.5	111.3	67.1	134.2	156.0	2.206	2.13
29	1310	2581.2	200.7	309.2	6.76	244.5	111.3	66.6	133.2	155.7	2.197	2.18
30	1330	2543.8	199.9	309.4	7.07	243.2	111.1	66.1	132.1	155.1	2.189	2.24
31	1331	2516.5	213.5	316.3	7.30	247.7	104.1	71.8	143.6	152.0	2.379	1.88
32	1332	2488.2	214.5	315.9	7.53	248.5	104.4	72.0	144.1	152.4	2.380	1.86
33	1333	2457.5	212.5	314.2	7.79	248.2	106.2	71.0	142.0	153.5	2.337	1.90
34	1334	2425.0	211.0	312.8	8.06	247.8	107.5	70.1	140.3	154.3	2.305	1.94
35	1335	2393.0	209.0	311.6	8.32	246.9	108.8	69.1	138.1	154.8	2.270	2.00
36	1338	2382.5	192.5	303.9	8.41	240.3	116.4	61.9	123.9	157.7	2.064	2.63
37	1350	2359.8	190.2	305.6	8.59	236.4	114.7	60.8	121.7	155.3	2.061	2.88
38	1420	2302.5	189.3	307.9	9.07	232.7	112.4	60.1	120.3	152.5	2.070	3.09
39	1445	2255.5	188.0	309.7	9.46	229.1	110.4	59.3	118.7	150.0	2.075	3.34
40	1446	2235.0	199.7	315.4	9.62	233.1	104.8	64.2	128.3	147.6	2.225	2.63
41	1447	2203.0	200.5	314.5	9.89	234.3	105.6	64.3	128.7	148.5	2.218	2.58
42	1448	2170.0	199.0	313.3	10.16	233.8	106.8	63.5	127.0	149.1	2.189	2.67
43	1449	2140.0	197.0	312.2	10.41	232.8	107.8	62.5	125.0	149.5	2.159	2.79
44	1450	2110.5	195.5	311.4	10.65	232.4	109.0	61.7	123.4	150.1	2.132	2.91
45	1453	2102.8	182.5	305.0	10.72	227.6	115.2	56.2	112.4	152.7	1.976	4.09
46	1510	2070.9	180.8	307.2	10.98	223.6	112.9	55.4	110.7	149.8	1.981	4.56
47	1530	2032.1	180.5	309.5	11.30	220.6	110.5	55.0	110.1	147.2	1.996	4.83
48	1535	2028.3	176.1	308.3	11.33	218.3	112.0	53.2	106.3	147.4	1.950	5.91

SAMPLE NO. = T 310 HOLE NO. = 4 DEPTH = 11.28 METRES TO 11.66 METRES

CONSOLIDATION AXIAL STRESS = 301.70 KPA
PRECONSOLIDATION PRESSURE = 218.00 KPA
NORMALIZING STRESS = 301.70 KPA

NORMALIZED SHEAR TEST RESULTS START 19801025 END 19801026

PT	PER CENT STRAIN	NRMLZD HALF DEV STRESS KPA	NRMLZD DEV STRESS KPA	NRMLZD OCT STRESS KPA	NRMLZD CHANGE IN PWP KPA
1	0.00	0.151	0.301	0.775	0.000
2	0.10	0.191	0.381	0.753	0.048
3	0.22	0.207	0.415	0.743	0.070
4	0.35	0.217	0.434	0.736	0.083
5	0.52	0.222	0.445	0.730	0.093
6	0.65	0.225	0.450	0.723	0.101
7	0.80	0.227	0.453	0.718	0.107
8	1.12	0.228	0.456	0.703	0.122
9	1.43	0.229	0.457	0.690	0.135
10	1.74	0.228	0.457	0.676	0.150
11	2.05	0.228	0.456	0.664	0.162
12	2.35	0.228	0.455	0.652	0.174
13	2.67	0.227	0.454	0.640	0.185
14	2.99	0.226	0.452	0.629	0.195
15	3.30	0.225	0.450	0.617	0.206
16	3.61	0.224	0.449	0.607	0.215
17	3.93	0.223	0.447	0.598	0.224
18	4.08	0.223	0.446	0.594	0.227
19	4.71	0.248	0.495	0.584	0.254
20	4.94	0.245	0.490	0.584	0.252
21	5.20	0.243	0.487	0.585	0.251
22	5.49	0.152	0.305	0.530	0.246
23	5.52	0.174	0.347	0.517	0.274
24	5.57	0.190	0.381	0.509	0.293
25	5.70	0.209	0.418	0.508	0.306
26	5.84	0.218	0.435	0.510	0.310
27	6.14	0.222	0.445	0.515	0.308
28	6.45	0.222	0.445	0.517	0.306
29	6.76	0.221	0.442	0.516	0.305
30	7.07	0.219	0.438	0.514	0.306
31	7.30	0.238	0.476	0.504	0.329
32	7.53	0.239	0.478	0.505	0.327
33	7.79	0.235	0.471	0.509	0.322
34	8.06	0.232	0.465	0.511	0.317
35	8.32	0.229	0.458	0.513	0.313
36	8.41	0.205	0.411	0.523	0.288
37	8.59	0.202	0.403	0.515	0.293
38	9.07	0.199	0.399	0.505	0.301
39	9.46	0.197	0.393	0.497	0.307
40	9.62	0.213	0.425	0.489	0.326
41	9.89	0.213	0.426	0.492	0.323
42	10.16	0.210	0.421	0.494	0.319
43	10.41	0.207	0.414	0.495	0.315
44	10.65	0.204	0.409	0.498	0.313
45	10.72	0.186	0.373	0.506	0.291
46	10.98	0.183	0.367	0.497	0.299
47	11.30	0.182	0.365	0.488	0.306
48	11.33	0.176	0.352	0.489	0.302

APPENDIX III

CONSOLIDATED-DRAINED STRESS-CONTROLLED TEST RESULTS

UNIVERSITY OF MANITOBA
SOIL MECHANICS LABORATORY
ENERGY CALCULATIONS

**** ENGINEERING STRAIN ****

SAMPLE NO. = T 302 HOLE NO. = 4 DEPTH = 11.28 METRES TO 11.68 METRES

TEST RESULTS START 19800722 END 19800802

PT	EFFECT SIGMA1 KPA	EFFECT SIGMA3 KPA	DEV STRESS KPA	EFFECT OCT STRESS KPA	AXIAL STRAIN %	RADIAL STRAIN %	VOL STRAIN %	LSSV KPA	LSNV %	DELTA ENERGY KN-M/VOL	TOTAL ENERGY KN-M/VOL
1	0.0	0.0	0.0	0.0	0.000	0.000	0.000	0.0	0.0		0.000
2	43.0	41.1	1.9	41.7	0.619	0.200	1.019	72.3	0.7	0.215	0.215
3	81.7	79.7	2.0	80.4	1.441	0.522	2.484	139.2	1.6	0.901	1.116
4	120.3	118.2	2.1	118.9	2.092	0.782	3.657	205.9	2.4	1.174	2.290
5	159.7	157.7	2.0	158.4	2.720	1.160	5.040	274.3	3.2	1.921	4.211
6	201.4	199.4	2.0	200.1	3.414	1.670	6.755	346.5	4.2	3.076	7.287
7	240.5	238.5	2.0	239.2	4.174	2.257	8.688	414.3	5.3	4.247	11.534
8	281.2	279.2	2.0	279.9	5.048	2.892	10.832	484.7	6.5	5.567	17.102
9	321.4	319.4	2.0	320.1	6.005	3.396	12.798	554.4	7.7	5.903	23.005
10	362.6	360.5	2.1	361.2	6.874	3.819	14.513	625.6	8.7	5.848	28.853
11	403.1	401.2	1.9	401.8	7.630	4.177	15.985	696.0	9.6	5.621	34.474
12	444.0	442.1	1.9	442.7	8.311	4.509	17.328	766.8	10.5	5.676	40.150

UNIVERSITY OF MANITOBA
SOIL MECHANICS LABORATORY
ENERGY CALCULATIONS

**** ENGINEERING STRAIN ****

SAMPLE NO. = T 303 HOLE NO. = 4 DEPTH = 11.28 METRES TO 11.68 METRES

TEST RESULTS START 19800725 END 19800805

PT	EFFECT SIGMA1 KPA	EFFECT SIGMA3 KPA	DEV STRESS KPA	EFFECT OCT STRESS KPA	AXIAL STRAIN %	RADIAL STRAIN %	VOL STRAIN %	LSSV KPA	LSNV %	DELTA ENERGY KN-M/VOL	TOTAL ENERGY KN-M/VOL
1	118.9	77.2	41.7	91.1	2.978	0.335	3.647	0.0	0.0		0.000
2	159.5	117.6	41.9	131.6	3.851	0.661	5.172	70.1	1.0	1.850	1.850
3	200.1	157.9	42.2	172.0	4.928	1.015	6.959	140.1	2.2	2.914	4.765
4	239.7	197.5	42.2	211.6	6.230	1.396	9.023	208.7	3.6	4.217	8.982
5	280.8	238.5	42.3	252.6	7.679	1.814	11.307	279.7	5.1	5.591	14.573
6	320.9	279.2	41.7	293.1	9.082	2.243	13.567	349.9	6.7	6.439	21.012
7	361.8	319.9	41.9	333.9	10.241	2.580	15.402	420.5	7.9	5.981	26.994
8	402.3	360.4	41.9	374.4	11.179	2.870	16.920	490.6	9.0	5.556	32.550
9	442.8	400.8	42.0	414.8	11.952	3.108	18.168	560.7	9.8	5.074	37.624

UNIVERSITY OF MANITOBA
SOIL MECHANICS LABORATORY
ENERGY CALCULATIONS

**** ENGINEERING STRAIN ****

SAMPLE NO. = T 304 HOLE NO. = 4 DEPTH = 11.28 METRES TO 11.68 METRES

TEST RESULTS START 19800904 END 19800910

PT	EFFECT SIGMA1 KPA	EFFECT SIGMA3 KPA	DEV STRESS KPA	EFFECT OCT STRESS KPA	AXIAL STRAIN %	RADIAL STRAIN %	VOL STRAIN %	LSSV KPA	LSNV %	DELTA ENERGY KN-M/VOL	TOTAL ENERGY KN-M/VOL
1	119.3	77.6	41.7	91.5	2.105	0.655	3.414	0.0	0.0		0.000
										0.397	
2	130.8	73.2	57.6	92.4	2.496	0.593	3.683	13.1	0.4		0.397
										0.360	
3	140.2	66.8	73.4	91.3	3.010	0.353	3.716	25.9	1.0		0.757
										1.353	
4	150.2	61.7	88.5	91.2	4.474	-0.248	3.977	38.2	2.7		2.110
										0.468	
5	161.7	56.3	105.4	91.4	4.952	-0.484	3.985	52.0	3.3		2.578

UNIVERSITY OF MANITOBA
SOIL MECHANICS LABORATORY
ENERGY CALCULATIONS

**** ENGINEERING STRAIN ****

SAMPLE NO. = T 305 HOLE NO. = 4 DEPTH = 11.28 METRES TO 11.68 METRES

TEST RESULTS START 19800908 END 19800914

PT	EFFECT SIGMA1 KPA	EFFECT SIGMA3 KPA	DEV STRESS KPA	EFFECT OCT STRESS KPA	AXIAL STRAIN %	RADIAL STRAIN %	VOL STRAIN %	LSSV KPA	LSNV %	DELTA ENERGY KN-M/VOL	TOTAL ENERGY KN-M/VOL
1	118.7	77.0	41.7	90.9	2.256	0.402	3.059	0.0	0.0		0.000
										0.143	
2	122.7	69.1	53.6	87.0	2.493	0.304	3.100	11.9	0.3		0.143
										0.181	
3	127.8	62.4	65.4	84.2	2.825	0.125	3.075	22.6	0.7		0.324
										0.432	
4	130.2	53.1	77.1	78.8	3.502	-0.257	2.987	35.7	1.6		0.756
										0.389	
5	134.4	45.2	89.2	74.9	3.994	-0.524	2.946	47.6	2.2		1.144

UNIVERSITY OF MANITOBA
SOIL MECHANICS LABORATORY
ENERGY CALCULATIONS

**** ENGINEERING STRAIN ****

SAMPLE NO. = T 306 HOLE NO. = 4 DEPTH = 11.28 METRES TO 11.68 METRES

TEST RESULTS START 19801003 END 19801004

PT	EFFECT SIGMA1 KPA	EFFECT SIGMA3 KPA	DEV STRESS KPA	EFFECT OCT STRESS KPA	AXIAL STRAIN %	RADIAL STRAIN %	VOL STRAIN %	LSSV KPA	LSNV %	DELTA ENERGY KN-M/VOL	TOTAL ENERGY KN-M/VOL
1	116.0	75.1	40.9	88.7	0.000	0.000	0.000	0.0	0.0		0.000
2	123.0	67.8	55.2	86.2	0.100	-0.050	0.000	12.5	0.1	0.048	0.048
3	125.2	63.6	61.6	84.1	0.260	-0.130	0.000	18.7	0.3	0.093	0.141
4	126.6	61.8	64.8	83.4	0.370	-0.185	0.000	21.6	0.5	0.070	0.211
5	127.2	60.0	67.2	82.4	0.510	-0.255	0.000	24.1	0.6	0.092	0.303
6	127.9	58.8	69.1	81.8	0.650	-0.325	0.000	25.9	0.8	0.095	0.399
7	128.1	57.5	70.6	81.0	0.790	-0.395	0.000	27.7	1.0	0.098	0.497
8	128.7	55.6	73.1	80.0	1.070	-0.535	0.000	30.4	1.3	0.201	0.698
9	128.9	54.3	74.6	79.2	1.360	-0.680	0.000	32.1	1.7	0.214	0.912
10	128.9	53.0	75.9	78.3	1.650	-0.825	0.000	33.8	2.0	0.218	1.130
11	129.0	52.2	76.8	77.8	1.940	-0.970	0.000	34.9	2.4	0.221	1.352
12	128.8	51.3	77.5	77.1	2.250	-1.125	0.000	36.0	2.8	0.239	1.591
13	128.8	51.2	77.6	77.1	2.520	-1.260	0.000	36.1	3.1	0.209	1.800
14	128.8	50.6	77.8	76.5	2.820	-1.410	0.000	36.8	3.5	0.233	2.033
15	127.3	50.2	77.1	75.9	3.260	-1.630	0.000	37.0	4.0	0.341	2.374
16	126.3	49.9	76.4	75.4	3.690	-1.845	0.000	37.1	4.5	0.330	2.704
17	125.0	49.6	75.4	74.7	4.140	-2.070	0.000	37.2	5.1	0.342	3.046
18	123.7	49.6	74.1	74.3	4.560	-2.280	0.000	36.9	5.6	0.314	3.360
19	121.7	49.8	71.9	73.8	5.020	-2.510	0.000	36.2	6.1	0.336	3.695
20	119.7	49.9	69.8	73.2	5.470	-2.735	0.000	35.8	6.7	0.319	4.014
21	117.8	50.2	67.6	72.7	5.920	-2.960	0.000	35.3	7.3	0.309	4.323
22	115.7	50.4	65.3	72.2	6.350	-3.175	0.000	34.9	7.8	0.286	4.609
23	110.3	51.5	58.8	71.1	7.580	-3.790	0.000	33.9	9.3	0.763	5.372
24	101.4	51.1	50.3	67.9	14.770	-7.385	0.000	36.9	18.1	3.922	9.294
25	99.8	50.4	49.4	66.9	17.160	-8.580	0.000	38.5	21.0	1.191	10.486
26	98.6	50.5	48.1	66.5	18.930	-9.465	0.000	38.9	23.2	0.863	11.349

UNIVERSITY OF MANITOBA
SOIL MECHANICS LABORATORY
ENERGY CALCULATIONS

**** ENGINEERING STRAIN ****

SAMPLE NO. = T 307 HOLE NO. = 4 DEPTH = 11.28 METRES TO 11.68 METRES

TEST RESULTS START 19801002 END 19801011

PT	EFFECT SIGMA1 KPA	EFFECT SIGMA3 KPA	DEV STRESS KPA	EFFECT OCT STRESS KPA	AXIAL STRAIN %	RADIAL STRAIN %	VOL STRAIN %	LSSV KPA	LSNV %	DELTA ENERGY KN-M/VOL	TOTAL ENERGY KN-M/VOL
1	117.1	76.1	41.0	89.8	2.705	0.357	3.418	0.0	0.0		0.000
2	130.6	80.6	50.0	97.3	3.130	0.347	3.824	14.9	0.4	0.511	0.511
3	144.1	84.2	59.9	104.2	3.768	0.260	4.287	29.3	1.1	0.732	1.244
4	157.6	87.8	69.8	111.1	4.437	0.177	4.792	43.7	1.8	0.868	2.112
5	171.2	91.5	79.7	118.1	5.354	-0.003	5.347	58.3	2.7	1.183	3.295
6	184.6	95.3	89.3	125.1	6.876	-0.403	6.070	72.8	4.3	1.961	5.256
7	195.8	98.3	97.5	130.8	10.509	-1.571	7.366	84.7	8.3	4.648	9.904
8	211.6	102.3	109.3	138.7	11.177	-1.877	7.424	101.5	9.0	0.749	10.653

UNIVERSITY OF MANITOBA
SOIL MECHANICS LABORATORY
ENERGY CALCULATIONS

**** ENGINEERING STRAIN ****

SAMPLE NO. = T 308 HOLE NO. = 4 DEPTH = 11.28 METRES TO 11.68 METRES

TEST RESULTS START 19801006 END 19801018

PT	EFFECT SIGMA1 KPA	EFFECT SIGMA3 KPA	DEV STRESS KPA	EFFECT OCT STRESS KPA	AXIAL STRAIN %	RADIAL STRAIN %	VOL STRAIN %	LSSV KPA	LSNV %	DELTA ENERGY KN-M/VOL	TOTAL ENERGY KN-M/VOL
1	117.2	76.3	40.9	89.9	2.469	0.438	3.385	0.0	0.0		0.000
2	149.6	96.6	53.0	114.3	3.343	0.504	4.352	43.3	0.9	1.281	1.281
3	180.9	115.9	65.0	137.6	4.463	0.488	5.440	84.8	2.0	1.817	3.098
4	213.3	136.5	76.8	162.1	6.224	0.379	6.983	128.4	3.8	3.196	6.294
5	245.0	156.4	88.6	185.9	9.045	0.072	9.190	170.8	6.6	5.565	11.859
6	276.7	176.7	100.0	210.0	12.303	-0.383	11.537	213.5	9.9	6.981	18.840
7	308.1	196.3	111.8	233.6	15.310	-0.799	13.713	255.4	13.0	7.243	26.082
8	340.8	216.6	124.2	258.0	17.607	-1.049	15.508	298.9	15.3	6.416	32.499
9	372.7	236.3	136.4	281.8	19.233	-1.229	16.774	341.3	16.9	4.986	37.484
10	404.7	256.3	148.4	305.8	20.727	-1.400	17.927	384.0	18.4	4.967	42.452

UNIVERSITY OF MANITOBA
SOIL MECHANICS LABORATORY
ENERGY CALCULATIONS

**** ENGINEERING STRAIN ****

SAMPLE NO. = T 309 HOLE NO. = 4 DEPTH = 11.28 METRES TO 11.68 METRES

TEST RESULTS START 19801015 END 19801029

PT	EFFECT SIGMA1 KPA	EFFECT SIGMA3 KPA	DEV STRESS KPA	EFFECT OCT STRESS KPA	AXIAL STRAIN %	RADIAL STRAIN %	VOL STRAIN %	LSSV KPA	LSNV %	DELTA ENERGY KN-M/VOL	TOTAL ENERGY KN-M/VOL
1	116.7	75.6	41.1	89.3	2.356	0.423	3.201	0.0	0.0		0.000
2	140.7	94.6	46.1	110.0	2.911	0.525	3.961	36.0	0.6	0.889	0.889
3	164.0	112.9	51.1	129.9	3.469	0.642	4.753	70.9	1.2	1.093	1.982
4	187.7	131.5	56.2	150.2	4.242	0.740	5.723	106.3	1.9	1.600	3.582
5	210.3	149.1	61.2	169.5	5.120	0.859	6.839	139.9	2.8	2.081	5.663
6	234.3	168.1	66.2	190.2	6.201	0.925	8.051	175.9	3.9	2.611	8.274
7	256.9	185.7	71.2	209.4	7.411	0.967	9.345	209.5	5.1	3.120	11.394
8	280.8	204.8	76.0	230.1	8.745	1.011	10.768	245.6	6.4	3.760	15.154
9	303.8	222.6	81.2	249.7	9.955	1.049	12.053	279.7	7.7	3.697	18.851
10	327.4	241.3	86.1	270.0	11.000	1.092	13.185	315.1	8.7	3.500	22.351
11	374.1	277.9	96.2	310.0	12.609	1.136	14.882	384.8	10.3	5.872	28.223
12	420.4	314.2	106.2	349.6	14.111	1.198	16.507	454.0	11.8	6.331	34.554

UNIVERSITY OF MANITOBA
SOIL MECHANICS LABORATORY
ENERGY CALCULATIONS

**** ENGINEERING STRAIN ****

SAMPLE NO. = T 311 HOLE NO. = 4 DEPTH = 11.28 METRES TO 11.66 METRES

TEST RESULTS START 19801027 END 19801116

PT	EFFECT SIGMA1 KPA	EFFECT SIGMA3 KPA	DEV STRESS KPA	EFFECT OCT STRESS KPA	AXIAL STRAIN %	RADIAL STRAIN %	VOL STRAIN %	LSSV KPA	LSNV %	DELTA ENERGY KN-M/VOL	TOTAL ENERGY KN-M/VOL
1	118.3	76.7	41.6	90.6	2.311	0.527	3.364	0.0	0.0		0.000
2	137.7	89.2	48.5	105.4	2.822	0.621	4.063	26.2	0.5	0.810	0.810
3	157.3	101.8	55.5	120.3	3.331	0.605	4.542	52.7	1.0	0.722	1.532
4	177.0	114.0	63.0	135.0	3.925	0.625	5.176	78.9	1.6	1.036	2.568
5	197.0	126.8	70.2	150.2	4.758	0.631	6.021	105.9	2.5	1.572	4.140
6	216.9	139.4	77.5	165.2	5.890	0.569	7.028	132.6	3.6	2.176	6.317
7	237.1	152.4	84.7	180.6	7.325	0.482	8.288	159.9	5.0	3.002	9.319
8	256.5	164.6	91.9	195.2	9.042	0.297	9.636	185.9	6.7	3.653	12.971
9	275.8	176.7	99.1	209.7	10.755	0.103	10.961	211.7	8.5	3.897	16.868
10	295.7	189.4	106.3	224.8	12.379	-0.083	12.212	238.5	10.1	3.958	20.826
11	315.8	201.9	113.9	239.9	13.740	-0.240	13.260	265.2	11.5	3.549	24.375
12	355.4	227.9	127.5	270.4	16.020	-0.616	14.788	319.3	13.8	6.036	30.411
13	394.0	252.2	141.8	299.5	18.697	-1.073	16.551	371.0	16.5	7.837	38.247
14	434.2	277.4	156.8	329.7	20.749	-1.400	17.949	424.7	18.6	6.766	45.013
15	473.7	302.2	171.5	359.4	22.577	-1.652	19.273	477.5	20.5	6.838	51.851
16	513.9	327.5	186.4	389.6	23.945	-1.820	20.305	531.3	21.9	5.697	57.548
17	554.3	353.3	201.0	420.3	25.189	-1.958	21.272	585.8	23.1	5.701	63.249
18	594.2	378.6	215.6	450.5	26.185	-2.079	21.987	639.3	24.1	4.608	67.857

UNIVERSITY OF MANITOBA
SOIL MECHANICS LABORATORY
ENERGY CALCULATIONS

**** ENGINEERING STRAIN ****

SAMPLE NO. = T 312 HOLE NO. = 4 DEPTH = 11.28 METRES TO 11.66 METRES

TEST RESULTS START 19801103 END 19801221

PT	EFFECT SIGMA1 KPA	EFFECT SIGMA3 KPA	DEV STRESS KPA	EFFECT OCT STRESS KPA	AXIAL STRAIN %	RADIAL STRAIN %	VOL STRAIN %	LSSV KPA	LSNV %	DELTA ENERGY KN-M/VOL	TOTAL ENERGY KN-M/VOL
1	118.5	76.9	41.6	90.8	2.136	0.552	3.240	0.0	0.0		0.000
2	137.2	88.9	48.3	105.0	2.666	0.577	3.821	25.3	0.5	0.720	0.720
3	157.3	101.7	55.6	120.2	3.206	0.650	4.506	52.3	1.1	0.933	1.653
4	177.1	114.1	63.0	135.1	3.781	0.676	5.134	78.8	1.7	1.019	2.672
5	197.1	126.9	70.2	150.3	4.750	0.692	6.134	105.7	2.6	1.850	4.522
6	216.8	139.3	77.5	165.1	6.055	0.636	7.327	132.1	3.9	2.552	7.074
7	236.5	151.8	84.7	180.0	7.525	0.542	8.608	158.6	5.4	3.057	10.130
8	256.4	164.5	91.9	195.1	9.004	0.395	9.793	185.4	6.9	3.180	13.310
9	276.1	176.9	99.2	210.0	10.543	0.246	11.035	211.7	8.4	3.591	16.901
10	295.9	189.5	106.4	225.0	11.998	0.102	12.203	238.4	9.9	3.636	20.537

UNIVERSITY OF MANITOBA
SOIL MECHANICS LABORATORY
ENERGY CALCULATIONS

**** ENGINEERING STRAIN ****

SAMPLE NO. = T 314 HOLE NO. = 4 DEPTH = 11.28 METRES TO 11.66 METRES

TEST RESULTS START 19801118 END 19801209

PT	EFFECT SIGMA1 KPA	EFFECT SIGMA3 KPA	DEV STRESS KPA	EFFECT OCT STRESS KPA	AXIAL STRAIN %	RADIAL STRAIN %	VOL STRAIN %	LSSV KPA	LSNV %	DELTA ENERGY KN-M/VOL	TOTAL ENERGY KN-M/VOL
1	0.0	0.0	0.0	0.0	0.000	0.000	0.000	0.0	0.0		0.000
2	52.2	50.2	2.0	50.9	0.570	0.535	1.641	88.1	0.9	0.418	0.418
3	67.2	65.2	2.0	65.9	0.802	0.663	2.129	114.1	1.2	0.286	0.704
4	82.1	80.1	2.0	80.8	1.029	0.802	2.633	139.9	1.5	0.371	1.075
5	97.0	95.0	2.0	95.7	1.251	0.938	3.128	165.7	1.8	0.438	1.512
6	112.1	110.2	1.9	110.8	1.420	1.073	3.567	192.0	2.1	0.454	1.966
7	127.1	125.1	2.0	125.8	1.610	1.226	4.063	217.8	2.4	0.587	2.553
8	142.1	139.5	2.6	140.4	1.895	1.372	4.639	243.1	2.7	0.769	3.322
9	156.9	154.9	2.0	155.6	2.057	1.568	5.192	269.5	3.0	0.818	4.140
10	171.5	169.4	2.1	170.1	2.299	1.767	5.834	294.6	3.4	1.046	5.186
11	187.1	185.1	2.0	185.8	2.558	1.995	6.549	321.8	3.8	1.273	6.458
12	201.1	199.0	2.1	199.7	2.863	2.249	7.361	345.9	4.3	1.566	8.024
13	217.2	215.1	2.1	215.8	3.209	2.559	8.328	373.8	4.8	2.009	10.033
14	232.3	230.3	2.0	231.0	3.708	2.736	9.181	400.0	5.4	1.910	11.943
15	246.9	244.9	2.0	245.6	4.099	3.000	10.100	425.3	5.9	2.191	14.135
16	261.9	259.9	2.0	260.6	4.495	3.266	11.026	451.3	6.4	2.345	16.480
17	276.8	274.9	1.9	275.5	4.876	3.513	11.903	477.2	7.0	2.353	18.832
18	291.3	289.2	2.1	289.9	5.263	3.738	12.740	502.1	7.5	2.368	21.201
19	306.9	304.9	2.0	305.6	5.648	3.948	13.545	529.3	7.9	2.399	23.600
20	588.6	587.3	1.3	587.7	9.023	5.653	20.329	1018.0	12.1	30.319	53.919

UNIVERSITY OF MANITOBA
SOIL MECHANICS LABORATORY
ENERGY CALCULATIONS

**** ENGINEERING STRAIN ****

SAMPLE NO. = T 313 HOLE NO. = 4 DEPTH = 11.28 METRES TO 11.66 METRES

TEST RESULTS START 19801117 END 19801217

PT	EFFECT SIGMA1 KPA	EFFECT SIGMA3 KPA	DEV STRESS KPA	EFFECT OCT STRESS KPA	AXIAL STRAIN %	RADIAL STRAIN %	VOL STRAIN %	LSSV KPA	LSHV %	DELTA ENERGY KN-M/VOL	TOTAL ENERGY KN-M/VOL
1	118.2	76.6	41.6	90.5	2.181	0.497	3.176	0.0	0.0		0.000
2	123.7	80.2	43.5	94.7	2.327	0.510	3.346	7.5	0.1	0.195	0.195
3	130.7	84.9	45.8	100.2	2.487	0.539	3.565	17.1	0.3	0.252	0.448
4	137.4	89.1	48.3	105.2	2.622	0.532	3.686	26.1	0.4	0.169	0.616
5	144.3	93.5	50.8	110.4	2.776	0.544	3.864	35.4	0.6	0.239	0.855
6	150.2	96.9	53.3	114.7	2.948	0.563	4.075	43.0	0.8	0.290	1.146
7	156.9	101.2	55.7	119.8	3.123	0.557	4.237	52.0	0.9	0.256	1.401
8	163.4	105.3	58.1	124.7	3.309	0.565	4.440	60.7	1.1	0.315	1.717
9	170.3	109.8	60.5	130.0	3.507	0.563	4.634	70.1	1.3	0.326	2.043
10	176.0	113.6	62.4	134.4	3.728	0.579	4.885	78.0	1.6	0.416	2.459
11	183.5	118.0	65.5	139.8	3.996	0.598	5.193	87.7	1.8	0.528	2.987
12	190.0	122.2	67.8	144.8	4.246	0.587	5.420	96.5	2.1	0.439	3.426
13	196.9	126.6	70.3	150.0	4.550	0.581	5.712	105.8	2.4	0.573	4.000
14	203.3	130.6	72.7	154.8	4.894	0.575	6.044	114.3	2.7	0.673	4.673
15	209.9	134.7	75.2	159.8	5.297	0.568	6.433	123.1	3.1	0.814	5.487
16	216.4	138.8	77.6	164.7	5.781	0.561	6.902	131.8	3.6	1.011	6.498
17	223.6	143.7	79.9	170.3	6.353	0.522	7.397	141.8	4.2	1.150	7.647
18	229.8	147.3	82.5	174.8	6.864	0.465	7.794	149.8	4.7	0.993	8.640
19	236.5	151.7	84.8	180.0	7.362	0.410	8.183	159.0	5.2	0.998	9.638
20	243.1	155.9	87.2	185.0	7.958	0.359	8.677	167.9	5.8	1.272	10.910
21	249.4	159.6	89.8	189.5	8.660	0.308	9.276	176.0	6.5	1.566	12.477
22	256.1	164.0	92.1	194.7	9.319	0.238	9.795	185.2	7.1	1.439	13.916
23	262.5	167.8	94.7	199.4	9.906	0.175	10.256	193.5	7.7	1.313	15.229
24	269.7	172.7	97.0	205.0	10.530	0.119	10.767	203.5	8.4	1.468	16.697
25	275.6	176.3	99.3	209.4	11.089	0.058	11.204	211.3	8.9	1.311	18.008
26	282.7	180.7	102.0	214.7	11.593	0.008	11.609	220.8	9.4	1.230	19.238
27	289.3	185.0	104.3	219.8	12.133	-0.027	12.079	229.7	10.0	1.416	20.655
28	295.9	189.2	106.7	224.8	12.649	-0.062	12.525	238.6	10.5	1.379	22.033
29	447.8	289.9	157.9	342.5	16.764	-2.063	12.638	446.8	15.0	5.715	27.748

UNIVERSITY OF MANITOBA
SOIL MECHANICS LABORATORY
ENERGY CALCULATIONS

**** ENGINEERING STRAIN ****

SAMPLE NO. = T 315 HOLE NO. = 5 DEPTH = 11.28 METRES TO 11.66 METRES

TEST RESULTS START 19810112 END 19810209

PT	EFFECT SIGMA1 KPA	EFFECT SIGMA3 KPA	DEV STRESS KPA	EFFECT OCT STRESS KPA	AXIAL STRAIN %	RADIAL STRAIN %	VOL STRAIN %	LSSV KPA	LSNV %	DELTA ENERGY KN-M/VOL	TOTAL ENERGY KN-M/VOL
1	118.7	77.1	41.6	91.0	1.656	0.280	2.215	0.0	0.0		0.000
										0.228	
2	129.1	71.6	57.5	90.8	2.005	0.142	2.289	13.0	0.4		0.228
										0.255	
3	140.2	66.8	73.4	91.3	2.316	0.023	2.363	26.0	0.8		0.483
										0.274	
4	150.0	60.8	89.2	90.5	2.725	-0.227	2.272	38.9	1.3		0.757
										0.333	
5	156.0	58.7	97.3	91.1	3.087	-0.411	2.264	45.5	1.7		1.090
										0.423	
6	160.7	55.8	104.9	90.8	3.589	-0.736	2.116	51.7	2.4		1.513
										0.184	
7	166.0	53.3	112.7	90.9	3.754	-0.815	2.124	58.1	2.6		1.697

UNIVERSITY OF MANITOBA
SOIL MECHANICS LABORATORY
ENERGY CALCULATIONS

**** ENGINEERING STRAIN ****

SAMPLE NO. = T 316 HOLE NO. = 5 DEPTH = 11.28 METRES TO 11.66 METRES

TEST RESULTS START 19810113 END 19810121

PT	EFFECT SIGMA1 KPA	EFFECT SIGMA3 KPA	DEV STRESS KPA	EFFECT OCT STRESS KPA	AXIAL STRAIN %	RADIAL STRAIN %	VOL STRAIN %	LSSV KPA	LSNV %	DELTA ENERGY KN-M/VOL	TOTAL ENERGY KN-M/VOL
1	118.3	76.8	41.5	90.6	1.542	0.080	1.701	0.0	0.0		0.000
										-0.161	
2	110.3	65.4	44.9	80.4	1.527	-0.022	1.483	18.0	0.1		-0.161
										-0.184	
3	102.2	53.9	48.3	70.0	1.496	-0.148	1.199	36.2	0.3		-0.345
										-0.141	
4	94.8	43.0	51.8	60.3	1.496	-0.295	0.907	53.3	0.5		-0.487
										-0.164	
5	87.2	32.1	55.1	50.5	1.520	-0.542	0.437	70.5	0.9		-0.650
										-0.072	
6	79.4	20.4	59.0	40.1	1.685	-0.939	-0.194	88.7	1.4		-0.722
										3.940	
7	66.8	9.2	57.6	28.4	8.673	-4.887	-1.102	108.6	10.0		3.218

UNIVERSITY OF MANITOBA
SOIL MECHANICS LABORATORY
ENERGY CALCULATIONS

**** ENGINEERING STRAIN ****

SAMPLE NO. = T 317 HOLE NO. = 5 DEPTH = 11.28 METRES TO 11.66 METRES

TEST RESULTS START 19810113 END 19810121

PT	EFFECT SIGMA1 KPA	EFFECT SIGMA3 KPA	DEV STRESS KPA	EFFECT OCT STRESS KPA	AXIAL STRAIN %	RADIAL STRAIN %	VOL STRAIN %	LSSV KPA	LSNV %	DELTA ENERGY KN-M/VOL	TOTAL ENERGY KN-M/VOL
1	118.3	76.8	41.5	90.6	0.000	0.000	0.000	0.0	0.0		0.000
2	126.0	76.7	49.3	93.1	0.083	-0.008	0.067	7.7	0.1	0.089	0.089
3	131.1	76.7	54.4	94.8	0.174	-0.020	0.134	12.8	0.2	0.099	0.188
4	142.3	76.8	65.5	98.6	0.443	-0.063	0.317	24.0	0.5	0.302	0.489
5	156.4	76.7	79.7	103.3	0.822	-0.165	0.492	38.1	0.9	0.409	0.899
6	158.1	76.7	81.4	103.8	0.875	-0.179	0.517	39.8	0.9	0.062	0.961
7	159.7	76.5	83.2	104.2	0.926	-0.192	0.542	41.4	1.0	0.061	1.022
8	162.6	76.9	85.7	105.5	1.004	-0.210	0.584	44.3	1.0	0.098	1.120
9	165.3	76.9	88.4	106.4	1.114	-0.248	0.618	47.0	1.2	0.122	1.242
10	171.7	77.0	94.7	108.6	1.305	-0.319	0.668	53.4	1.4	0.213	1.455
11	173.8	77.0	96.8	109.3	1.403	-0.355	0.693	55.5	1.5	0.113	1.568
12	182.1	77.3	104.8	112.2	1.744	-0.488	0.768	63.8	1.9	0.402	1.970
13	182.7	77.0	105.7	112.2	1.797	-0.510	0.776	64.4	1.9	0.062	2.032
14	183.6	76.6	107.0	112.3	1.863	-0.543	0.776	65.3	2.0	0.070	2.102
15	184.4	76.7	107.7	112.6	1.928	-0.563	0.801	66.1	2.1	0.089	2.191
16	185.7	77.0	108.7	113.2	2.003	-0.592	0.818	67.4	2.2	0.094	2.285
17	186.5	76.9	109.6	113.4	2.086	-0.622	0.843	68.2	2.3	0.110	2.395
18	187.5	76.7	110.8	113.6	2.211	-0.672	0.868	69.2	2.4	0.157	2.552
19	189.0	76.7	112.3	114.1	2.336	-0.726	0.885	70.7	2.6	0.152	2.704
20	191.4	76.8	114.6	115.0	2.770	-0.918	0.935	73.1	3.1	0.531	3.235
21	191.8	76.7	115.1	115.1	2.964	-0.998	0.968	73.5	3.3	0.248	3.483
22	192.6	77.0	115.6	115.5	3.233	-1.141	0.951	74.3	3.6	0.297	3.781
23	192.6	76.7	115.9	115.3	3.372	-1.223	0.926	74.3	3.8	0.142	3.922
24	189.6	76.8	112.8	114.4	3.810	-1.433	0.943	71.3	4.3	0.514	4.436
25	187.1	76.6	110.5	113.4	4.043	-1.529	0.985	68.8	4.6	0.292	4.728
26	183.9	76.5	107.4	112.3	4.300	-1.653	0.993	65.6	4.9	0.286	5.015
27	182.2	76.6	105.6	111.8	4.414	-1.710	0.993	63.9	5.0	0.121	5.136
28	175.4	76.8	98.6	109.7	4.837	-1.947	0.943	57.1	5.6	0.394	5.530
29	171.2	76.4	94.8	108.0	5.129	-2.080	0.968	52.9	5.9	0.302	5.831

UNIVERSITY OF MANITOBA
SOIL MECHANICS LABORATORY
ENERGY CALCULATIONS

**** ENGINEERING STRAIN ****

SAMPLE NO. = T 319 HOLE NO. = 5 DEPTH = 11.28 METRES TO 11.66 METRES

TEST RESULTS START 19810130 END 19810130

PT	EFFECT SIGMA1 KPA	EFFECT SIGMA3 KPA	DEV STRESS KPA	EFFECT OCT STRESS KPA	AXIAL STRAIN %	RADIAL STRAIN %	VOL STRAIN %	LSSV KPA	LSNV %	DELTA ENERGY KN-M/VOL	TOTAL ENERGY KN-M/VOL
1	117.1	76.2	40.9	89.8	0.000	0.000	0.000	0.0	0.0		0.000
2	124.6	66.8	57.8	86.1	0.100	-0.050	0.000	15.3	0.1	0.049	0.049
3	129.2	62.0	67.2	84.4	0.220	-0.110	0.000	23.4	0.3	0.075	0.124
4	132.6	58.4	74.2	83.1	0.340	-0.170	0.000	29.6	0.4	0.085	0.209
5	136.5	55.9	80.6	82.8	0.470	-0.235	0.000	34.6	0.6	0.101	0.310
6	139.8	53.8	86.0	82.5	0.600	-0.300	0.000	39.0	0.7	0.108	0.418
7	145.1	51.3	93.8	82.6	0.790	-0.395	0.000	45.0	1.0	0.171	0.589
8	151.6	49.5	102.1	83.5	1.050	-0.525	0.000	51.1	1.3	0.255	0.844
9	156.9	49.5	107.4	85.3	1.330	-0.665	0.000	54.9	1.6	0.293	1.137
10	159.5	51.8	107.7	87.7	1.600	-0.800	0.000	54.7	2.0	0.290	1.427
11	159.7	53.9	105.8	89.2	1.880	-0.940	0.000	53.0	2.3	0.299	1.726
12	156.1	56.1	100.0	89.4	2.170	-1.085	0.000	48.3	2.7	0.298	2.025
13	136.7	68.0	68.7	90.9	2.580	-1.290	0.000	22.8	3.2	0.346	2.370
14	130.5	69.9	60.6	90.1	3.070	-1.535	0.000	16.1	3.8	0.317	2.687
15	128.2	70.5	57.7	89.7	3.580	-1.790	0.000	13.7	4.4	0.302	2.989
16	127.4	70.9	56.5	89.7	4.000	-2.000	0.000	12.7	4.9	0.240	3.229

A P P E N D I X IV

ENERGY CALCULATION PROGRAM

(LSSV and LSNV included)

Data Preparation Instructions

(REVISED FREE-FORMAT VERSION)

SUMMARY

The ENERGY CALCULATION program is a simple FORTRAN program for the calculation of Strain-Energy stored in a triaxial clay sample during Drained Triaxial Consolidation or during Undrained Shear. In addition, the program will also calculate the Length of the Stress Vector (LSSV) and the Length of Strain Vector (LSNV) from the approximate in-situ stress state to the stress state at the end of each successive stress increment.

PREPARATION OF INPUT INFORMATION

Stress-Strain values at each stress increment should be first calculated, either by hand or by using the TRIAXIAL TEST program (LEW, 1981).

The program is written in WATFIV and "Free-Format" input is used. Input should be presented in the order shown below as Integer or Real. Real number data require decimal points. Data should be separated by commas, or at least two spaces.

The order of the input information is as follows:

Card Type			Format
1.	JSAMP	Sample No.	Integer
	NHOLE	Hole No.	Integer
	TDPTHM	Depth of Sample (Top)	Real
	BDPTHM	Depth of Sample (Bottom)	Real

2.	N	Counting Index (Total No. of points in test series)	Integer
3.	JDATES	Starting Data of Test	Integer
	JDATEE	Ending Data of Test	Integer
4.	ESIMA1	Effective Sigma 1	Real
	ESIMA3	Effective Sigma 3	Real
	ASTRN1	Axial Strain	Real
	VOLSTN	Volumetric Strain	Real
	JPT	Stress Point	Integer

NOTE:

(1) Stresses are read in kPa.

(2) Strains are read in percent in terms of Engineering strain.

(3) Sample depths are read in metres.

OUTPUT INFORMATION

1. The program will first print out the following input data:

Sample No.	JSAMP
Hole No.	NHOLE
Depth of Sample (Top)	TDPTHM

Depth of Sample (Bottom)	BDPTHM
Starting Date of Test	JDATES
Ending Date of Test	JDATEE

2. Printout of Results

The calculated results are printed in a form of a well organized table in terms of both Engineering and Natural strain which consists of the following:

Stress Point	JPT
Effective Sigma 1	ESIMA1
Effective Sigma 3	ESIMA3
Deviator Stress	DEVSTM
Effective Normal Octahedral Stress	OCTSTM
Axial Strain	ASTRN1
Radial Strain	RSTRN3
Volumetric Strain	VOLSTN
Length of Stress Vector	LSSV
Length of Strain Vector	LSNV
Delta Energy	DELENE
Total Energy	TOTENE

ALGORITHM

(1) Strain-Energy

$$W = \Sigma \left(\left(\frac{\sigma'_{1(j+1)} + \sigma'_{1(j)}}{2} \right) \left(\varepsilon_{1(j+1)} - \varepsilon_{1(j)} \right) + 2 \left(\frac{\sigma'_{3(j+1)} + \sigma'_{3(j)}}{2} \right) \right.$$

$$\left. x \left(\varepsilon_{3(j+1)} - \varepsilon_{3(j)} \right) \right) \qquad j = 1, M$$

(2) Length of Stress Vector (LSSV)

$$LSSV = \left((\sigma'_{1(j)} - p'_o)^2 + 2 (\sigma'_{3(j)} - K_o p'_o)^2 \right)^{1/2} \qquad j = 1, N$$

(3) Length of Strain Vector (LSNV)

$$LSNV = \left((\varepsilon_{1(j)} - \varepsilon_{1(0)})^2 + 2 (\varepsilon_3 - \varepsilon_{3(0)})^2 \right)^{1/2}$$

NOTES:

(1) p'_o and $K_o p'_o$ are the approximate in-situ stresses.

(2) $\varepsilon_{1(0)}$ and $\varepsilon_{3(0)}$ are strains that occurred from initial building-in to the approximate in-situ stress levels.

OPERATIONAL PROCEDURE

The program is written in WATFIV and can be operated on the system currently in operation at the 5th Floor Computer Terminal, Engineering Building, University of Manitoba. The control cards are as follows:

```
//jobname[1] JOB 'XXXX,YYYY,,L=2,T=10,C=Ø,CO=1','username'
  (Note XXXX denotes the users' 4-digit    account number,
  and YYYY their security code)
// EXEC WATFIV
//SYSIN DD *
$JOB  WATFIV   username,NOEXT
  (PROGRAM CARD DECK)
$ENTRY
  (DATA CARDS)
/*
```

[1]Maximum 8 characters commencing with a letter

CONCLUSION

A FORTRAN program has been developed for the computer in use at the University of Manitoba in 1981, which will perform the calculation of Strain-Energy stored in a triaxial clay sample during Drained Triaxial Consolidation or during Undrained Shear. In addition, Length of Stress Vector (LSSV) and Length of Strain Vector (LSNV) from in-situ stress levels to the stress state at the end of each stress increment are calculated and reported.

ACKNOWLEDGEMENT

The writer would like to acknowledge Dr. J. Graham for his supervision and useful comments.

TERMS AND DEFINITIONS

ASIMA1	Average Effective Sigma 1
ASIMA3	Average Effective Sigma 3
ASTRN1	Axial Strain in Percent (Eng. Strain)
BDPTHM	Depth of Sample (Top)
DELENE	Change in Strain Energy (Eng. Strain)
DELENN	Change in Strain Energy (Natural Strain)
DESTRN1	Change in Axial Strain (Eng. Strain)
DESTRN3	Change in Radial Strain (Eng. Strain)
DEVSTM	Deviator Stress
ESIMA1	Effective Sigma 1
ESIMA3	Effective Sigma 3
I	Counting Index
II	Counting Index
INCSN1	Incremental change in Axial Strain in Percent (Natural Strain)
INCSN3	Incremental change in Radial Strain in Percent (Natural Strain)
INVOL	Incremental change in Volumetric Strain in Percent (Natural Strain)

ISTRN1	Axial Strain that occurred when restressed to in-situ stress levels (Eng. Strain)
ISTRN3	Radial Strain that occurred when restressed to in-situ stress levels (Eng. Strain)
J	Counting Index
JJ	Counting Index
JDATEE	Ending Date of Test
JDATES	Starting Date of Test
JPT	Stress Point
JSAMP	Sample Number
K	Counting Index
KK	Counting Index
L	Counting Index
LSNV	Length of Strain Vector
LSNVE	Length of Strain Vector (Eng. Strain)
LSNVN	Length of Strain Vector (Natural Strain)
LSSV	Length of Stress Vector
M	Counting Index
N	Counting Index
NHOLE	Hole Number

NSTRN1	Axial Strain in Percent (Natural Strain)
NSTRN3	Radial Strain in Percent (Natural Strain)
NVOLSN	Volumetric Strain in Percent (Natural Strain)
OCTSTM	Effective Normal Octahedral Stress
OSIMA1	Approximate p'_o
OSIMA3	Approximate $K_o\ p'_o$
OSTRN1	Axial Strain that occurred when restressed to in-situ stress levels (Natural Strain)
OSTRN3	Radial Strain that occurred when restressed to in-situ stress levels (Natural Strain)
RSTRN3	Radial Strain in Percent (Eng. Strain)
TDPTHM	Depth of Sample (Bottom)
TOTENE	Total Strain Energy (Eng. Strain)
TOTENN	Total Strain Energy (Natural Strain)
VOLSTN	Volumetric Strain in Percent (Eng. Strain)

```
$JOB  WATFIV   LEW,NOEXT
C
C      ************************************
C      *                                  *
C      *    ENERGY  CALCULATION  PROGRAM  *
C      *    ::::::::::::::::::::::::::    *
C      *                                  *
C      ************************************
C
C      NOTE : IN THIS VERSION OF THE PROGRAM
C
C             (1)  STRESSES ARE READ IN KPA
C
C             (2)  STRAINS ARE READ IN PERCENT (ENGINEERING STRAINS)
C
C             (3)  SAMPLE DEPTHS ARE READ IN METRES
C
      DIMENSION JPT(90),ESIMA1(90),ESIMA3(90),ASTRN1(90),RSTRN3(90),
     1DEVSTM(90),OCTSTM(90),VOLSTN(90),ASIMA1(90),ASIMA3(90),
     1DESTN1(90),DESTN3(90),LSSV(90),DELENE(90),TOTENE(90),
     1NSTRN1(90),NSTRN3(90),DELENN(90),TOTENN(90),INCSN1(90),
     1INCSN3(90),INVOL(90),NVOLSN(90),LSNVE(90),LSNVN(90)
      REAL LSSV,NSTRN1,NSTRN3,NVOLSN,INCSN1,INCSN3,INVOL,LSNVE,LSNVN
      REAL ISTRN1,ISTRN3
C
C      READING IN ESSENTIAL INFORMATION
C      ::::::::::::::::::::::::::::::::
C
      READ,  JSAMP,NHOLE,TDPTHM,BDPTHM
      READ,  N
      READ,  JDATES,JDATEE
      PRINT  60
      PRINT  70
      PRINT  71
      PRINT  72
      PRINT  80,  JSAMP,NHOLE,TDPTHM,BDPTHM
      PRINT  100, JDATES,JDATEE
      PRINT  81
      PRINT  82
      PRINT  83
      PRINT  84
      DO     10  I=1,N
C
C      READING IN STRESS-STRAIN VALUES
C      ::::::::::::::::::::::::::::::::
C
      READ,  ESIMA1(I),ESIMA3(I),ASTRN1(I),VOLSTN(I),JPT(I)
      DEVSTM(I)=ESIMA1(I)-ESIMA3(I)
      OCTSTM(I)=(ESIMA1(I)+2*ESIMA3(I))/3
      RSTRN3(I)=(VOLSTN(I)-ASTRN1(I))/2
   10 CONTINUE
      L=N-1
      NSTRN1(1)=ASTRN1(1)/(1-ASTRN1(1)/200)
      NVOLSN(1)=VOLSTN(1)/(1-VOLSTN(1)/200)
      NSTRN3(1)=(NVOLSN(1)-NSTRN1(1))/2
      DO     12  II=1,L
      INCSN1(II)=(ASTRN1(II+1)-ASTRN1(II))/
     1           (1-(ASTRN1(II+1)+ASTRN1(II))/200)
      INVOL(II)=(VOLSTN(II+1)-VOLSTN(II))/
     1          (1-(VOLSTN(II+1)+VOLSTN(II))/200)
      INCSN3(II)=(INVOL(II)-INCSN1(II))/2
   12 CONTINUE
      DO     13   K=1,L
      NSTRN1(K+1)=INCSN1(K)+NSTRN1(K)
      NSTRN3(K+1)=INCSN3(K)+NSTRN3(K)
      NVOLSN(K+1)=INVOL(K)+NVOLSN(K)
   13 CONTINUE
      OSIMA1=ESIMA1(1)
      OSIMA3=ESIMA3(1)
      OSTRN1=ASTRN1(1)
      OSTRN3=RSTRN3(1)
      ISTRN1=NSTRN1(1)
      ISTRN3=NSTRN3(1)
```

```
43          DO      11  I=1,N
44          LSSV(I)=SQRT((ESIMA1(I)-OSIMA1)**2+2*(ESIMA3(I)-OSIMA3)**2)
45          LSNVE(I)=SQRT((ASTRN1(I)-OSTRN1)**2+2*(RSTRN3(I)-OSTRN3)**2)
46          LSNVV(I)=SQRT((NSTRN1(I)-ISTRN1)**2+2*(NSTRN3(I)-ISTRN3)**2)
47       11 CONTINUE
C
C
C           ENERGY CALCULATIONS
C           ::::::::::::::::::
C
48          M=N-1
49          DO      20  J=1,M
50          ASIMA1(J)=(ESIMA1(J+1)+ESIMA1(J))/2
51          ASIMA3(J)=(ESIMA3(J+1)+ESIMA3(J))/2
52          DESTN1(J)=ASTRN1(J+1)-ASTRN1(J)
53          DESTN3(J)=RSTRN3(J+1)-RSTRN3(J)
54          DELENE(J)=(ASIMA1(J)*DESTN1(J)+2*ASIMA3(J)*DESTN3(J))/100
55          DELENN(J)=(ASIMA1(J)*(NSTRN1(J+1)-NSTRN1(J))   +
           1          2*ASIMA3(J)*(NSTRN3(J+1)-NSTRN3(J)))/100
56       20 CONTINUE
57          TOTENE(1)=0.0
58          TOTENN(1)=0.0
59          DO      30 K=1,M
60          TOTENE(K+1)=DELENE(K)+TOTENE(K)
61          TOTENN(K+1)=DELENN(K)+TOTENN(K)
62       30 CONTINUE
C
C
C           PRINT CALCULATED RESULTS
C           ::::::::::::::::::::::::
C
53          DO      40 KK=1,N
64          PRINT  90, JPT(KK),ESIMA1(KK),ESIMA3(KK),DEVSIM(KK),OCTSIM(KK),
           1ASTRN1(KK),RSTRN3(KK),VOLSTN(KK),LSSV(KK),LSNVE(KK),TOTENE(KK)
55          IF (KK.EQ.N)  GO TO 40
66          PRINT  91, DELENE(KK)
57       40 CONTINUE
68          PRINT  60
69          PRINT  70
70          PRINT  71
71          PRINT  73
72          PRINT  80,  JSAMP,NHOLE,TDPTHM,BDPTHM
73          PRINT  100, JDATES,JDATEE
74          PRINT  81
75          PRINT  82
76          PRINT  83
77          PRINT  84
78          DO      41 JJ=1,N
79          PRINT  90, JPT(JJ),ESIMA1(JJ),ESIMA3(JJ),DEVSIM(JJ),OCTSIM(JJ),
           1NSTRN1(JJ),NSTRN3(JJ),NVOLSN(JJ),LSSV(JJ),LSNVN(JJ),TOTENN(JJ)
80          IF (JJ.EQ.N)  GO TO 41
81          PRINT  91, DELENN(JJ)
82       41 CONTINUE
83          PRINT  99
84       60 FORMAT(1H1,////,23H UNIVERSITY OF MANITOBA)
85       70 FORMAT(26H SOIL MECHANICS LABORATORY)
86       71 FORMAT(20H ENERGY CALCULATIONS/)
87       72 FORMAT(31H ****  ENGINEERING STRAIN  ****//)
88       73 FORMAT(31H ****    NATURAL STRAIN    ****//)
89       80 FORMAT(15H SAMPLE NO. = T,I4,5X,11H HOLE NO. = ,I4,5X,
           1  9H DEPTH = ,F6.2,11H METRES TO ,F6.2,8H METRES  //)
90       81 FORMAT(47H  PT    EFFECT    EFFECT    DEV      EFFECT    AXIAL,
           150H    RADIAL    VOL       LSSV    LSNV     DELTA     TOTAL)
91       82 FORMAT(48H        SIGMA1    SIGMA3    STRESS  OCT       STRAIN,
           151H  STRAIN    STRAIN                    ENERGY    ENERGY )
92       83 FORMAT(45H        KPA       KPA       KPA     STRESS      %,
           154H        %         %       KPA      %      KN-M/VOL KN-M/VOL)
93       84 FORMAT(36H                                    KPA/)
94       90 FORMAT(I4,2X,F6.1,3X,F6.1,2X,F6.1,3X,F6.1,4X,F6.3,2X,F6.3,
           13X,F6.3,2X,F6.1,2X,F4.1,11X,F7.3)
95       91 FORMAT(81X,F7.3)
96      100 FORMAT(22H TEST RESULTS    START,  I10,5H     ,
           13HEND, I10     ///)
97       99 FORMAT(1H1,////)
98          STOP
99          END

$ENTRY
```

UNIVERSITY OF MANITOBA
SOIL MECHANICS LABORATORY
ENERGY CALCULATIONS

**** ENGINEERING STRAIN ****

SAMPLE NO. = T 312 HOLE NO. = 4 DEPTH = 11.28 METRES TO 11.66 METRES

TEST RESULTS START 19801103 END 19801221

PT	EFFECT SIGMA1 KPA	EFFECT SIGMA3 KPA	DEV STRESS KPA	EFFECT OCT STRESS KPA	AXIAL STRAIN %	RADIAL STRAIN %	VOL STRAIN %	LSSV KPA	LSNV %	DELTA ENERGY KN-M/VOL	TOTAL ENERGY KN-M/VOL
1	118.5	76.9	41.6	90.8	2.136	0.552	3.240	0.0	0.0		0.000
2	137.2	88.9	48.3	105.0	2.666	0.577	3.821	25.3	0.5	0.720	0.720
3	157.3	101.7	55.6	120.2	3.206	0.650	4.506	52.3	1.1	0.933	1.653
4	177.1	114.1	63.0	135.1	3.781	0.676	5.134	78.8	1.7	1.019	2.672
5	197.1	126.9	70.2	150.3	4.750	0.692	6.134	105.7	2.6	1.850	4.522
6	216.8	139.3	77.5	165.1	6.055	0.636	7.327	132.1	3.9	2.552	7.074
7	236.5	151.8	84.7	180.0	7.525	0.542	8.608	158.6	5.4	3.057	10.130
8	256.4	164.5	91.9	195.1	9.004	0.395	9.793	185.4	6.9	3.180	13.310
9	276.1	176.9	99.2	210.0	10.543	0.246	11.035	211.7	8.4	3.591	16.901
10	295.9	189.5	106.4	225.0	11.998	0.102	12.203	238.4	9.9	3.636	20.537

UNIVERSITY OF MANITOBA
SOIL MECHANICS LABORATORY
ENERGY CALCULATIONS

**** NATURAL STRAIN ****

SAMPLE NO. = T 312 HOLE NO. = 4 DEPTH = 11.28 METRES TO 11.66 METRES

TEST RESULTS START 19801103 END 19801221

PT	EFFECT SIGMA1 KPA	EFFECT SIGMA3 KPA	DEV STRESS KPA	EFFECT OCT STRESS KPA	AXIAL STRAIN %	RADIAL STRAIN %	VOL STRAIN %	LSSV KPA	LSNV %	DELTA ENERGY KN-M/VOL	TOTAL ENERGY KN-M/VOL
1	118.5	76.9	41.6	90.8	2.159	0.567	3.293	0.0	0.0		0.000
2	137.2	88.9	48.3	105.0	2.702	0.597	3.896	25.3	0.5	0.743	0.743
3	157.3	101.7	55.6	120.2	3.258	0.676	4.610	52.3	1.1	0.970	1.714
4	177.1	114.1	63.0	135.1	3.854	0.708	5.270	78.8	1.7	1.065	2.779
5	197.1	126.9	70.2	150.3	4.866	0.732	6.330	105.7	2.7	1.951	4.730
6	216.8	139.3	77.5	165.1	6.246	0.682	7.609	132.1	4.1	2.721	7.451
7	236.5	151.8	84.7	180.0	7.823	0.589	9.001	158.6	5.7	3.305	10.756
8	256.4	164.5	91.9	195.1	9.435	0.435	10.306	185.4	7.3	3.488	14.244
9	276.1	176.9	99.2	210.0	11.141	0.276	11.692	211.7	9.0	3.996	18.240
10	295.9	189.5	106.4	225.0	12.781	0.117	13.014	238.4	10.6	4.107	22.347

A P P E N D I X V

ON CURVE-FITTING, AND LABORATORY DATA

(TECHNICAL NOTE)

ON CURVE-FITTING, AND LABORATORY DATA

by

J. Graham[1], R.B. Pinkney[1], K.V. Lew[2] and P.G.S. Trainor[2]

[1]Associate Professor, Civil Engineering Department, University of Manitoba, Winnipeg, Manitoba.

[2]Graduate Student, Civil Engineering Department, University of Manitoba, Winnipeg, Manitoba.

ABSTRACT

The evaluation of soil properties in laboratory tests involves interpretation of data on the basis of accepted empirical procedures. In limit-state studies, it has proved difficult to establish procedures for identifying yield, which are independent of stress path, and independent of the plotting method used. Mini-computers and automatic curve-fitting techniques have been examined as possible sources of rational, repeatable, inexpensive results. Results show that the conclusions drawn from the tests may depend strongly on the evaluation procedures. Careful examination and judgement are still necessary.

INTRODUCTION

For some years, one of us has been involved with the acquisition and interpretation of data like those shown in Figures 1a, b, c. The data are normally collected from drained stress-controlled triaxial tests on carefully trimmed samples consolidated anisotropically to in-situ stresses. Basic soil properties of the three soils are listed in Table 1. Figure 1a shows σ'_{oct} versus $\Delta V/V$ results from a soft marine clay from N. Ireland which was tested at constant shear stress (Crooks and Graham, 1976). In Figure 1b, the results come from a triaxial test under approximately K_o-conditions on plastic lacustrine clay from Manitoba (Lew, 1981). Figure 1c shows the strain energy W absorbed during undrained shearing versus stress vector length LSSV from a sample of highly sensitive marine clay from Norway (Graham, 1969). If results of this general shape are obtained in many branches of materials science, they are interpreted as showing evidence of yielding, or material property changes, at limit state conditions defined by empirical procedures which are commonly accepted in the field.

Workers in solid mechanics define yielding as the limit-state at which non-reversible plastic straining commences. Prior linear elastic behaviour is not a prerequisite. A clay soil is not a continuum, but a particulate material, and the classical definition of yielding is not appropriate. Non-recoverable strains occur in clays, even at low stresses.

TABLE 1 Soil Classification Data

Site	Mastemyr	Kinnegar	Winnipeg 5.5 m	Winnipeg 11.5 m
Moisture Content %	43-47	63-69	55	55-62
Liquid Limit %	31-35	78-86	95	79-86
Plasticity Index %	8-12	51-57	65	54-57
Und. Shear Strength kPa	10	19	81	45
Sensitivity	100	6-8	2-3	3-4
Compression Index	0.6	0.35	0.72	1.0
Overconsolidation Ratio	1.3	1.3	7.0	1.8
Clay Fraction %	12-15	35-40	85	75
Dominant Mineralogy	-	illite	smectite	smectite
Reference	Graham, 1969	Crooks and Graham, 1976	Trainor, 1981	Lew, 1981

However, in a more general sense, the concept of yielding in clays is now commonly accepted (Crooks and Graham, 1976; Tavenas et al., 1979) to be the limit-state when soils reach a well-defined boundary in p', q, e - space. At stresses lower than yield stresses, the clay is relatively incompressible, creep rates are slow, porewater pressure generation small, and porewater pressure dissipation rapid. At stresses higher than yield stresses, the clay is more compressible, creep rates are faster, larger porewater pressures are generated, and their dissipation is slower.

Questions then arise regarding the empirical procedures to be

adopted for determining the magnitude of the stresses at yield. Bi-linear curve-fitting has frequently been used with data similar to those shown in Figure 2a, for example by Mitchell (1970). Its use with oedometer results is commonly limited to lean, sensitive, kaolin-illite clays. In contrast, the soil in Figure 2a is a plastic, insensitive, illite-montmorillonite clay (Baracos et al., 1980). Figure 2b shows the oedometer test data from Figure 2a replotted as an "e-log p" curve, with the p'_c-yield interpreted using the well known Casagrande construction.

The procedures used should ideally be rational and repeatable, and should minimise the influence of the person using them. It is sometimes suggested that the use of mini-computers and automatic curve-fitting techniques would reduce personal influences, and therefore provide more rational, repeatable results. This Note outlines some experiences which show that the suggestion must be used with discretion.

EXAMPLES

Test data such as those shown in Figure 3 for Lake Agassiz clay (Lew, 1981) can be represented as two fairly linear sections separated by a curved transitional section. At one stage during the review of these data, it was suggested that yielding could perhaps be associated with the point on the test curve where the curvature was maximum, (minimum radius of curvature, $\delta R/\delta s = 0$). A program which had previously been used successfully for fitting stress-strain data in metals was adapted to superimpose a best-fit Ramberg-Osgood function

(1) $$x/x_o = (y/y_o)(1 + |y/y_o|^{r-1})$$

through the test data using the method of least squares (Popov and Pinkney, 1969). This was then differentiated numerically, and the point of maximum curvature determined. The process was essentially automatic, once the experimental data had been read into the computer. However, when the function was examined visually, the Ramberg-Osgood function was in this case a relatively poor representation of the test data, although it had worked well for other materials. The data were then fitted by simple polynomial functions. Very good agreement was obtained using 4th order and higher polynomials. Unfortunately however, there was no obvious agreement between limit-state stresses obtained by numerical differentiation of the polynomial, and values decided intuitively on the basis of judgement.

It then seemed appropriate to return to bilinear fitting of the data, and to interpret yielding as the intersection of the initial and final linear sections. This was done by using a bilinear function with a slope discontinuity at x = c. This can be represented conveniently by

(2) $$y = y_o + ax + (b - a) < x - c >^1 ,$$

where $$< x - c >^1 \equiv \begin{cases} x - c, & x \geq c \\ o, & x < c \end{cases} ,$$

and a, b are the slopes of the function for $x < c$, and $x \geq c$ respectively.

If (x_i, y_i) represents the i-th observation of the independent and

dependent variables respectively, then the difference, or "error" in prediction between the observed value of y, and the value predicted by (2) is

$$e_i = y_o + ax_i + (b - a) < x_i - c >^1 - y_i \tag{3}$$

The method of least squares was used to determine y_o, a, b, and c such that the sum of the squares of the errors in N observations was minimized. The resulting computer program was applied to the results from a variety of tests similar to those shown in Figure 1.

The program worked well with most sets of test data, and it appeared that a reliable, impersonal procedure had been developed. It was possible, (but not advisable), to proceed from tabulated laboratory data to a numerical prediction of yield stresses without visually examining the detailed shape of the stress-strain curve. The authors advise against this automatic process. In recent studies of the use of mini-computers to process bilinear data, the authors found that only 6 out of 43 tests could be handled without using discretionary judgement. It is always necessary to be fully aware of the general shape of the stress-strain relationship which is being fitted.

Two separate examples from recent studies on Lake Agassiz clay will show why this is important. In Figure 4a, the data points have been shown as open circles in the initial and final linear sections, and as solid circles in the transition section. As programmed, the computer cannot exercise judgement to identify the data points on the transition section, and it fits two straight lines through all the data points, as shown by the dashed lines. If judgement is permitted, then the solid

points can be ignored and the curve-fitting is shown by solid lines in the figure. The difference in the yield stresses can be significant. In Figure 4b, a sample of sensitive clay was tested in undrained extension after it had been anisotropically consolidated to in-situ stresses. It gave out a small amount of energy in the early stages of testing, and then changed markedly, as failure was approached, until it was absorbing energy at a high rate. It is unreasonable to interpret the yield stress as the intersection of the two straight lines shown in Figure 4b.

In contrast with the previous examples in which yielding is self-evident and the difficulty lies in establishing acceptable procedures for consistently evaluating the yield stresses, Figure 5a shows oedometer results from two samples of brown, fissured, plastic Lake Agassiz clay which appear not to have yielded (Trainor, 1981). However, if the same data are plotted in the traditional way as an e-log p' curve, then Figure 5b shows results which might be readily acceptable for many plastic swelling clays. Unthinking application of the Casagrande construction would produce values for p'_c, even though the samples did not yield (Figure 5a) in the sense of the compressibility increasing markedly at some identifiable limit stress. The inferred value of p'_c has little significance. Care should be taken that the plotting technique - in this case semi-logarithmic plotting - does not imply behaviour which is absent from the original data.

This point is developed further in Figure 6. In Figure 6a, some non-yielding data are shown, together with three straight lines with different slopes which could represent this type of behaviour. The same data and lines are plotted in e, log p'-space in Figure 6b.

Not only is there a tendency to infer p'_c values from non-yielding data, but the value of p'_c depends on the slope of the line. It also depends on the relative dimensional scales which are used for the void ratio and log(pressure) axes.

The semi-logarithmic construction for p'_c requires the identification of the point of maximum curvature. If a straight line

(4) $$e = a - b\,p'$$

in e, p'-space is transformed into e, log p'-space, then

(5) $$P' = K \log_{10}(p'), \quad \text{and therefore}$$

(6) $$e = a - b \exp(P'/0.434K), \quad \text{where}$$

(7) (dimension of 1 log cycle of p') = K x (dimension of $\Delta e = 1.0$)

The curvature of (6) is given by

(8) $$C(P') = \{ 1 + (de/dP')^2 \}^{-1.5} \times d^2e/d(P')^2$$

This is maximum when

(9) $$p' = \frac{0.434\ K}{\sqrt{2}\ b}$$

Thus the points of maximum curvature, and therefore the p'_c-value, depend directly on the physical scales which are used for plotting the data. It is perhaps fortunate that only a limited range of plotting scales are used in practice. The problem is not acute when the maximum curvature in the semi-logarithmic plot is clearly identified, and the virgin consolidation behaviour is straight.

Finally, attention should be drawn to the definition of engineering strain which is commonly used in soil mechanics, namely the total change in a representative dimension, say sample height, divided by the dimension at the beginning of the test. Similarly, in void ratio calculations $\Delta e = \Delta H/H_s$, the divisor H_s is constant throughout the test. Oedometer tests on compressible clays often measure vertical compressions of 20%, and void ratio changes of 0.8. Other branches of engineering commonly limit the use of engineering strain to only a few percent. Figure 7a shows results from an oedometer test on Winnipeg clay. The curve drops steeply after p'_c is exceeded, but at high strains it becomes concave upwards. In sensitive marine clays, this has been attributed to changes in porewater electrolyte conditions following deposition (Bjerrum, 1967). In other cases, part of the curvature of the post-p'_c section may simply depend on how the laboratory data have been processed and plotted. Figures 7a and 7b show the same observational data. In Figure 7b, vertical strains have been calculated as "natural" strains

$$\varepsilon_v = \Sigma \{(H_i - H_{i-1})/0.5 \times (H_i + H_{i+1})\}, \tag{9}$$

and the post-p'_c line is straighter than in Figure 7a.

DISCUSSION

Previous paragraphs have shown examples of curve-fitting techniques which in some cases have failed to identify yield points which are clearly present in the data; and in other cases have implied

yields for which there is no justification. The authors have recently become aware of similar problems faced by colleagues in mechanical and electrical engineering. Little is apparently available in the literature concerning the influence of empirical data-handling methods on the conclusions which are drawn from the data. The interaction of measuring systems with observations is well known. Influences at the interpretive stage of reducing laboratory data appear to be less generally appreciated.

CONCLUSIONS

Procedures used for manipulating and presenting laboratory data may themselves significantly affect the conclusions which can be drawn from testing programs. It might appear that impersonal treatment of data by automatic computation, should produce more consistent and rational results with less effort and cost. However, the results may not be more relevant to practical applications. Computer convenience and efficiency challenge engineers with more careful exercise of experience, judgement and common sense.

ACKNOWLEDGEMENTS

Funding support was provided by the Natural Sciences and Engineering Research Council of Canada under Grant Number A3712, and a Graduate Fellowship from the University of Manitoba. The interest of our colleague Andrew Baracos is gratefully acknowledged.

REFERENCES

Baracos, A., Graham, J., and Domaschuk, L. 1980. "Yielding and Rupture In a Lacustrine Clay". Canadian Geotechnical Journal, 17, pp. 559-573.

Bjerrum, L. 1967. "The Engineering Geology of Norwegian Normally Consolidated Marine Clays as Related to the Settlement of Buildings". Geotechnique 17, pp. 81-118.

Crooks, J.H.A., and Graham, J. 1976. "Geotechnical Properties of the Belfast Estuarine Deposits". Geotechnique 26, pp. 293-315.

Graham, J. 1969. "Laboratory Results from Mastemyr Quick Clay After Reconsolidation to the In-Situ Stresses". Norwegian Geotechnical Institute, Oslo, Norway, Internal Report F372-5.

Lew, K.V. 1981. "Yielding Criteria and Limit-State in a Winnipeg Clay". M.Sc. Thesis, University of Manitoba, Winnipeg, Manitoba, 197p.

Mitchell, R.J. 1970. "On the Yielding and Mechanical Strength of Leda Clays". Canadian Geotechnical Journal, 7, pp. 297-312.

Popov, E.P., and Pinkney, R.B. 1969. "Cyclic Yield Reversal in Steel Building Connections". A.S.C.E. Journal of the Structural Division, 95, ST3, pp. 327-353.

Tavenas, F., J.P. Des Rosiers, S. Leroueil, P. La Rochelle, and M. Roy. 1979. "The Use of Strain Energy as a Yield and Creep Criterion for Lightly Overconsolidated Clays". Geotechnique 29, pp. 285-304.

Trainor, P.G.S. 1981. M.Sc. Thesis, University of Manitoba, Winnipeg, Manitoba. In Preparation.

NOTATION

b	=	slope of linear data in e, p'-space
e	=	void ratio, error
H	=	sample height
K	=	ratio of scale dimensions in e, log p'-space (Eqn. 6)
K_o	=	ratio of horizontal to vertical effective stresses under conditions of zero lateral strain
LSSV	=	length of stress vector in p', q-space
q	=	deviator stress $(\sigma_1 - \sigma_3)$
p'	=	mean principal effective stress $(\sigma'_1 + 2\sigma'_3)/3$
$\Delta V/V$	=	volumetric strain
W	=	energy absorbed/unit volume
ε_v	=	vertical strain
σ'_{oct}	=	effective normal octahedral stress = p'

LIST OF FIGURES

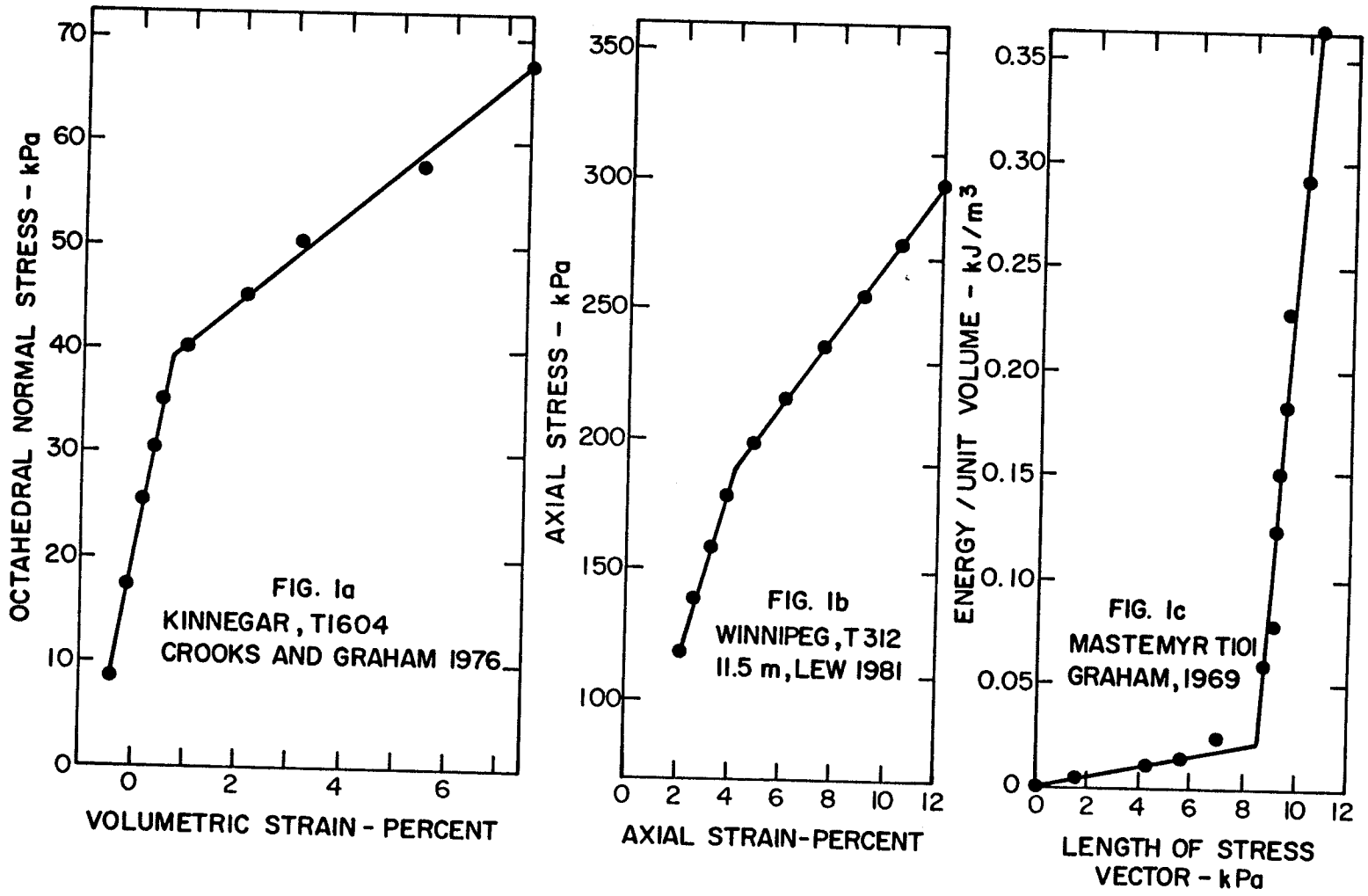

FIGURE 1 Typical Laboratory Data for Yielding Samples

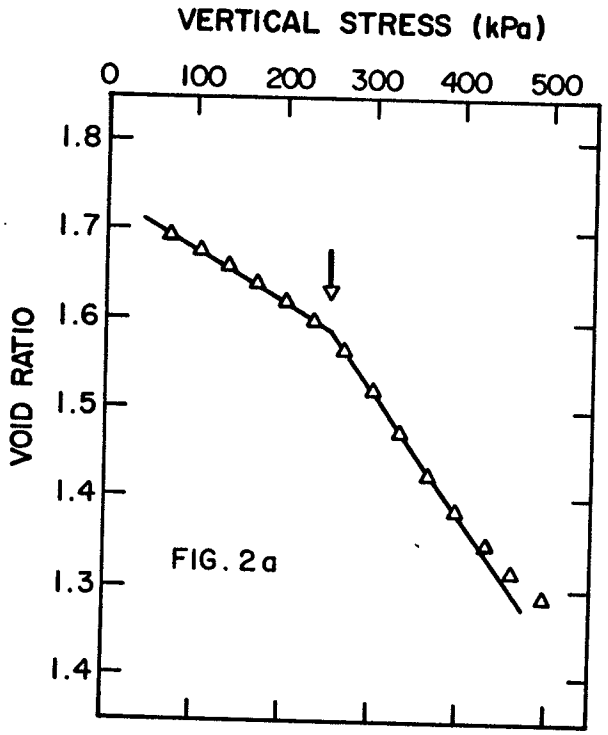

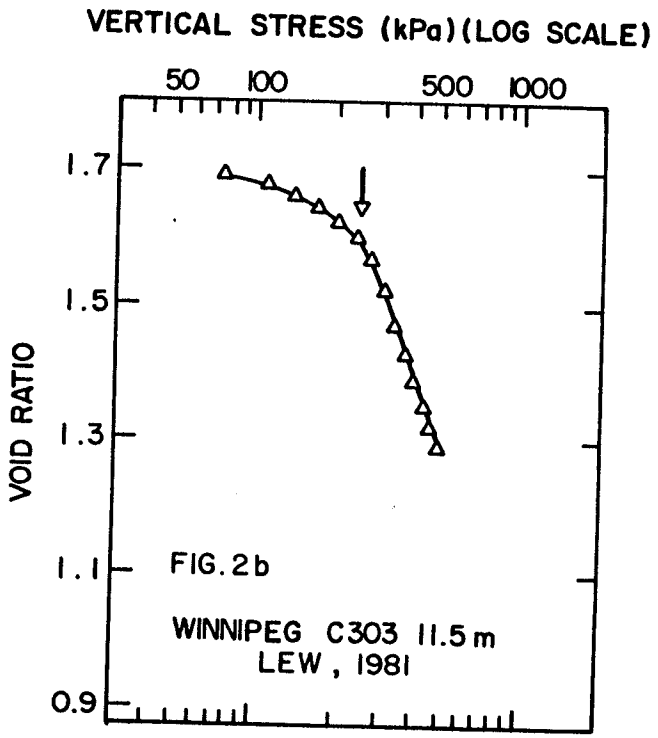

FIGURE 2 Alternative Plots of Oedometer Test Data

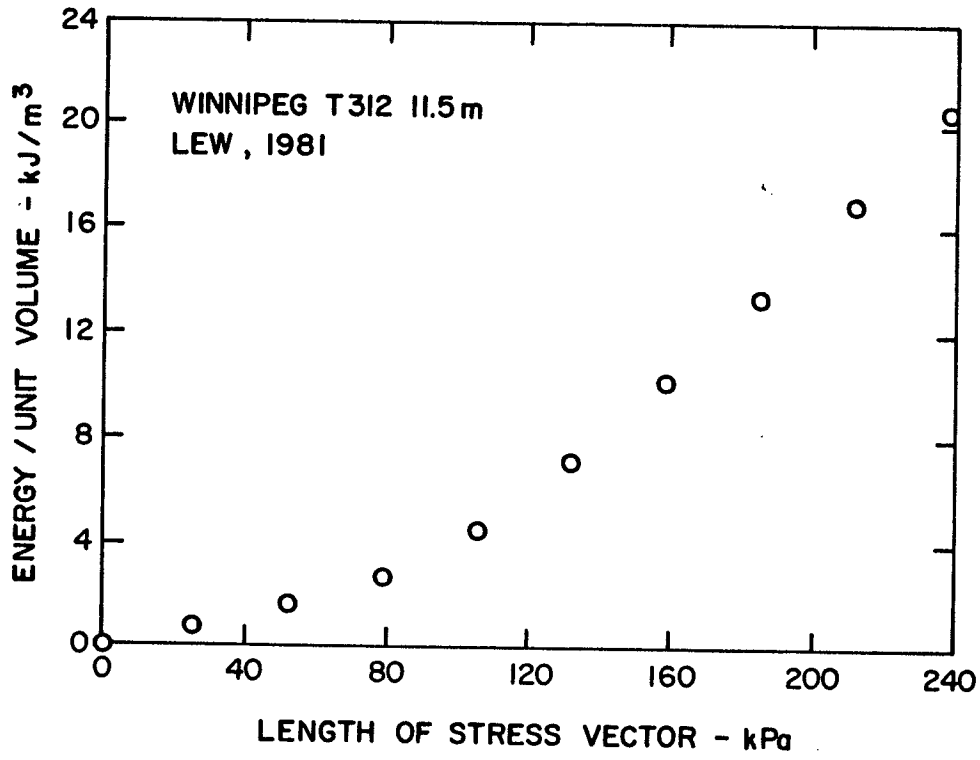

FIGURE 3 K_o-Consolidation Triaxial Test Results

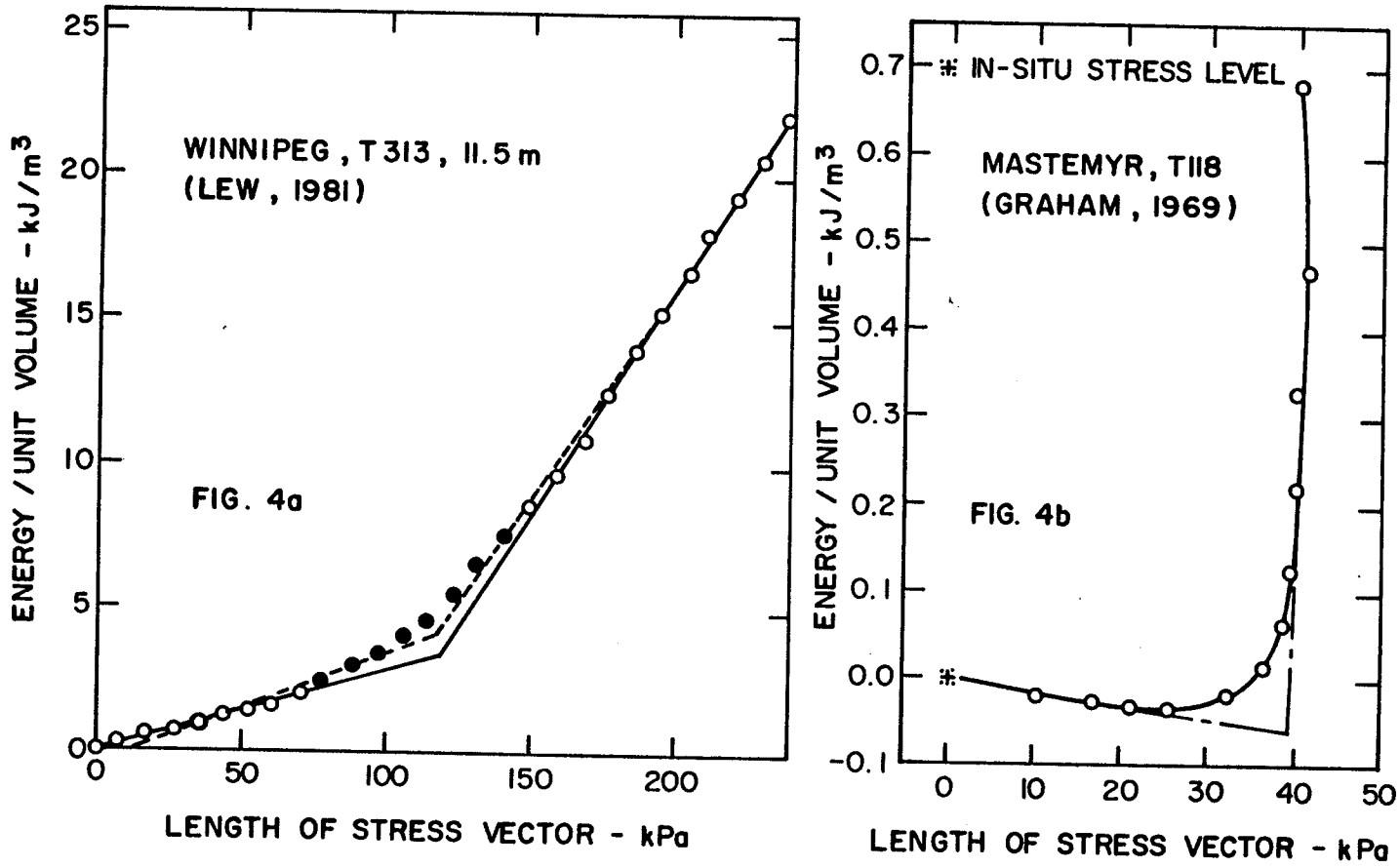

FIGURE 4 Automatic Curve-Fitting of Experimental Data

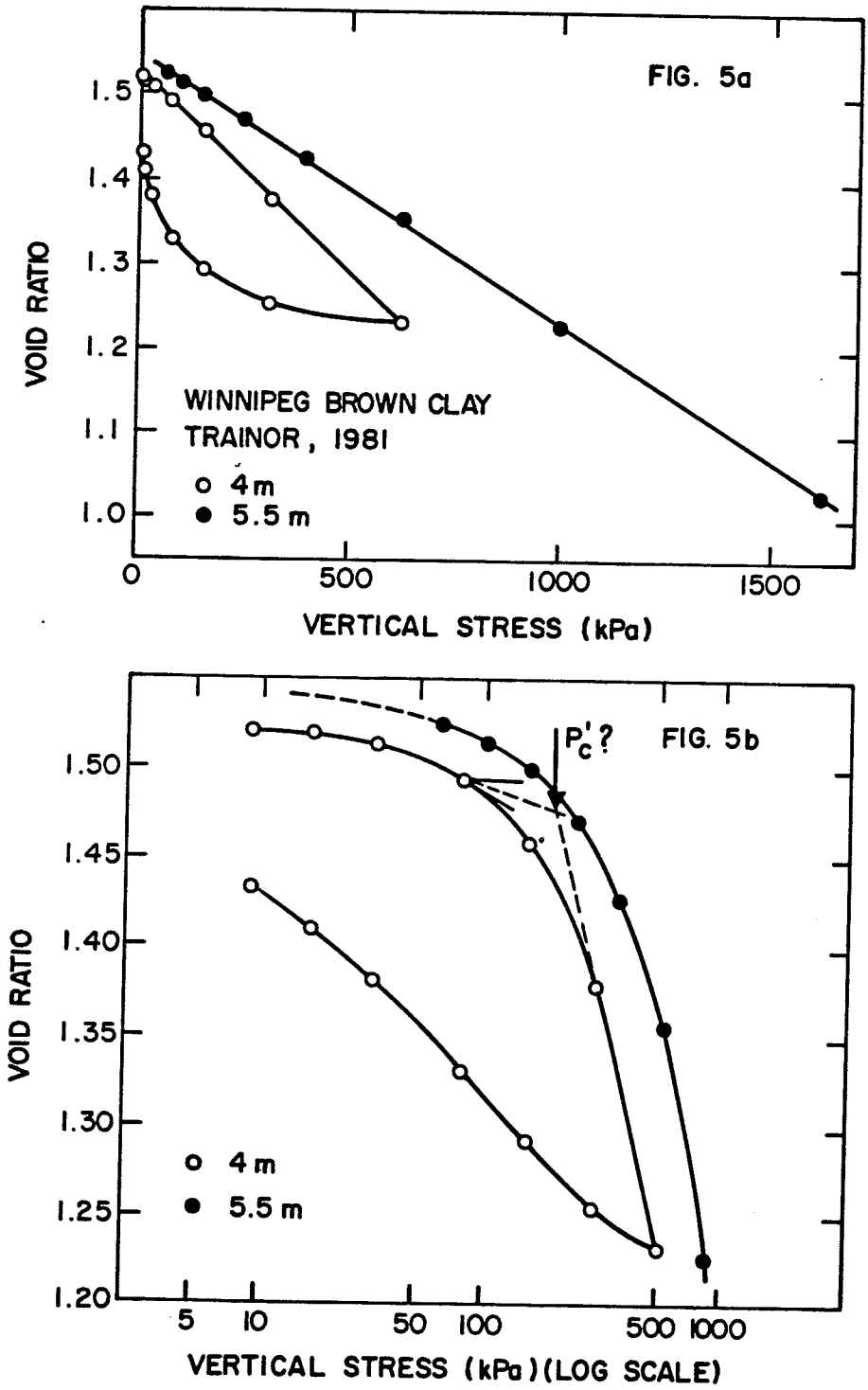

FIGURE 5 Oedometer Results in Arithmetic and Semi-Logarithmic Plots

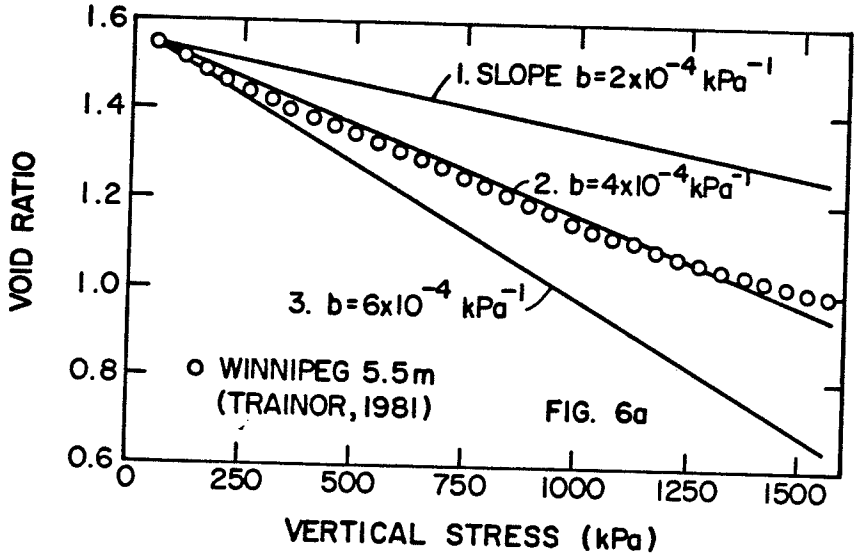

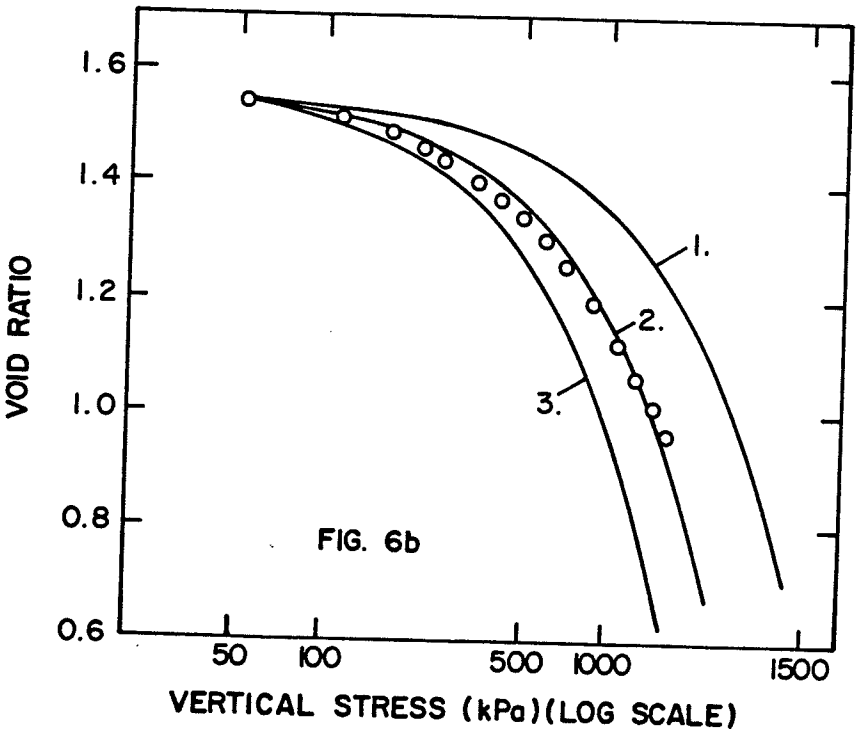

FIGURE 6 Implications of Semi-Logarithmic Plotting

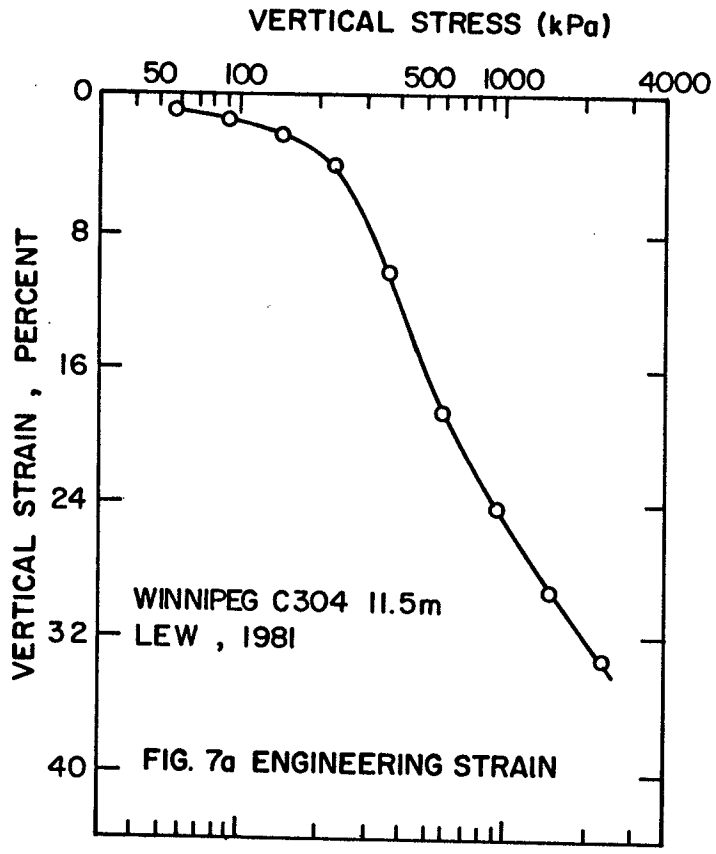

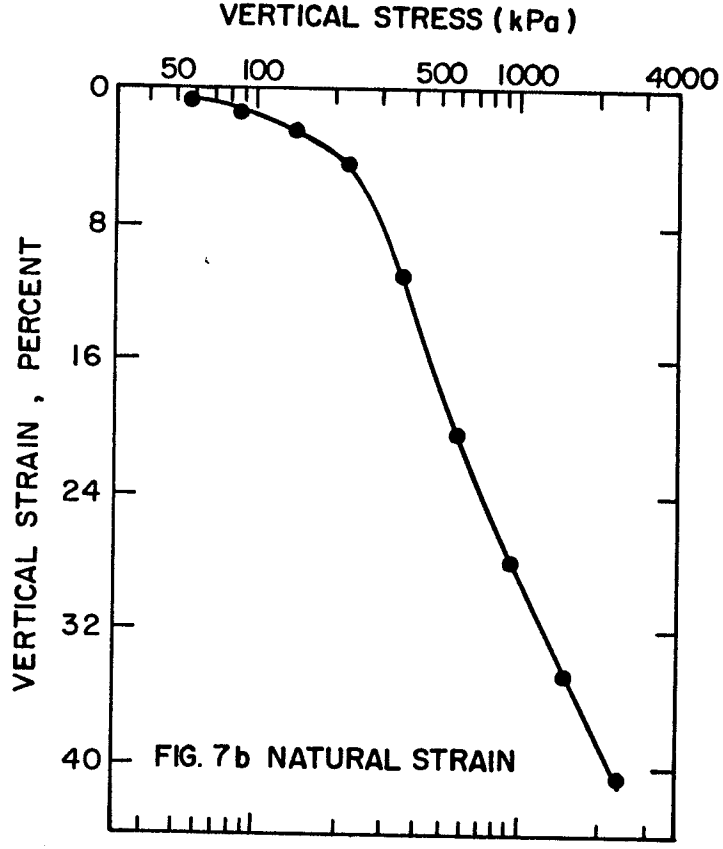

FIGURE 7 Comparison of Engineering and Natural Strains